ABSTRACT

Title of Thesis: INVERSE HYBRID METHOD FOR DETERMINING EXPLOSIVE LOADING ON PLATES DUE TO BURIED MINES

Damien Carl Bretall, Master of Science, 2007

Thesis Directed By: Professor William Fourney
Department of Mechanical Engineering

Due to the changing face of warfare there is an ever growing need to protect the underside of combat vehicles from mine blasts. This research effort presents a new method to better characterize the pressure profiles experienced by a plate as the blast develops. The explosive deformation of a small-scale plate was recorded using synchronized high-speed digital cameras, and then analyzed using 3D Digital Image Correlation software. Time-varying pressure profiles were input into an axisymmetric FEM simulation by fitting curves to data obtained from tests using Kolsky bars to measure pressures. These were then modified to find possible profiles that produce the measured deformations. It was discovered that the final deformation cannot be determined from only total impulse or peak pressures, it is very sensitive to the time and spatial decay of the pressures, and a deforming plate travels with greater initial velocity than a nondeforming plate of equal mass.

INVERSE HYBRID METHOD FOR DETERMINING EXPLOSIVE LOADING ON PLATES DUE TO BURIED MINES

By

Damien Carl Bretall

Thesis submitted to the Faculty of the Graduate School of the
University of Maryland, College Park, in partial fulfillment
of the requirements for the degree of
Master of Science
2007

Advisory Committee:
Professor William Fourney, Chair
Professor Henry Haslach, Jr.
Professor Deborah Goodings

Dedication

This is dedicated to my late grandfather Carl F. Bretall, whose lifelong vigor for learning motivates me to constantly better myself. I take great pride in knowing that I am beginning to earn my middle name by modeling my work ethic, organization and workmanship after his.

Acknowledgements

First of all I would like to thank my advisor Dr. Fourney for granting me the privilege of working in the Dynamic Effects Lab as his graduate student. This has been a remarkable experience for me, and I was able to tremendously expand my engineering abilities and awareness. No one could have asked for a more trusting, encouraging and knowledgeable advisor. I would also like to thank my committee, Dr. Goodings and Dr. Haslach, for what I've learned from them in our group meetings or in class, respectively.

This work was performed under contract to the Office of Naval Research as part of a larger effort. General direction of the overall effort was provided by Mr. Lee Mastroianni and Maj. Billy Short, USMC (Expeditionary Warfare and Combating Terrorism Department). It is continuing under the sponsorship of the US Army Tank Automotive Research, Development and Engineering Center (TARDEC).

Also critical to my research was Uli Leiste, who was always patient whilst instructing me on the many intricacies of small-scale explosive testing. Thanks to Les Taylor for always answering any question I may have, and to Dr. Robert Bonenberger for assisting me with my force-deformation material tests.

Daniel Casem from the Army Research Lab was essential to my development of the DYNA computer model, and I appreciate the many hours he spent answering my questions and teaching me about computer simulations. I also appreciate Dr. Michael Sutton and Vikrant Tiwari from the University of South Carolina for lending us a high-speed camera and helping me conduct Vic-3D tests, and Dr. Steve McNeill for traveling to our lab to help further my knowledge of Vic-3D.

Thanks also go to Sasha Tsarev for helping me out when I was new to the lab, to my German colleagues Dominik Weinlein, Thomas Welker and Joschka Neumann for always lending a hand with my work, teaching me various techniques, and motivating me, and to my most recent labmates Rob Benedetti, Dana Colegrove and Suad Drekovic for making it such a pleasure to work in the Dynamic Effects Lab.

The graduate level classes would have been much harder to bear if it was not for the motivation, assistance, and support of some of my closest friends throughout graduate school, including Silas Nesson, Rifat Jafreen, Chrissy Ikeda and Crystal Robinson, who always found time to study with me, do homework together, or bring me food to keep me going.

Last, but of course not least, thanks to my family for always being there for me, and helping me successfully make it through college. You have always strongly supported me throughout my college years and allowed me to take on many opportunities. It is immensely motivating to know that there is someone wishing you well and hoping to see you succeed.

Table of Contents

List of Tables

List of Figures

Chapter 1: Introduction and Background

1.1 Overview

Research for this thesis was conducted at the University of Maryland, College Park within the Mechanical Engineering Department in the A. James Clark School of Engineering. Tests were performed in the Dynamic Effects Lab by utilizing the sand pit located in the basement of the Engineering Lab Building. Computer simulations were also employed using LS-DYNA finite element analysis (FEA) software.

Previous small-scale research conducted at the Dynamic Effects Lab measured the impulse delivered to a plate positioned at various distances from the sand subjected to an explosive buried at varying depths. The effect of the geometry of the plate has also been examined by using pyramidal and V-shaped non-deformable hulls [1]. However, for current research, thinner plates have been employed to ensure that adequate deformation is induced using only moderate amounts of explosive. The scope of this research is limited to blasts that do not penetrate the floorboard of the vehicle. Floor rupture has been established as the leading cause of serious crew injuries. Without rupture, "only floor bulging is experienced, [and] the vehicle is then subjected to displacement and acceleration off the ground" [2]. A flat plate was chosen for experimentation to represent the bottom surface of a vehicle, also known as the hull.

Videos of the small-scale tests were recorded using two synchronized high-speed cameras, and data of the deformation over time was obtained through 3D Digital Image Correlation (DIC) software. The final deformed profile of each plate

was measured using a FARO arm, and the crater generated by the blast was measured using a profilometer. For the FEM simulations, curves were fit to data that was obtained from previously conducted Kolsky bar pressure tests. Time-varying pressure curves were generated for each requisite node by interpolating this data. The results of the FEM simulation were then compared to the 3D DIC results, and the curves were next modified to determine possible profiles that produce the observed deformations and accelerations. The overall goal of this research is to present this new inverse hybrid method to better characterize the pressure profiles experienced by flat plates subjected to an explosive blast. Research was also done to determine any possible correlations between the crater volume and the volume under the deformed plate, as well as the difference in initial velocities between a deforming plate and a nondeforming plate of the same mass.

1.2 Land Mines and Improvised Explosive Devices

Due to the ever-changing tactics of warfare, there is a rapidly evolving need for better protection against mine and improvised explosive device attacks. By 2005 it was reported that in Iraq “more than half of all American fatalities are now being caused by powerful roadside bombs that blast fiery, lethal shrapnel into the cabins of armored vehicles” [3]. An example of one such demolished vehicle is shown as Figure 1.1 [4]:

Figure 1.1: IED Damaged HMMWV

In modern warfare there has been “a dangerous shift from the familiar standard issue weapons, to the use of improvised explosive devices (IEDs)” [4]. These roadside bombs are fabricated in many different ways due to their homemade nature. They are often buried with the intention of damaging a vehicle and can be detonated by various means. One such recovered IED is shown in Figure 1.2 [3]:

Figure 1.2: Unexploded IED

The United States “Army officials don't disclose statistics on IED casualties, saying that aids the enemy” [5]. However, there are still reputable sources dedicated to providing accurate casualty statistics. One commonly cited source, the Iraq Coalition Casualty Count, shows a steady increase in the number of IED fatalities, as seen in Figure 1.3 [6]:

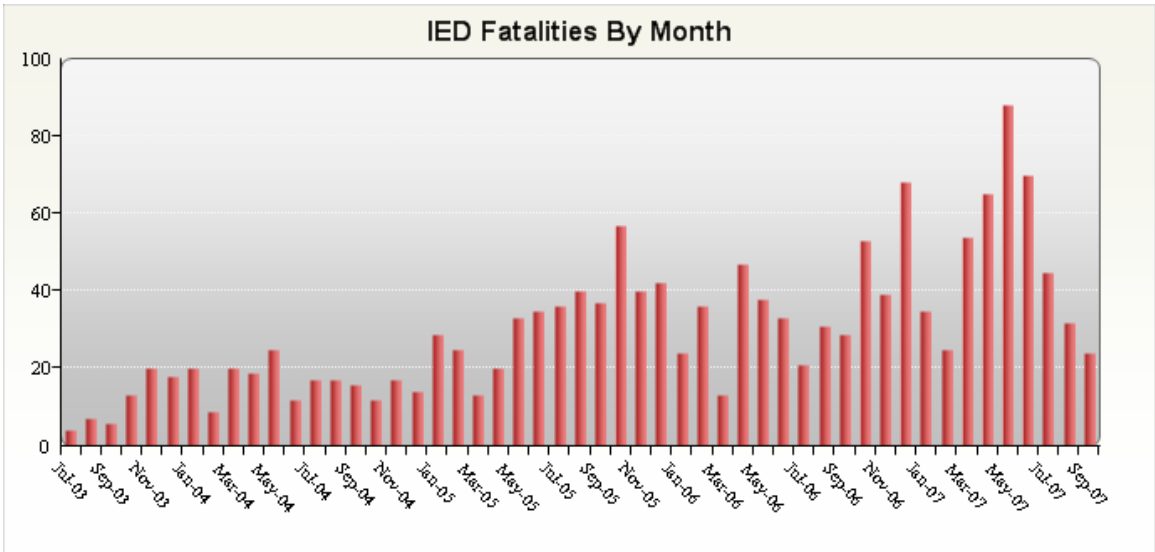

Figure 1.3: U.S. Fatalities by Month

It is especially troubling that the proportion of US fatalities that are caused by IEDs is, in general, growing. This increase is evident from Figure 1.4 which was compiled using data from the same source:

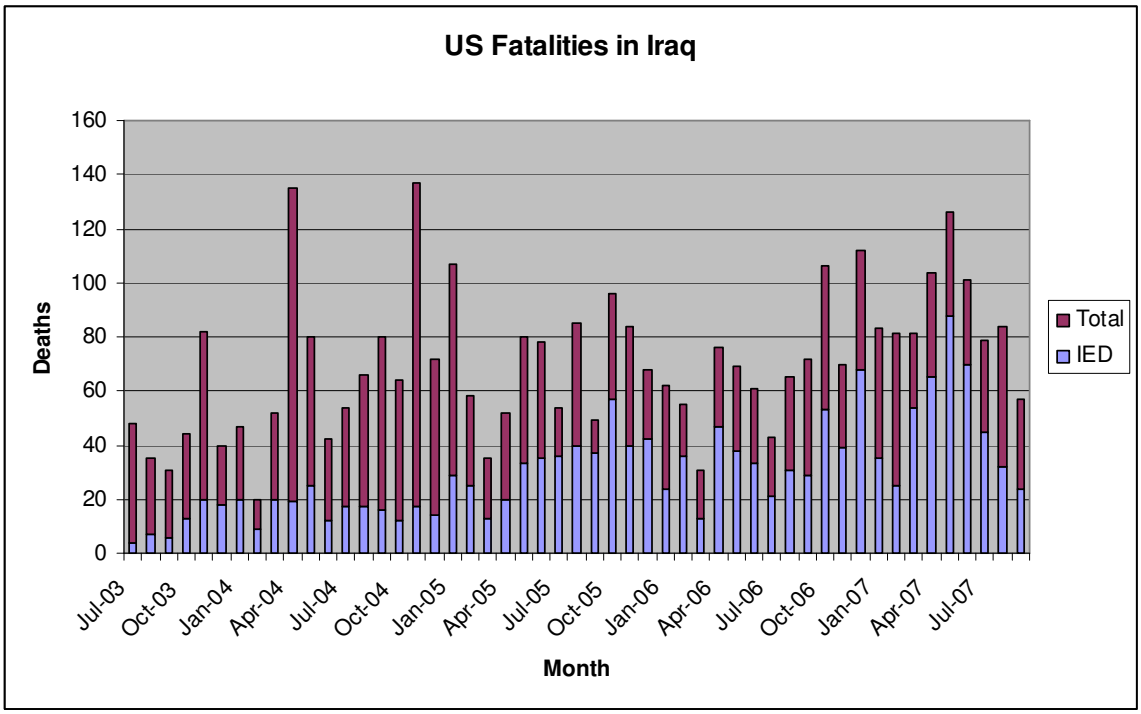

Figure 1.4: Increasing Proportion Fatalities by IEDs

Although much research has been directed towards the effects of buried explosives, there is not a comprehensive understanding of the pressures driving the damage. It is well known that "injuries sustained during a mine strike are caused by the pressure wave of the primary blast, the penetrating and nonpenetrating wounds of the secondary blast, and the injuries associated with being thrown some distance," [7] yet there is an incomplete understanding of these pressures. A full understanding not only includes the magnitudes of pressures experienced, but also the time duration of the pulse as well as the decay rate with respect to distance from the center. Increased comprehension of the pressure profiles and the damage they induce would allow for development of more sophisticated and advanced protective measures.

1.3 Scaling

The vehicles used in full-scale testing "are very expensive, and each damage test by land mine detonation expends not only the vehicle but also many man-hours of skilled engineering and support labor" [2]. Instead, small-scale tests are commonly employed due to the lower cost, quicker execution, and increased accessibility. The Dynamic Effects Lab primarily uses cube-root scaling to correlate the small-scale results with the full-scale setup. In this case, the "explosion is characterized by a mass dimension" [8].

When choosing a scaling factor, it was important to ensure that the plate experiences significant permanent deformation yet remains intact and non-penetrated in order to allow for easy measurement of the damage. It was also important to use target plates of a readily available thickness. After some initial trial and error an effective charge size of 1 gram was selected, in conjunction with a 1/16" plate thickness. The full-scale situation of interest is chosen to be a 5 pound charge (2268 g). The scaling factor is then determined by dividing the full-scale charge mass by the small-scale, and taking it to the 1/3 power:

$$SF = \left(\frac{mass_{full-scale}}{mass_{small-scale}} \right)^{1/3} = \left(\frac{2268g}{1g} \right)^{1/3} = 13.14$$

1 gram of effective explosive is used for each test conducted, so the scaling factor of 13.14 applies to all of them. In order to go from a full-scale linear dimension to the small scale, the full-scale length is divided by this scaling factor. One common test setup is a plate 16" off of the ground (known as standoff distance or SOD), with an

explosive buried 4” deep (known as depth of burial or DOB). These distances are scaled-down using the following equation:

$$SF = \left(\frac{mass_{full-scale}}{mass_{small-scale}} \right)^{1/3} = \frac{length_{full-scale}}{length_{small-scale}}$$

With a scaling factor of 13.14, 16” becomes 1.22”, and 4” becomes 0.30”. A similar calculation can also be performed to determine the plate thickness. The 1/16” test plate corresponds to a 0.82” thick full-scale plate. With this scaling method the full-scale velocity is the same as the small scale. In order to obtain full-scale acceleration, the small-scale observed acceleration needs to be divided by the scaling factor.

Chapter 2: Research Equipment

2.1 Explosive Charge – RP-87 and Deta Sheet

The charges used for all the experiments are made by coupling a precision secondary explosive detonator with a malleable sheet explosive. The detonator is an RP-87 Exploding Bridge Wire (EBW) Detonator manufactured by Teledyne RISI. The EBW detonators contain a small wire that is vaporized when electricity is suddenly discharged through it, which initiates a secondary explosive. It consists of 26 mg PETN initiating explosive, and 43 mg RDX output explosive, as shown in Figure 2.1 [9]:

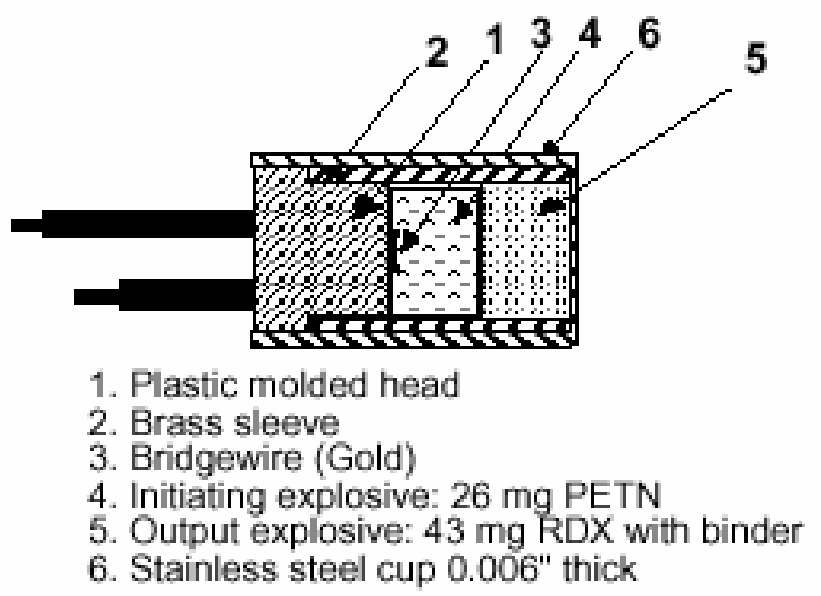

Figure 2.1: RP-87 Explosive Train

PETN stands for pentaerythritol tetranitrate, a very powerful high explosive. RDX is cyclotrimethylenetrinitramine, a common military high explosive also known as cyclonite. The dimensions of the RP-87 detonator are shown in Figure 2.2 [9], and the firing parameter specifications are listed in Table 2.1 [9]:

Figure 2.2: RP-87 Dimensions

Threshold Burst Current	210 amps
Threshold Voltage	Approx. 500 volts
Threshold Voltage Std. Deviation	75 volts maximum
Function Time	1.95 µsec typical
Function Time Simultaneity Standard Deviation	0.125 µsec maximum

Table 2.1: RP-87 Firing Parameters

The moldable sheet explosive, purchased from Omni Explosives [10], is similar to the compound commonly known as Deta Sheet. It consists of 63% PETN by weight. The required mass of Deta Sheet was chosen based on the goal of creating a charge with 1 gram of effective explosive material. As shown in the above Figure 2.1, an RP-87 consists of 69 mg of explosive. In order to get 1000 mg of total explosive, 1478 mg of Deta Sheet must be used because it contains 931 mg of PETN. Along with the RP-87 detonator and Deta Sheet, the charge also consists of a Delrin plastic casing. This ring is made on a lathe from a piece of 5/8th inch stock. The center is drilled using a 19/32nd inch bit (approximately 15 mm inner diameter), and the outer surface is turned down until the wall thickness is thinner than about a millimeter. The ring is parted off so it is about 6.5 mm tall. These components are shown in Figure 2.3. The foreground of Figure 2.4 shows a partially assembled charge, with the Deta Sheet pressed into the casing. Figure 2.5 shows the finished charge, with the components held in place using 5-minute epoxy.

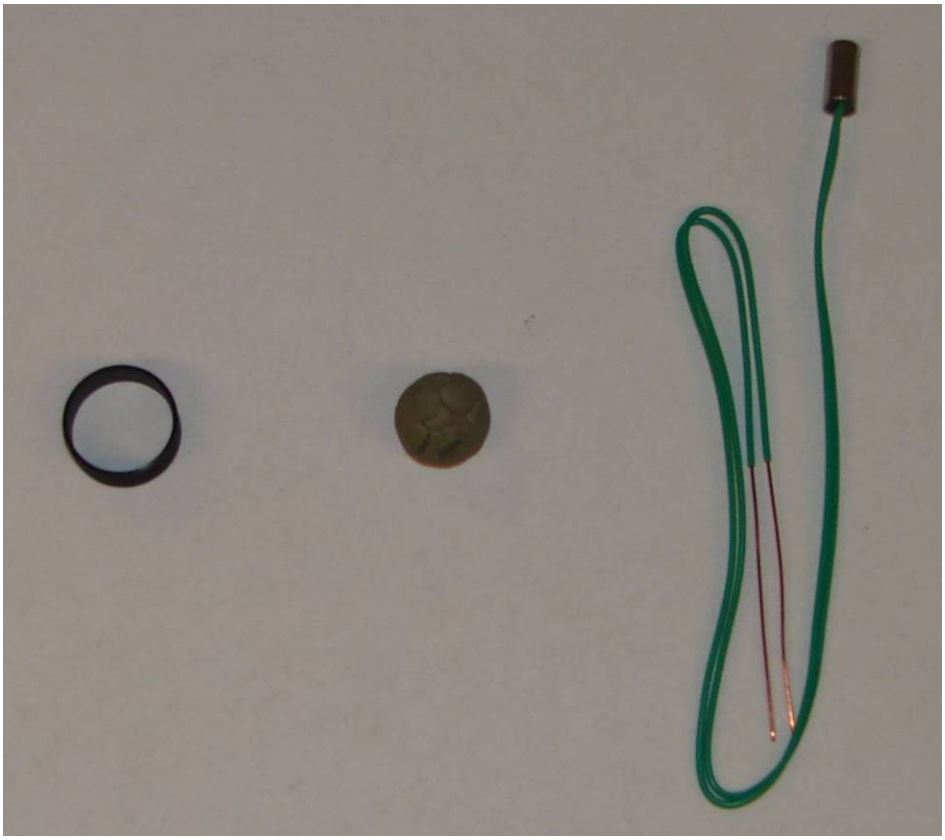

Figure 2.3: Delrin Casing, Deta Sheet, and RP-87

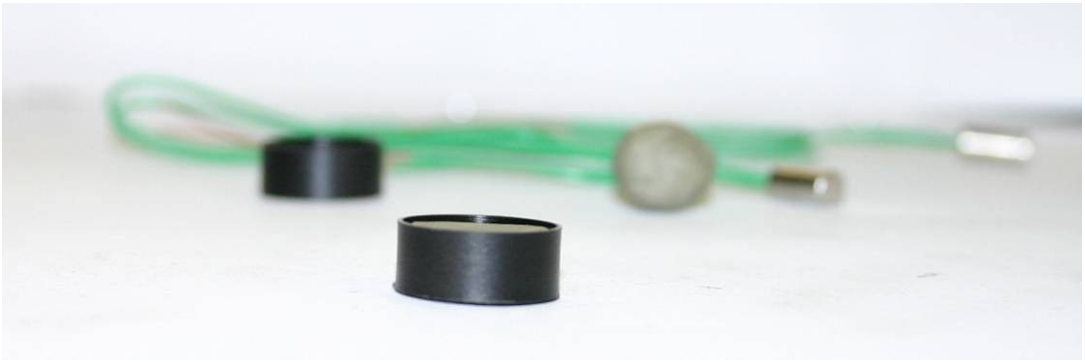

Figure 2.4: Delrin Casing with Deta Sheet Inside

Figure 2.5: Finished Charge

2.2 FS-17 Exploding Bridge Wire Firing System

In order to trigger the RP-87 an FS-17 Exploding Bridge Wire Firing System is used, which ensures the EBW detonator is supplied the appropriate sudden pulse required for proper firing [11]. The system consists of a Control Unit as well as a Firing Module, as shown in Figure 2.6. In the figure the Firing Module is the smaller rectangular box demarcated by blue brackets, which is inserted into the Control Unit. The Trigger Mechanism for the camera is also shown.

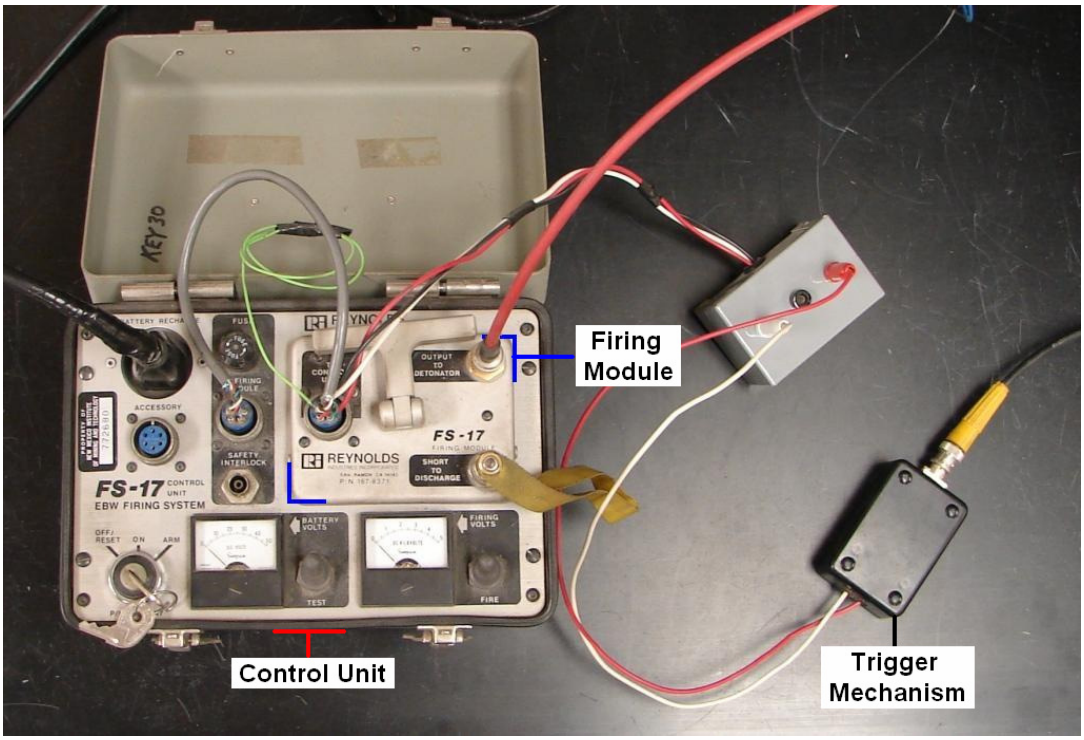

Figure 2.6: FS-17 Firing System

The Control Unit supplies low voltage (40 volt) electrical energy to the Firing Module, which charges a one microfarad capacitor. In order to operate the unit, the safety is removed from the "Short to Discharge" connection and inserted into the one labeled "Safety Interlock." The key is then rotated clockwise from the "Off" position, and held in the "Arm" position until the "Firing Volts" gauge reads at least 3500 volts. At this point the countdown can begin; while still holding the key in the "Arm" position, the switch labeled "Fire" is then toggled to initiate detonation. This applies a 30 volt pulse to a spark gap in the Firing Module, which causes the capacitor to discharge through a cable to the detonator. At this point a signal is also sent to the trigger mechanism, which in turn is connected to the cameras. This ensures the cameras are triggered at the same time as the explosion.

2.3 Dummy Charges

Before executing the test it is prudent to ensure that the equipment is properly connected. A dummy charge is employed before connecting the Firing System to the detonator. It is just a simple aluminum cylinder that holds two exposed wires a short distance apart, as seen in Figure 2.7:

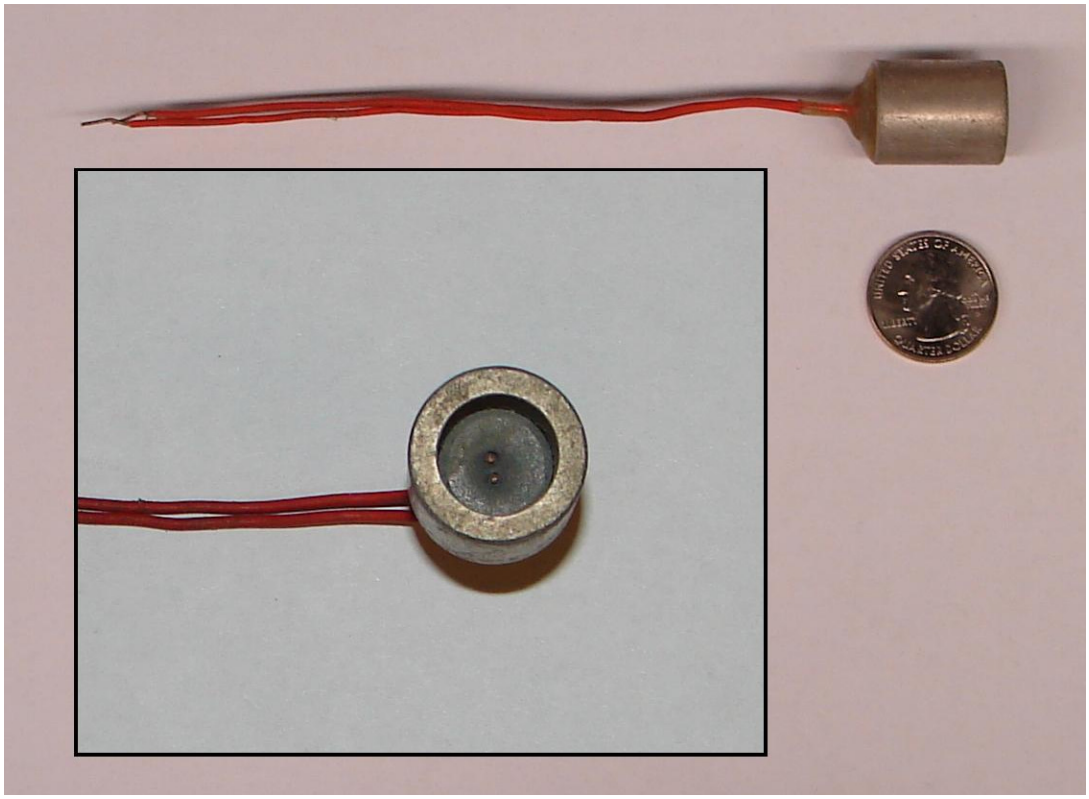

Figure 2.7: Dummy Charge (Top and Side Views)

The dummy charge is hooked to the Firing System, which is then triggered in the same manner as it would be with a live explosive. The current arcs through the air between the leads and creates an audible noise as well as a flash of light. If everything is hooked up properly, the cameras will both trigger and record a video of this flash at the time of trigger.

2.4 Sand Pit

All explosive tests discussed in this paper were conducted in the sand pit located in the basement of the Dynamic Effects Lab using fully saturated sand. It has a 5 foot by 5 foot area, and is 2 feet deep. The sand pit, often referred to as the test bed, is shown in Figure 2.8. The leveling tool is also shown in the figure, which is used to obtain a smooth and level top surface.

Figure 2.8: Sand Pit with Leveling Tool

Underneath the sand is a layer of coarse gravel as well as a layer of mesh. This allows for the sand to be saturated from below with water, and then drained after the test is performed. When the drain valve is closed and the water is turned on, the sand pit begins to fill from underneath the sand. Figure 2.9 shows the sand pit with its system of tubes for filling and draining, including the gray stand column.

Figure 2.9: Sand Pit with Water Piping System

The procedure for preparing, saturating and leveling the test bed of the sand pit is described in the next chapter on experimental procedures.

2.5 Deformable Target Plate

Due to the destructive nature of the tests, a new target plate was constructed for every experiment. The same specifications were used for each one. The plate is simply a 1/16” thick sheet of 6061 T6 aluminum alloy, cut to a 16” by 14” rectangle. Holes were drilled in the plate so it could be bolted to a heavy frame. The center points were marked on the plate by using the frame and a transfer punch, and the side holes drilled using a 25/64” drill bit. A typical test plate has a mass of about 610 g after preparation. Depending on the test goals the plate was spray painted as well. One of the test plates, as well as the frame, is shown in Figure 2.10:

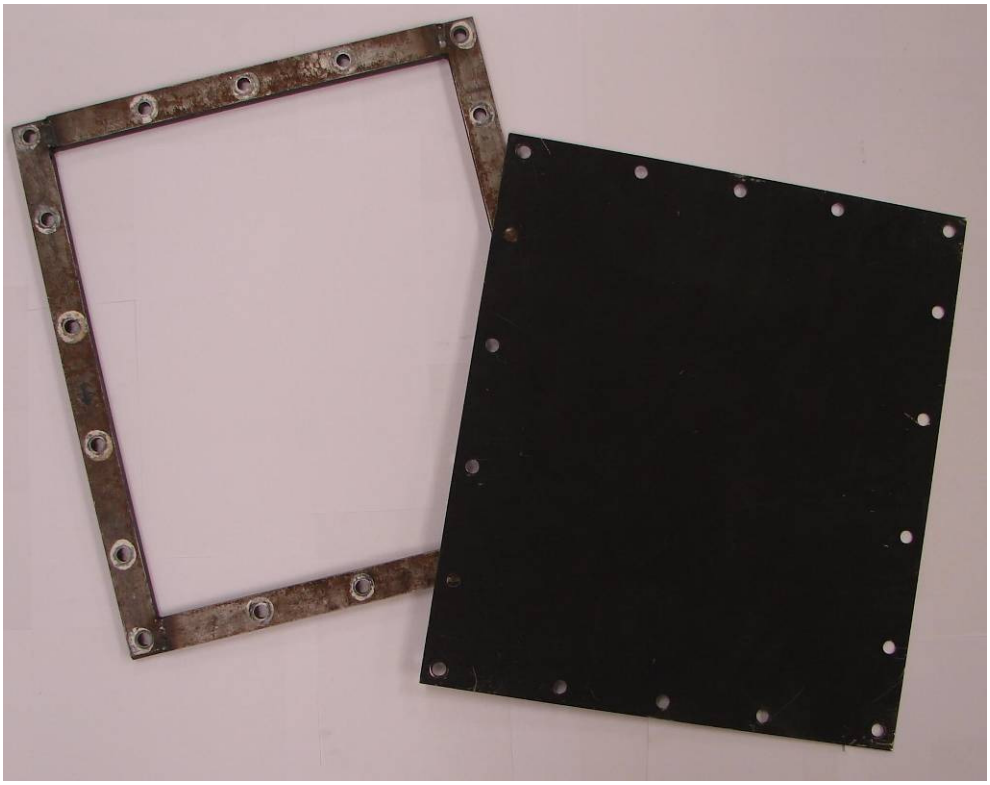

Figure 2.10: Frame and Test Plate (Before Deformation)

2.6 Frame

A steel frame was used in order to increase the weight of the target, as well as to fix the edges. It was constructed by welding ½" by 1" steel stock into a rectangle and drilling the holes for holding the plate. The frame is ½" thick, and the other dimensions are shown in Figure 2.11:

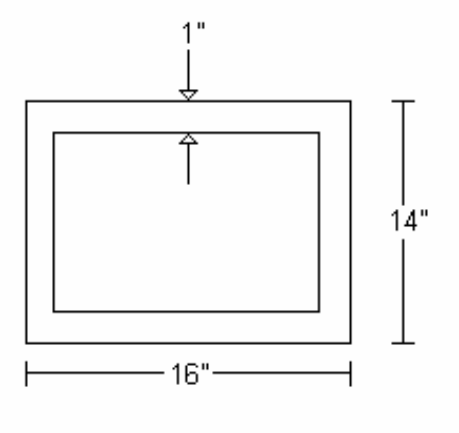

Figure 2.11: Frame Dimensions

Including the weight of the 18 nuts and bolts required to hold the plate in place, the frame has a mass of about 4050 g. The approximate total mass of the frame, plate, and mounting hardware is 4660 g.

2.7 Lighting

250W halogen photography lights from North Star were used for the test. The flexible mounts allow for easy placement and positioning. Adequate lighting is especially crucial for high speed photography where the exposure time is as low as 5 μs. Depending on the selected frame rate and exposure time, up to 5 photo lights are used at one time. It is especially important to ensure that they are pointed at the center of the plate, and that the light is not reflecting directly into the cameras. As the surface of the plate deforms, the light is reflected in different directions. Care must be taken to ensure that these reflections do not over saturate the camera images.

2.8 High Speed Cameras and Lenses

The high speed cameras used were made by Vision Research. Two cameras were run simultaneously for each test in order to record the images from different

angles, especially for the experiments with 3D Digital Image Correlation. A Phantom v7.1 was used along with the Phantom v7.2 shown in Figure 2.12:

Figure 2.12: Phantom v7.2 and Zoom Lens

Phantom v7.1 and v7.2 are nearly identical cameras. The Phantom v7.2 runs at up to 190,476pps [12], but resolution must be sacrificed to achieve this. Typical camera parameters used for the experiments are shown in Table 2.2:

Resolution	Frame Rate
256 x 256	26143
128 x 128	61538
320 x 128	55555

Table 2.2: Phantom Camera Parameter Combinations

The listed frame rates are the maximum the camera will allow at the specified resolution. The third combination listed is the only non-square field of view used, and was only employed in rare cases where this shape was more suitable. The 3D DIC tests exclusively used the square field of views. These parameters are selected in the Phantom Camera Control software, which must be run on a laptop that is connected

to the camera. During testing the images are recorded by connecting the BNC trigger cable to the trigger mechanism, which is hooked to the firing system as pictured in Figure 2.6.

The above Figure 2.12 also shows one of the lenses used for the tests. Most of the tests were photographed with a 28-75mm variable focal length zoom lens set to 28mm for each camera, with the aperture set at 8 (this lets almost the maximum amount of light in). Instead of zoom lenses, 28mm fixed focal length lenses were used for the high precision tests that required image distortion to be minimized.

Chapter 3: General Experimental Procedures

3.1 Test Procedure

All the tests were performed in the sand pit at the Dynamic Effects Lab using saturated sand. Due to conflicting requirements between software applications and conventions, values are reported in either SI or English. Prior testing concluded that saturated sand produces the highest impulse in a buried mine blast, and is therefore the worst case scenario. A test cannot be conducted unless water has been drained and the sand has dried out adequately from any previous testing. At this point preparation can begin by loosening and turning over the surface of the sand, especially around the area for where the charge will be buried. It is also often necessary to build up this area with enough sand to ensure that after compaction it is higher than the height of the leveling tool. The sand is then compacted with a concrete block, and the excess is scraped off with the leveling tool (see Figure 2.8 in Chapter 2). At this point, a trench is dug around the perimeter of the tank to ensure proper water saturation. The finished test bed is shown in Figure 3.1, along with the area where the test is to be conducted:

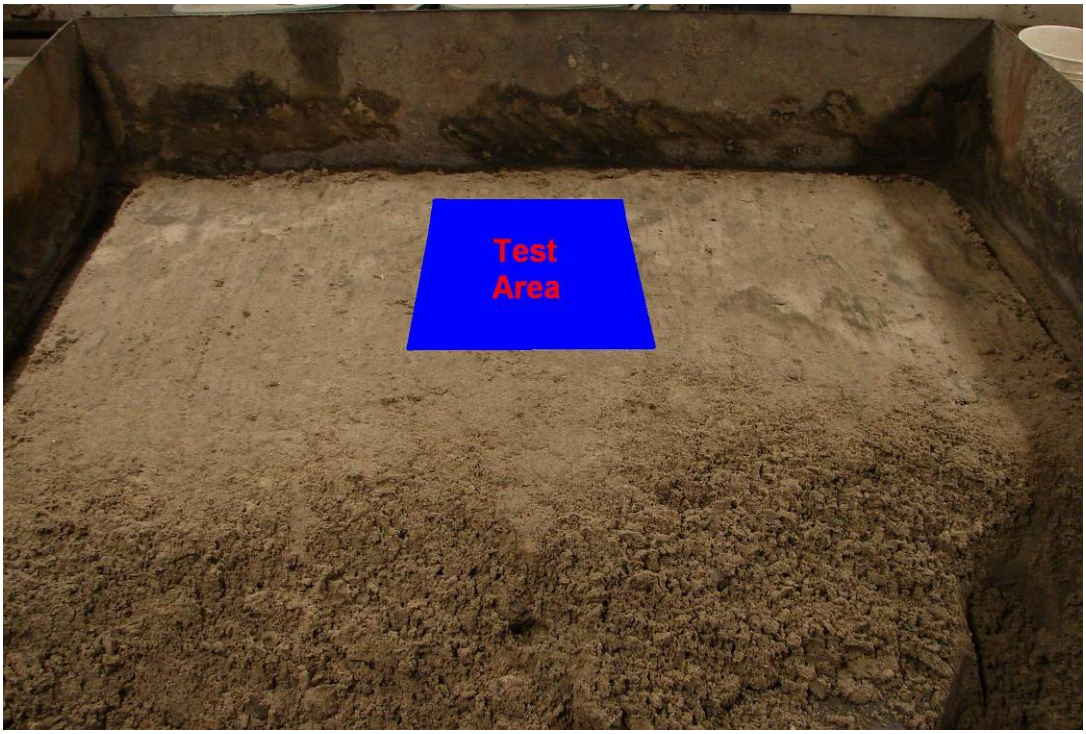

Figure 3.1: Prepped Sand Pit with Test Area Highlighted

The next step is burying the charge at the selected depth. This is done by taking the plate and frame (already bolted together) and placing it in the desired test position, and then tracing an outline in the sand around the perimeter using a thin, sharpened dowel rod. The plate and frame are then removed so that the center of the rectangle can be located by connecting the opposite corners of the sketched rectangle using a ruler and dowel. A small hole is dug at the center and the charge is buried at the desired depth of burial (DOB). DOB is defined as the distance from the top of the charge to the surface of the sand, as shown in Figure 3.2. This measurement is taken using the depth probe of a caliper. After the depth is correct, the hole needs to be filled in and lightly compacted to approximately the same density as the surrounding area. Care must be taken to carefully smooth the surface of the sand above the charge

by using a small wooden block. Prior experimentation showed that the faintest lines left in the sand can alter the shape of the developing blast.

The other parameter of interest is the distance from the surface of the sand to the bottom of the plate, known as the standoff distance (SOD). This is controlled by adjusting the bolts in the four corners of the frame that serve as legs. Small pieces of sheet metal are placed under each of the legs to ensure that they do not sink into the sand once water is introduced. The plate and frame setup are shown in Figure 3.3 immediately before conducting a test. Water is introduced to the tank through the piping system described in Chapter 2 until it reaches the surface of the sand, which is then fully saturated and develops a glossy sheen.

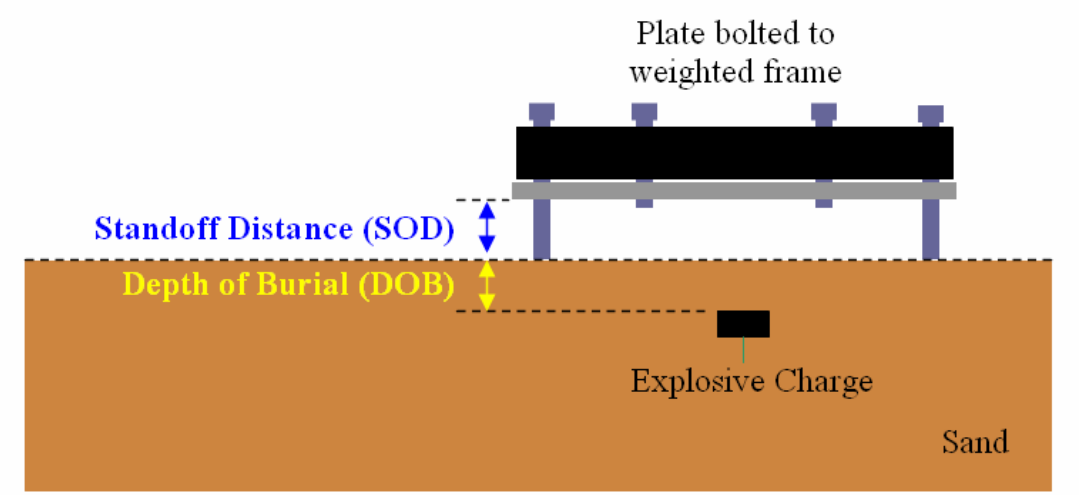

Figure 3.2: Test Diagram

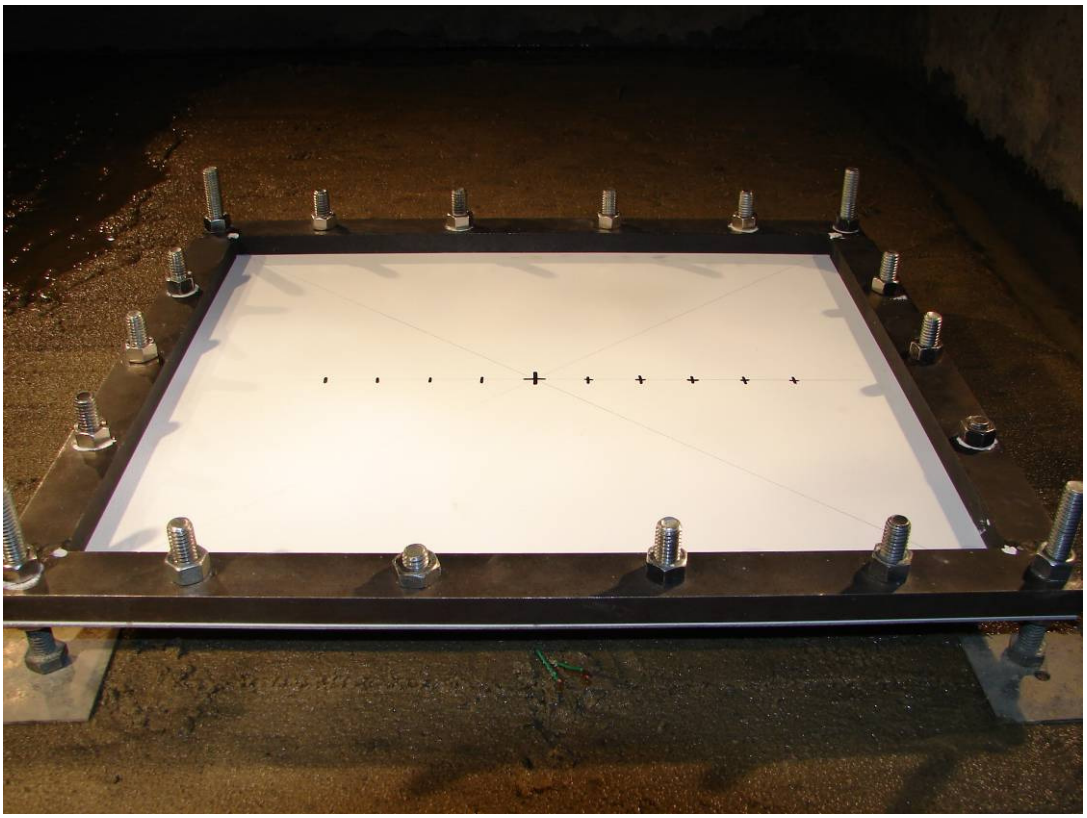

Figure 3.3: Plate and Frame Ready for a Test

Once the plate is in place the dummy charge (described in Chapter 2) can be connected to the alligator clips from the detonator cable. The dummy is then fired using the Firing System with the procedure described in Chapter 2 to ensure the cameras are triggering correctly. If the cameras successfully record the spark at or around frame 0, then the charge can be hooked up and the test can be run.

3.2 Measurement of Final Deformation

Although the transient deformation of the plate was obtained using 3D Digital Image Correlation, the final deformation is also important. A FARO Platinum Arm was used to measure the plastic deformation of the test samples. The arm is capable of achieving accuracies of up to 0.0005” which is more than adequate for this

purpose. These measurements obviously do not need to be taken at the time of the test. Figure 3.4 [13] shows the device, which is located in the Kim Building at the University of Maryland:

Figure 3.4: FARO Platinum Arm

The aim of these measurements was not only to quantify the final deformation but to determine its degree of axisymmetry. The FARO was set up to collect series of points as the probe was moved along the surface of the plate. The machine is calibrated by placing the probe at a fixed location on the workbench and capturing the point from many different approach angles. This method is referred to as Hole Calibration in the FARO CAM2 Measure software and is found by going to the Devices menu, and then selecting Probes. After calibration a coordinate system must then be developed. The first step is to select 3-D line from the Line option under the Measure menu and create two lines by tracing intersecting edges of the plate. From the Construct menu a plane of best fit must be created using these two lines. Also

from the Construct menu, a point is created using the intersection of the lines, and then a coordinate system is constructed from the plane and point. The plate was clamped to the workbench and the coordinate system was constructed at the top left as shown in Figure 3.5:

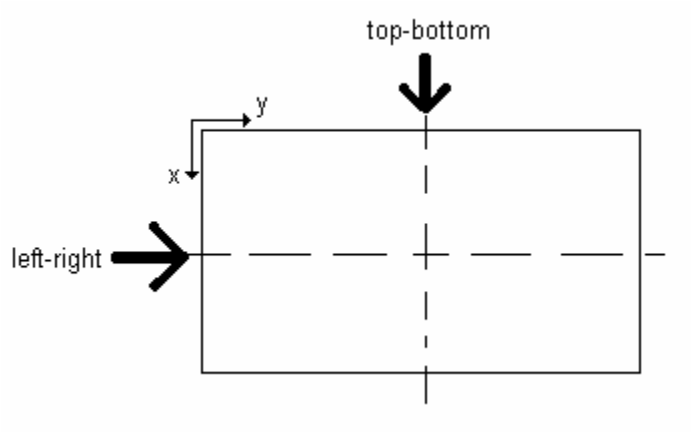

Figure 3.5: Schematic of Coordinate System and Measurement Paths

After the calibration and coordinate system are completed, data is taken by going to the Measure menu, selecting Scan, and then Freehand. Points were collected by following a path from the left side of the plate to the right side through the area of maximum deformation, minimizing deviations of the path in the x direction as much as possible. The same procedure was also used to trace from the top to the bottom of the plate, as well as across the diagonal. An example of the resulting data lines is shown in Figure 3.6, including a line traced diagonally along the plate:

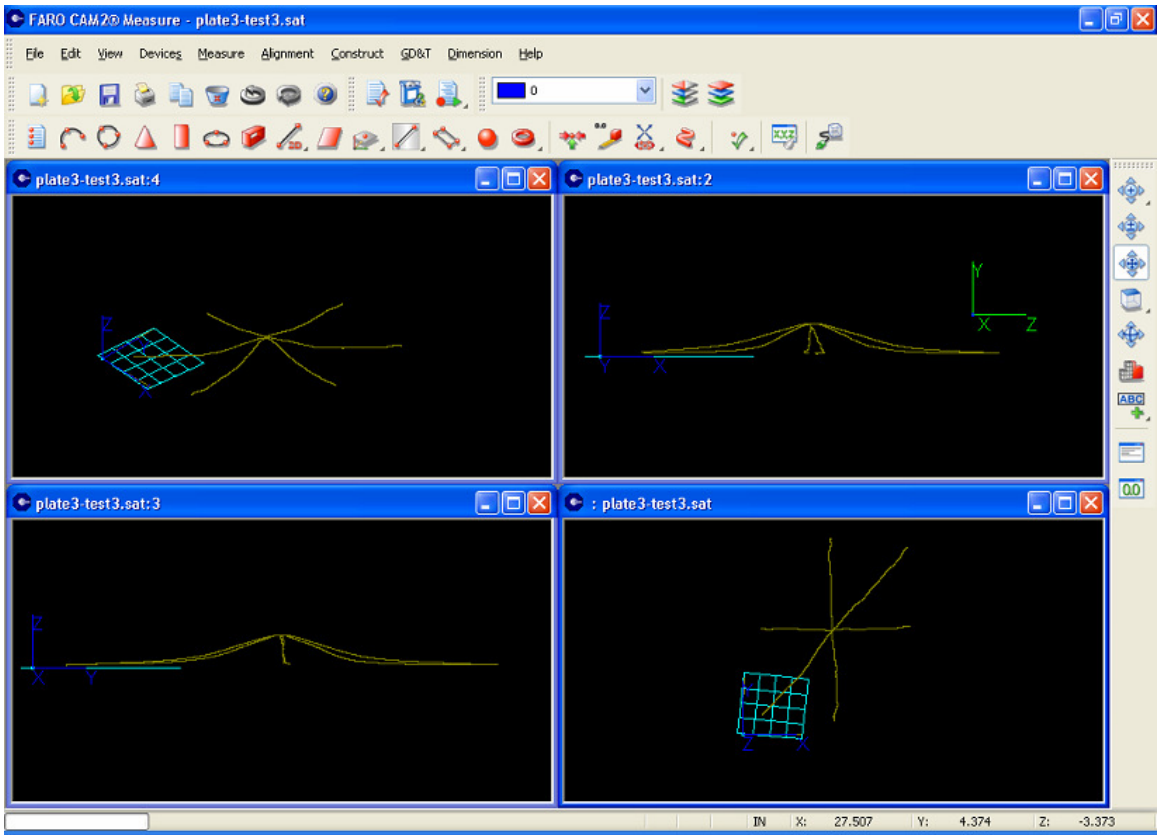

Figure 3.6: Final Deformation Profile Data in FARO Software

From this point the XYZ data can be exported to a text file through the Export XYZ option under the File menu, by selecting XYZ Out. The csv file can then be opened in a spreadsheet program and the 2D profiles can be plotted. In the spreadsheet the point with the largest deformation is assumed to be the center of the plate, and the data is shifted accordingly. The area under the entire displacement curve is calculated, as is the volume generated by rotating the area in the first quadrant around the y-axis. This data is presented in Chapter 4.

3.3 Crater Measurement

A crater measurement can be taken after the test has been conducted and the water has been drained from the sand pit, but before the surface of the sand is

disrupted. A custom-made profilometer tool is used that consists of several depth probes mounted with a grid behind them. The profilometer is placed across the sand pit directly above the center of the crater, and the probes are lowered until they barely make contact with the surface of the sand. The profilometer is shown in Figure 3.7 after the probes have been lowered to follow the crater's surface:

Figure 3.7: Profilometer after Taking Measurements

At this point the profilometer can be removed from the sand pit. The bottom of the probes should now be positioned to closely follow the profile of the crater, as seen in Figure 3.8. At this point the depth measurements can be recorded using the top edge of the depth probes and the built-in grid, as seen in Figure 3.8 and Figure 3.9:

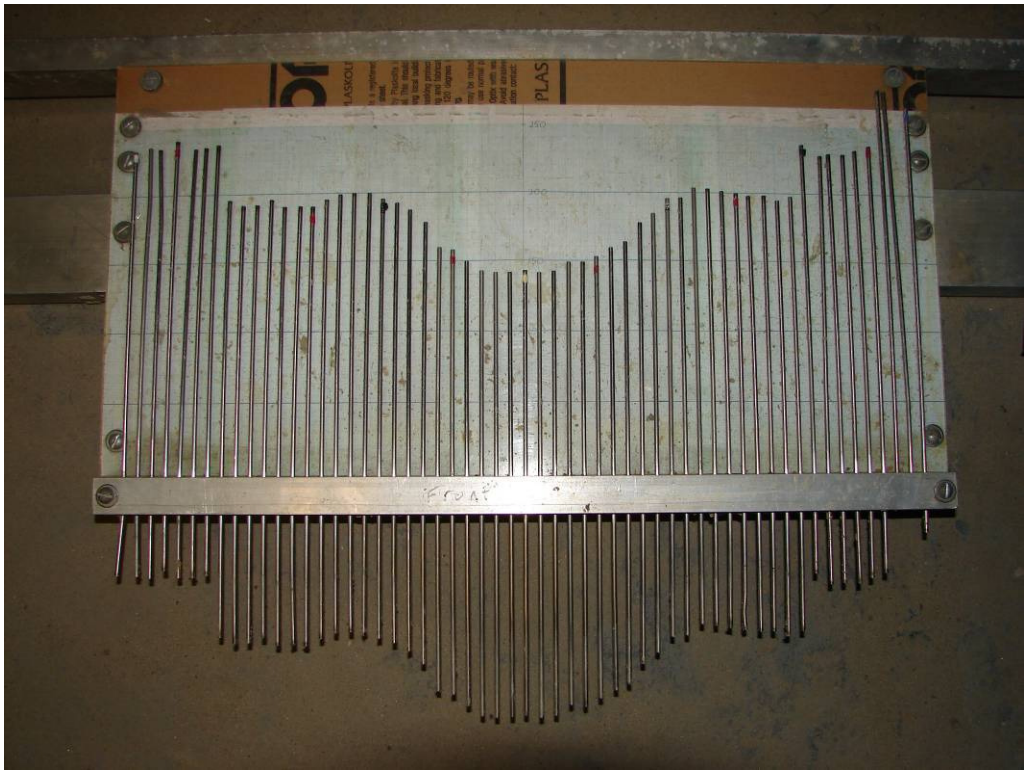

Figure 3.8: Recording Measurements from the Profilometer

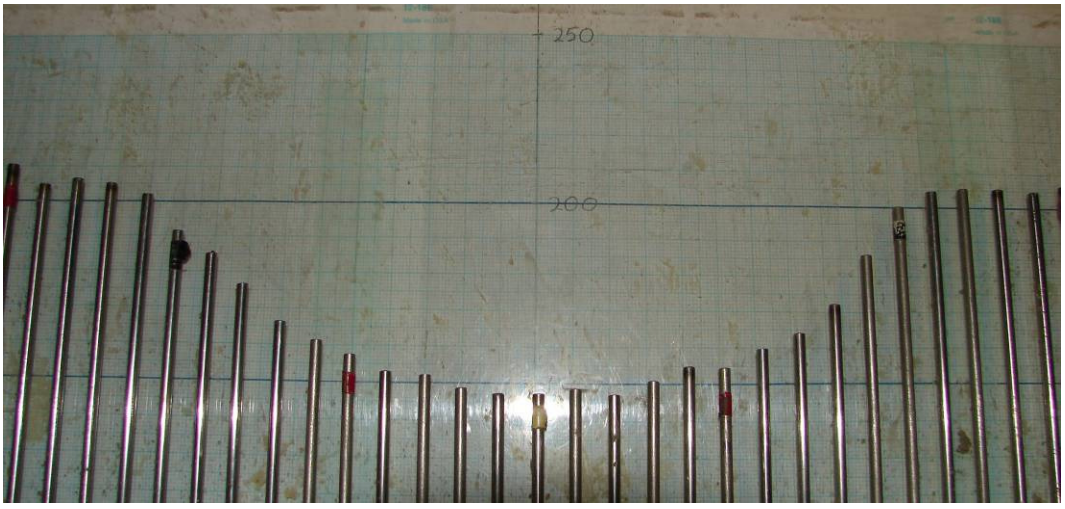

Figure 3.9: Recording Measurements from the Profilometer

Results were obtained for most, but not all, of the craters. The crater measurement results are discussed in Chapter 4.

Chapter 4: Specific Experimentation

The primary focus of this thesis is taking transient measurements with 3D DIC and developing an inverse hybrid method to determine the pressure experienced by a plate during the explosion by using finite element analysis. However, other useful results were obtained. The first is the final deformation analysis, obtained through use of a FARO measurement arm. This data was measured for nearly every test conducted, even if the 3D DIC data was not. The second set of useful results is the crater analysis, obtained by using the profilometer for all of the tests towards the end of the experimental program. The third set of specific experimentation results compare the movement of a semi-rigid nondeforming plate of comparable mass to the deformable plate and frame used for all the other experimentation.

4.1 Final Deformation Analysis

After the experiments were completed, final deformation measurements were taken for the plate. Data was obtained for the test conditions described in Table 4.1:

Description	DOB (in)	SOD (in)	Test Name
Surface Blast	0	1.22	DT 8
	0	1.22	DT 9
Shallow	0.3	1.22	USC 3
	0.3	1.22	USC 4
Mid-Depth	0.65	1.22	DT 10
Deep	1	1.22	USC 2
Deepest	1.22	1.22	DT 11
0" SOD	*1.22*	*0*	*DT 12*

Table 4.1: Experiments with Final Deformation Data

As discussed in the previous chapter, data was taken for each plate along two paths: one from left to right following the longer dimension of the plate, and another from

top to bottom (front to back) along the shorter dimension. For all of the plates, both paths produce approximately the same data near the center of the plate, but begin to deviate near the boundaries, as seen in Figure 4.1:

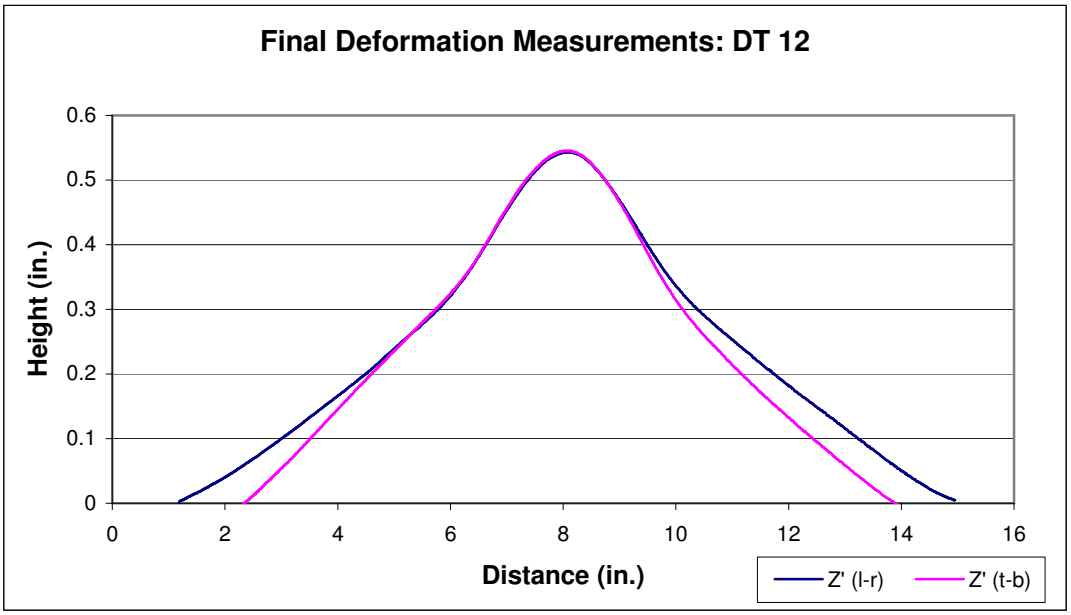

Figure 4.1: Comparison of Left-to-Right and Top-to-Bottom Measurement Path

After examining the permanent deformation experienced by the plates, it is reasonable to assume that they are approximately axisymmetric until the boundaries are approached. In Chapter 6 the FEM computer simulation is discussed, which uses an axisymmetric model. The 14" x 16" rectangular plate has therefore been modeled as a circular plate with a 7" radius. For these reasons, Faro data will only be reported along the shorter, 14" path, but not including the inch on each side used to bolt the plate to the frame.

4.1.1. Final Deformation: Surface Blast 0” DOB, 1.22” SOD (DT 8, DT9)

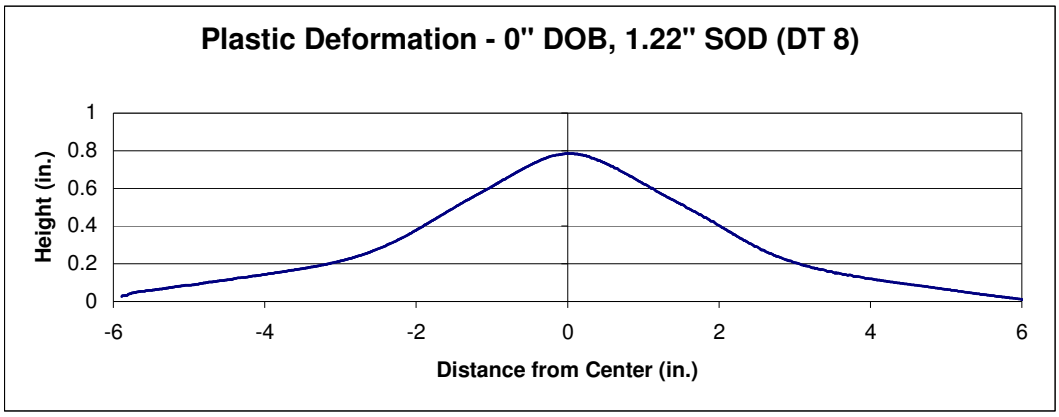

Figure 4.2: Final Deformation Profile – 0” DOB, 1.22” SOD

Maximum Deformation	Area under Curve (in^2)	Volume under Plate (in^3)
0.785 in	**3.66 in^2**	**18.77 in^3**

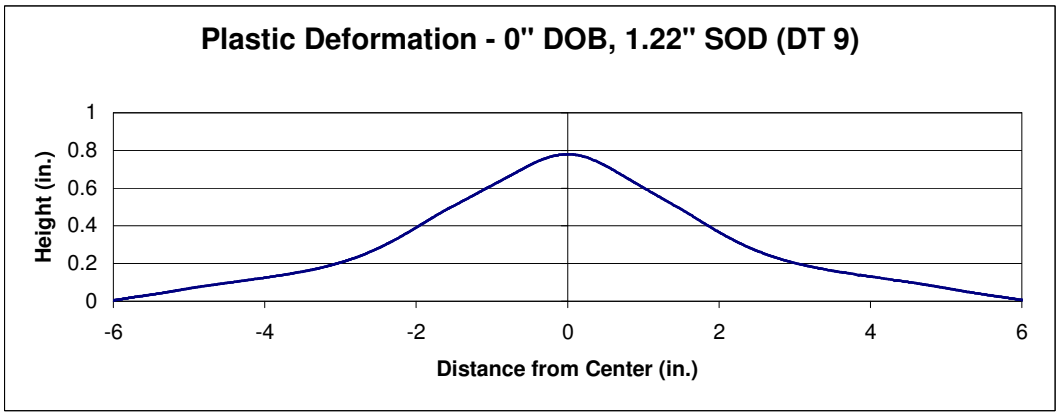

Figure 4.3: Final Deformation Profile – 0” DOB, 1.22” SOD

Maximum Deformation	Area under Curve (in^2)	Volume under Plate (in^3)
0.780 in	**3.57 in^2**	**18.46 in^3**

4.1.2. Final Deformation: Shallow 0.3” DOB, 1.22” SOD (USC 3, USC 4)

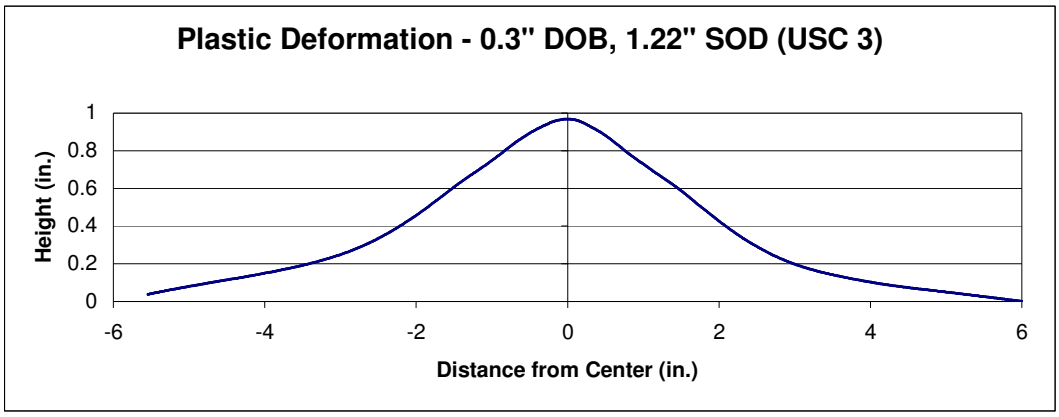

Figure 4.4: Final Deformation Profile – 0.3” DOB, 1.22” SOD

Maximum Deformation	Area under Curve (in^2)	Volume under Plate (in^3)
0.968 in	**4.17 in^2**	**18.59 in^3**

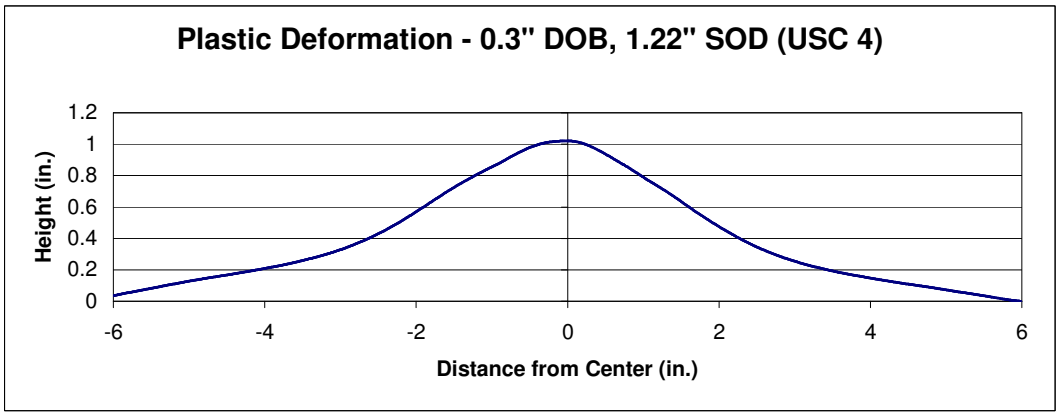

Figure 4.5: Final Deformation Profile – 0.3” DOB, 1.22” SOD

Maximum Deformation	Area under Curve (in^2)	Volume under Plate (in^3)
1.021 in	**4.89 in^2**	**22.48 in^3**

4.1.3. Final Deformation: Mid-Depth 0.65" DOB, 1.22" SOD (DT 10)

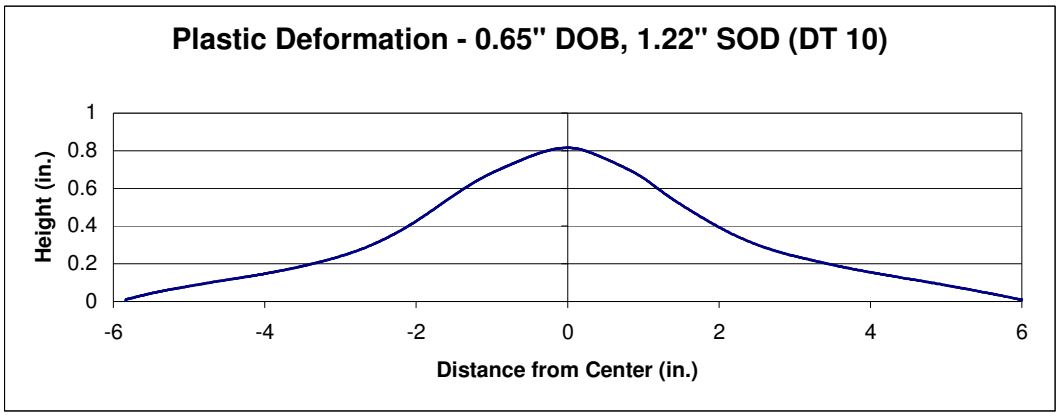

Figure 4.6: Final Deformation Profile – 0.65" DOB, 1.22" SOD

Maximum Deformation	Area under Curve (in^2)	Volume under Plate (in^3)
0.816 in	**3.91 in^2**	**21.03 in^3**

4.1.4. Final Deformation: Deep 1" DOB, 1.22" SOD (USC 2)

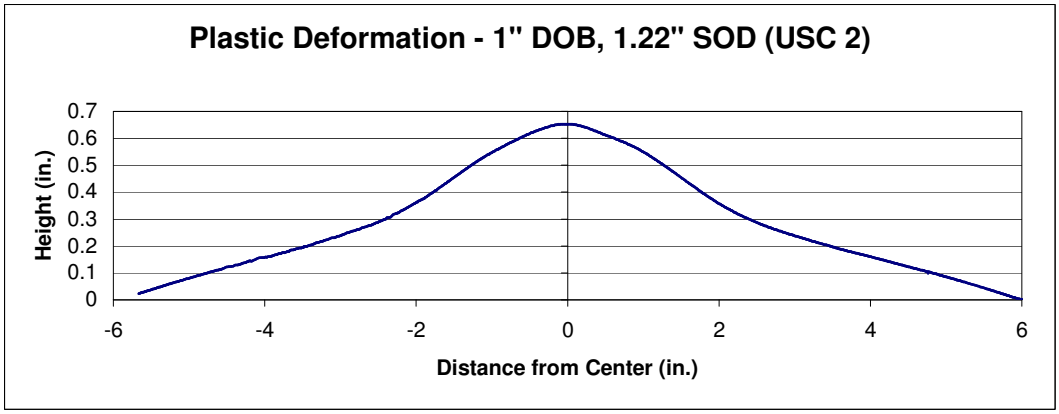

Figure 4.7: Final Deformation Profile – 1" DOB, 1.22" SOD

Maximum Deformation	Area under Curve (in^2)	Volume under Plate (in^3)
0.653 in	**3.37 in^2**	**19.76 in^3**

4.1.5. Final Deformation: Deepest 1.22” DOB, 1.22” SOD (DT 11)

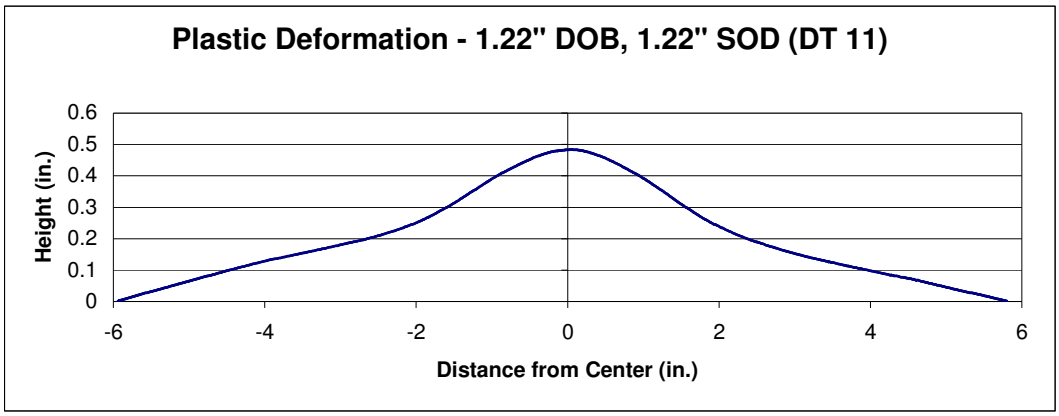

Figure 4.8: Final Deformation Profile – 1.22” DOB, 1.22” SOD

Maximum Deformation	Area under Curve (in^2)	Volume under Plate (in^3)
0.484 in	**2.43 in^2**	**12.55 in^3**

4.1.6. Final Deformation: Zero Standoff 1.22” DOB, 0” SOD (DT 12)

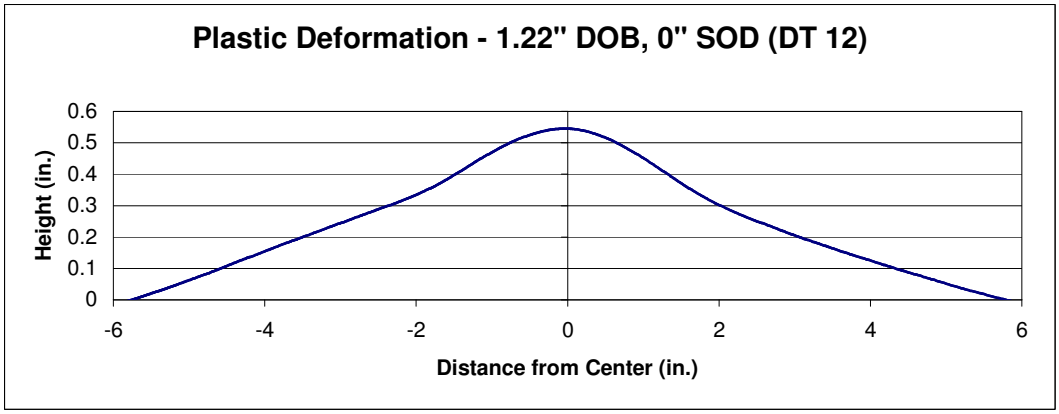

Figure 4.9: Final Deformation Profile – 1.22” DOB, 0” SOD

Maximum Deformation	Area under Curve (in^2)	Volume under Plate (in^3)
0.544 in	**3.00 in^2**	**15.45 in^3**

4.1.7. Comparison of Tests

A summary of the final deformation parameters is given in Table 4.2:

Description	Maximum deformation (in)	Area under curve (in^2)	Volume under plate (in^3)	DOB (in)	SOD (in)	Test Name
Surface Blast	0.785	3.66	18.77	0	1.22	DT 8
	0.780	3.57	18.46	0	1.22	DT 9
Shallow	0.968	4.17	18.59	0.3	1.22	USC 3
	1.021	4.89	22.48	0.3	1.22	USC 4
Mid-Depth	0.816	3.91	21.03	0.65	1.22	DT 10
Deep	0.653	3.37	19.76	1	1.22	USC 2
Deepest	0.484	2.43	12.55	1.22	1.22	DT 11
0" SOD	*0.545*	*3.00*	*15.45*	*1.22*	*0*	*DT 12*

Table 4.2: Final Deformation Values

The final deformation profiles from each test condition are plotted together in Figure 4.10:

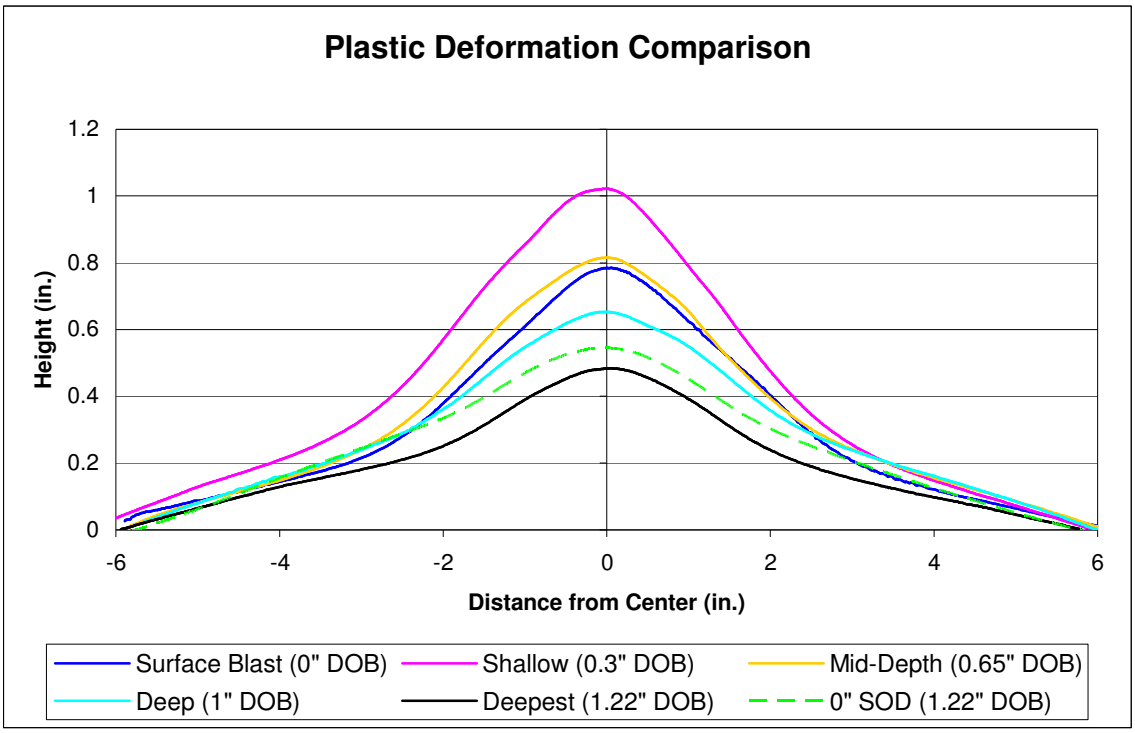

Figure 4.10: Comparison of Final Deformation Profiles

The peak final deformation values for each DOB have been plotted for all tests in which the standard 1.22” SOD was used, as shown in Figure 4.11:

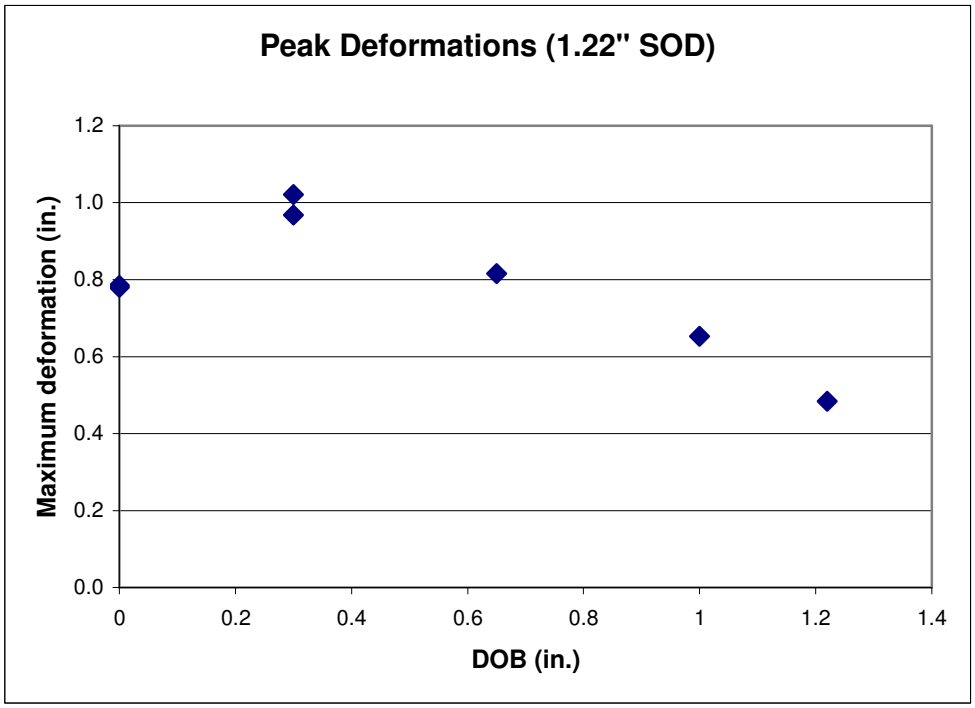

Figure 4.11: Comparison of Peak Deformation Values vs. DOB

This demonstrates that the amount of final deformation first increases as the charge is buried deeper, and then begins to drop off as the charge becomes further buried. The tests conducted with 0.3” DOB cause the largest final deformation. The same trend can be noticed in a plot of the area under the deformation curves, shown in Figure 4.12:

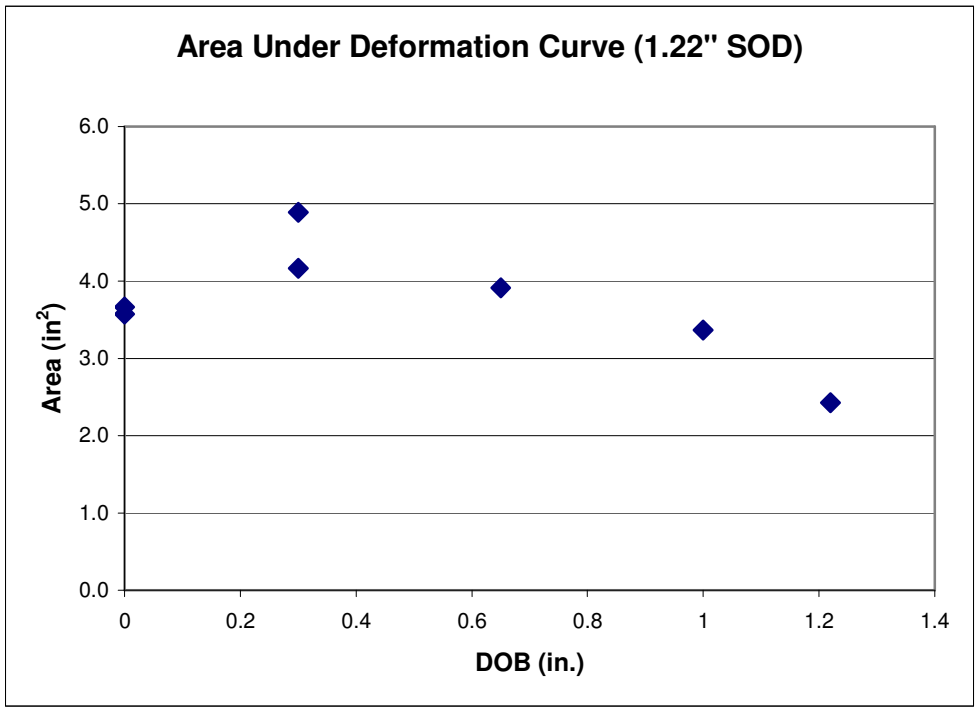

Figure 4.12: Comparison of Area Under the Deformation Curves vs. DOB

This similar trend is largely because the area under the curve is heavily influenced by the maximum deformation value. However, the shapes of these curves vary with the DOB, which affects the revolved volume of the curves, shown in Figure 4.13:

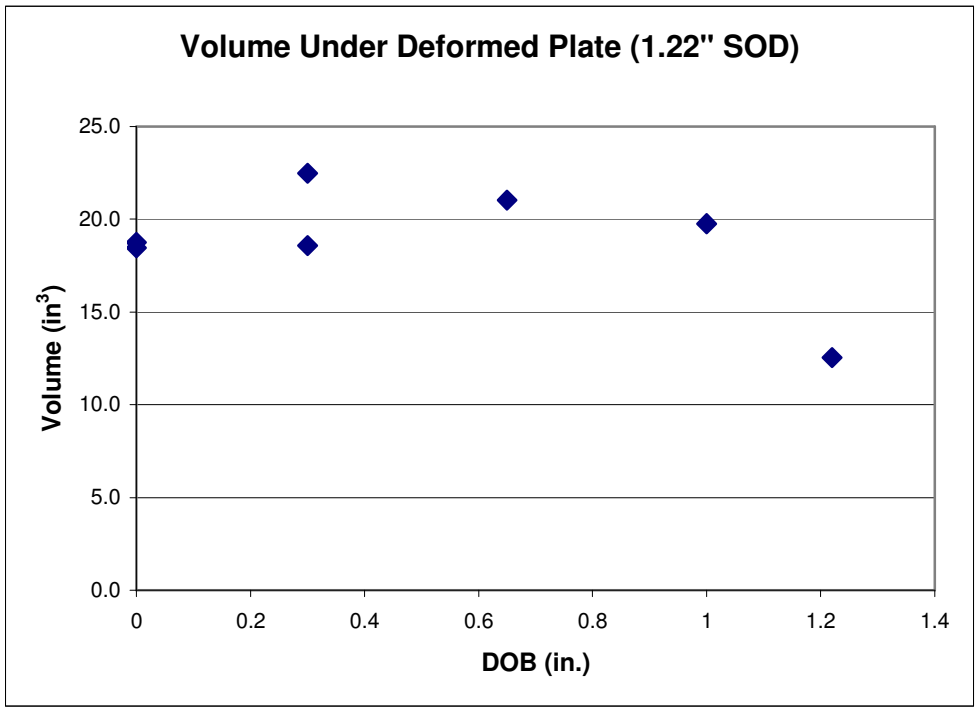

Figure 4.13: Comparison of Volume Under the Deformed Plates vs. DOB

These values suggest that while the DOB greatly influences the maximum deformation in one manner, the deformed volume is affected differently. This is also observable from the deformation plots; for 0" DOB it can be seen that the deformation has a higher peak than for 1.0" DOB but has less deformation farther from the center. Because of this, these two tests have similar values for area but quite different values for volume. This spreading-effect of the deformation can be seen in Figure 4.14, with the more localized deformation occurring for 0" DOB:

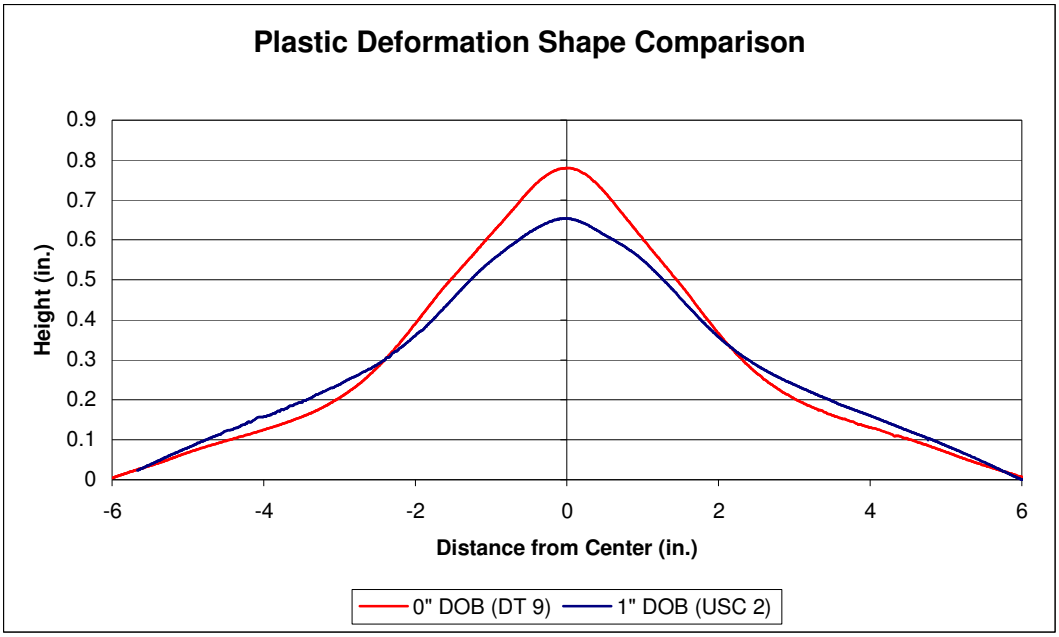

Figure 4.14: Degree of Deformation Localization for Deformed Plates

Thus far, the focus of this discussion has been restricted to the tests with a constant 1.22" SOD. However, a single test was conducted varying the SOD. Although extensive testing was not conducted with a varying SOD, there are still a few interesting findings. First of all it seems that the total distance between the charge and the plate matters less than what material occupies that area. In the original test setup with 1.22" total distance charge-to-plate (0" DOB and 1.22" SOD) there is about 0.783" of deformation, whereas for the test with the modified standoff distance (1.22" DOB and 0" SOD) there is only 0.545". This value falls in between the 1.22" SOD tests that have 1" DOB and 1.22" DOB (for a total distance of 2.22" to 2.44" charge-to-plate), suggesting that the final damage delivered is more sensitive to the material between the plate and charge than the total distance. This agrees with prior

research that determined that the damage is not caused by the charge alone, but primarily by the sand thrown by the charge.

4.2 Crater Analysis

After the first series of tests were conducted, it was realized that some insight may be gained through the use of crater measurements. Although it is by no means a primary focus of this research, the measurements were easily obtained without having to conduct additional tests. Crater profile data was obtained for the test conditions described in Table 4.3:

Description	DOB (in)	SOD (in)	Test Name
Surface Blast	0	1.22	DT 8
	0	1.22	DT 9
	0	1.22	DT 13
Shallow			
Mid-Depth	0.65	1.22	DT 7
	0.65	1.22	DT 10
Deep	1	1.22	DT 5
Rigid plate	*1*	*1.22*	*DT 6*
Deepest	1.22	1.22	DT 11
0" SOD	1.22	0	DT 12

Table 4.3: Experiments with Crater Profile Data

Immediately after the test, the water was drained from the tank. Measurements were taken using a profilometer once the water level was below the crater, as described in Chapter 3. These results were shown in Figure 4.15 through Figure 4.20:

4.2.1. Crater Measurements: Surface Blast 0” DOB, 1.22” SOD (DT 8, 9, 13)

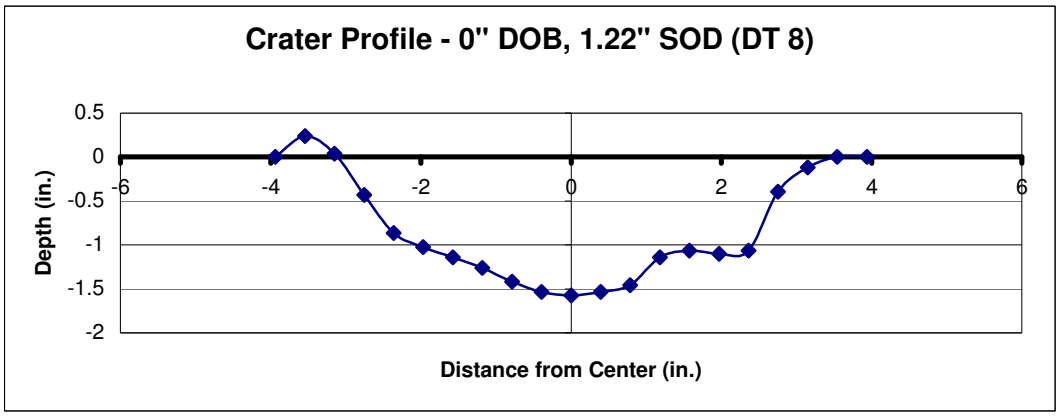

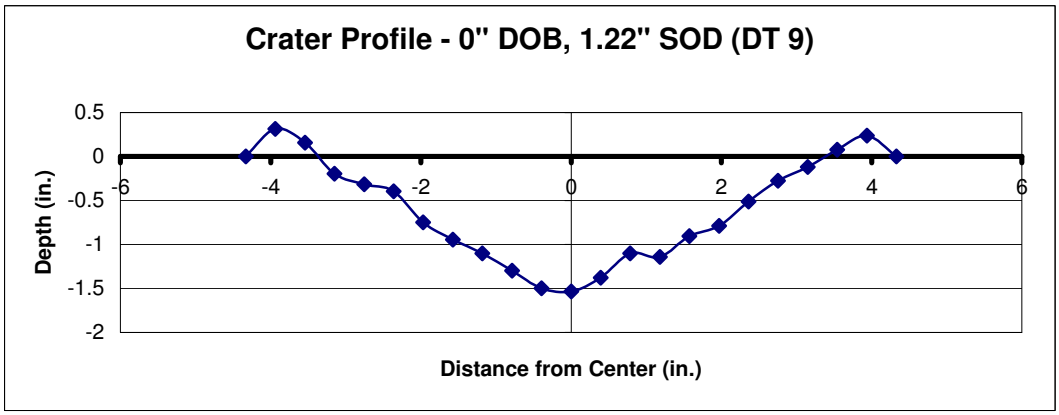

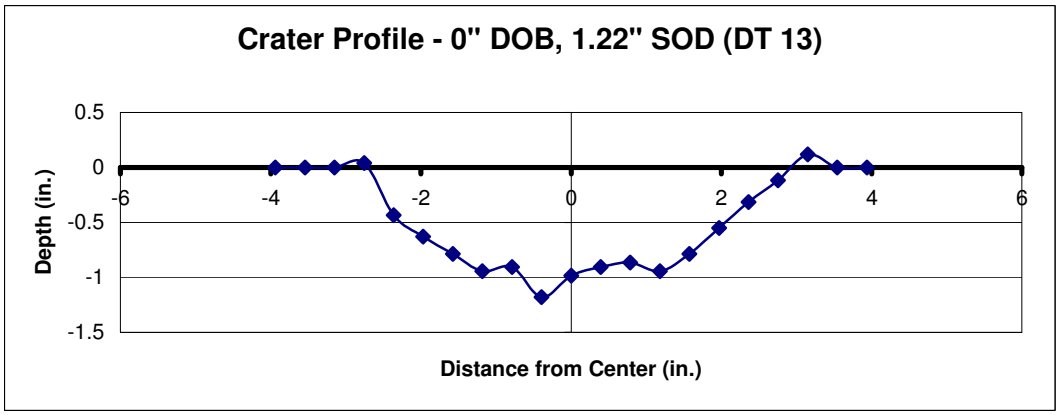

Figure 4.15: Crater Profiles – 0” DOB, 1.22” SOD

Maximum Depth	Profile Area (in^2)	Crater Volume (in^3)
1.6 in	**6.7 in^2**	**27.0 in^3**
1.5 in	**5.6 in^2**	**20.1 in^3**
1.2 in	**4.0 in^2**	**14.0 in^3**

4.2.2. Crater Measurements: Mid-Depth 0.65” DOB, 1.22” SOD (DT 7, 10)

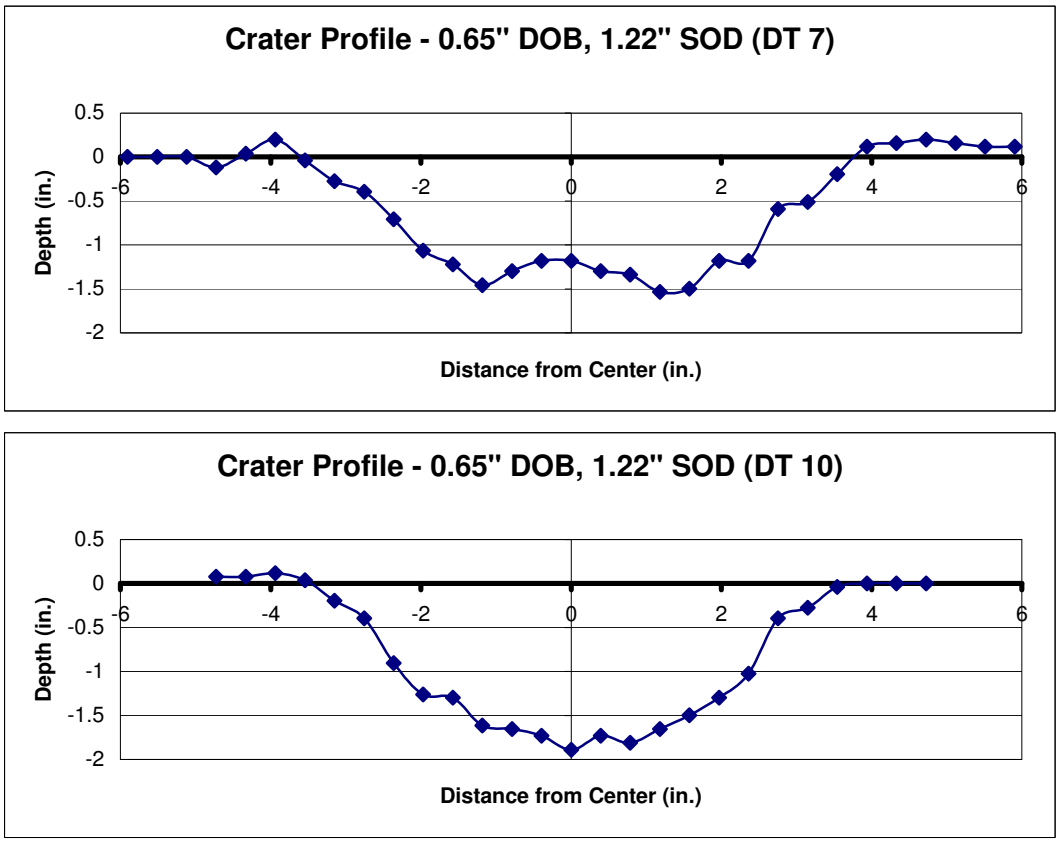

Figure 4.16: Crater Profiles – 0.65” DOB, 1.22” SOD

Maximum Depth	Profile Area (in^2)	Crater Volume (in^3)
1.5 in	**7.1 in^2**	**31.8 in^3**
1.9 in	**8.1 in^2**	**32.2 in^3**

4.2.3. Crater Measurements: Deep 1” DOB, 1.22” SOD (DT 5)

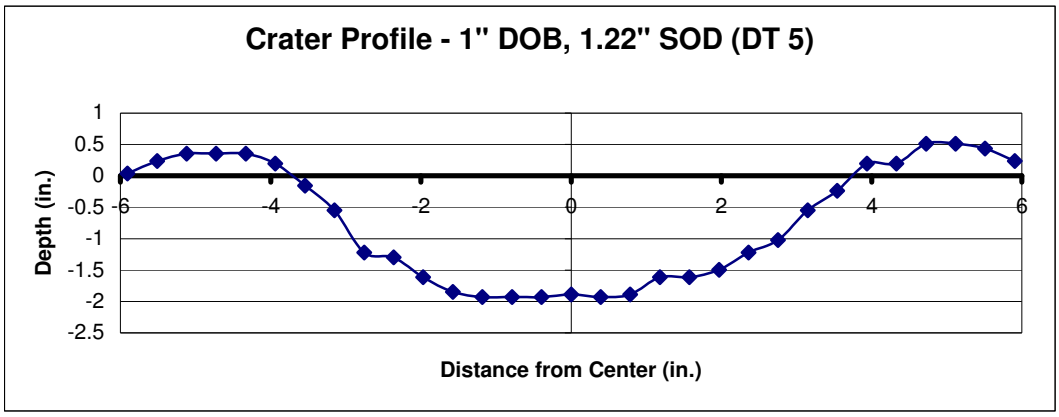

Figure 4.17: Crater Profile – 1” DOB, 1.22” SOD

Maximum Depth	Profile Area (in^2)	Crater Volume (in^3)
1.9 in	**10.1 in^2**	**45.8 in^3**

4.2.4. Crater Measurements: Rigid Plate, Deep 1” DOB, 1.22” SOD (DT 6)

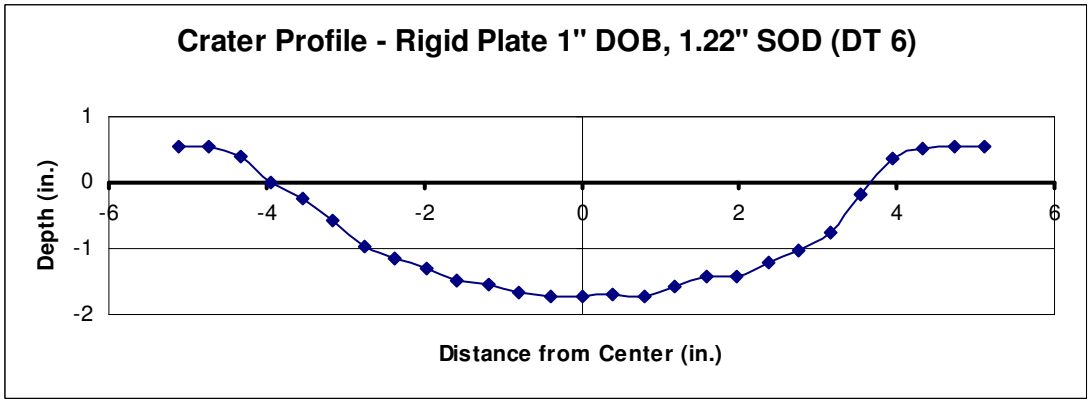

Figure 4.18: Crater Profile – Rigid Plate, 1” DOB, 1.22” SOD

Maximum Depth	Profile Area (in^2)	Crater Volume (in^3)
1.7 in	**9.2 in^2**	**42.6 in^3**

4.2.5. Crater Measurements: Deepest 1.22” DOB, 1.22” SOD (DT 11)

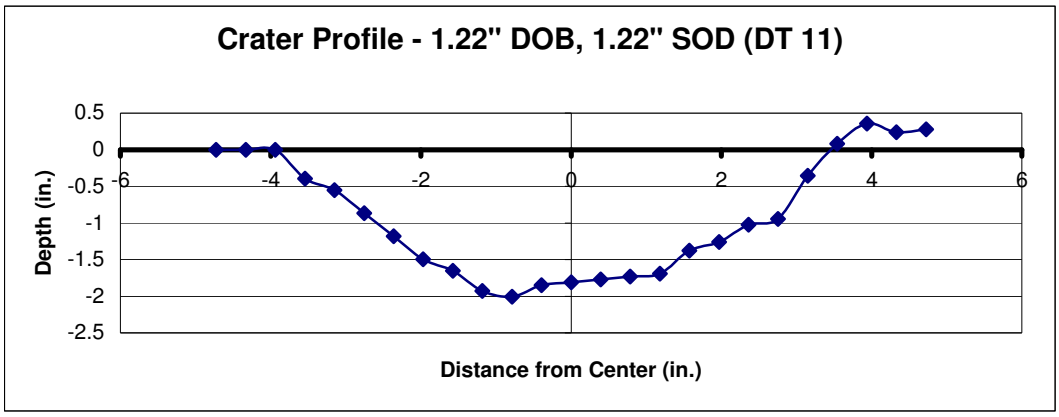

Figure 4.19: Crater Profile – 1.22” DOB, 1.22” SOD

Maximum Depth	Profile Area (in^2)	Crater Volume (in^3)
2.0 in	**9.4 in^2**	**41.5 in^3**

4.2.6. Crater Measurements: Zero Standoff 1.22” DOB, 0” SOD (DT 12)

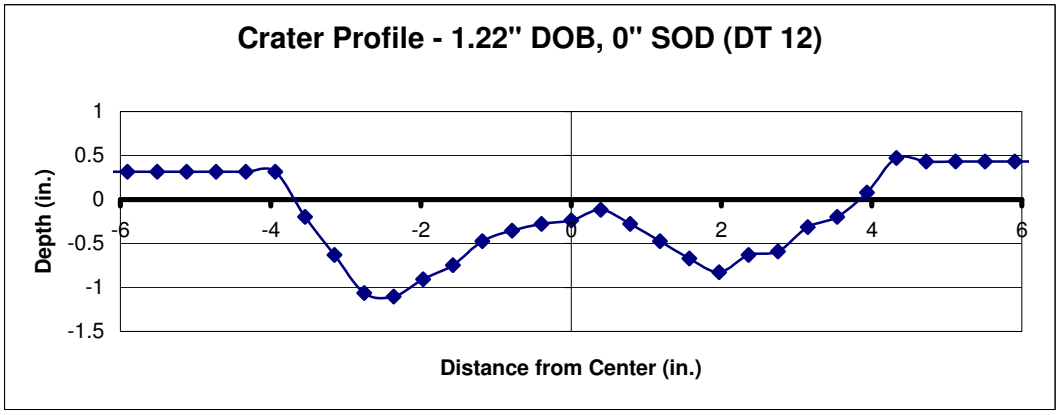

Figure 4.20: Crater Profile – 1.22” DOB, 0” SOD

Maximum Depth	Profile Area (in^2)	Crater Volume (in^3)
1.1 in	**3.9 in^2**	**24.7 in^3**

4.2.7. Comparison of Tests

A summary of the measured crater values is given in Table 4.4:

Description	Maximum Depth (in)	Profile Area (in^2)	Crater Volume (in^3)	DOB (in)	SOD (in)	Test Name
Surface Blast	1.6	6.7	27.0	0	1.22	DT 8
	1.5	5.6	20.1	0	1.22	DT 9
	1.2	4.0	14.0	0	1.22	DT 13
Shallow						
Mid-Depth	1.5	7.1	31.8	0.65	1.22	DT 7
	1.9	8.1	32.2	0.65	1.22	DT 10
Deep	1.9	10.1	45.8	1	1.22	DT 5
Rigid plate	1.7	9.2	42.6	*1*	*1.22*	*DT 6*
Deepest	2.0	9.4	41.5	1.22	1.22	DT 11
0" SOD	1.1	3.9	24.7	1.22	0	DT 12

Table 4.4: Crater Measurement Values

The values of the deepest portion of the crater for each DOB have been plotted for all tests in which the standard 1.22" SOD was used, as shown in Figure 4.21:

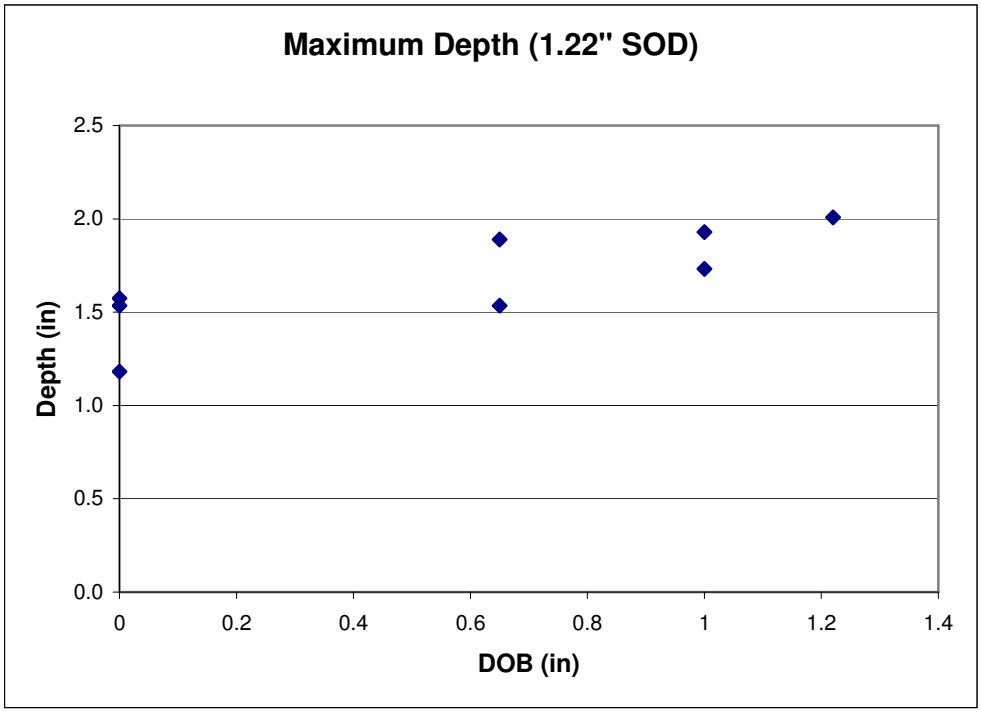

Figure 4.21: Comparison of Maximum Crater Depths vs. DOB

As expected, the depth of the crater increases as the charge is buried deeper. Although the crater depth seems to increase with charge depth, it does not increase at the same rate. For instance, when the depth of the charge is increased from 0.65” to 1.22”, the maximum depth of the crater only increases by about 0.3”. Also, as the depth of charge burial increases, the area of the crater profile and the calculated volume of the crater actually begin to decrease after 1”, as seen in Figure 4.22 and Figure 4.23:

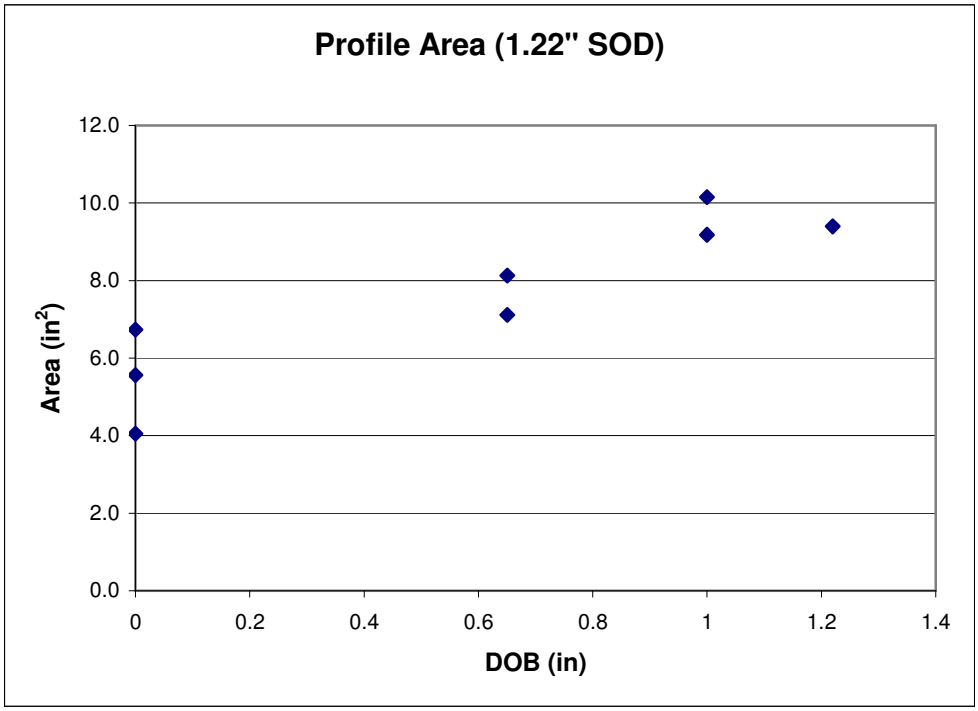

Figure 4.22: Comparison of Crater Profile Area vs. DOB

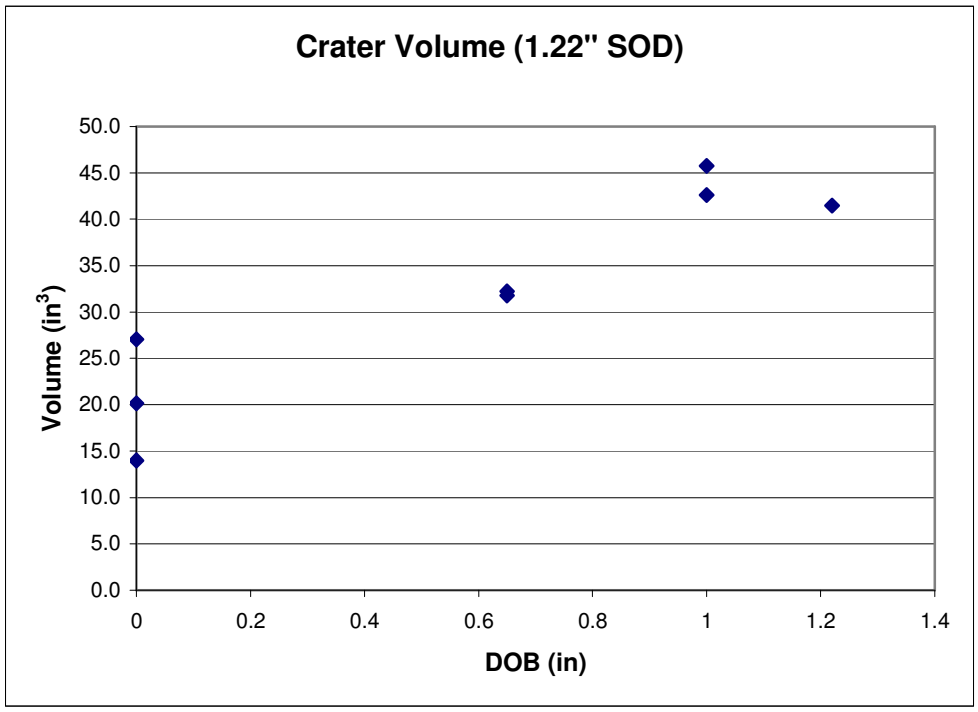

Figure 4.23: Comparison of Crater Volume vs. DOB

This trend is not surprising; a charge buried at very large depths would not break the surface of the sand and would create no crater.

4.2.8. Craters vs. Final Deformation

For most test conditions there are data from the crater profile as well as the final deformation. The resulting measurements have been plotted together for each of these conditions, and the averages of the height/depth, profile area, and volume have been shown for comparison.

4.2.9. Crater vs. Final Deformation: Surface Blast 0" DOB, 1.22" SOD

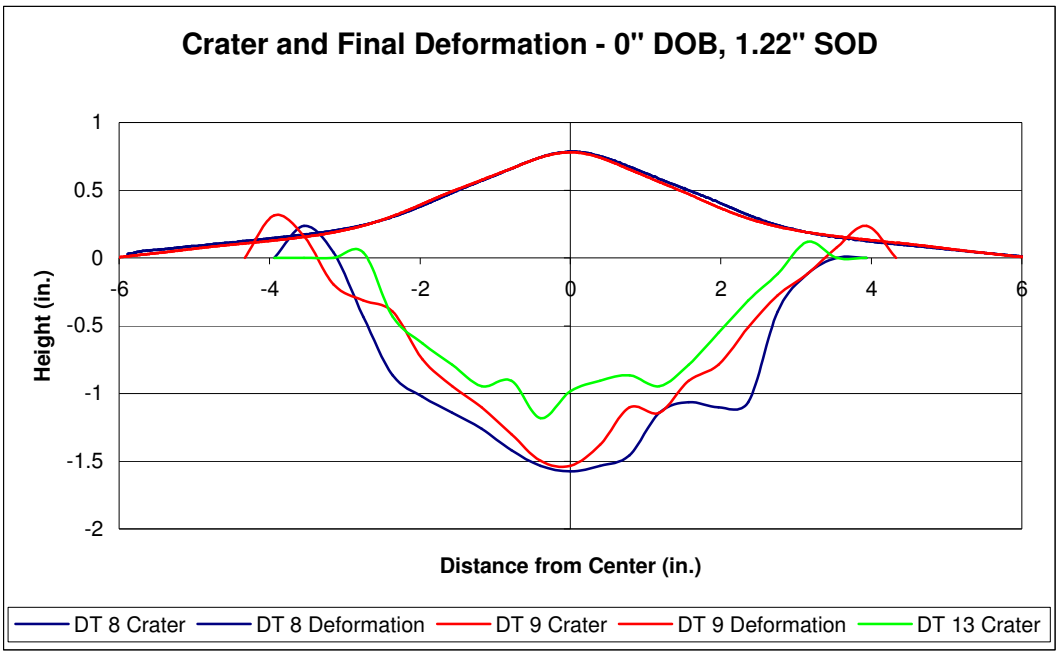

Figure 4.24: Crater and Final Deformation Profiles – 0" DOB, 1.22" SOD

	Deformation	Area (in^2)	Volume (in^3)
Crater	**1.4 in**	**5.4 in^2**	**20.4 in^3**
Plate	**0.783 in**	**3.62 in^2**	**18.62 in^3**

The surface blast setup has the most data of all the test conditions. Initial observation shows that while the final deformations take on very similar values, there is much more variability with the crater measurements. The measurement technique for final deformation was much more precise than the technique for crater deformation, however this does not account for the variation. It seems as if the crater is much more sensitive to slight variations in the blast pressures, whereas there is a type of averaging effect with the plate's deformation. It has been noticed that the blast pressure profiles have dramatic peaks, often referred to as "fingers" due to the way they look under high-speed imaging. This could be why the crater often appears jagged, but the plate's deformation seems to be smooth. Although the sand projected by the blast does not always appear to be axisymmetric, the final deformation measurements all show a high degree of axisymmetry near the center, away from the rectangular boundary.

It is also notable that in the region 3" to 6" from the center of the plate the deformation can be approximated as a straight line. For this test condition the crater has an approximately 3" radius. This is discussed in the crater vs. final deformation summary section.

4.2.10. Crater vs. Final Deformation: Mid-Depth 0.65” DOB, 1.22” SOD

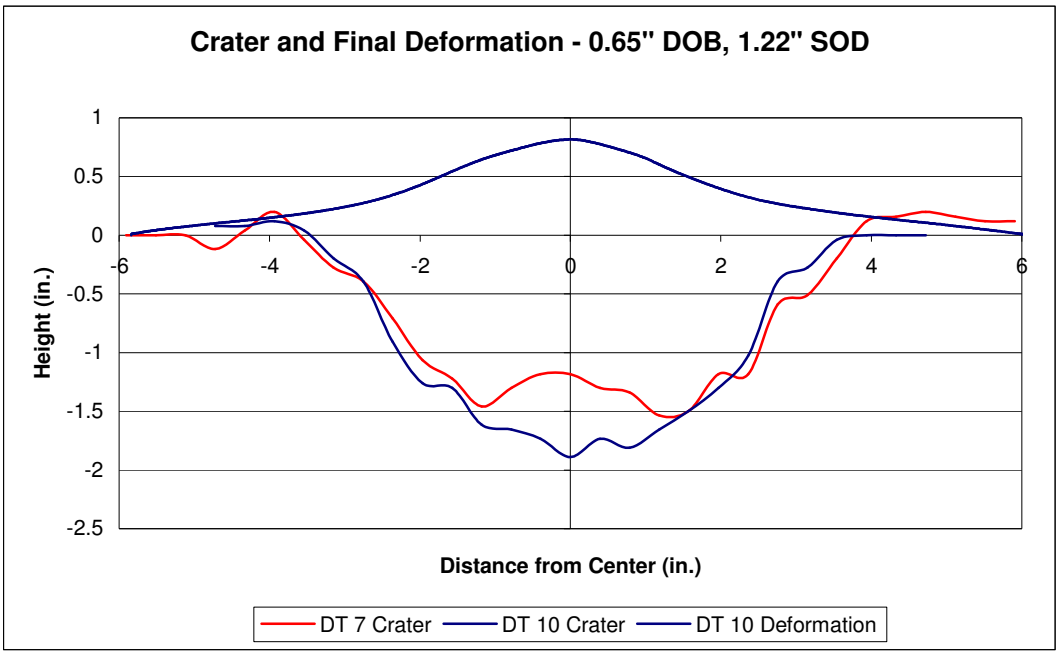

Figure 4.25: Crater and Final Deformation Profiles – 0.65” DOB, 1.22” SOD

	Deformation	Area (in^2)	Volume (in^3)
Crater	**1.7 in**	**7.6 in^2**	**32.0 in^3**
Plate	**0.816 in**	**3.91 in^2**	**21.03 in^3**

No crater data was obtained for the shallow depth of burial, so it cannot be compared to the final deformation for that test setup. However, data was obtained for the mid-depth setup, and is presented above.

4.2.11. Crater vs. Final Deformation: Deep 1” DOB, 1.22” SOD

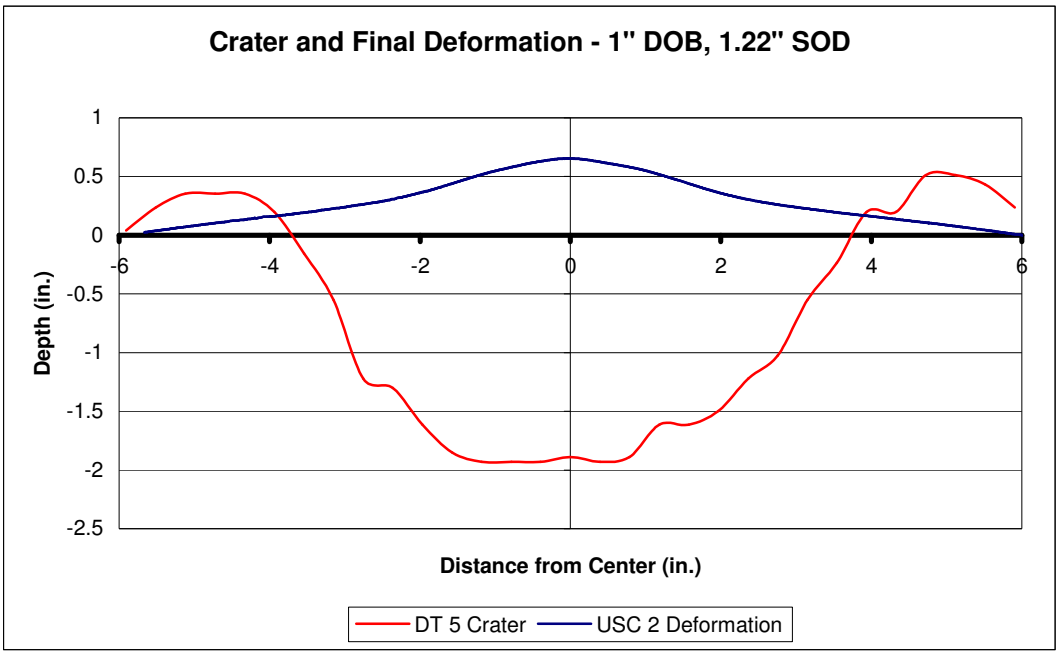

Figure 4.26: Crater and Final Deformation Profiles – 1” DOB, 1.22” SOD

	Deformation	Area (in^2)	Volume (in^3)
Crater	**1.9 in**	**10.1 in^2**	**45.8 in^3**
Plate	**0.653 in**	**3.37 in^2**	**19.76 in^3**

4.2.12. Crater vs. Final Deformation: Deepest 1.22” DOB, 1.22” SOD

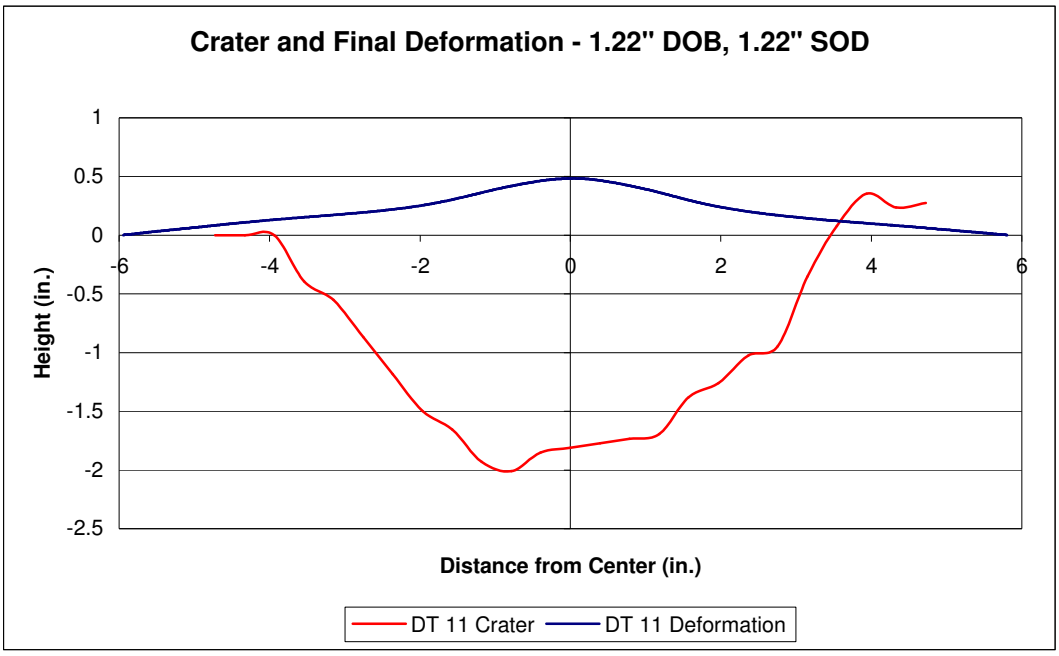

Figure 4.27: Crater and Final Deformation Profiles – 1.22” DOB, 1.22” SOD

	Deformation	Area (in^2)	Volume (in^3)
Crater	**2.0 in**	**9.4 in^2**	**41.5 in^3**
Plate	**0.484 in**	**2.43 in^2**	**12.55 in^3**

4.2.13. Crater vs. Final Deformation: Zero Standoff 1.22” DOB, 0” SOD

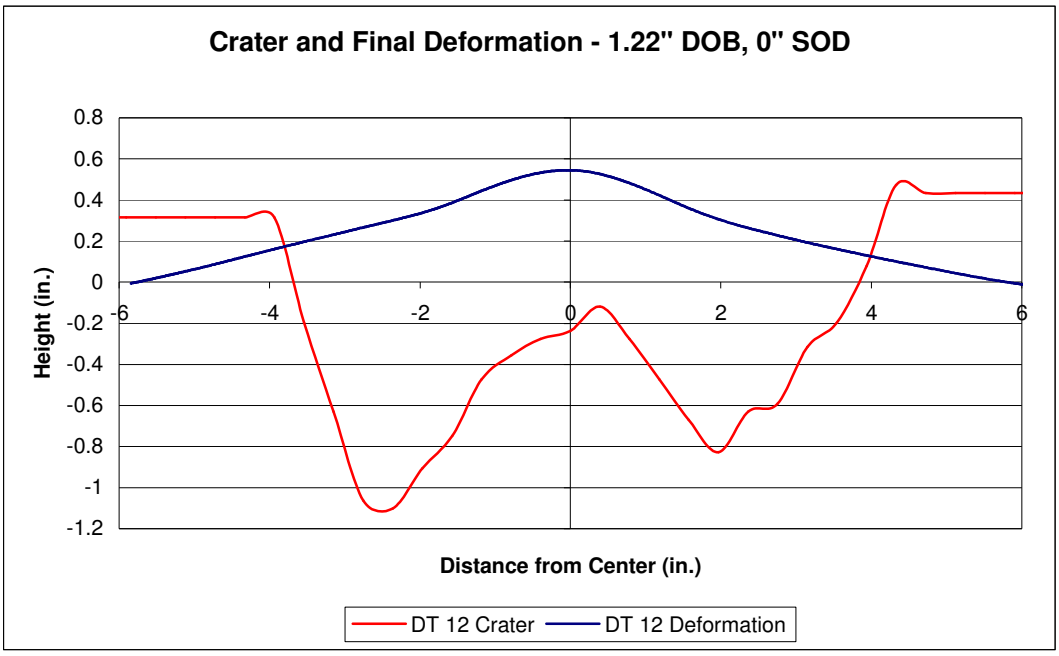

Figure 4.28: Crater and Final Deformation Profiles – 1.22” DOB, 0” SOD

	Deformation	Area (in^2)	Volume (in^3)
Crater	**1.1 in**	**3.9 in^2**	**24.7 in^3**
Plate	**0.545 in**	**3.00 in^2**	**15.45 in^3**

Unlike the tests with 1.22” of standoff distance, the plate was sitting directly on the sand’s surface. This caused a much different crater shape, with the deepest point not at the center of the crater. The blast appears to have caused deformation that becomes linear after approximately 2” from the center. It is also at this location that the crater appears the deepest. Since the center of the crater is much shallower than the charge burial depth, it is possible that the sand was propelled upward by the blast and reflected off of the plate, settling back into the crater.

4.2.14. Crater vs. Final Deformation Summary

Some observations can be made after examining the combined crater-deformation plots. Starting from the boundary, the slope of the plate appears to be linear until the edge of the crater is reached. It is at this point that the plate becomes curved. This was observed for several test conditions as discussed above. It possibly indicates that the deformation is caused by the pressure in the region of the plate above the crater, creating a curvature to the center region but dragging the rest of the plate along with it. It is reasonable to hypothesize that the outer deformation is caused by forces transmitted through the plate from this region. A numerical comparison of the resulting measurements is given in Table 4.5:

	Maximum Height/Depth (in)		Area (in^2)		Volume (in^3)	
Description	Plate	Crater	Plate	Crater	Plate	Crater
Surface Blast	0.783	1.4	3.62	5.4	18.62	20.4
Mid-Depth	0.816	1.7	3.91	7.6	21.03	32.0
Deep	0.653	1.9	3.37	10.1	19.76	45.8
Deepest	0.484	2.0	2.43	9.4	12.55	41.5
0" SOD	0.545	1.1	3.00	3.9	15.45	24.7

Table 4.5: Final Deformation vs. Crater

In order to uncover any possible correlation, the plate and crater measurements were plotted against each other as shown in Figure 4.29, Figure 4.30, and Figure 4.31. The blue diamonds represent tests for which the SOD was 1.22”, whereas the red is for the test with 0” SOD.

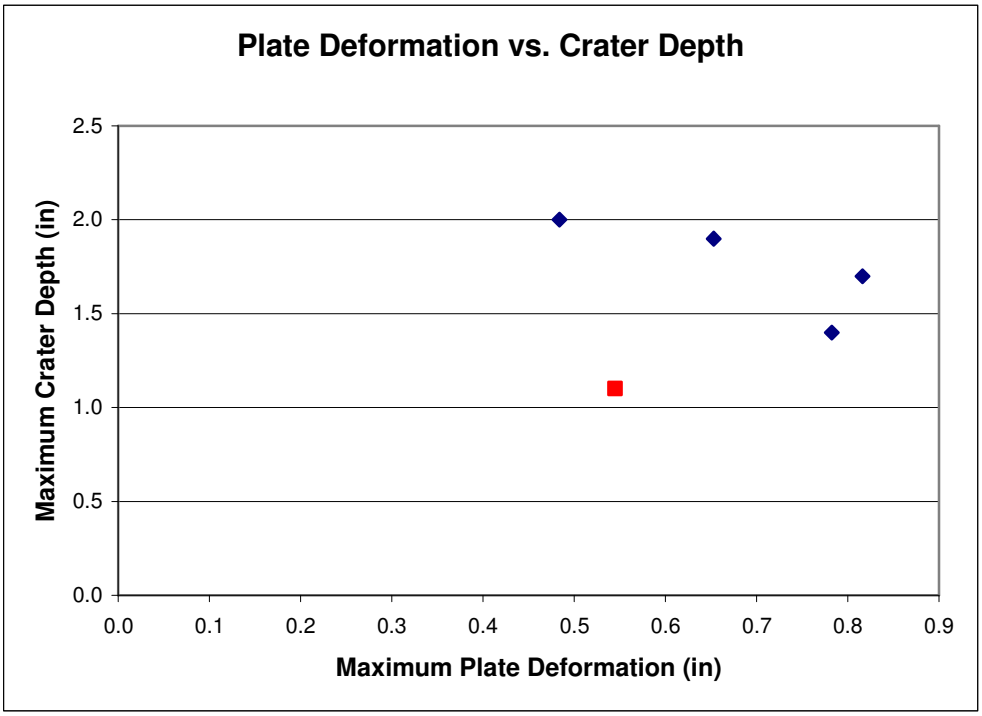

Figure 4.29: Comparison of Maximum Crater Depth and Plate Deformation

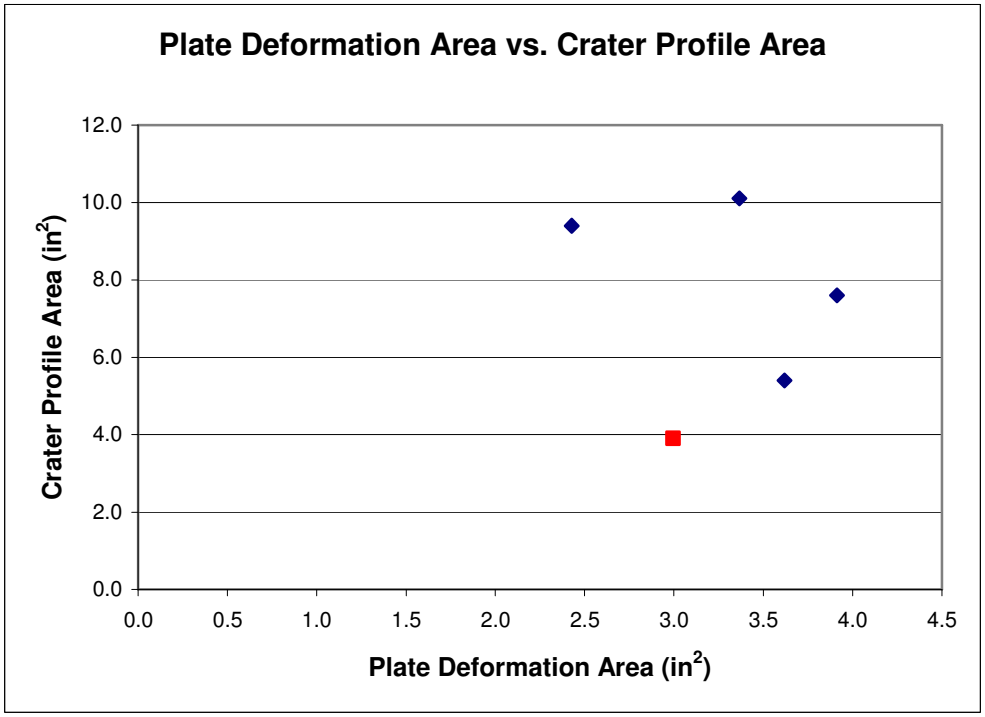

Figure 4.30: Comparison of Crater Profile Area and Plate Deformation Area

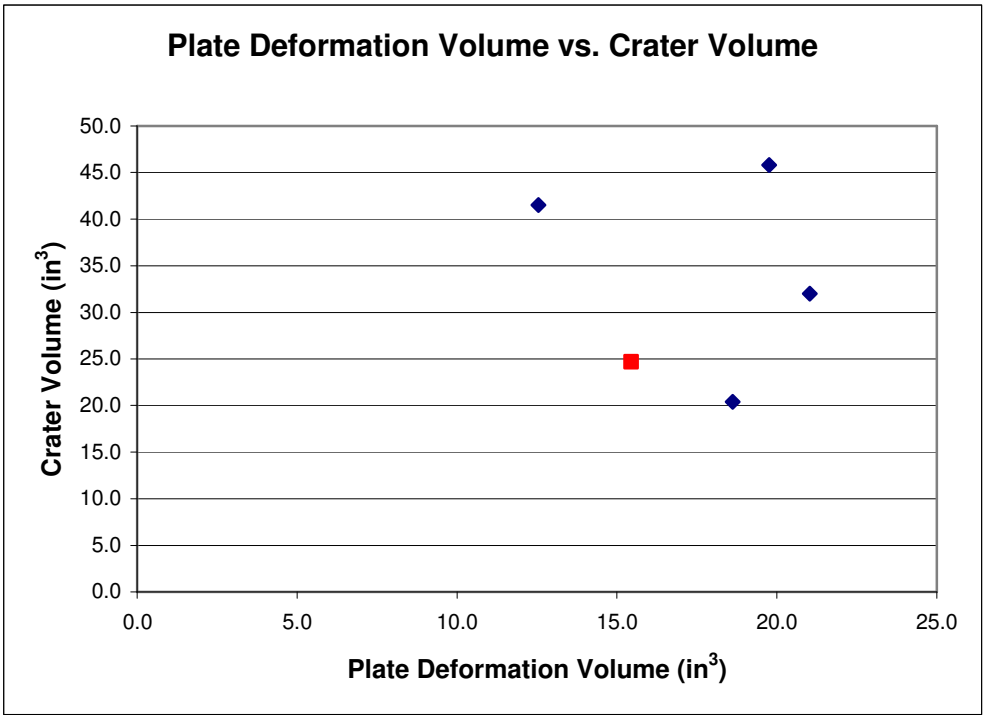

Figure 4.31: Comparison of Crater Volume and Plate Deformation Volume

There does not appear to be any strong relationship between the plate and crater values. However, by holding the SOD constant (and ignoring the red data point) some general trends begin to emerge. If the plate experiences a high maximum deformation, the crater depth tends to be lower. From Figure 4.29 this even appears to be a linear relationship. However, it is unlikely that these variables directly affect each other; it is more probably that the depth of burial is affecting both.

4.3 Rigid Plate vs. Deformable

Throughout the research process one aspect of interest was how the velocity and acceleration of the plate is affected by the deformation it is undergoing. It was hypothesized that since a portion of the charge's energy is going towards deforming the plate there would be less rigid body motion for the plate and frame rig. A pair of

tests was designed to test this hypothesis. The first consisted of an experiment with the same deformable plate as in all the other experimentation, with a DOB of 1" and a SOD of 1.22". The plate, frame, and hardware have a combined mass of 4673 grams. The second test was conducted with the same explosive parameters but using a ½" thick plate with the same 16" x 14" area as the deformable plate. The semi-rigid plate is also made of 6061 T6 aluminum with a density of 2.7 g/cc, and has a mass of 5074 grams (about 8% heavier than the deformable setup). The thick plate is shown in Figure 4.32 in position for the test, with the corners and center marked for easy identification:

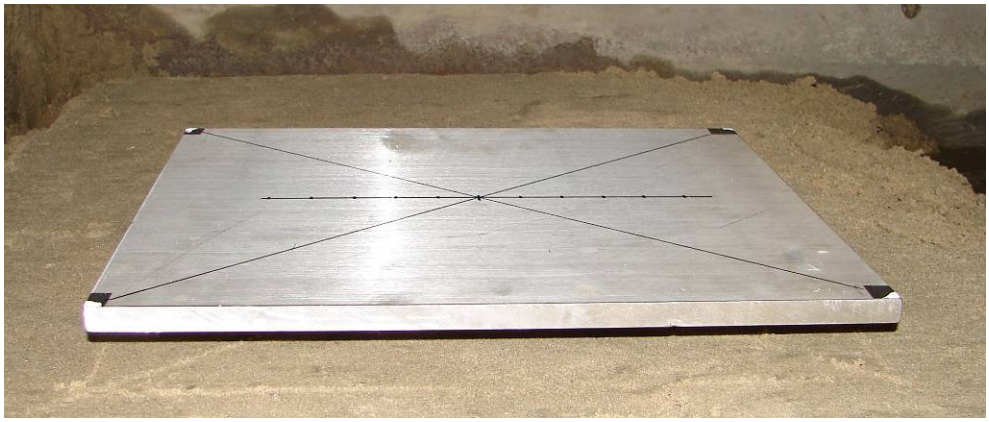

Figure 4.32: Semi-Rigid Plate

Although the plate flexed elastically during the test, there was no visible permanent deformation. These tests were conducted with the use of the Phantom 7 high speed camera system, and the video files were analyzed using the Phantom software.

4.3.1. Phantom Software Analysis Procedure

The Phantom Camera Control software was used to manually track each point of interest, as opposed to the 3D Digital Image Correlation techniques used for all the other tests. 3D DIC is discussed in depth in Chapter 5, but there are some major

differences between these methods that must be noted. Unlike 3D DIC, manual tracking requires the deformation to be approximately planar, and the camera to be set up normal to this plane. Any deviation from the plane of deformation will record less deformation than is actually occurring. However, if this setup is not possible small deviations can be accounted for if the angle is measured. The test plate is set up parallel to the sand surface, which is leveled since uniform water saturation is desired. For this reason the camera can be easily positioned so that only the angle from the horizontal position needs to be measured. This can be accomplished in a number of ways. High accuracy was not required and a digital inclinometer was not available, so a photograph was taken of the Phantom camera relative to the horizontal position, as shown in Figure 4.33. The angle was then measured using Photoshop, and compensated for in the spreadsheet calculations. The advantages of the manual tracking method are that it only requires one camera, takes much less time to set up and run, requires no expensive software, and can be analyzed quickly. However, data is only available for a few points as opposed to across the entire plate's surface, and values for strain are unobtainable. The Phantom Camera Control software graphical user interface is shown in Figure 4.34.

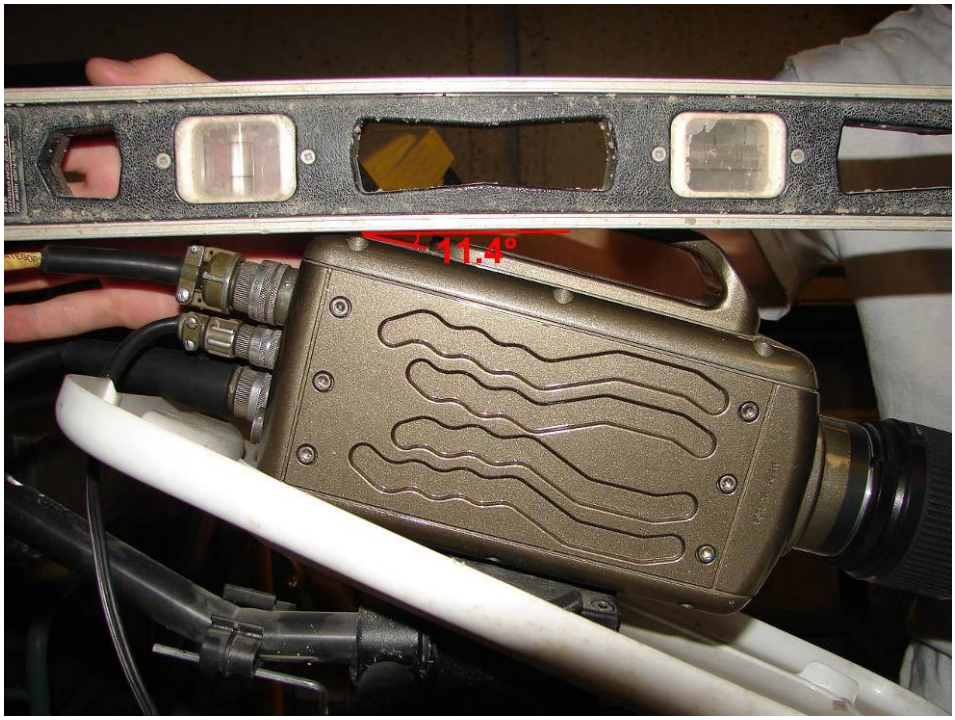

Figure 4.33: Camera Angle Measurement

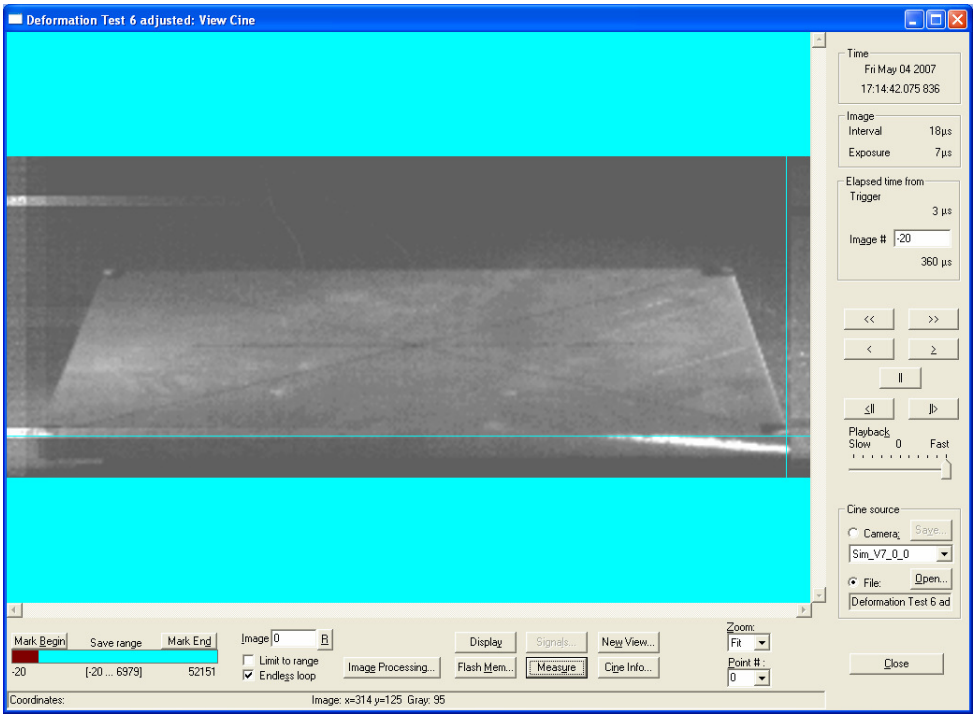

Figure 4.34: Phantom Camera Control Software Graphical User Interface

The Phantom software allows the user to track a data point by manually locating the point in each desired frame. For this series of tests (deformable vs. rigid) the four corners were tracked, as well as the center point. By clicking on the Measure button the unit system can be selected. The reference distance can be input by first choosing the Scaling option (also under Measure) and entering the gauge length, which is a known distance between any two points on the plate at any frame in time, and then clicking once on each of these points. A new report file can be opened from within the Measure button, and then the origin can be selected. It is easiest to set the origin at the initial location of the point being tracked. The coordinates of the point at each frame is reported by clicking once on the point. After advancing to the next frame, the point's new coordinates can be reported by clicking on its new location. The report file contains the time of each frame so it is permissible to skip frames if there is no visible movement of the point of interest, but the analysis will be easiest if the same amount of frames are skipped between images for each report file. Once data has been taken to an adequate time the report file should be closed. The process is then repeated from the beginning frame for the next point of interest.

At this point there will be a different report file for each point, with a .rep extension. These are simply text files, and can be opened in Excel using the Text Import Wizard and defining the cell spacing through use of the fixed width option. The files can then be combined into an .xls file, which allows for data plotting and analysis.

4.3.2. Rigid vs. Deformable Data Analysis

Ideally the camera's line of sight would be normal to the plane of deformation so the amount of deformation could be directly read from the images. However, due to limitations with the sides of the sand box this is not possible, so before plotting the data the camera angle compensation must be determined. The geometry is shown in Figure 4.35 with the plate shown with two different amounts of deformation. For this example the blue point is the reference state of deformation, the green point is the new location of the center, and the red point is where the camera records the point. The blue line segment B representing the amount of deformation measured by the camera, and the red line segment A representing the actual amount of deformation.

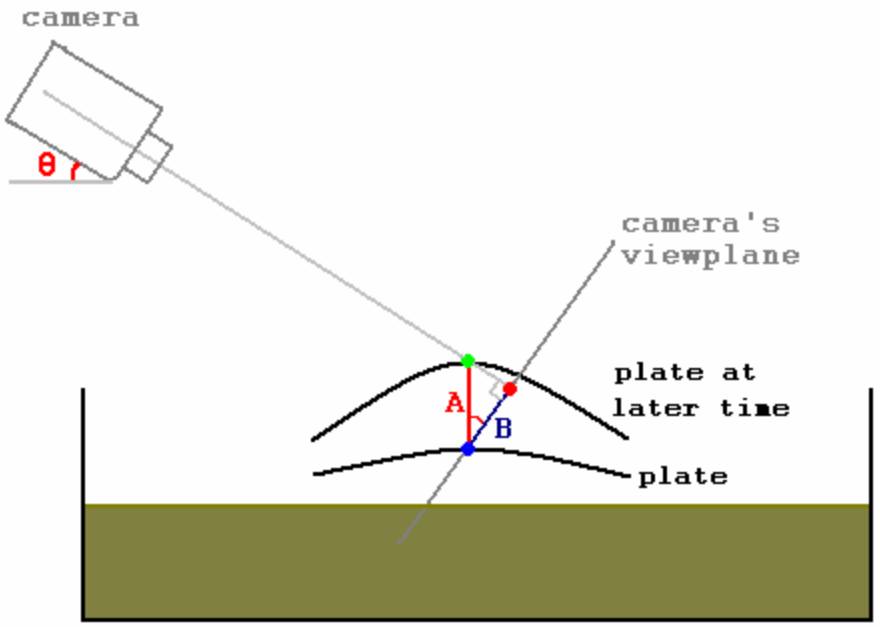

Figure 4.35: Camera Angle Geometry

By constructing a right triangle the actual amount of deformation can be calculated using simple trigonometry:

$$A = \frac{B}{\cos(\theta)}$$

A quick check shows that if the camera angle θ is 0 then the images contain the actual deformation and no compensation is necessary. As the camera angle increases, the compensation gets much larger, but the amount of time that data can be obtained is longer. This is because the point of interest will be moving a shorter distance through the camera's field of view. However, this also means that the data will be less accurate, and can be severely limited by the resolution. Also, as the camera angle approaches 90° it will appear as if the point is not moving at all since the deformation action will be occurring directly towards the camera.

At this point a spreadsheet can be compiled with all displacement values for each tracked point, along with the corresponding times. The data can then be plotted after dividing all these values by the cosine of the camera angle.

Semi-Rigid Plate

For the semi-rigid plate all four corners were tracked as well as the center point. This data is presented in Figure 4.36:

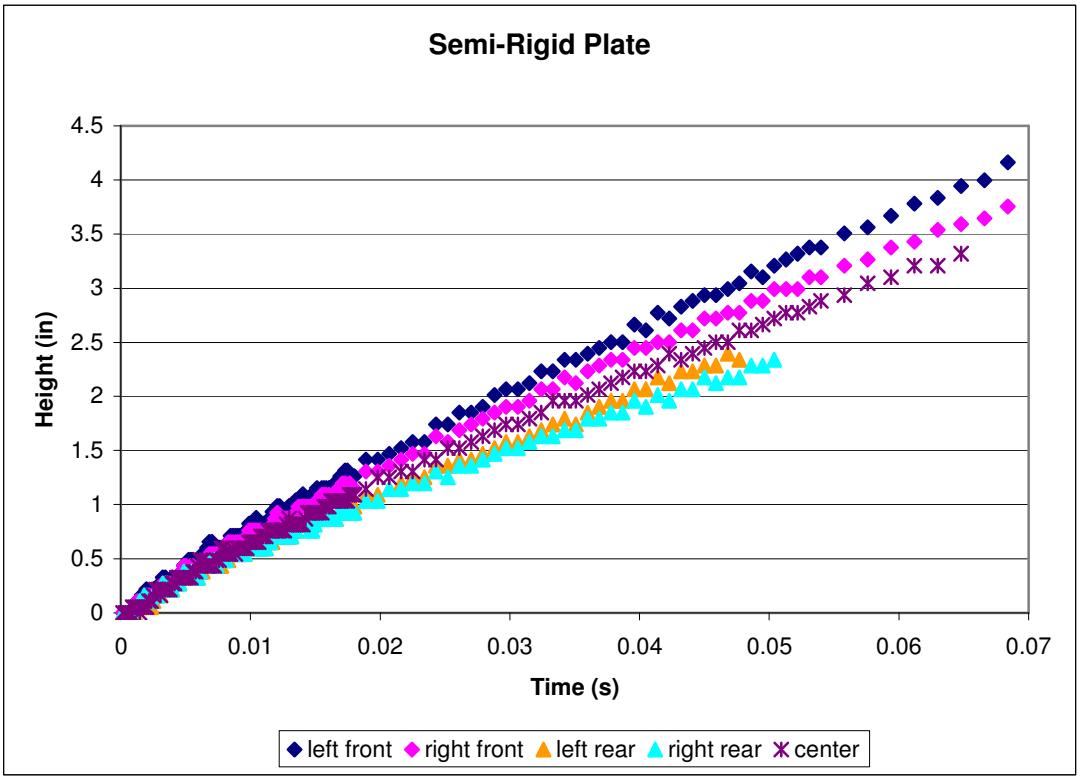

Figure 4.36: Semi-Rigid Plate Point Displacements

The diamonds represent the front corners, and the triangles represent the back corners. The center point is demarcated with "X"s. Although the data suggests the front of the plate was traveling faster than the rear, there did not appear to rotation in the movie file. The camera was pointed directly at the center of the plate, so the angle to the front points of the plate and to the back points is slightly different. However, a bigger contribution to the difference was caused by the camera's perspective. The input gauge length was chosen along the center of the plate, so distances at the front of the plate appear slightly longer than they are and distances at the rear of the plate appear slightly shorter. In order to properly use this data, an average was taken of the four corners and the center point, as shown in Figure 4.37. This average is very similar to the center point values, as should be expected for a nearly rigid plate. In

order to determine the initial velocity a straight line was fit through the early, approximately linear region of the data, as shown in Figure 4.38.

Figure 4.37: Semi-Rigid Plate Average Displacement

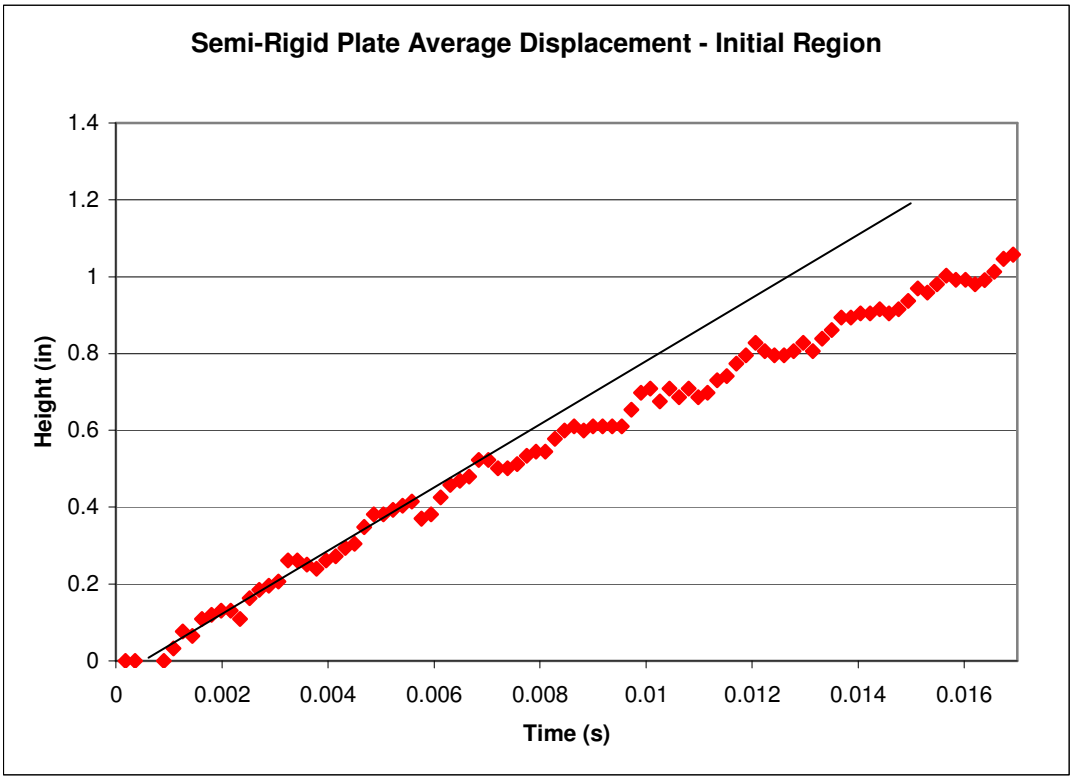

Figure 4.38: Semi-Rigid Plate Average Displacement - Early Region

The slope of the line represents the initial velocity of the plate with units of in/s. By using two points on the line the velocity is calculated to be 84.9 in/s, or 7.1 ft/s. Due to the poor spatial and temporal resolution of the video, accurate acceleration values cannot be obtained.

Deformable Plate

All four corners of the frame were tracked for the rigid plate in order to determine the rigid-body motion, as shown in Figure 4.39:

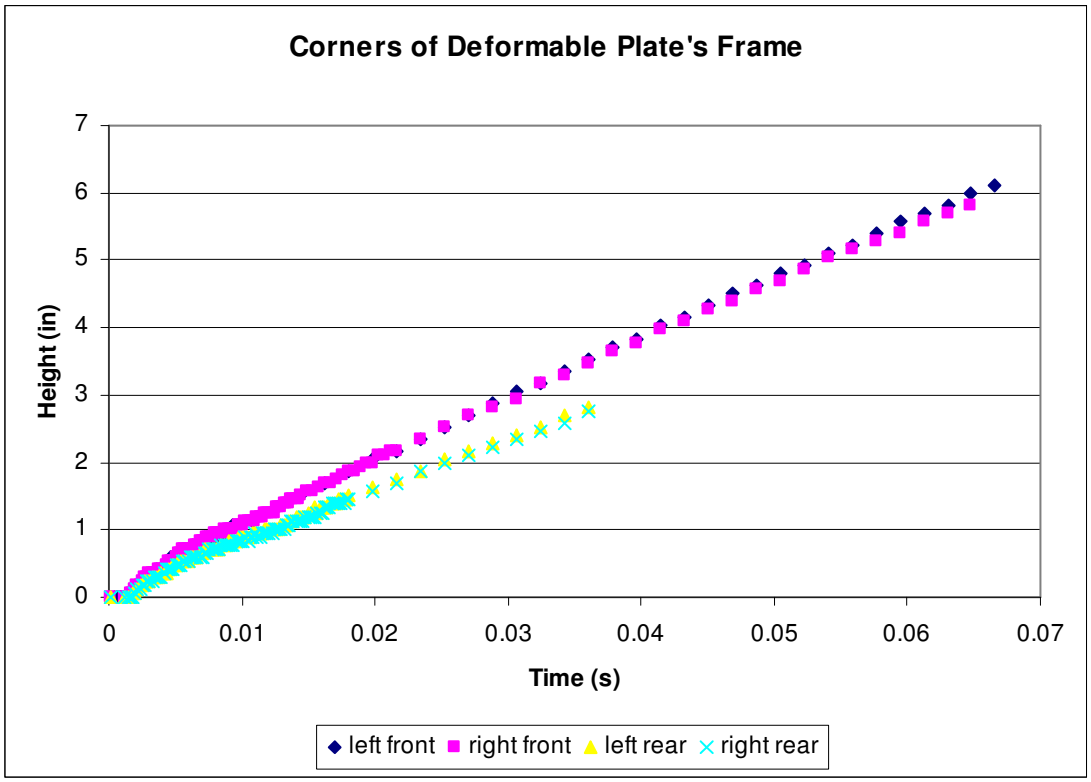

Figure 4.39: Deformable Plate Corner Point Displacements

These corner values were then averaged in order to determine the initial velocity of the frame. The center of the deforming plate was also tracked, and these were plotted together in Figure 4.40:

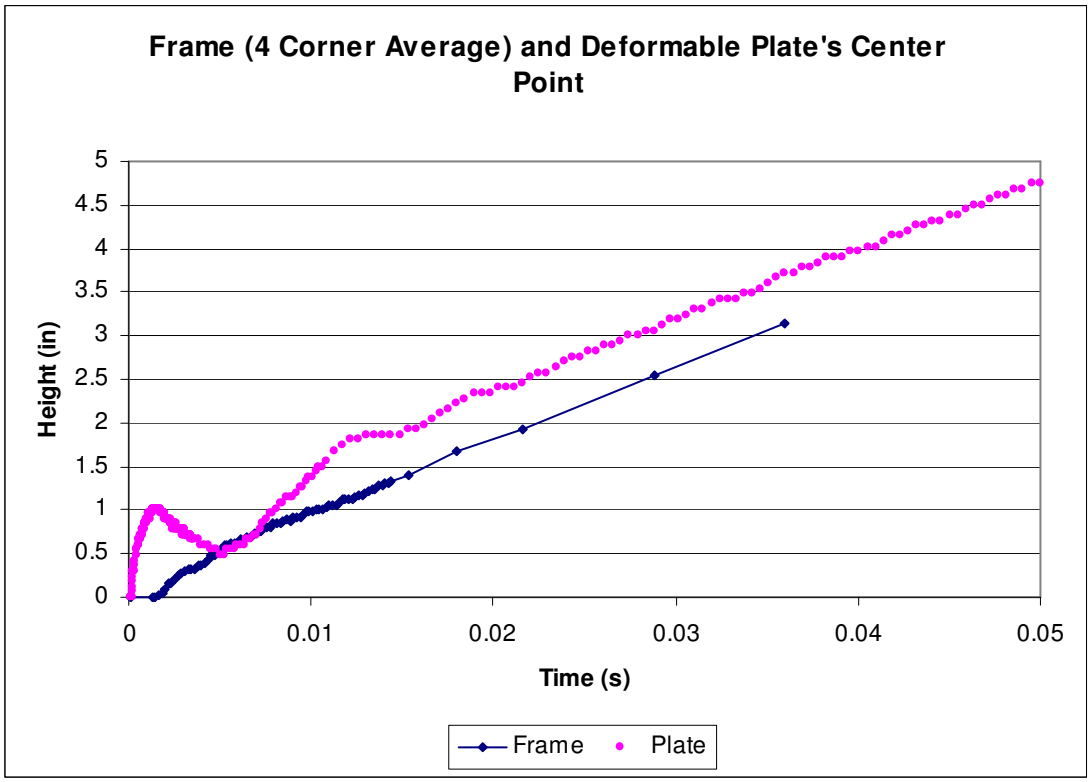

Figure 4.40: Frame and Deformable Plate Displacements

A few important characteristics of the displacement can be easily noticed from this plot. First of all, the plate begins to accelerate a significant amount of time before the frame, because it is initially just deforming. Rigid-body motion initiates when the frame begins its upward displacement. At this point the plate is experiencing a rebound. In fact, the center of the plate even drops below its initial starting point relative to the frame (which is in motion) for a brief moment at around 5 ms. It then begins to outpace the frame once again until it reaches equilibrium at around 15 ms, and begins to travel with the frame as a rigid body. As the frame and plate continue upward, the plate stays about 0.53" above the frame. From data previously presented (in section 4.1.4), this test condition yielded 0.653" of final deformation in another test plate, so the results seem reasonable. In order to approximate the initial velocity a

straight line was fit through the early, linear region of the data, as shown in Figure 4.41:

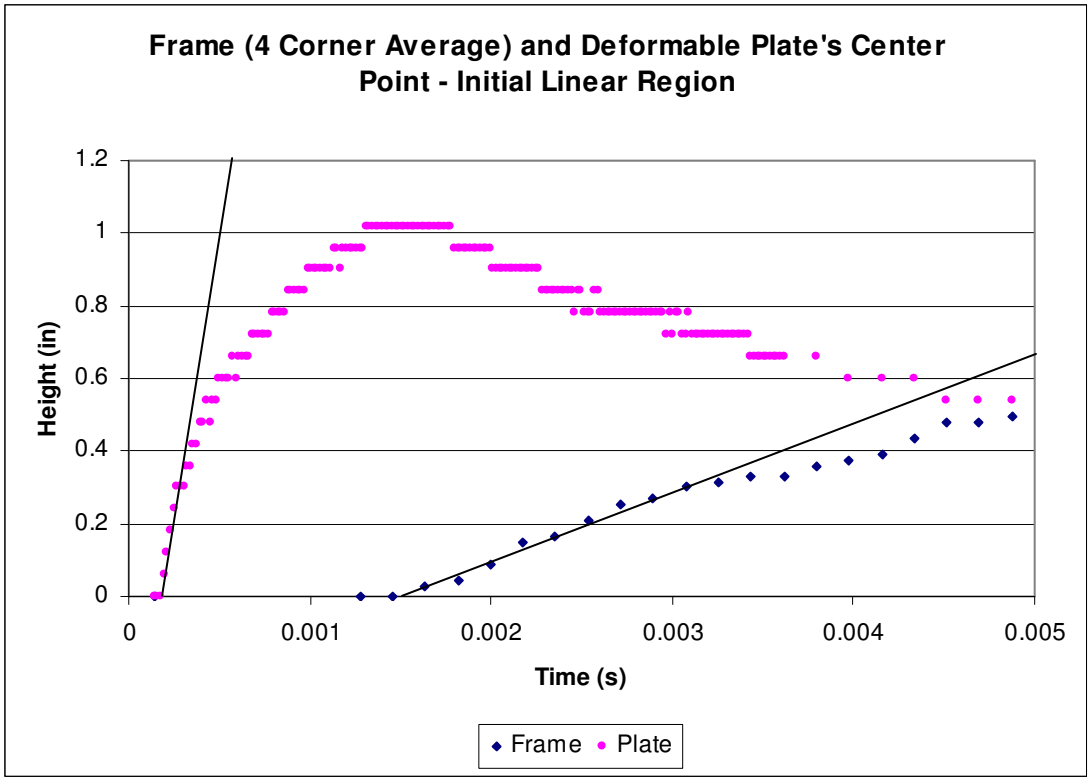

Figure 4.41: Frame and Deformable Plate Displacements – Early Region

These lines produce an estimated initial velocity of 222.2 ft/s for the plate and an initial velocity of 15.6 ft/s for the frame.

Comparison

The initial velocities for both tests are given in Table 4.6. The rigid-body motions (RBM) are the values that should be compared, since these both represent an acceleration of the same masses. This is representative of the velocity which the entire vehicle would be accelerated to in a full-scale mine blast.

	Initial velocity (ft/s)
Semi-Rigid Plate (RBM)	7.1
Frame (RBM)	15.6
Deformable Plate	222.2

Table 4.6: Initial Velocities of Rigid-Body Motion and Deforming Plate

These findings are contrary to what was initially expected. It was hypothesized that the deformable plate's frame would travel at a lower speed because some of the blast's energy was dissipated through deforming the plate. However, the initial velocity of the frame was measured to be more than double the rigid plate's initial velocity. The first concern was that the semi-rigid plate was heavier, but this difference in weight is not great enough to produce such a dramatic difference in initial velocity. The increased velocity of the deformable plate's frame may be due to the effectiveness of the cupped plate capturing the blast's energy. Whereas the semi-rigid plate can be seen to divert the sand towards the sides, it is possible that the deformed plate is acting like a parachute and capturing this pressure. Another plausible explanation is that the deforming plate may be acting as a sort of spring. From the initial blast pressure it is deformed plastically as well as elastically, and after the plate reaches its peak it begins to recover the elastically stored energy. This mechanism could be launching the frame upward at a greater rate.

4.3.3. Rigid vs. Deformable Crater Analysis

For this test it was also interesting to know if the plate affects the crater. Both craters are plotted as Figure 4.42, and their respective measurements are shown:

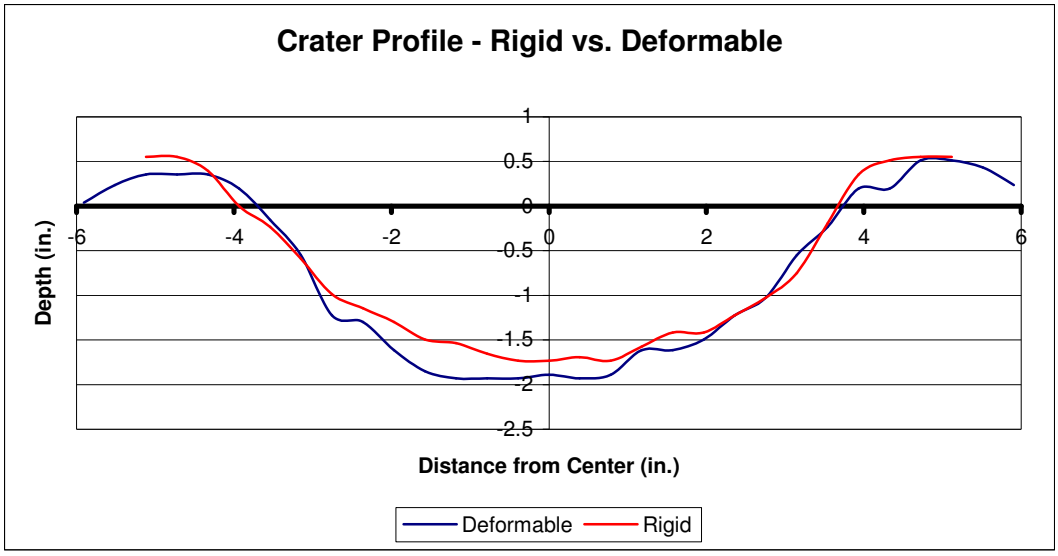

Figure 4.42: Crater Profile – 1" DOB, 1.22" SOD

	Maximum Depth	Profile Area (in^2)	Crater Volume (in^3)
Deformable	**1.9 in**	**10.1 in^2**	**45.8 in^3**
Rigid	**1.7 in**	**9.2 in^2**	**42.6 in^3**

Since the craters have an inherently high level of variability it is hard to draw any conclusions from this small sample size. However, the crater is slightly smaller for the rigid plate, possibly due to its slower initial velocity. It could also be the case that the rigid plate is reflecting more sand back into the crater since it remains flat.

Chapter 5: 3D Digital Image Correlation Experimentation

5.1 Data Acquisition Procedure

The primary goal of this research is to develop an inverse hybrid method for determining the pressure experienced by a flat plate during an explosion. In order to accomplish this, it is necessary to obtain data from physical experimentation. 3D Digital Image Correlation is a technique used to measure the three-dimensional deformation of a surface through use of two simultaneous images taken from different angles. The software "tracks the gray value pattern in small neighborhoods called subsets (indicated in red in the figure) during deformation," as shown in Figure 5.1 [14]:

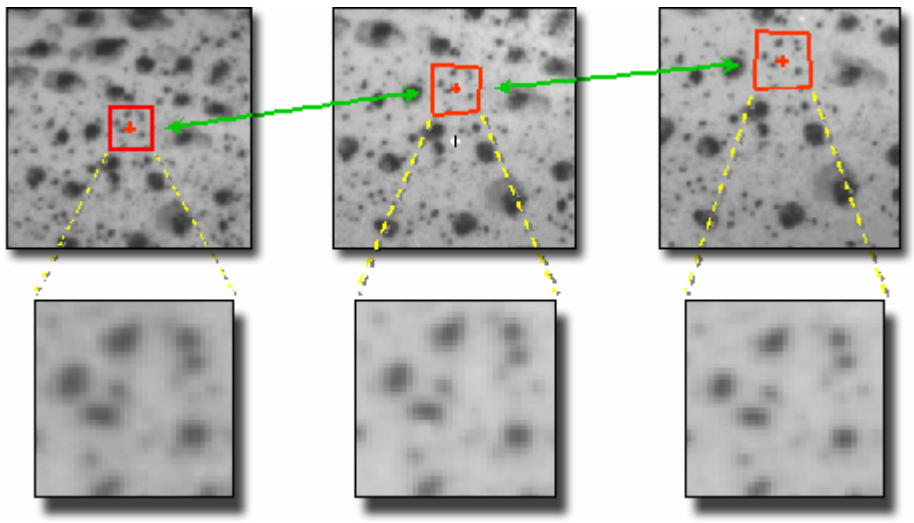

Figure 5.1: Tracking a Subset as it Deforms

A random pattern assures that each subset (also referred to as an interrogation window) is unique and can be recognized in subsequent images.

5.1.1 Preparing the Test Specimen

The first step in performing a 3D image correlation experiment is to create an appropriate test sample. A random pattern must be produced in order for the software to be able to track individual points. This pattern must deform with the specimen, so it is typically painted on. Creating a speckle pattern, as they are referred to, is often described as more of an art than a science. Each speckle should be at least twice as big as the pixel size, but if the marks are too big there will not be enough points to track and the data will have a very low spatial resolution. The pattern also has to have high contrast, so it is typical to use black speckles on a white background (or vice-versa).

Specimens were prepared by first spray painting the plate a flat white color. The plate must not be painted too far in advance or the paint will become brittle and chip off during testing. After the white basecoat was dry enough not to smudge speckles were added using black markers of various tip sizes. The test results turn out better if there speckle density is high because the white space reflects more light into the cameras as the deformation is occurring, which can cause overexposure. One such speckle pattern used for a test is shown in Figure 5.2:

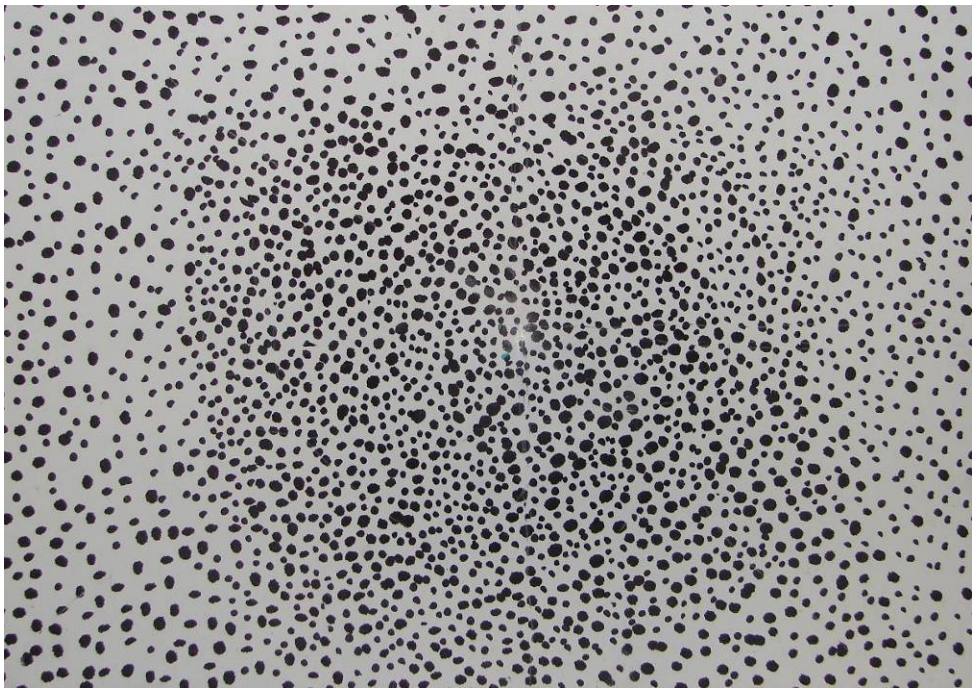

Figure 5.2: Random Speckle Pattern on Test Plate

The center of the plate is marked in order to help properly orient the cameras. It is also helpful to include one readily identifiable mark in the corner of the plate, such as the one shown in Figure 5.3. This must be visible to both cameras, and ideally not undergo much deformation during the explosion. The mark helps locate 3 common points on the plate in both images during the analysis process, which the Vic-3D software uses as an initial guess during calculations, as described later in this section. A border should be traced on the plate around the area that can be seen by both cameras using a light marker line. This is done by looking at the live images from each camera and plotting several points that can be seen by both, and then roughly connecting them. This border is useful for determining the area in which data will be obtained.

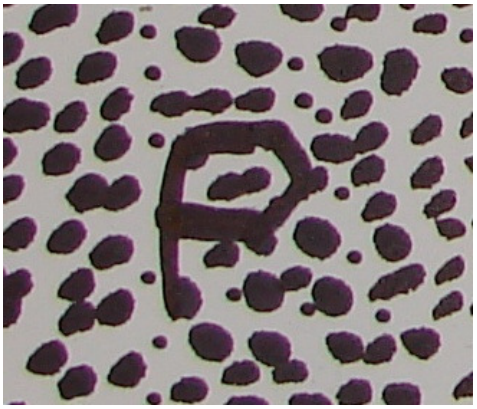

Figure 5.3: Uniquely Identifiable Mark

5.1.2 Stereo-Imaging Test Setup

In order to perform 3D DIC, it is necessary to use two high-speed cameras. The Phantom 7 cameras were used for the tests conducted at the Dynamic Effects Lab. The cameras need to be precisely synchronized together for the data to be processed. This is accomplished by connecting the F-Sync cables between the cameras, and using the Phantom control software to set one camera as internally synchronized and the other as external. The camera that is set to "External" will rely on the other camera for the image timing and frame rate. The trigger cables are also connected together, with a T-splitter connecting them both to the firing system. This signals the cameras that the explosive has been triggered. The F-Sync and Trigger Cables are both coaxial with BNC connections. Lastly, Cat 5 cable (commonly known as Ethernet cable) is used to connect both of the cameras to a hub, which then connects to the controlling laptop. The complete setup is diagrammed in Figure 5.4:

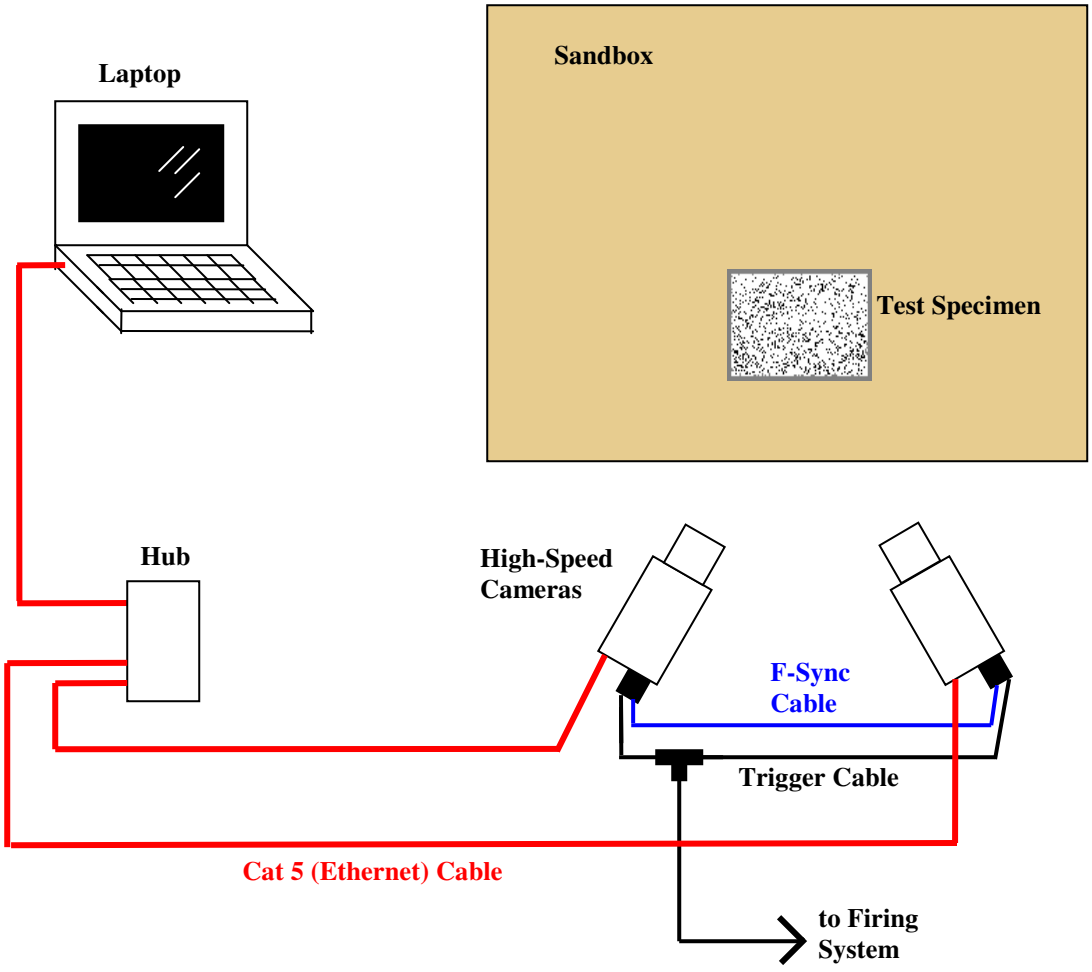

Figure 5.4: 3D Digital Image Correlation Setup

There are several camera settings that must be selected. The most important ones are the resolution and the sample rate. Due to inherent hardware limitations, there is a tradeoff: the higher the resolution, the lower the possible sample rate. The resolution determines how much area of the test specimen can be seen, as well as the amount of pixels available for analysis. A greater number of pixels provide more spatial resolution, but the sample rate must provide enough pictures per second to capture several dozen frames of the event. Another important setting is exposure time. This must be low enough that the images appear to be still. If blurring occurs, the data

will not be usable. For most levels of explosive, it is typical to keep the exposure time under 10μs. Lastly, the PostTrigger must be set so that several images before triggering are saved to ensure detonation is not missed. The camera is continuously taking images and this setting determines which ones to save.

5.1.3 Camera Positioning and Calibration Imaging

When setting up the cameras, a balance must be struck between keeping the specimen in focus and obtaining adequate depth resolution. If the cameras were directly above the plate the data would have superior depth resolution, but after the plate travels too far vertically it would be out of focus and the data would be unusable. Conversely, if the cameras were looking at the plate from the side it would stay in focus longer, yet the deformation would begin to block the back-side of the plate.

Once the cameras are in place they must be focused so that the specimen is clear during the time of interest of the event. If the cameras are outfitted with variable zoom lenses, it must be ensured that the focal length is not changed after it is initially set. This can be achieved by placing a piece of tape along the outside of the lens. Once both cameras are properly positioned and focused, a calibration must be conducted, in order to determine the internal camera parameters "(focal length, image center, distortions, skew)" [15]. This process also determines the relative position and angles of the cameras, which the software needs to perform triangulation.

Although the Phantom software can be used, the easiest tool for taking calibration images is the Vic-Snap software. It allows for simultaneous images to be taken from both cameras, and properly names and numbers them in the convention

required for Vic-3D. The calibration consists of collecting stereo images of a rigid grid positioned at multiple angles. Two of the grids used are shown in Figure 5.5. In order for the software to recognize the positioning of the grid, all three hollow spots must appear in both images of every pair. Therefore different grid sizes are needed depending on the camera resolution selected. For a white grid the hallow spots are black with a white center, and for a black grid the hallow spots are white with a black center.

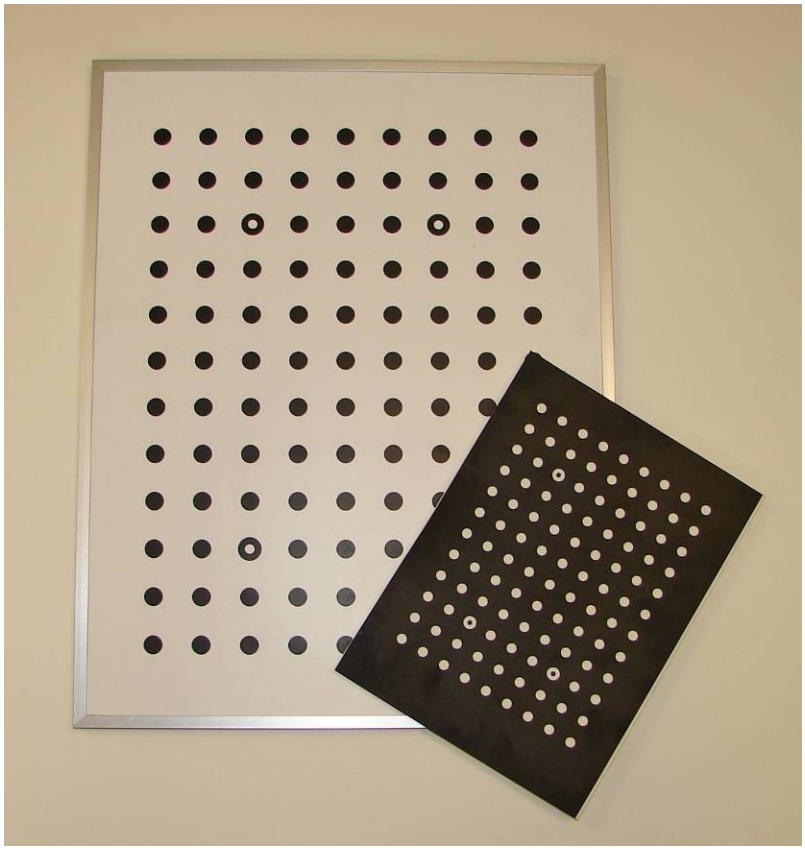

Figure 5.5: Various Calibration Grids

Theoretically only 3 quality calibration images are needed, but to reduce error it is typical to take 20 or more. There are two ways the images can be obtained. The first is by using the Vic-Snap software, which is relatively automated and simple but

prone to locking up, especially when using cameras that are not identical to each other. With this method the images are recorded by clicking the space bar. The second way images were taken is through the Continuous Recording option in the Phantom Camera Control software. After loading two instances of the software, the path and file names must be input. When entering the file name, the "@" symbol followed by a number indicates the amount of digits used for the image number. For example, DT9_@2_0 would refer to camera 0 for Deformation Test 9, whereas DT9_@2_1 should be entered for the other camera. The first image would be named DT9_00_0 for camera 0 and DT9_00_1 for camera 1. In the same "Cine file paths and save parameters" options box, the image count should be set to 1 and the first image to 0, and the file type set to TIFF 8,24 images. Images can then be taken by using a hand trigger. Care must be paid to ensure that the images are both saved before clicking the trigger again, and that the numbers match for both images.

Using either method, a variety of images should be taken with the grid in different positions, rotated along all 3 axes by at least 20°. The software uses the images to determine the camera parameters such as focal length and the orientation vectors. It also determines the scaling from the known distance between the dots on the grid, which is later input into Vic-3D. The calibration can be done using any resolution, but it is preferable to use the same resolution as the test if possible. The lighting does not have to be the same for the calibration and the test.

In the event that a camera is bumped after calibration but before the test, the procedure does not need to be repeated. The calibration can be salvaged in the Vic-3D by simply selecting the Calibrate Camera Orientation option. If, however, the

lenses setups are changed in any way, including the focus or the focal length, the calibration images must be retaken.

The next section discusses how to process the calibration images. It is prudent to ensure the calibration images are adequate by quickly running through the Vic-3D calibration procedure. Afterwards, the test can be conducted in the same manner as an experiment without image correlation. Figure 5.6 shows the completed setup, immediately before a test is conducted. The cameras are covered by plastic boxes in order to provide protection, and the lenses are protected by a simple UV filter.

Figure 5.6: 3D Digital Image Correlation Test Setup

A dummy charge is set off to ensure the images are being properly captured, and then the test is performed. Videos can be collected either using the Phantom software, which is more robust but requires the files to be converted into TIFF format before

analysis, or by using the previously mentioned Vic-Snap software. Vic-Snap will not function properly with cameras that are not exactly identical to each other; for this reason the tests described in this thesis used the Phantom software.

5.2 Data Analysis Procedure

After the test has been conducted the Vic-3D software is used to analyze the results. It is made by Correlated Solutions, and build 2006 was used.

5.2.1 Vic-3D Calibration Procedure

The first step is to load the calibration images into Vic-3D. After creating a new file, the Calibration images option is selected from the Project menu. All of the desired calibration should be highlighted and opened. By selecting Calibrate stereo system the images can then be processed. The first step is to enter the parameters for the specific grid that was used. The values for one commonly used grid are shown in Figure 5.7. The pattern, as previously shown in Figure 5.5, includes three identifier dots with hollow centers. Besides entering the number of dots and the location of these identifiers from the edge, the distance between identifiers is also input as the number of spaces between them. Lastly, the distance in mm between dot centers must be entered.

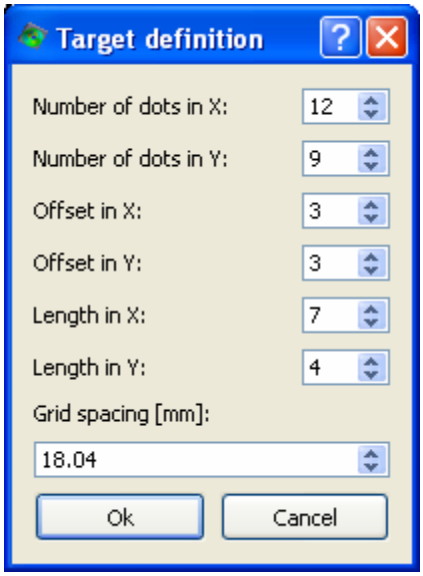

Figure 5.7: Values for Commonly Used Calibration Grid

Typically the grid points can be extracted for enough images by simply clicking the Auto button. If the points are not automatically recognized, the images can be modified by adjusting the threshold slider, taking off glare reduction, or changing the minimum or maximum amount of pixels per dot. After enough image pairs are recognized, the Calibration button is selected to begin the procedure. In order to improve the quality of the calibration, the images with the highest standard deviations should be noted, and the procedure should be repeated without these images included.

If a different resolution is used for testing, an adjustment must be made to the calibration. Adjust for cropping is selected from the Calibration menu, and the offset is entered. This ensures the center of the calibration and the center of the test images coincide. Figure 5.8 shows the process for using a 512 x 512 pixel calibration resolution along with 128 x 128 test images:

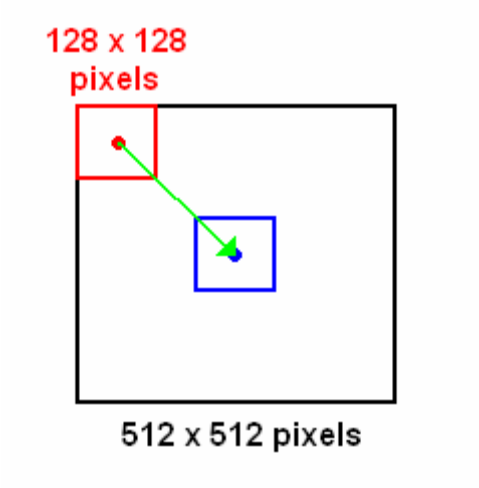

Figure 5.8: Cropping for Different Calibration Resolution

In this example the center of the large image is at 256 and the center of the smaller image is at 64, so the offset is calculated to be 192 in both the x and y direction.

After completing the calibration, the quality should be double-checked by ensuring the given center values are approximately in the middle of the resolution. For the above example, the x and y centers for both camera calibrations should be around 64. The focal length values should also be checked to ensure that they are about the same for each camera, assuming the same lenses are used. It is also prudent to check the reported measurement for the Stereo Baseline, which is the distance between the two lenses reported in mm. The alpha, beta, and gamma angles of the two cameras can also be observed, although with most camera setups these are extremely hard to measure.

5.2.2 Vic-3D Data Processing

In order to load the images from the deformation into Vic-3D, they must first be extracted from the Phantom cine files. This is done by loading the Phantom Camera Control software and choosing Convert&Process cine from the File menu.

After picking the cine and selecting Open, first image should be entered for the frame number immediately before the plate undergoes noticeable deformation. In the case where the Phantoms do not trigger at the same time, this number will be different for each camera. The file type should be set to TIFF 8,24 images and the desired image count must also be entered (typically about 200 to 400 images can be analyzed before the plate leaves the field of view or becomes unfocused). If either of the cameras' images are too dark, this is also the easiest time to brighten them, but the desired Image Processing values must first be determined in the View Cine playback window. Lastly, the file name must be entered using a similar naming convention to the one described in the above section on obtaining calibration images using the Phantom software. In this field the file name should include a "+" symbol followed by a number, which indicates the amount of digits used for the image number. For example, DT9_+3_0 would refer to camera 0 for Deformation Test 9, and the images would be saved as DT9_001_0.tif for the first one, DT9_002_0.tif for the second one, and so on. Returning to Vic-3D once again, the newly extracted images can be loaded similarly to the calibration images, except by clicking the Speckle images button this time.

After a successful calibration has been performed and the deformation images have been extracted and loaded, the first step in processing the data is to determine the area of interest. By using the first image as the reference, a region is drawn using one of the Aoi tools. This is the area for which the data will be processed. In order to minimize processing time, this area should be drawn so that the other camera can see the entire region, but it is not detrimental to include too much area. The next items

that must be set are the subset size and the step size. The subset size is the area in which the software will track displacement between frames. This should be as small as possible while still containing several spots. The step size determines the number of pixels between data points, with smaller step sizes taking longer to process yet providing finer data resolution. If the data is not processing cleanly (or at all), these values can be tweaked in order to obtain better results. The reference (undeformed) image along with the chosen area of interest can be seen in Figure 5.9:

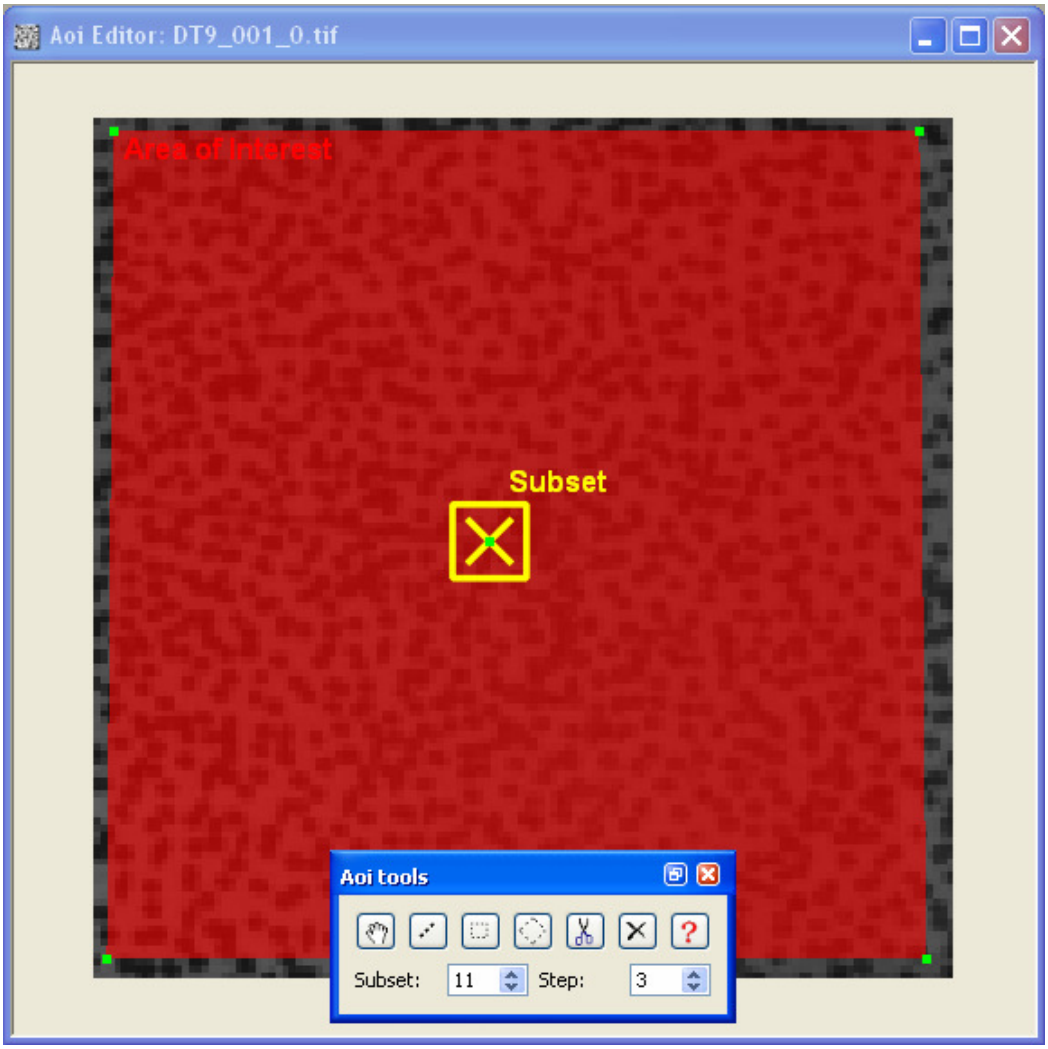

Figure 5.9: Reference Image with Highlighted Area of Interest and Aoi Tools

After defining the parameters, the selection box should be moved to encompass the uniquely identifiable mark, an example of which was previously shown in Figure 5.3. This determines the location of the seed point, which is where the correlation begins. An initial guess correlating the two cameras must be made by selecting the question mark button. Next the Guess Type is set to Complete, and a point is chosen in one of the images. The corresponding point is selected in the other displayed image, and the point is then saved by selecting Add Point. This must be done for 2 more corresponding points in order to obtain a comprehensive guess. As previously discussed, this can be a very easy task to find the same location in two different camera images if a unique identifier mark was placed in an area undergoing minimal deformation, or an incredibly impossible one if there was no unique mark on the plate. If the guess was close enough, the red question mark next to the image name will turn to a green arrow. After the first guess is made, the computer can typically figure out the correspondence for the rest of the images. By clicking through the frames it can be determined if the seed point was good enough for automatic detection.

The analysis can be started by clicking the green arrow button if the computer is able to automatically detect the seed point in subsequent images after the initial guess. For these tests, all of the options in the Thresholding tab are unchecked, and under the Post-Processing tab the Auto plane-fit coordinate transform is selected. If desired, strain computations can also be performed at this point. All of the images to be processed with these initial guesses and subset sizes should be selected, and the

analysis can then be run. It is not uncommon to use different settings for the initial and later deformation stages in order to obtain a comprehensive data set.

The full-field data for the entire shared area of the two cameras can be viewed at each instance of time. Although many different variables can be viewed, the most relevant to this experiment is the vertical displacement, which is represented as W. The displacements U and V (in the x and y directions) are between 1 to 2 orders of magnitude smaller than W. The major principal strain is a more useful output. This is calculated using the partial derivatives of the displacements along with the Lagrange strain tensor equations, which is commonly used for finite (large) strains. Written in terms of displacements, the strain is:

$$E_{ij} = \frac{1}{2}\left(\frac{\partial u_i}{\partial x_j} + \frac{\partial u_j}{\partial x_i} + \frac{\partial u_k}{\partial x_j}\frac{\partial u_k}{\partial x_i} \right)$$

Any of these desired results can be displayed as either a 3D plot, as shown on the left side of Figure 5.10, or as a 2D overlay on either of the cameras' images, as shown on the right side:

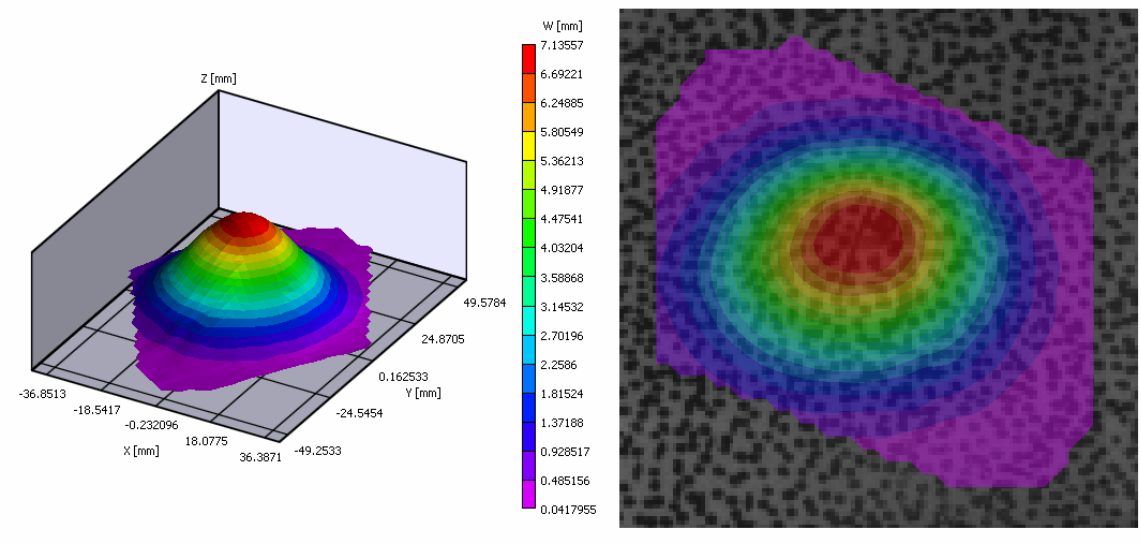

Figure 5.10: Out of Plane Deformation at One Instance In Time

These full-field deformation plots serve as a great tool to visualize the deformation process as it is occurring, but the complexity of the data can be greatly reduced due to the axisymmetric nature of the experiment. The results can be more easily represented and visualized through the use of profile plots and center point tracking, which are obtained through data extraction as discussed in the next section.

5.2.3 Vic-3D Data Extraction: Plate Center Point

In order to obtain the data for the center point, a 2D plot (as shown on the right in the above Figure 5.10) must be displayed. This should bring up the Inspector tools. After the Inspect point tool is selected, the center must be located by moving the cursor around the image and manually locating the point with the highest deformation. The deformation value is actively displayed at the bottom of the screen as the cursor is moved throughout the data area (along with the x and y pixel location of the cursor). Once the center of deformation has been located, clicking the X button

in the Inspector tools allows for extraction of the data. After clicking Extract, the data can be exported by clicking Save Data under the Plot tab.

After opening the comma-separated values (csv) file in a spreadsheet program the displacement of the center point can be plotted as a function of time. Since the time between images is not known to Vic-3D, this must manually be entered into the spreadsheet. This can easily be found based on the camera parameters that were used for testing.

Most of the center point data was compiled in this manner. However, for the tests that were not analyzed in-house the Vic-3D files were unobtainable. In these cases the center point data was extracted manually from the provided csv line data files, which should give the same results as the above discussed method.

The values for the major principal strain at this center point can also be exported in the same manner after choosing e1 as the contour variable from the 2D plot. The major principal strain value is reported for the center point because this is the maximum normal strain experienced. Most of the strain at this location occurs in the first several frames, as is evident from the set of data included as Figure 5.11. The plot on the right shows the early time region of the plot on the left.

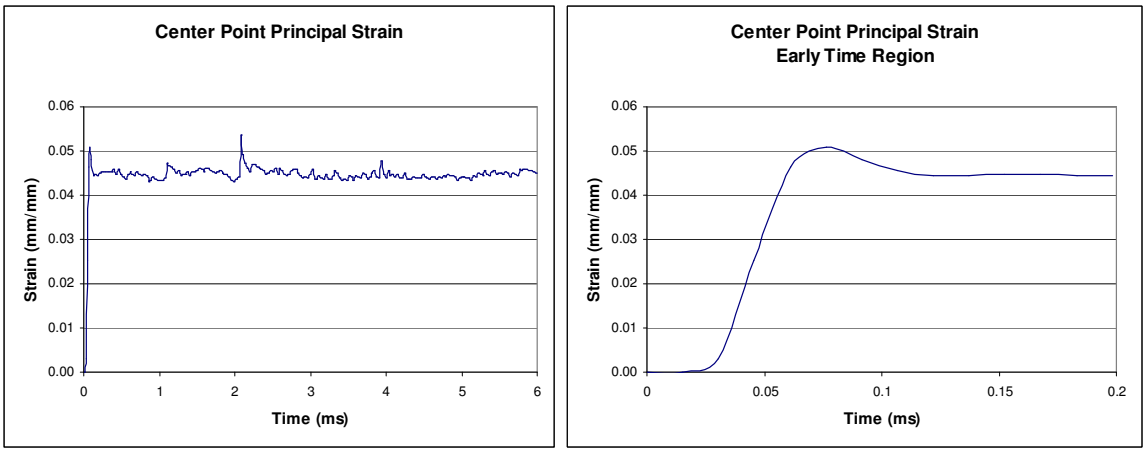

Figure 5.11: Deformation Test 9 Strain Data Plot Comparison

For this reason, it is more meaningful to only use data from the initial time frame when significant strain is occurring.

5.2.4 Vic-3D Data Extraction: Deformation Profiles

Another useful tool for visualizing the deformation process is a series of 2D profiles of the plate at various instances of time. The first step in obtaining these is to use the Inspect polyline tool (similar to the Inspect point tool previously mentioned). The reason the Inspect line tool would not work is because it is crucial that the center point remains on the line at all times, and with this tool this is not guaranteed. By using the first frame as a reference, a three node straight line should be constructed, with a node occurring at the center point of the plate. This can be seen on the left in Figure 5.12:

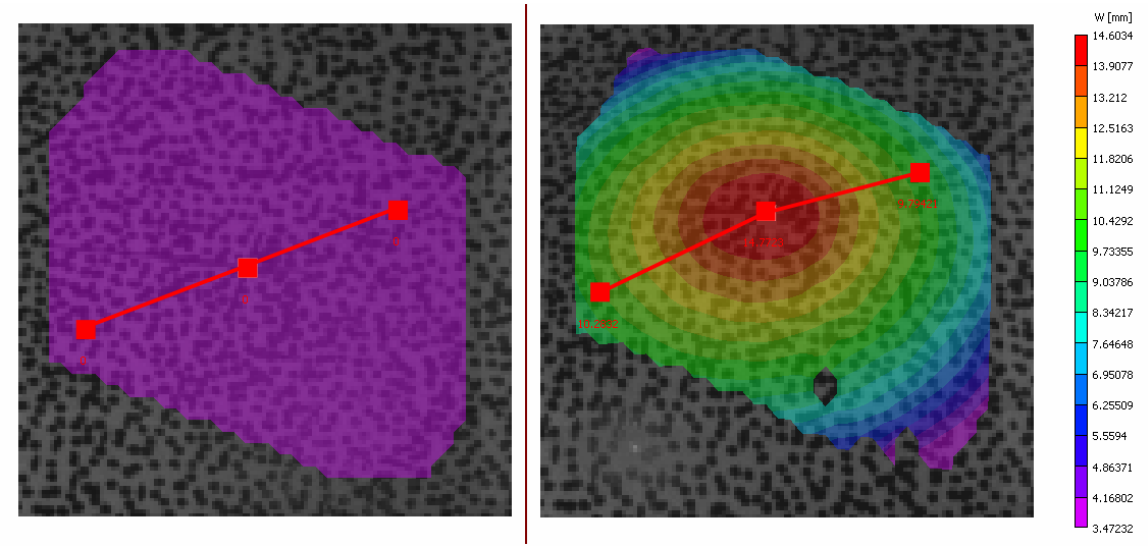

Figure 5.12: Polyline as Originally Drawn and as It Follows Center Node

By constructing the extraction line like this it can be seen on the right side of the above figure that the data will always be presented for the center point of the plate, along with the corresponding profile. After constructing this line, the data is extracted by clicking the X button under Inspection tools and selecting the number of data points desired (usually about 201 points). After clicking Save Data the file name must be manually entered. This procedure must be repeated for each instance in time that the deformation profile is desired. Typically data was extracted until a few frames after the visible area of the plate is just no longer deforming (and is just translating vertically).

The next task is combining the CSV files into one spreadsheet. Occasionally data will be unavailable at a few points along the polyline. This is typically due to excess reflection and over saturation of the camera sensor. In this case the output file will ignore this empty data point and continue on with the next. This creates a problem while combining files because they are of different lengths and will no longer line up nicely. In order to compensate for this a Matlab code was written to

automatically combine the files and, in case there is any missing data, line them up correctly. The code is included in Appendix A.

After the line plots are all combined into one file, they need to be copied into a new spreadsheet and properly labeled. The appropriate time needs to be calculated for each frame based on the camera's frame rate, and the distance (in millimeters) between each of the data points must be calculated. This is done by first calculating the distance between the end nodes of the polyline. By opening one of the line data output files the X and Y coordinates for these nodes can be used to calculate the total length of the line by simple use of Pythagorean theorem. The distance between data points can be easily calculated by assuming that it remains the same as deformation is occurring.

5.2.5 Potential Sources of Error

Throughout the analysis, there are sources contributing to potential error. For each data set the specific error conditions are discussed, but they fall into one of several types. For a few tests the camera synchronization was problematic. In one instance the explosive event did not occur at the same frame, so the cine files had to be adjusted to line up. In this case the images may not have been taken at precisely the same time. In another instance the exposure time varied, causing a flickering appearance. Also, due to slight differences between the two cameras, often the image was darker in one than in the other, so brightening compensation was applied before processing. However, even with these sources of error, while processing the data the error values were not unacceptably high.

5.3 Results

Results were obtained for several different test setups by following the data acquisition and analysis procedures outline in the previous sections. It is not possible to be certain that the data will be usable until after the tests have been conducted. In general, each set of parameters was repeated twice to ensure there would be usable data for each test condition. In the end, two of the test conditions have two sets of data reported, whereas the rest only have one. Figure 5.1 describes the tests for which results were obtained, along with the test number and parameters:

Description	DOB (in)	SOD (in)	Test Name
Surface Blast	0	1.22	DT 9
Shallow	0.3	1.22	USC 4
Mid-Depth	0.65	1.22	DT 7
	0.65	1.22	DT 10
Deep	1	1.22	USC 2
	1	1.22	USC 5
Deepest	1.22	1.22	DT 11
0" SOD	*1.22*	*0*	*DT 12*

Table 5.1: Experiments with 3D DIC Data

Most of the tests were conducted with the standoff distance held fixed at 1.22" while varying the depth of burial of the charge. For one such test the SOD was altered. All tests were conducted in the Dynamic Effects Lab at the University of Maryland, and most were analyzed at UMD. Chronologically, the USC (University of South Carolina) test series was conducted first, followed by the DT (Deformation Test) series.

5.3.1 3D DIC Test Results: Surface Blast 0" DOB, 1.22" SOD (DT 9)

Description of test conditions

As is common throughout all tests, 1 gram of effective charge was used, along with a $1/16^{th}$ inch aluminum plate. In this particular surface blast setup, the top of the charge was exposed and at the same level as the sand. The test setup and camera parameters are listed in Table 5.2:

DOB (in)	SOB (in)	Frame Rate	Exposure Time (μs)	Resolution
0	1.22	65573	7	128 x 128

Table 5.2: Deformation Test 9 Parameters

Sources of Error

Due to the poor placement of the unique identifiable mark for this test, it was necessary to use a different seed point for the initial frames. This causes a slight change in the appearance of the data set at this point. It was also necessary to brighten all of the images from one of the cameras. For this test the exposure times remained constant but the synchronization was off, and the explosive event did not occur in the same frame number for each camera. For this reason images had to be realigned and renumbered, and the Vic-3D error values were quite high, although not unacceptable.

Center Point Displacement and Strain

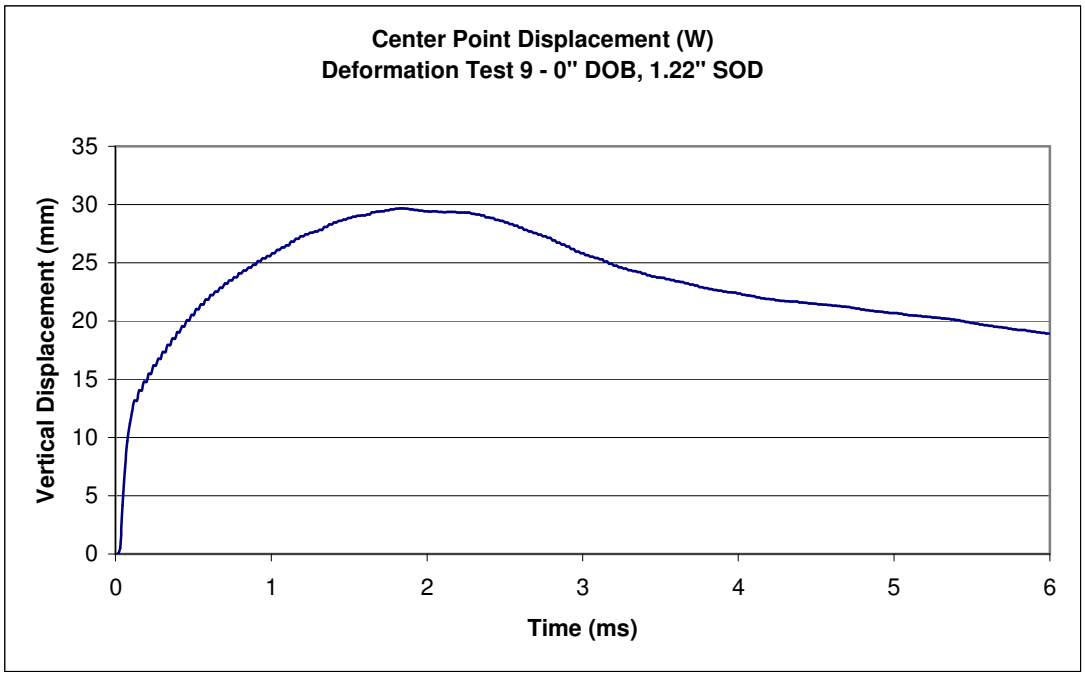

Figure 5.13: Center Point Displacement vs. Time – 0" DOB, 1.22" SOD

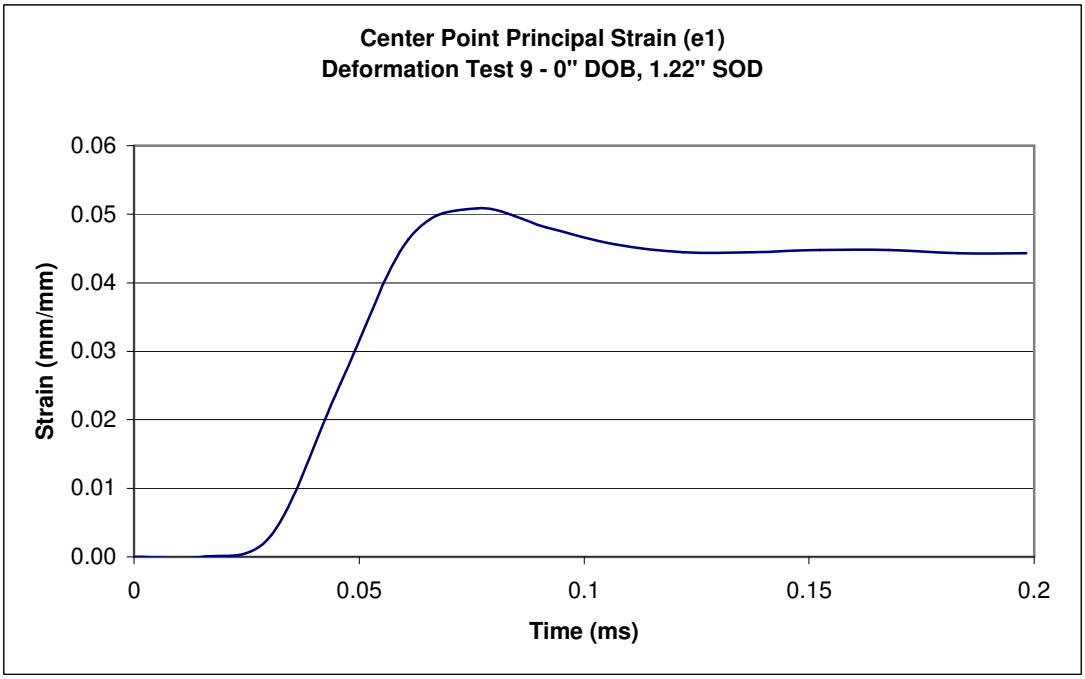

Figure 5.14: Center Point Principal Strain vs. Time – 0" DOB, 1.22" SOD

Deformation Profiles

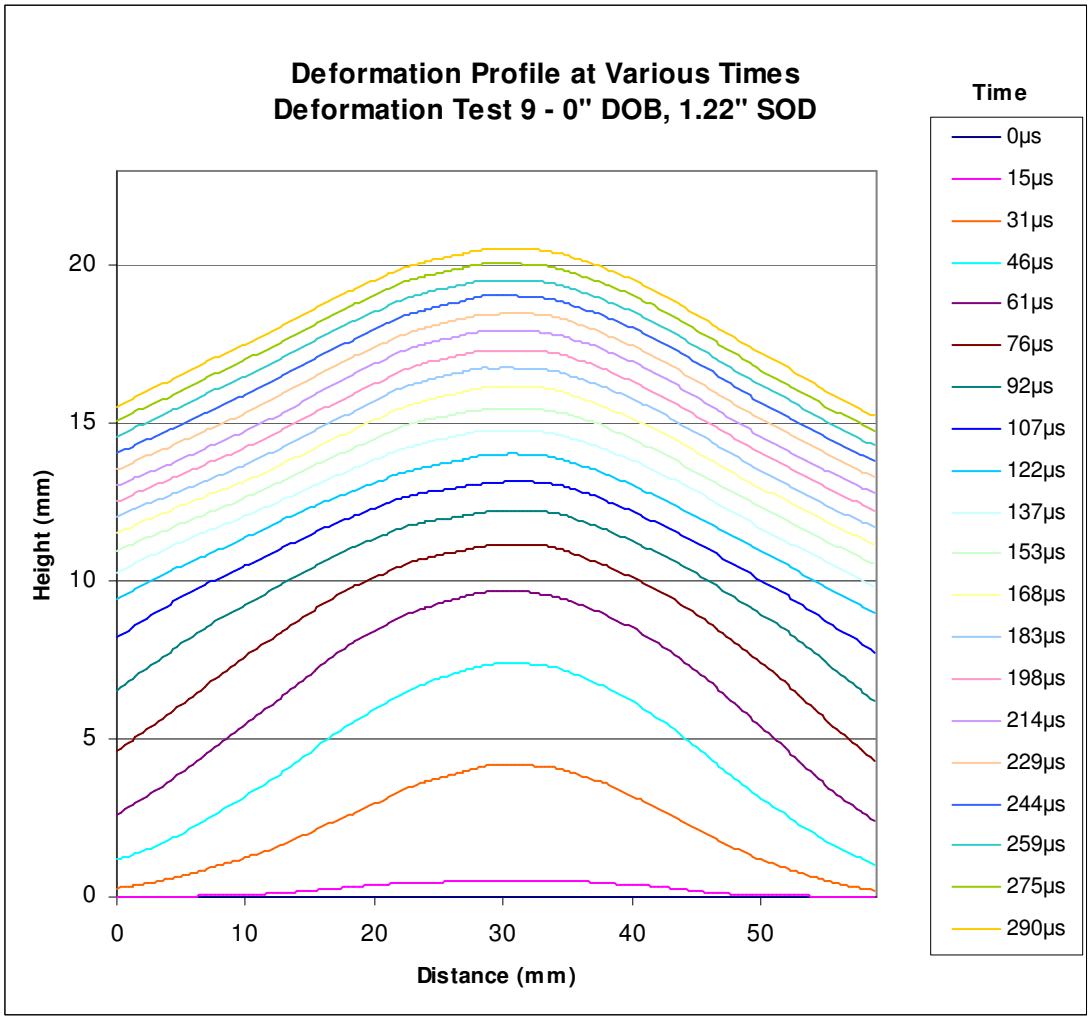

Figure 5.15: Deformation Profile at Various Times – 0" DOB, 1.22" SOD

5.3.2 3D DIC Test Results: Shallow 0.3" DOB, 1.22" SOD (USC 4)

Description of test conditions

This test was conducted with the 1 gram charge at the shallowest depth (besides the surface blast). It was performed in conjunction with visitors from the University of South Carolina, and processed at USC. The test setup and camera parameters are listed in Table 5.3:

DOB (in)	SOB (in)	Frame Rate	Exposure Time (μs)	Resolution
0.3	1.22	61538	10	128 x 128

Table 5.3: USC Test 4 Parameters

Sources of Error

The biggest source of error in this test was that one of the cameras used for this test experienced fluctuating time intervals, causing the cine file to flicker. Since this was one of the first 3D DIC tests conducted, the importance of a uniquely identifiable mark was not yet realized, so inputting the seed point into the analysis was quite difficult. This series of tests was processed using a copy of Vic-3D located at the University of South Carolina, and the raw data is unavailable. It is ideal to report the larger principal strain e1 but in this case exx, eyy, and exy were reported. However, the shear strain (exy) is negligible at the center, so exx and eyy can be treated as if they are be principal strains.

Center Point Displacement and Strain

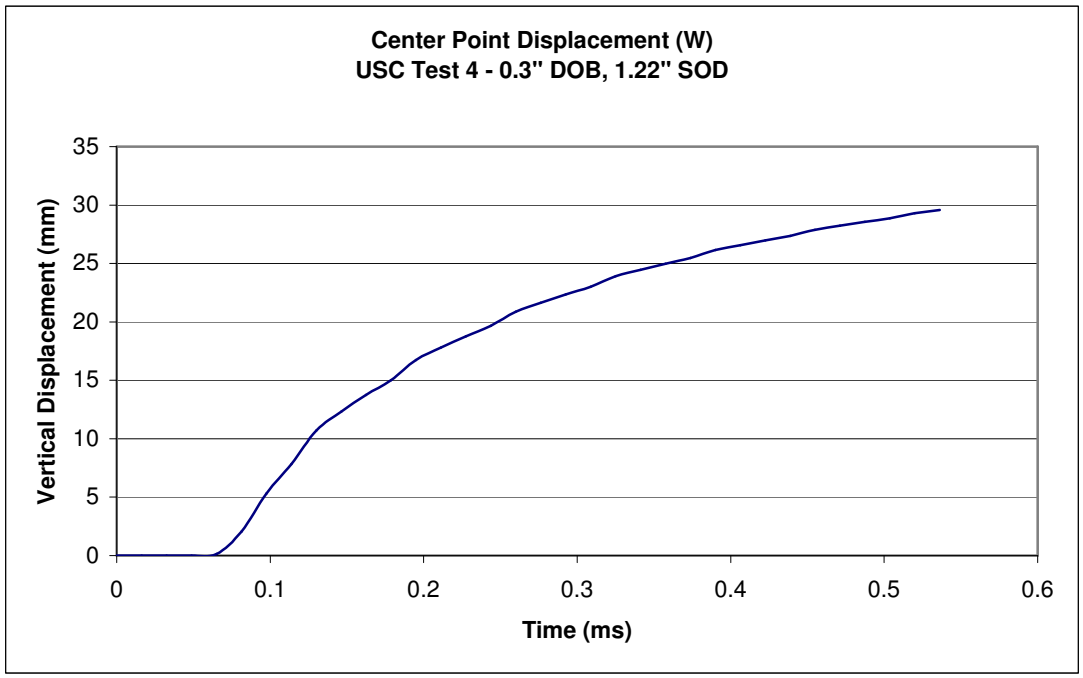

Figure 5.16: Center Point Displacement vs. Time – 0.3" DOB, 1.22" SOD

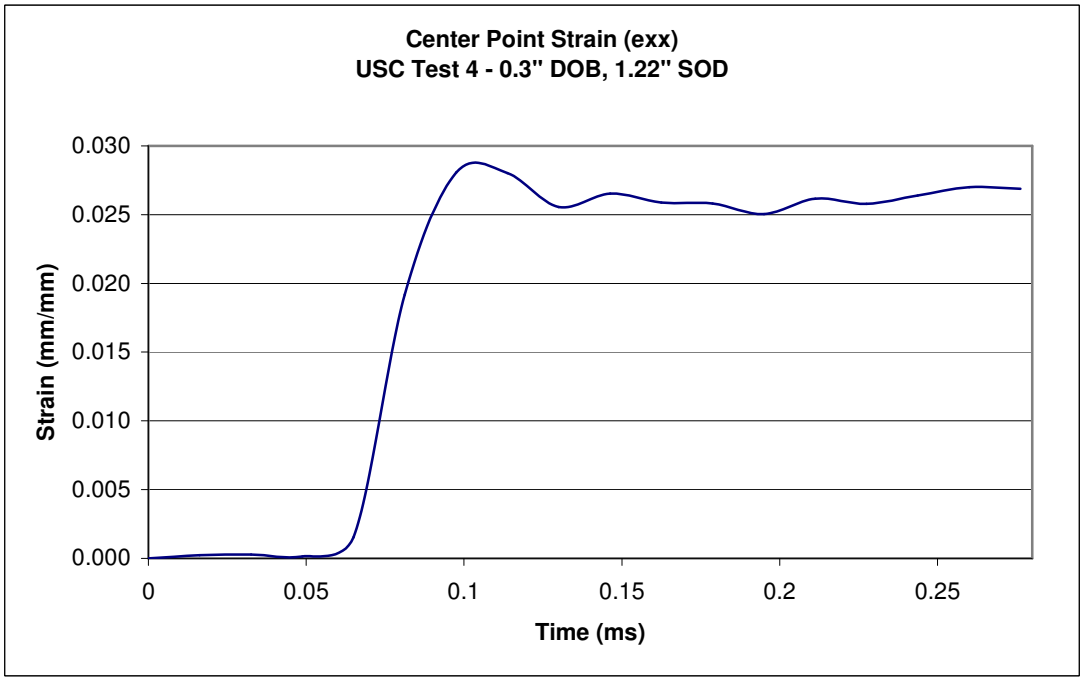

Figure 5.17: Center Point Principal Strain vs. Time – 0.3" DOB, 1.22" SOD

Deformation Profiles

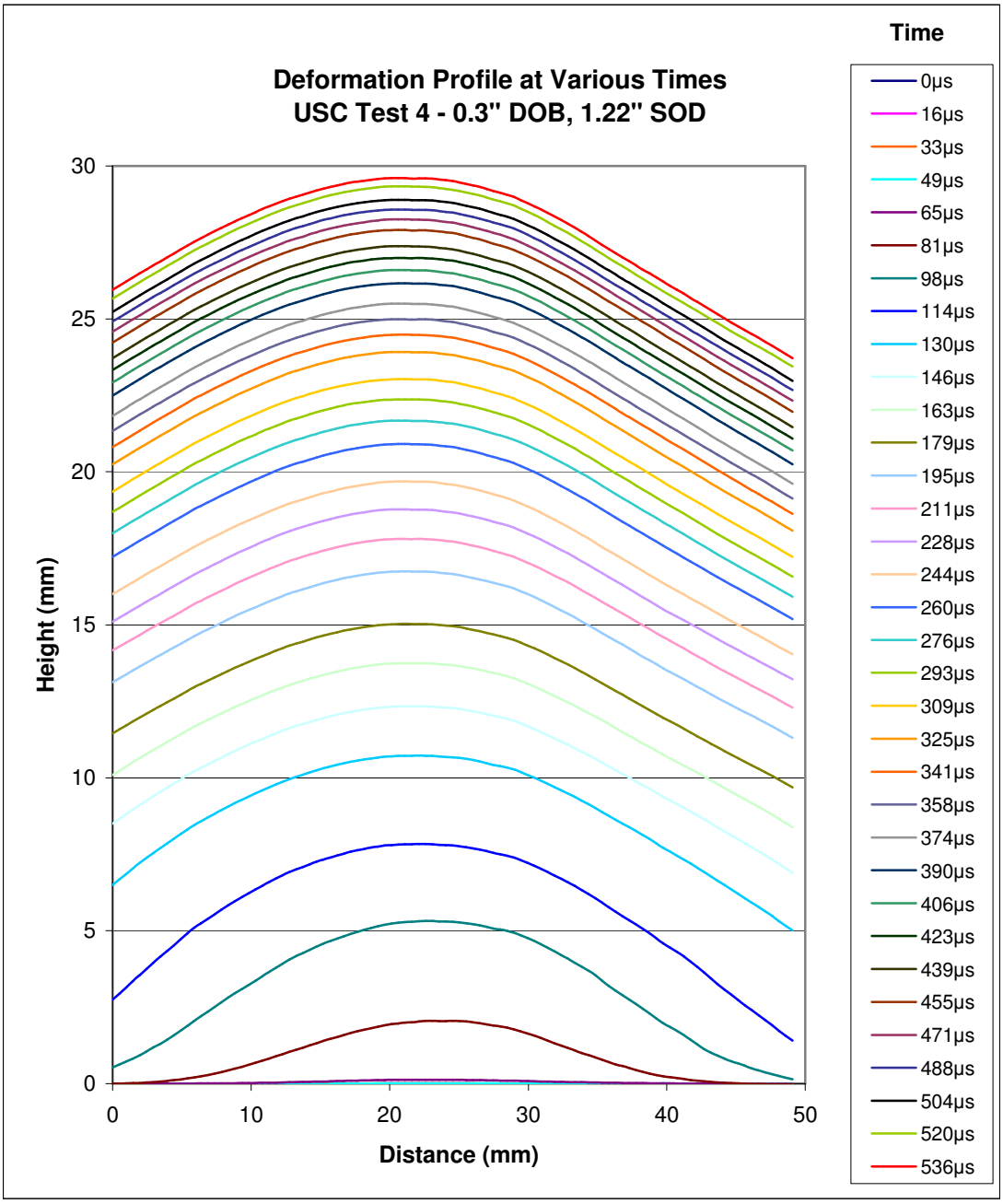

Figure 5.18: Deformation Profile at Various Times – 0.3" DOB, 1.22" SOD

5.3.3 3D DIC Test Results: Mid-Depth 0.65” DOB, 1.22” SOD (DT 7)

Description of test conditions

This test uses one of the intermediate depth of burials. Deformation Test 10 has the same DOB and SOD but a quicker frame rate and lower resolution. This test was performed with the direct assistance of a representative from Correlated Solutions to ensure the correct 3D experimental procedure was implemented. For this test a wide field of view was used which allowed for the cameras to track the plate well after the initial deformation. The test setup and camera parameters are listed in Table 5.4:

DOB (in)	SOB (in)	Frame Rate	Exposure Time (μs)	Resolution
0.65	1.22	26143	5	256 x 256

Table 5.4: Deformation Test 7 Parameters

Sources of Error

One of the cameras used for this test experienced some timing problems. Although the cameras were properly synchronized the exposure rate fluctuates from 4 to 7 μs. Because of this it was necessary to manually find the seed point every few frames. Although it was tedious, it was eventually possible to properly perform the analysis. It is also important to note that in the fourth frame the reported strain value jumped up to a value several orders of magnitude higher than the other values, and has been omitted due to this unreliability. One potential reason for this is that the frame rate was too low; too much deformation occurred between these frames which can distort the analysis procedure. Lastly, there was a bright reflection occurring for several frames causing portions of deformation profile data to be unobtainable.

Center Point Displacement and Strain

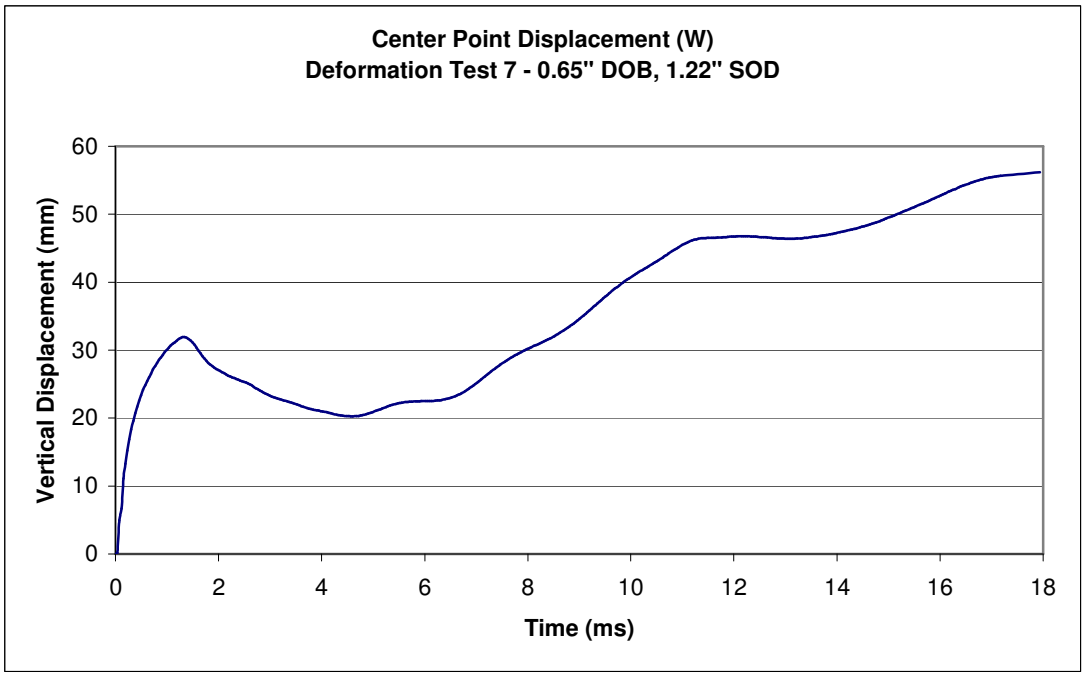

Figure 5.19: Center Point Displacement vs. Time – 0.65" DOB, 1.22" SOD

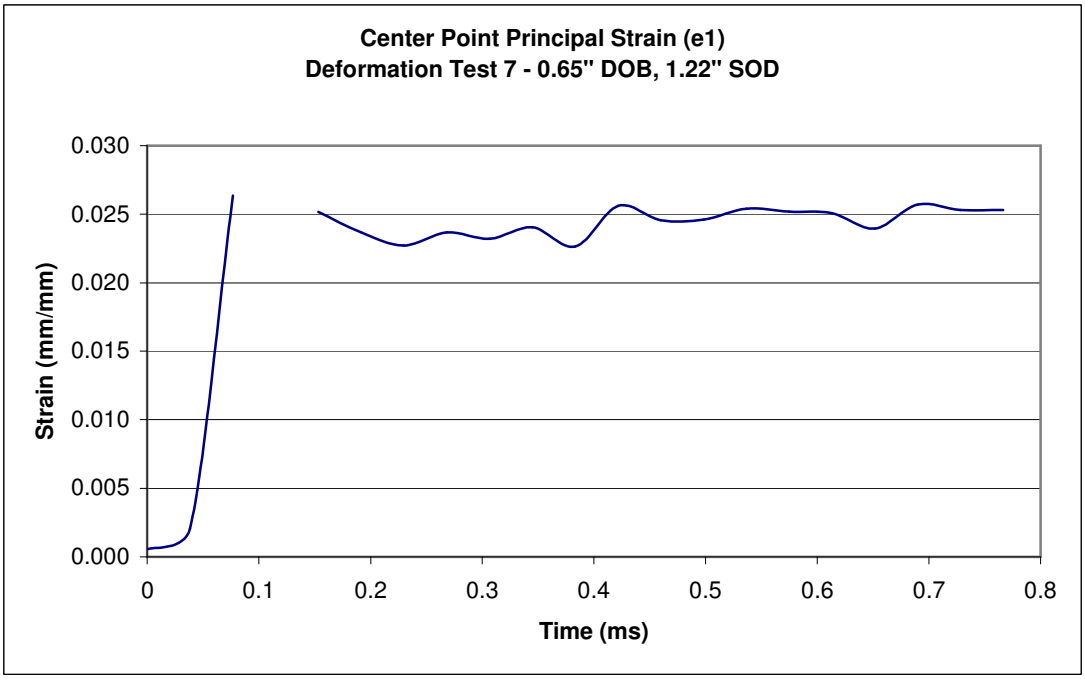

Figure 5.20: Center Point Principal Strain vs. Time – 0.65" DOB, 1.22" SOD

Deformation Profiles

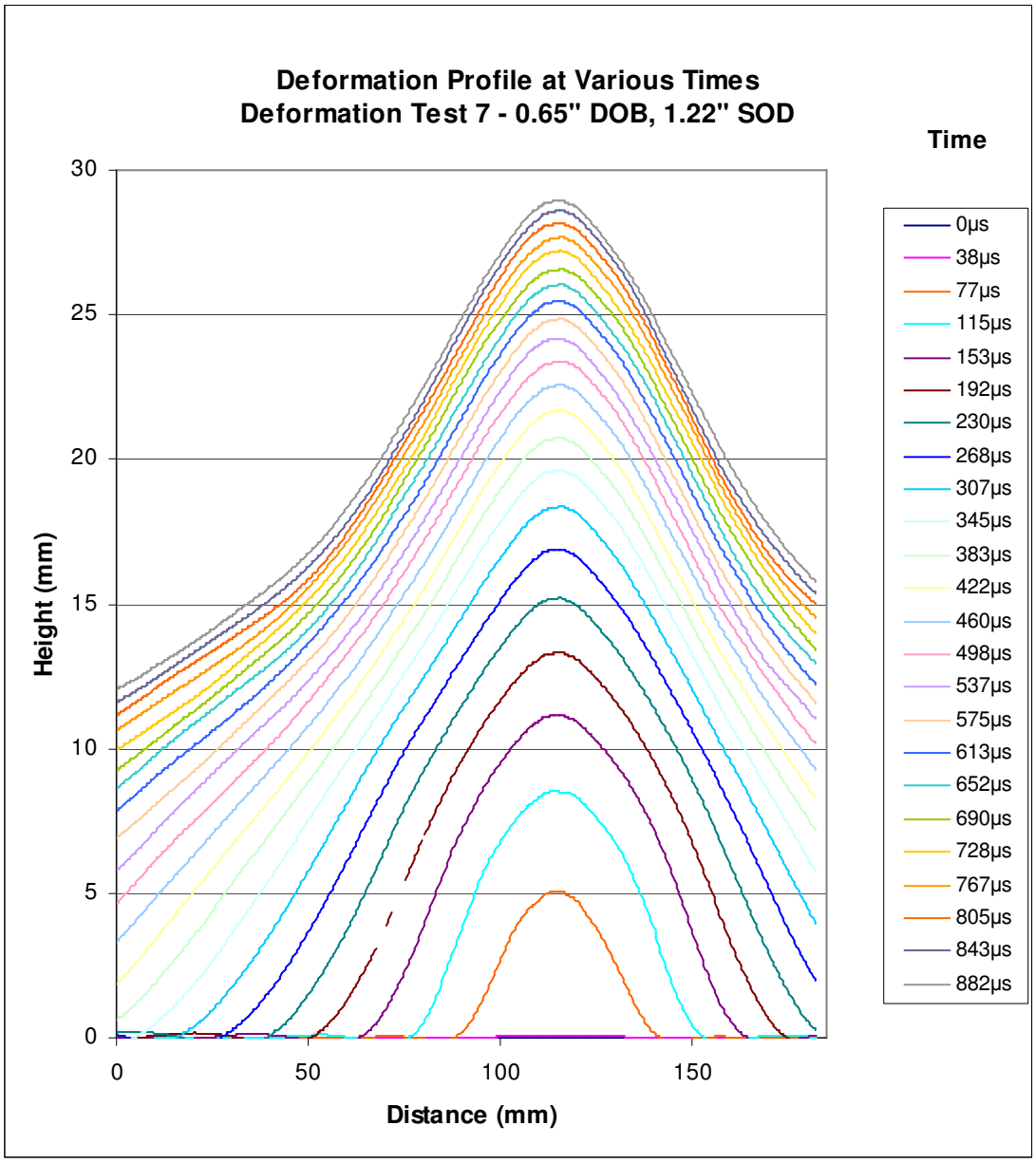

Figure 5.21: Deformation Profile at Various Times – 0.65" DOB, 1.22" SOD

5.3.4 3D DIC Test Results: Mid-Depth 0.65” DOB, 1.22” SOD (DT 10)

Description of test conditions

Deformation Test 10 uses the exact same conditions as the previously discussed one, except with a higher frame rate and lower resolution. The test setup and camera parameters are listed in Table 5.5:

DOB (in)	SOB (in)	Frame Rate	Exposure Time (μs)	Resolution
0.65	1.22	65573	7	128 x 128

Table 5.5: Deformation Test 10 Parameters

Sources of Error

For this test the calibration images were not ideal, and the software calibration took a considerable amount of time and tweaking. The biggest problem was that the center pixel of the image was reported to be a negative number. However, it was eventually possible to salvage the test and obtain a successful calibration by using the right subset of images. The data was analyzed automatically using the same seed point throughout, although it was necessary to manually locate it later on in the deformation. For this reason the center point displacement was not tracked for as many frames as some of the other tests, but the crucial earlier region has been obtained. Also, as with other tests in this series, it was necessary to renumber the files due to synchronization problems.

Center Point Displacement and Strain

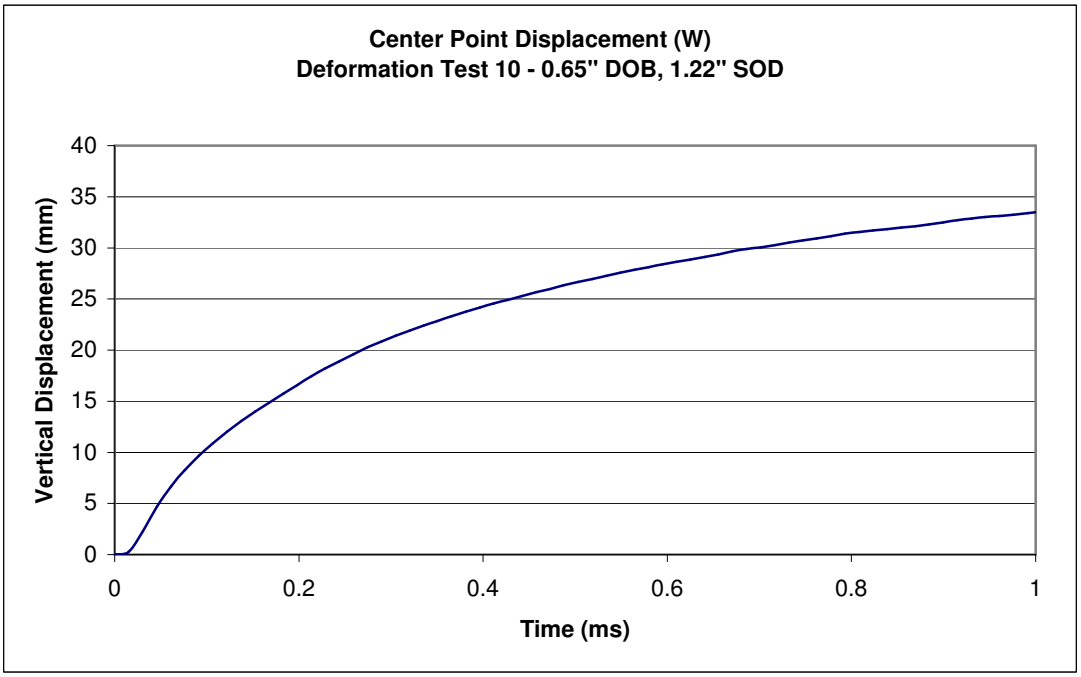

Figure 5.22: Center Point Displacement vs. Time – 0.65" DOB, 1.22" SOD

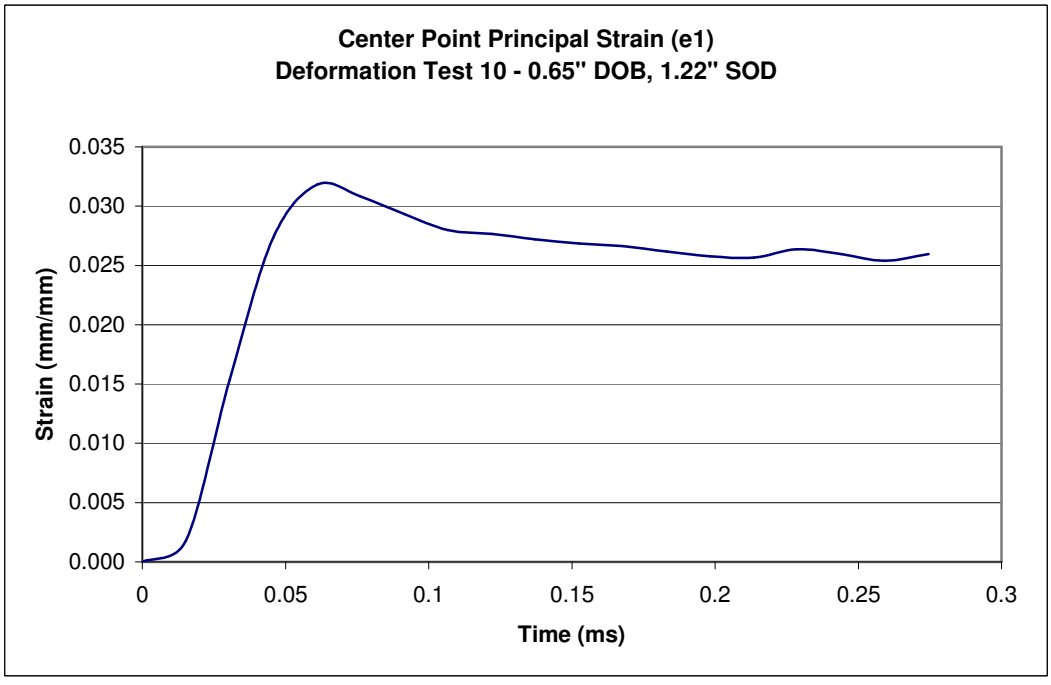

Figure 5.23: Center Point Principal Strain vs. Time – 0.65" DOB, 1.22" SOD

Deformation Profiles

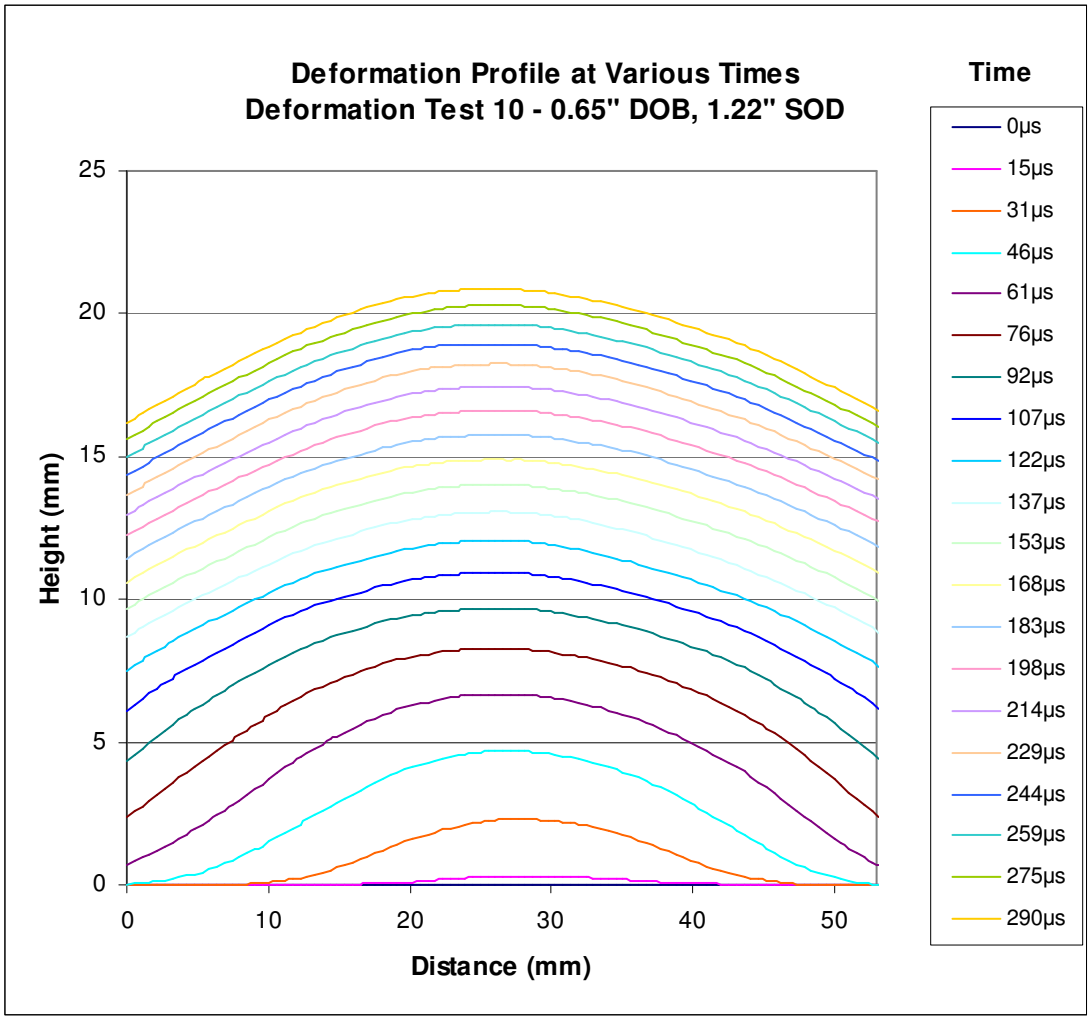

Figure 5.24: Deformation Profile at Various Times – 0.65" DOB, 1.22" SOD

5.3.5 3D DIC Test Results: Deep 1" DOB, 1.22" SOD (USC 2)

Description of test conditions

This test was one of two done with the charge buried deeply; USC Test 5 uses the same physical test parameters but with the camera running at a higher frame rate but obtaining data for a smaller area. These tests were performed in conjunction with visitors from the University of South Carolina, and were processed at USC. The test setup and camera parameters are listed in Table 5.6:

DOB (in)	SOB (in)	Frame Rate	Exposure Time (μs)	Resolution
1	1.22	26143	12	256 x 256

Table 5.6: USC Test 2 Parameters

Sources of Error

The biggest source of error in this test was that one of the cameras used for this test experienced fluctuating time intervals, causing the cine file to flicker. Since this was one of the first 3D DIC tests conducted the importance of a uniquely identifiable mark was not yet realized, so inputting the seed point into the analysis was quite difficult. This series of tests was processed using a copy of Vic-3D located at the University of South Carolina, and the raw data is unavailable. It is ideal to report the larger principal strain e1 but in this case exx, eyy, and exy were reported. However, the shear strain (exy) is negligible at the center, so exx and eyy can be treated as if they are be principal strains.

Center Point Displacement and Strain

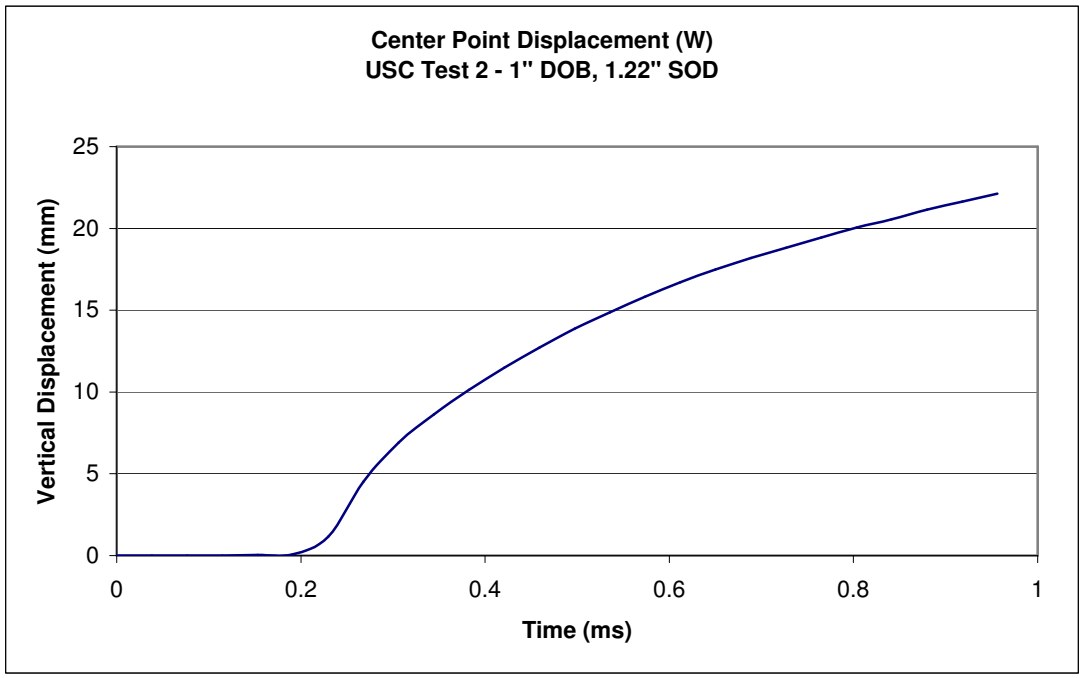

Figure 5.25: Center Point Displacement vs. Time – 1” DOB, 1.22” SOD

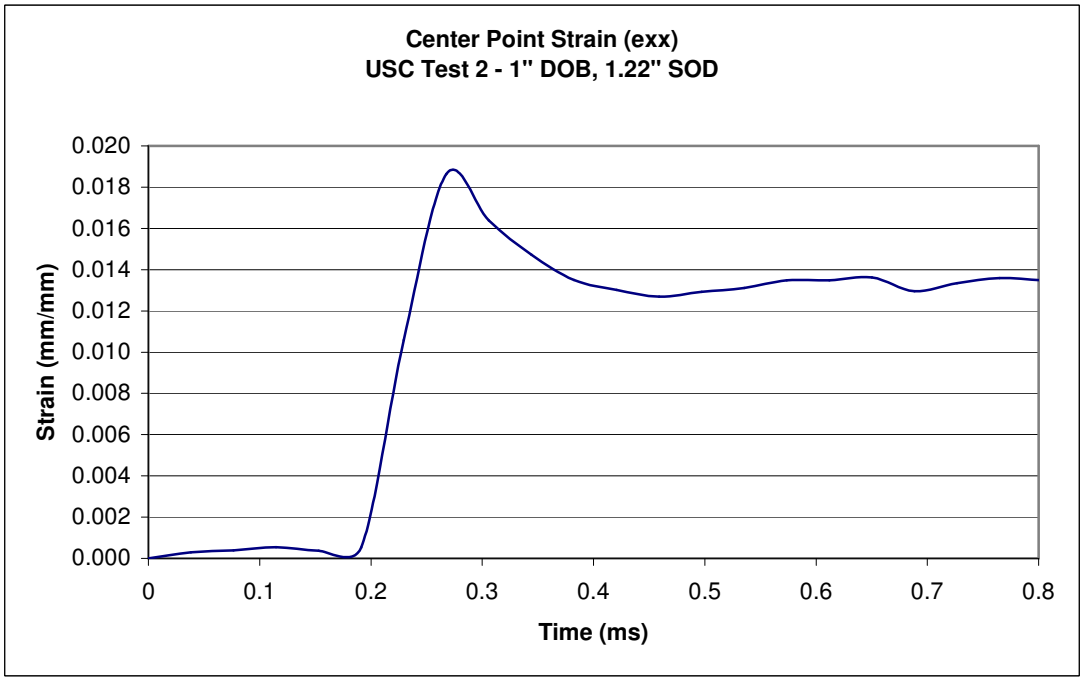

Figure 5.26: Center Point Principal Strain vs. Time – 1” DOB, 1.22” SOD

Deformation Profiles

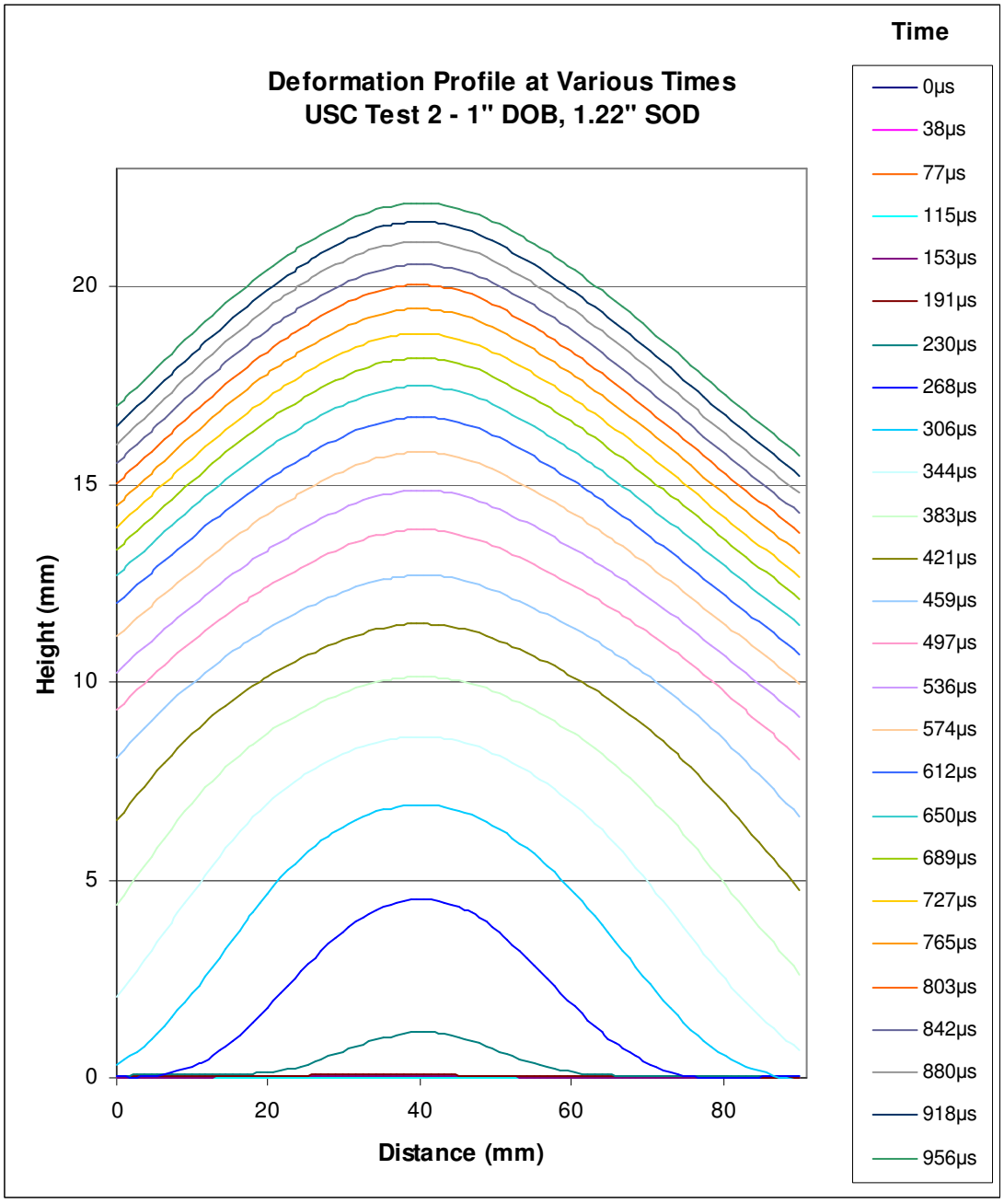

Figure 5.27: Deformation Profile at Various Times – 1" DOB, 1.22" SOD

5.3.6 3D DIC Test Results: Deep 1" DOB, 1.22" SOD (USC 5)

Description of test conditions

This test was the second of two done with the charge buried deeply; USC Test 2 uses the same physical test parameters but with the camera running at a lower frame rate but obtaining data for a larger area. The test setup and camera parameters are listed in Table 5.7:

DOB (in)	SOB (in)	Frame Rate	Exposure Time (μs)	Resolution
1	1.22	61538	10	128 x 128

Table 5.7: USC Test 5 Parameters

Sources of Error

In this test one of the cameras experienced fluctuating time intervals, causing the cine file to get brighter every few frames. Since this was one of the first 3D DIC tests conducted the importance of a uniquely identifiable mark was not yet realized, so inputting the seed point into the analysis was quite difficult. This series of tests was processed using a copy of Vic-3D located at the University of South Carolina, and the raw data is unavailable.

Center Point Displacement and Strain

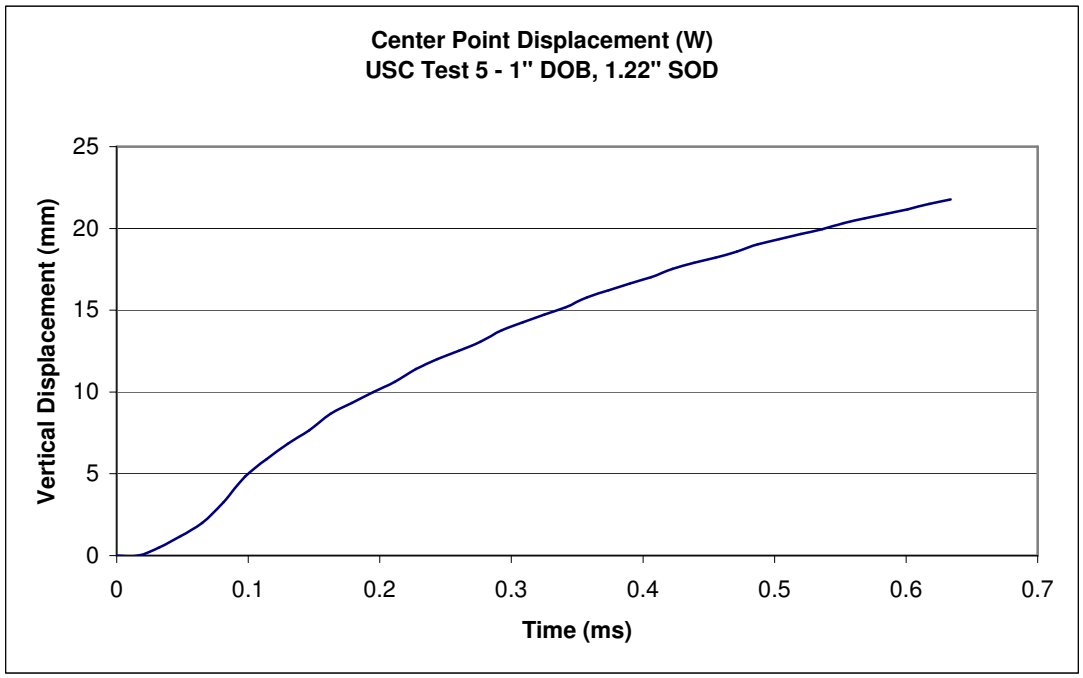

Figure 5.28: Center Point Displacement vs. Time – 1” DOB, 1.22” SOD

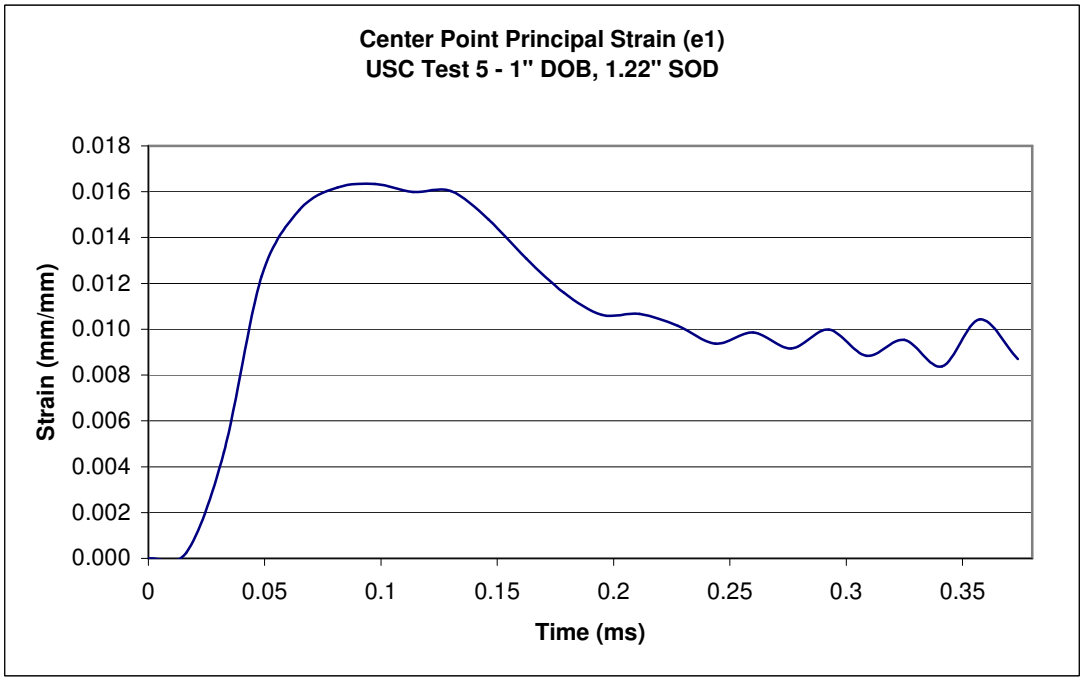

Figure 5.29: Center Point Principal Strain vs. Time – 1” DOB, 1.22” SOD

Deformation Profiles

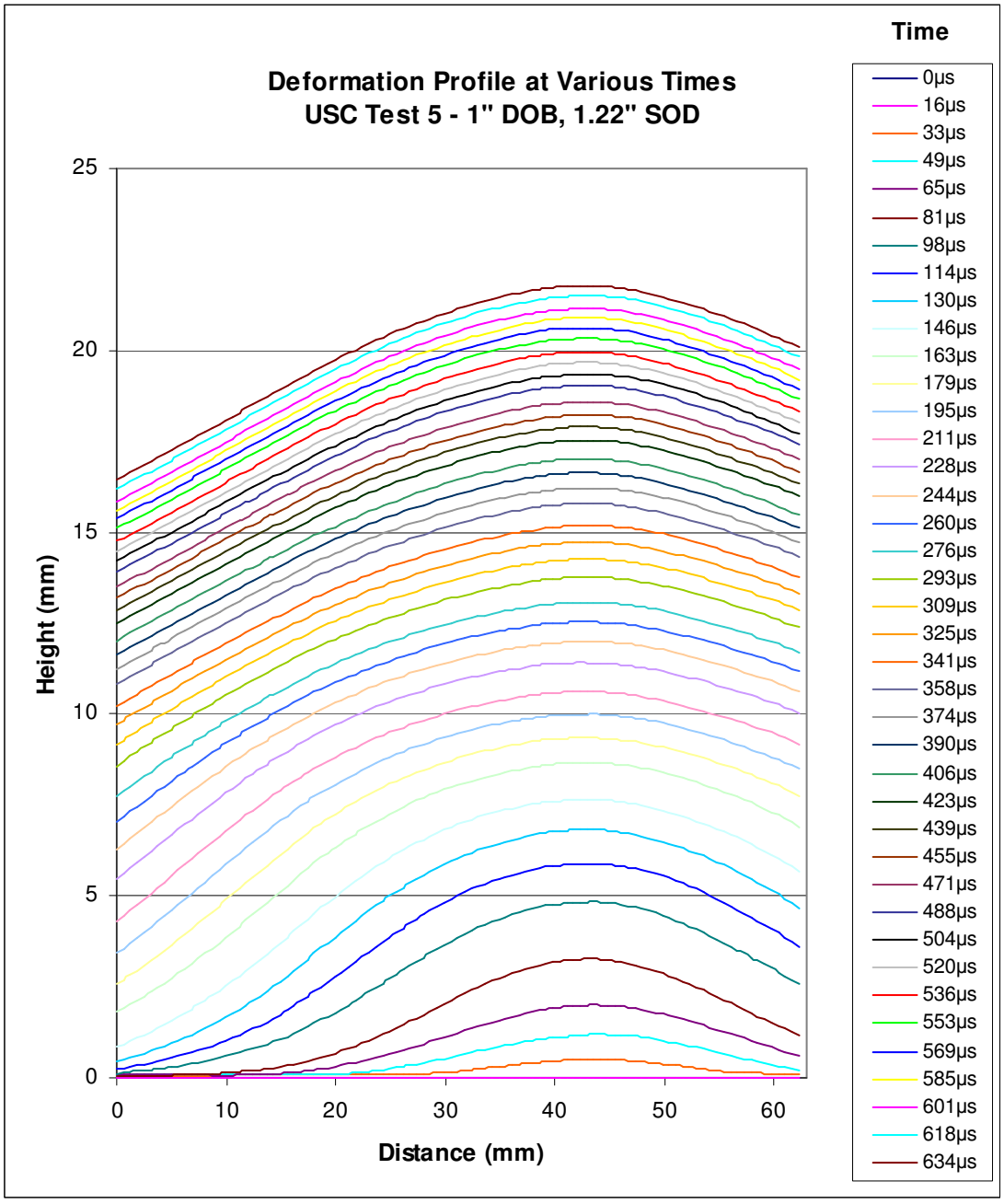

Figure 5.30: Deformation Profile at Various Times – 1" DOB, 1.22" SOD

5.3.7 3D DIC Test Results: Deepest 1.22” DOB, 1.22” SOD (DT 11)

Description of test conditions

As is common throughout all tests, 1 gram of effective charge was used, along with a 1/16th inch aluminum plate. This was the deepest depth of burial used. The test setup and camera parameters are listed in Table 5.8:

DOB (in)	SOB (in)	Frame Rate	Exposure Time (μs)	Resolution
1.22	1.22	65573	7	128 x 128

Table 5.8: Deformation Test 11 Parameters

Sources of Error

For this test the calibration images were not perfect, and the software calibration took a considerable amount of time and tweaking. The detected center pixel value reported by the calibration process was not close to the actual image center. Depending on how the calibration was performed the displacement numbers were off by up to a few millimeters, which is usually less than a few percent. For this test it was also necessary to renumber the files due to synchronization problems.

Center Point Displacement and Strain

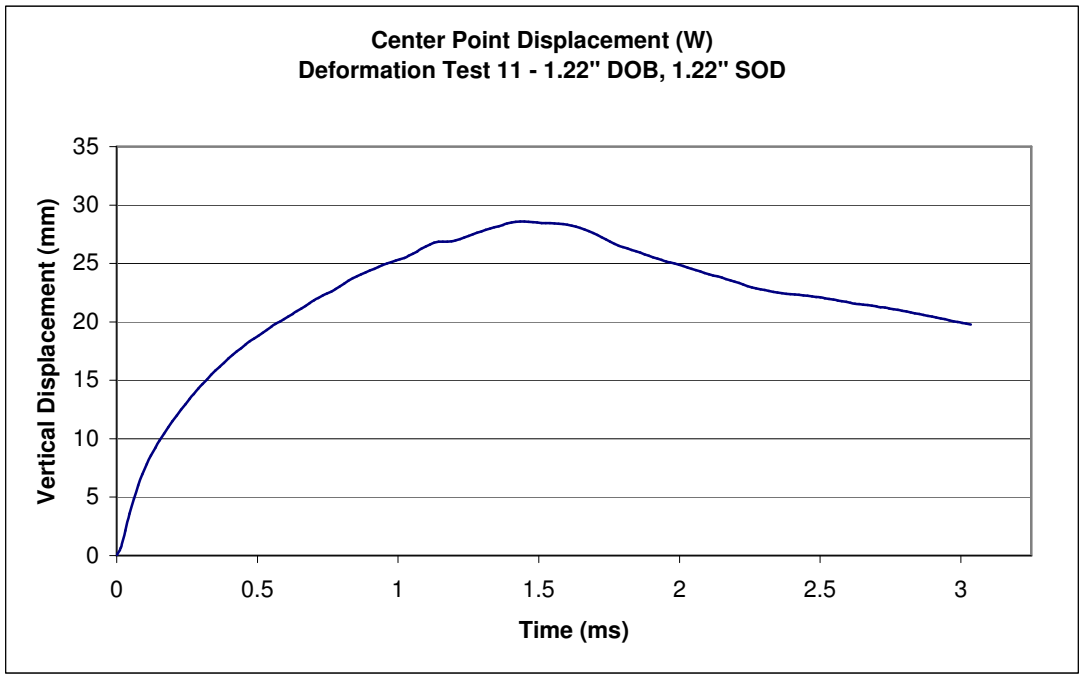

Figure 5.31: Center Point Displacement vs. Time – 1.22” DOB, 1.22” SOD

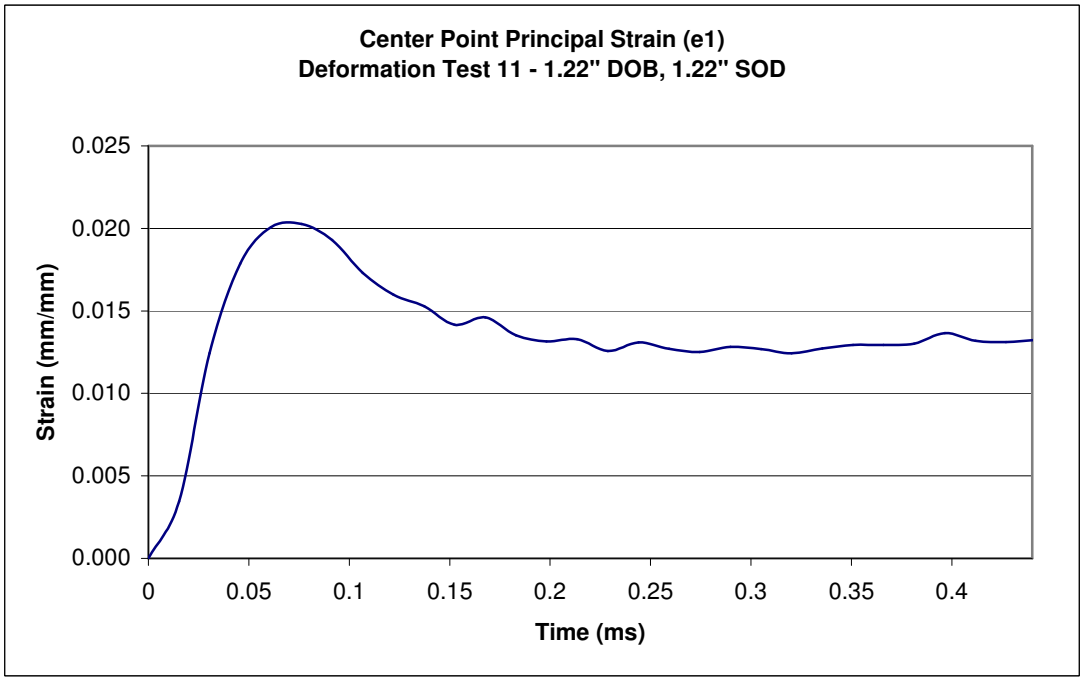

Figure 5.32: Center Point Principal Strain vs. Time – 1.22” DOB, 1.22” SOD

Deformation Profiles

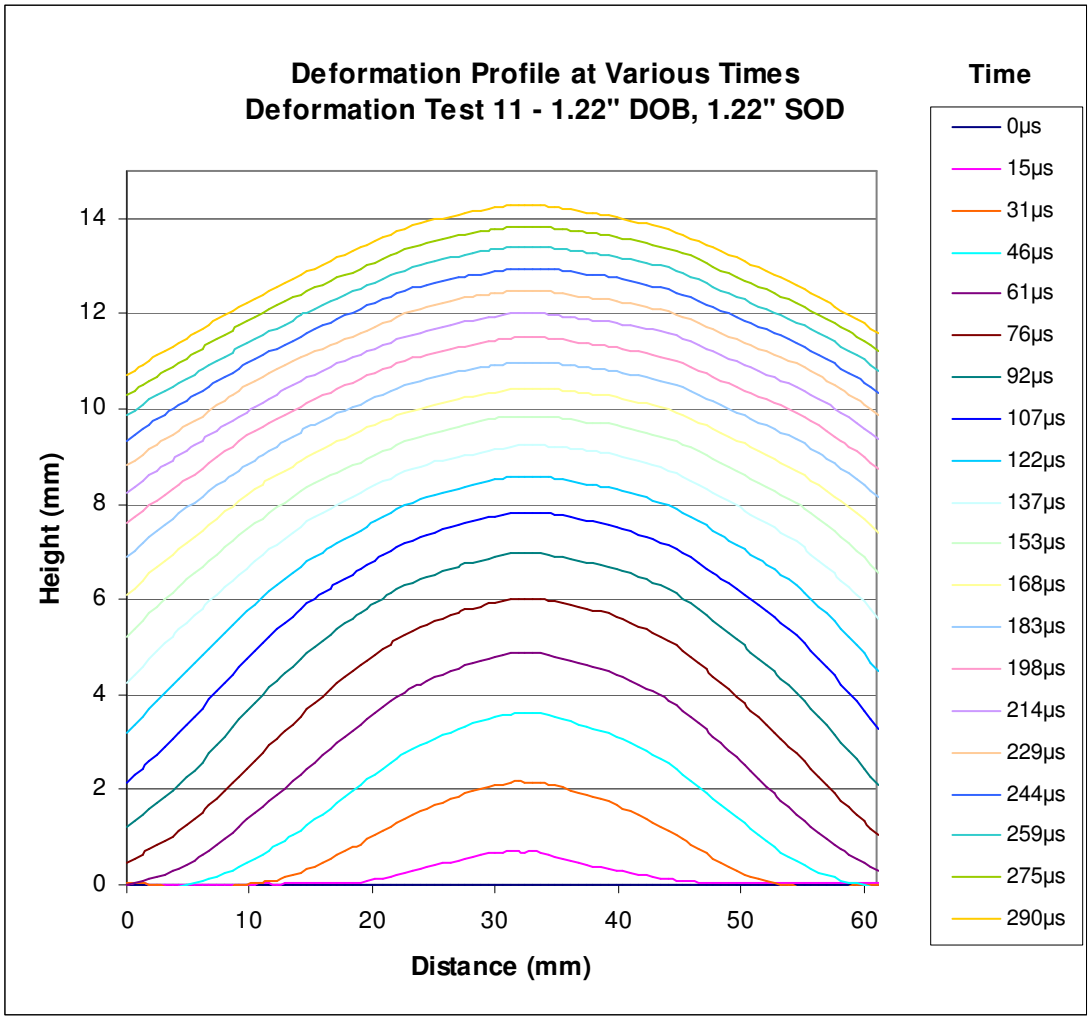

Figure 5.33: Deformation Profile at Various Times – 1.22" DOB, 1.22" SOD

5.3.8 3D DIC Test Results: Zero Standoff 1.22" DOB, 0" SOD (DT 12)

Description of test conditions

Although the standoff distance was kept at 1.22" for all other tests, this one was conducted with the plate sitting directly on the surface of the sand. As is common throughout all tests, 1 gram of effective charge was used, along with a $1/16^{th}$ inch aluminum plate. This test was conducted with the deepest depth of burial. The test setup and camera parameters are listed in Table 5.9:

DOB (in)	SOB (in)	Frame Rate	Exposure Time (μs)	Resolution
1.22	0	65573	7	128 x 128

Table 5.9: Deformation Test 12 Parameters

Sources of Error

Data processing was quite difficult for this test because there was no unique identifiable mark to seed the analysis. For this reason it was necessary to carefully examine the pictures and find corresponding spots in each one. However, once this was accomplished the analysis went smoothly. The calibration images were not of high quality either, but enough were taken that a useable set was obtainable. Data accuracy is also slightly compromised by the fact that it was necessary to renumber the files due to synchronization problems with the Phantom cameras. Lastly, there was a bright reflection into one of the camera lenses once the deformation began, but this only slightly warped the data in a small area.

Center Point Displacement and Strain

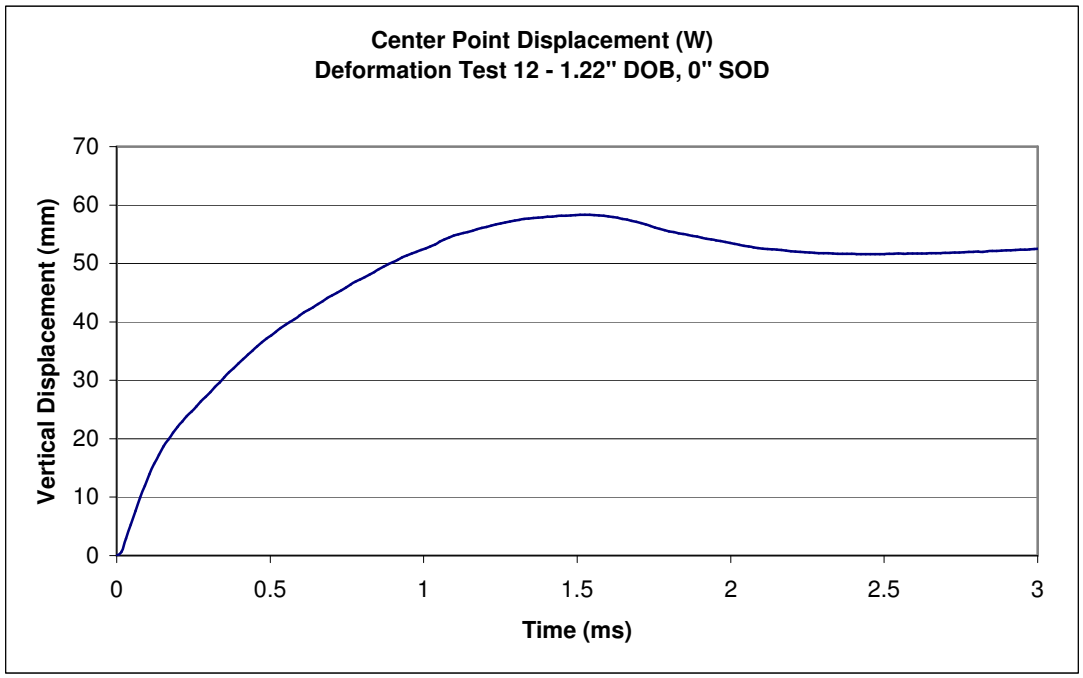

Figure 5.34: Center Point Displacement vs. Time – 1.22” DOB, 0” SOD

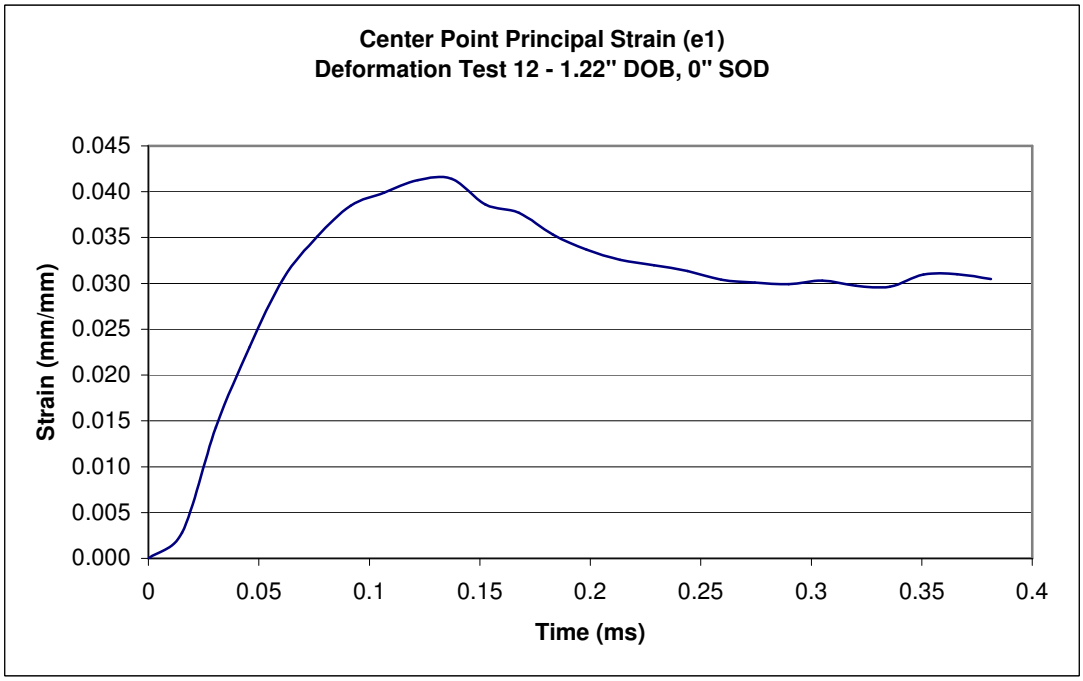

Figure 5.35: Center Point Principal Strain vs. Time – 1.22” DOB, 0” SOD

Deformation Profiles

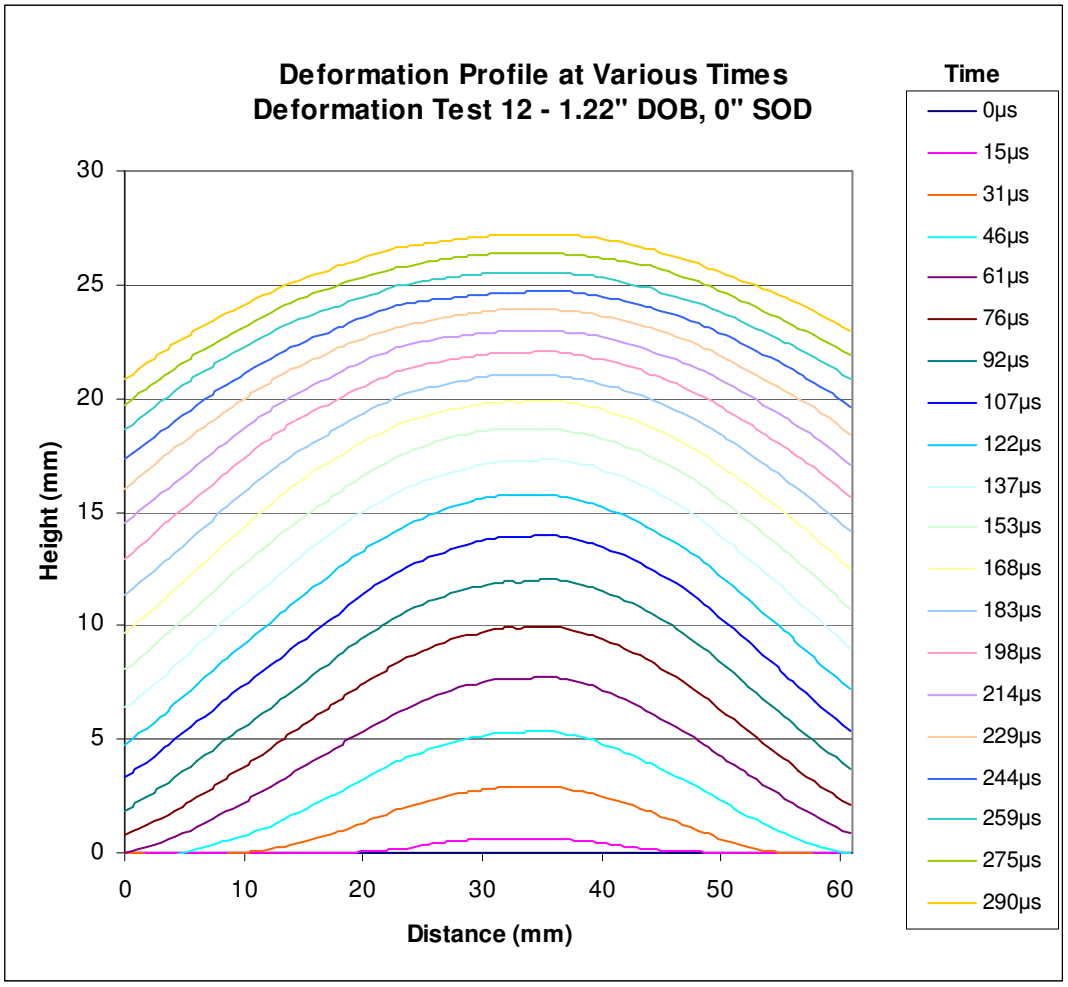

Figure 5.36: Deformation Profile at Various Times – 1.22” DOB, 0” SOD

5.3.9 Comparison of Tests

Various quantities were computed using the center point displacement and strain data reported in the previous section. Using the displacement curves the initial velocity was approximated by drawing a line through the first few points of the data, in the region that is approximately linear. The slope of this line was computed to determine the initial velocity. Initial strain rates were computed in the same manner by using the strain curves and fitting a straight line to the initial region. The maximum strain value and the final (steady-state) strain of the center of the plate were also noted. Lastly, acceleration calculations were done to determine the peak acceleration of the center of the plate. Unfortunately, only rough accelerations could be obtained. This is due to camera frame-rate limitations. The interval between images is too high to capture enough frames in the early stages of deformation, and the maximum acceleration reported ends up being dependent on which frame rate was used. In reality, the plate most likely experienced accelerations for a short period of time that were higher than the calculated values. The approximate maximum acceleration values are shown in Table 5.10, along with the other results:

Description	Name	Initial Vel. (m/s)	Max. center strain	Final center strain	Strain rate (/s)	Approx. max. accel. (m/s^2)
Surface Blast	DT 9	200	0.0508	0.0445	1417	13,400,000
Shallow	USC 4	163	0.0281	0.0258	1086	6,900,000
Mid-Depth	DT 7	78	0.0263	0.0252	633	3,100,000
	DT 10	157	0.0318	0.0260	838	7,300,000
Deep	USC 2	75	0.0186	0.0135	263	1,600,000
	USC 5	87	0.0163	0.0095	473	1,900,000
Deepest	DT 11	87	0.0203	0.0127	472	3,400,000
0" SOD	*DT 12*	148	0.0414	0.0303	664	7,000,000

Table 5.10: 3D DIC Data

Plots have been generated from this data for the tests conducted with the standard 1.22" SOD. They are shown as Figure 5.37, Figure 5.38, Figure 5.39, and Figure 5.40:

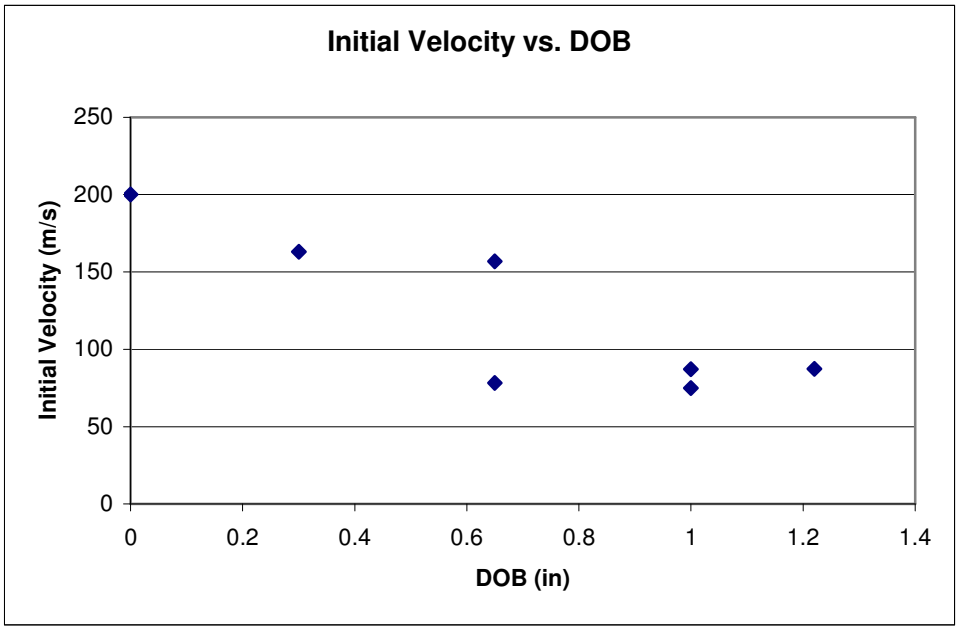

Figure 5.37: 3D DIC Results for Center Point Initial Velocity vs. DOB

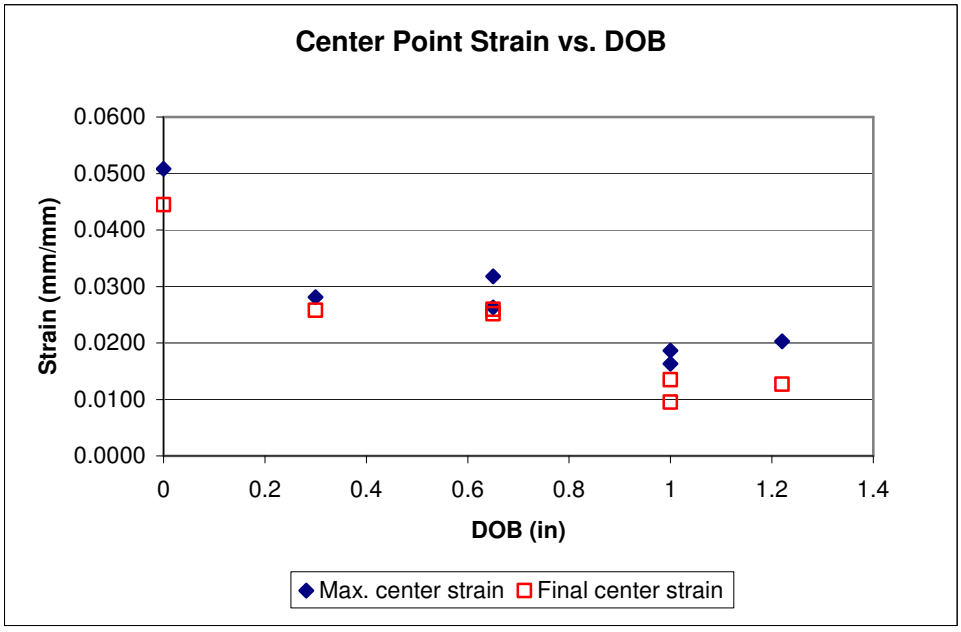

Figure 5.38: 3D DIC Results for Maximum and Final Strain vs. DOB

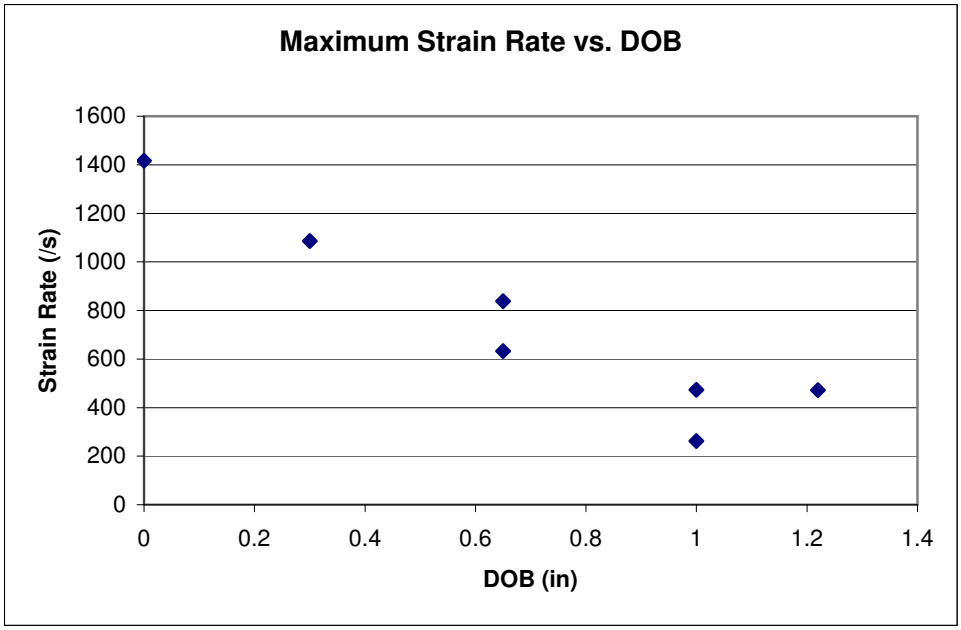

Figure 5.39: 3D DIC Results for Center Point Strain Rate vs. DOB

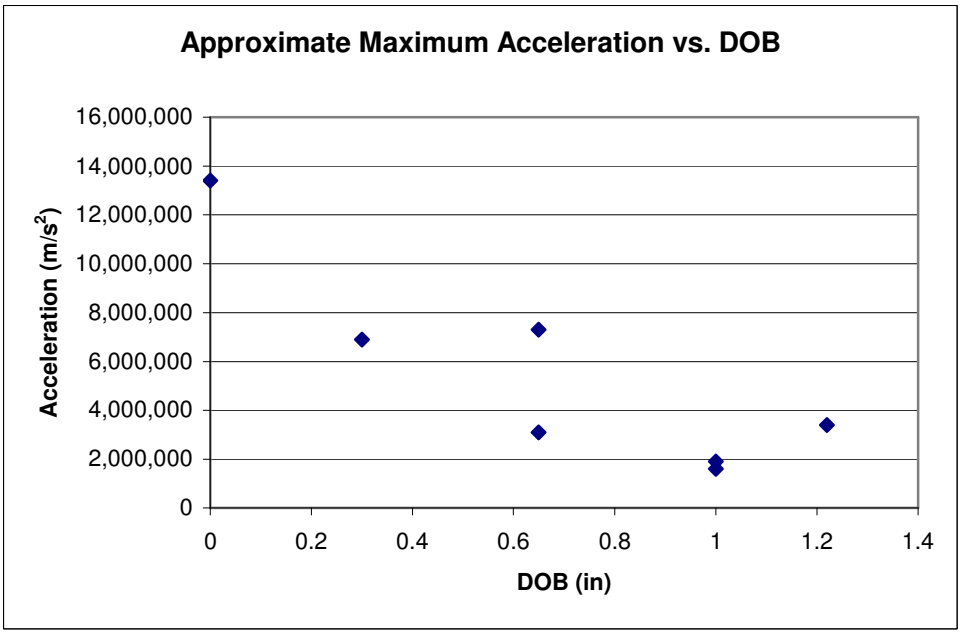

Figure 5.40: 3D DIC Results for Maximum Center Point Acceleration vs. DOB

For most depths of burial it was only possible to obtain data from a single test. For 1" DOB two tests were performed with different resolutions, and similar results were obtained. However, for 0.65" DOB the test data does not agree well. The test (DT 7)

producing the lower acceleration and initial velocity values used a very large field of view and was quite difficult to analyze. The resolution may not have been high enough because this test attempted to photograph the entire plate while maintaining an adequate frame rate. For this reason the data at the center point may not have been composed of enough pixels, and the other test point for 0.65" is likely more accurate.

It is somewhat surprising that all of these measured values tend to decrease as the DOB is increased. It was established in Chapter 4 that the damage done by the charge initially increases as it is buried deeper, and then begins to decrease, but this trend is not observed in initial velocity and center point strains. It seems that although an unburied charge (0" DOB) inflicts less total damage, it causes greater localized strains and accelerations at the center of the plate than a blast with sand ejecta.

Chapter 6: FEM Computer Analysis

6.1 Basics of the Finite Element Method

The Finite Element Method (FEM) is a numerical technique used for finding approximate solutions to problems that typically cannot be solved analytically or in closed form. This is especially useful for non-linear plasticity problems such as the explosive deformation of a flat plate. Pressures can be applied by dividing the plate into nodes and discrete elements, and the resulting dynamic deformation can be calculated. As discussed in Section 4.1, it is assumed that the pressure distribution and plate characteristics are the same along any circumferential path. This "symmetry of the structure and its loading about the vertical axis" means that "this class of system is two-dimensional in nature," and the elements "are actually complete rings in the third dimension" [16]. It is easy to visualize that an "axisymmetric element is developed by rotating a triangle or quadrilateral about a fixed axis located in the plane of the element through 360°" [17]. Each nodal point is in fact a complete circular line. Rectangular ring elements were used to model the flat plate, as shown in Figure 6.1:

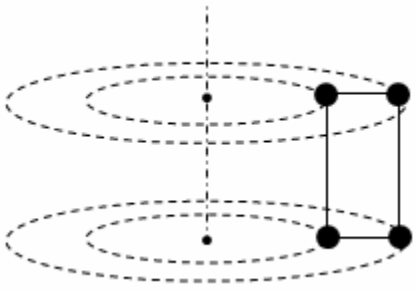

Figure 6.1: Rectangular Ring Element

By modeling the geometry as a simplified axisymmetric circular plate the complexity and runtime of the simulation is greatly reduced.

After selecting an element type, it is necessary to choose a material model. A simple material representation is not possible because the problem at hand involves very high rates of strain; "the strain rate dependence of flow stress is necessary in computational codes if these are to be realistic" [18]. In the field of dynamic material behavior, a model known as the Johnson-Cook equation is the de facto "'workhorse' of constitutive modeling" [18]. It is an important tool in applications where there are large plastic strains, high strain rates, high temperatures, and significant strain hardening. Strain rates of over 1000 s^{-1} have been observed during experimentation, along with plastic strain of over 1, so this model should be suitable.

The Johnson-Cook equation is used to determine the von Mises flow stress as a function of strain, strain rate, and temperature. Von Mises stress is a scalar value that relates a three-dimensional loading to the uniaxial yield stress of a material through use of the deviatoric stress tensor. This is closely related to distortion energy and the von Mises failure theory, which assumes that "yielding is independent of the hydrostatic stress" [19]. The Johnson-Cook constitutive equation is expressed as [20]:

$$\sigma = [A + B\varepsilon^{n}] [1 + C\ln \dot{\varepsilon}^{*}] [1 - T^{*m}]$$

where:

σ = von Mises tensile flow stress

ε = equivalent plastic strain

$\dot{\varepsilon}^{*} = \frac{\dot{\varepsilon}}{\dot{\varepsilon}_0}$ = dimensionless plastic strain rate for $\dot{\varepsilon}_0 = 1.0\ s^{-1}$

$T^* = \frac{T - T_{room}}{T_{melt} - T_{room}}$ = homologous temperature

along with 5 material constants:

A = yield stress

B = hardening coefficient (in units of stress)

n = hardening exponent

C = strain rate coefficient

m = softening exponent

The material constants for 6061-T6 aluminum were not published in the original Johnson-Cook papers, so they were retrieved from a computer material library [21]. The obtained values are similar to the values Johnson and Cook published for 7039 aluminum, and are given in Appendix B. A stress-strain curve was generated using these parameters by holding the material temperature at room temperature and inputting two different strain rates, shown as Figure 6.2:

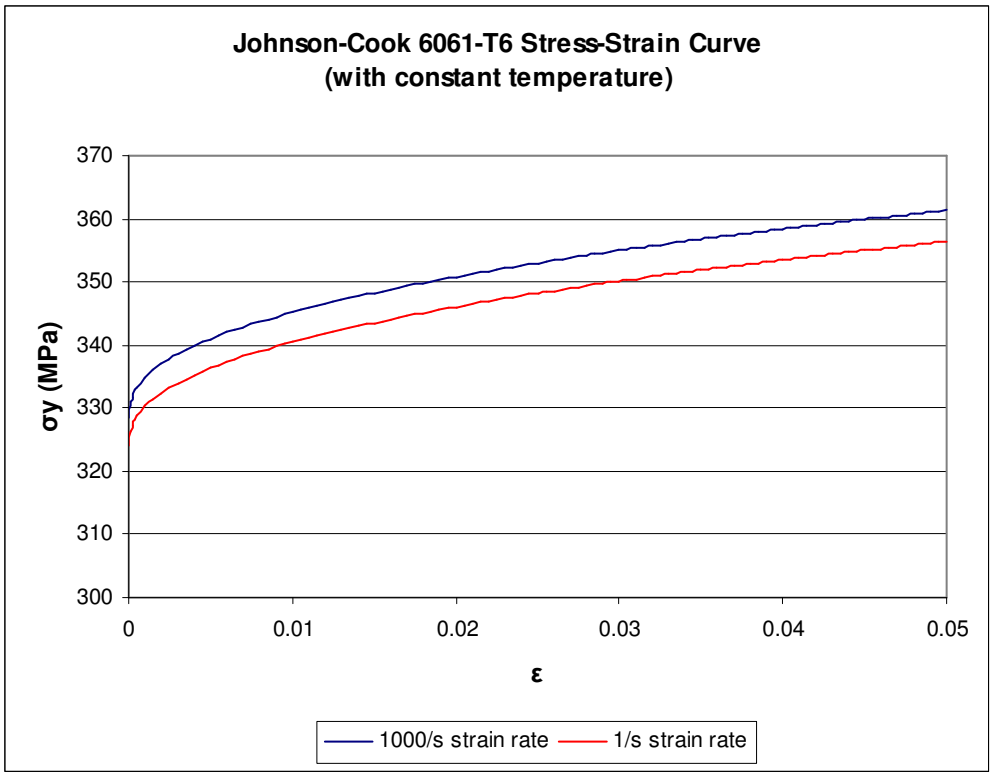

Figure 6.2: Johnson-Cook 6061-T6 Aluminum Stress-Strain Curve

The code does not directly use this strain curve, but rather recalculates the strength at each time instance based on all of the input Johnson-Cook parameters and variables. The simulation also requires an equation of state to determine the pressure response of the material, although it should not noticeably affect the results since there are not significantly high pressures within the material. A simple elastic pressure response was input by defining the EOS pressure as equal to the bulk modulus.

The last important FEM inputs are the boundary conditions. The experimental boundary conditions are quite complex, with the plate held in position through the use of several bolts, and the frame allowed to move freely. This would require very complex modeling and necessitate consideration of gravitational forces. Although the

axisymmetric assumption has thus far been justified, it would greatly simplify the simulation if the outer boundary could be approximated as uniform clamp that does not significantly affect the deformation process. From the high-speed footage this seems to be the case; it is evident that the plastic deformation is complete before the frame begins to move. In Deformation Test 5, the frame is still stationary 1350 μs after the first frame with noticeable deformation, yet the plate has already reached it maximum deformation. This can be noticed in Figure 6.3 and Figure 6.4:

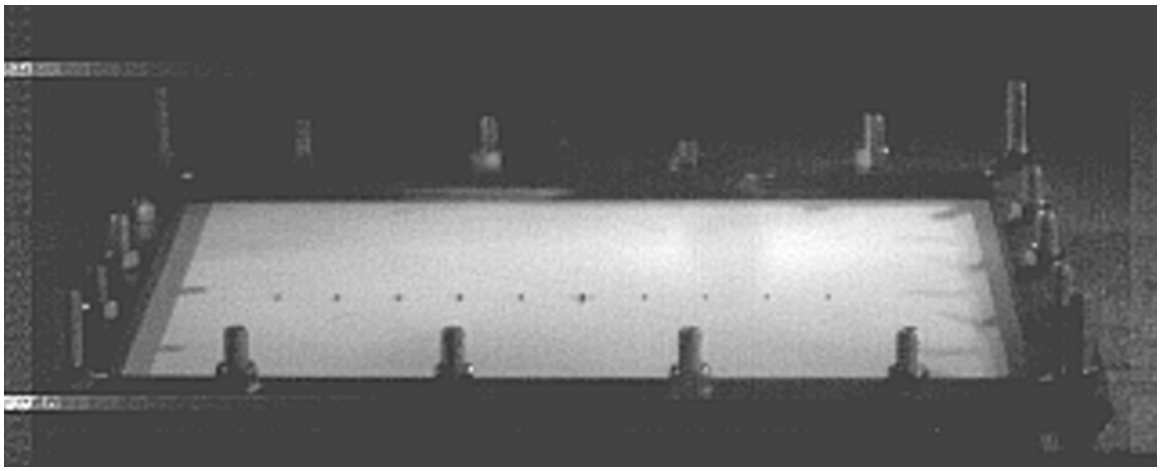

Figure 6.3: Start of Deformation (160 μs After Trigger)

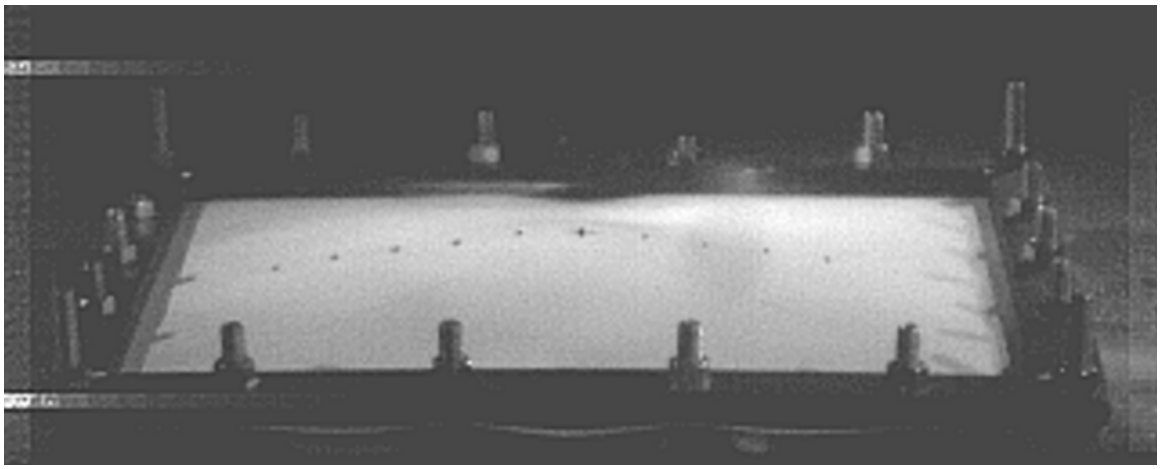

Figure 6.4: Plate at Maximum Deformation (1510 μs After Trigger)

After the plate has achieved its maximum deformation it continues to oscillate as the frame begins to move vertically. By using a rigidly constrained the edge the simulation accurately models the real-life conditions during the time period that the plastic deformation is occurring, but not the subsequent rigid body motion. Also, the reported elastic oscillations may not be accurate due to the simplified boundary condition, but this is not within the scope of this research. The goal of the simulation is to correlate pressure profiles to final deformations and to examine the plastic deformation as it is occurring, neither of which are compromised by this boundary condition.

6.2 LS-DYNA Input Procedure

FEM analysis was conducted using the LS-DYNA software developed by the Livermore Software Technology Corporation. It is a finite element analysis (FEA) program especially designed for nonlinear dynamic analysis of inelastic structures. LS-PrePost (also known as LSTC PrePost-Processing) was used to generate the keyword files that are input into the LS-DYNA solver. It can be accessed through the LS-DYNA Program Manager. LS-PrePost organizes all the commands into seven categories referred to as “Pages.” After initial generation of the keyword file it was often much more efficient to edit the keyword files directly in a word processing program, especially just to tweak certain parameters such as the duration of the simulation.

Using LS-PrePost, the geometry was created using the 2Dmesh option from Page 7. The first step is to select the Create/delete line button, labeled as 1 in Figure 6.5. From here the four lines are created by the using the KeyIn method. The

coordinates of corner point (which are superimposed on the figure) represent a 2D profile of a circular plate. In this software the y-axis is the default axis of revolution.

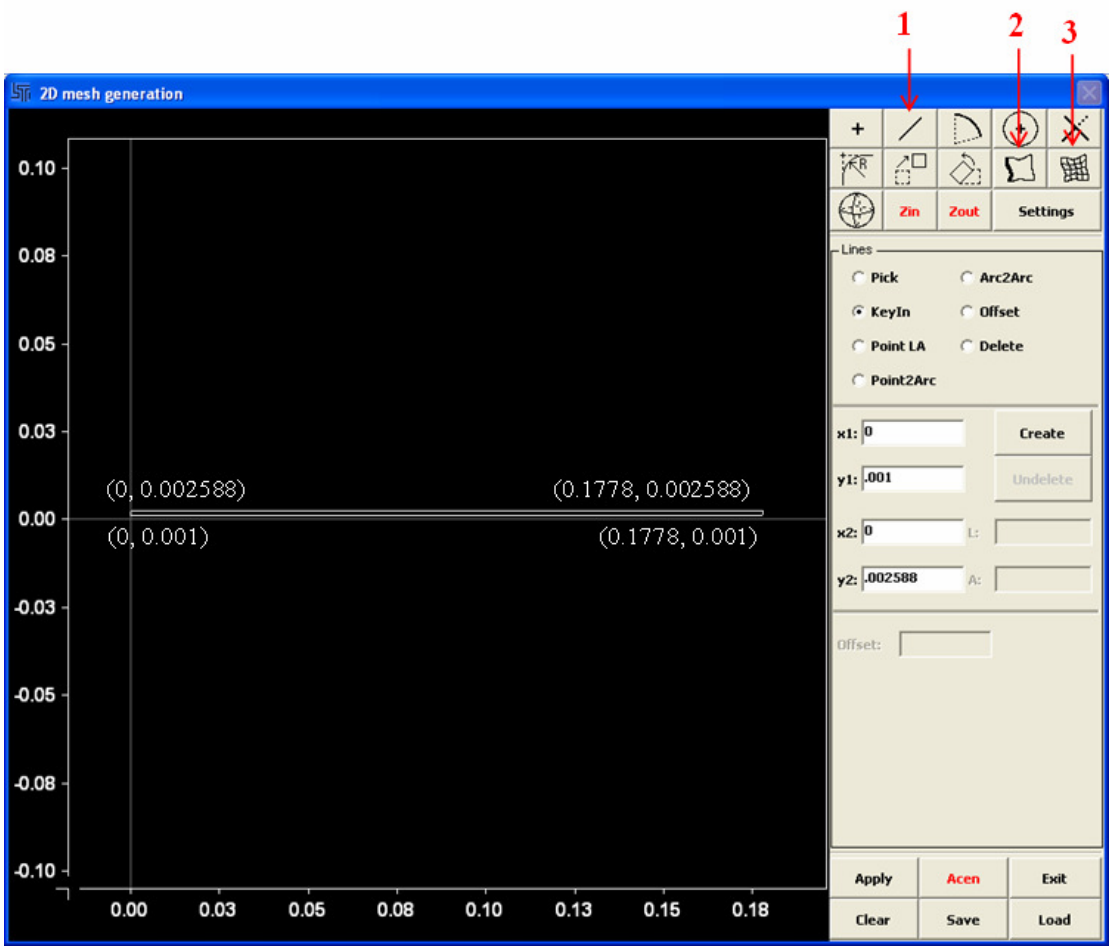

Figure 6.5: LS-PrePost 2D Mesh Generator

The second step in modeling the geometry is to define the number of elements. Each of the four drawn lines must be transformed into an edge using the button labeled 2, where the numbers of elements are selected for each. A different grid density is used depending on the sensitivity of the pressure curves. The vertical edges are divided into 4 elements, whereas the horizontal edges are divided into either 40 or 80 elements. The third and final step in the 2D mesher is generating the mesh. A structured quad mesh is created by selecting the four edges using the button labeled

3, starting with the bottom edge and then proceeding counter-clockwise. This ensures the node convention is sequential along the area of pressure application. Once the geometry is created the rest of the keyword file generation is more straightforward. The keyword inputs are located throughout the LS-PrePost pages. The best resource for locating the necessary commands is the LS-PrePost Online Documentation [22], which also has useful tutorials. The keywords are described more in depth in the Keyword User's Manual [23]. Keywords need to be defined for boundary conditions, material properties, data outputs, and more. Appendix C explains the different commands used for the thesis simulations. In Section 6.5 the unique method used to input the pressure curves into the DYNA code is discussed. After the keyword file has been created preprocessing is complete. Simulations were then run using version 971 of the LS-DYNA solver.

6.3 LS-DYNA Data Extraction

After the simulation has been run, the data can be extracted using the post-processing features of the LS-PrePost software. It is first necessary to open the binary output file that was generated by the simulation. The file is typically called d3plot. A final deformation profile plot can be created as long as the simulation was run long enough to allow the vibration to cease. After selecting the Mesh render option from the bottom, the Ident option is selected from Page 1 of the commands. The Area select method is used to choose all of the nodes on the top surface of the plate. This surface was selected because it is the most important in a full-scale vehicle since it represents the inside of the floorboard. This is in closest proximity to the passengers. The 3D displacement fields and the final deformations are also relative to the top

surface. Due to the thinness of the plate the deformation of the mid-surface or the bottom surface would be very similar to the top, but consistency was maintained by always selecting the top surface. This data can be exported by clicking the History button from page 1, selecting the Nodal option, Y-displacement, and then clicking the Plot button. By selecting the Save option the data can be exported into the comma-separated values (csv) file which can be easily manipulated in Excel. After selecting a row of data at a late time the final deformation profile can be plotted.

The History option can also be used to output the nodal time history results for the center node. A plot can be generated of the Y-displacement, velocity or acceleration, and can be exported in the same manner.

6.4 Code Validation

In order to validate the results of the DYNA FEM code, a test was performed for which the pressure and deformation could be easily controlled and measured. Since it was not feasible to apply known dynamic pressures similar to those caused by an explosion, a slowly increasing force was applied. A Tinius Olsen H25KT Universal Testing Machine (UTM) was used to deform the plate at a rate of about 0.1 inches per minute, as show in Figure 6.6:

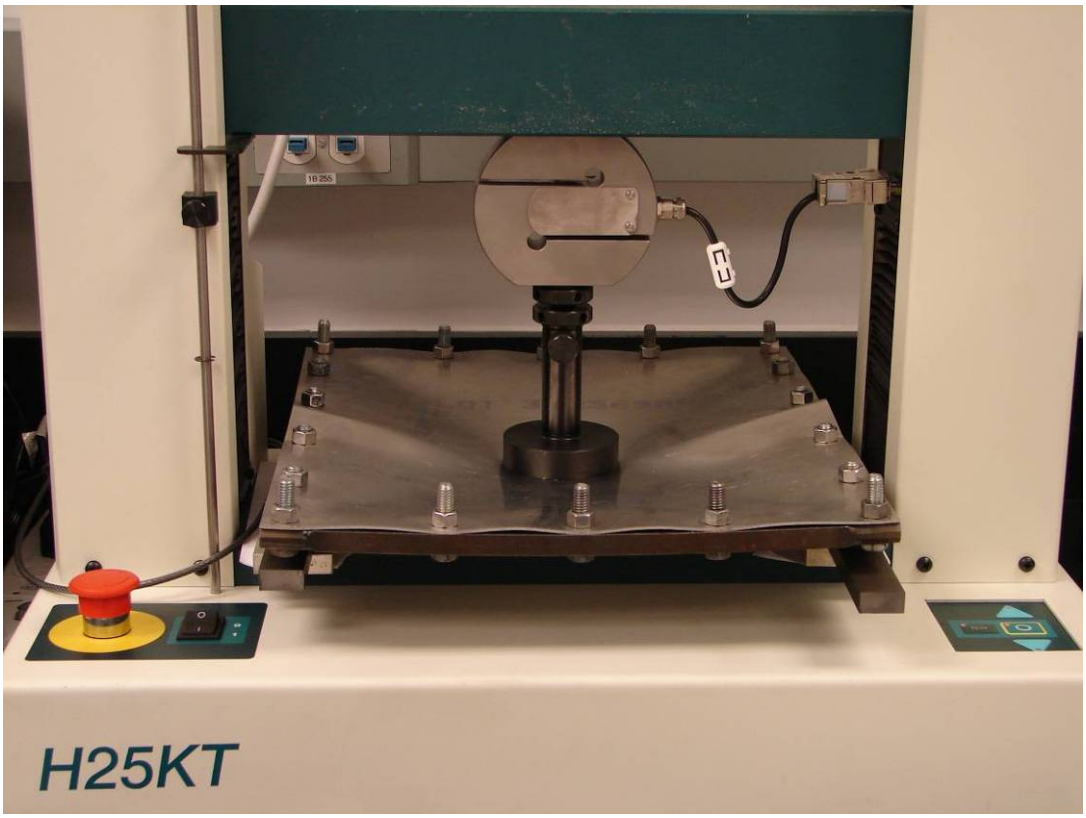

Figure 6.6: Plate in Universal Testing Machine at Maximum Deformation

The load was applied to the center of the plate using a 3 inch diameter attachment, and the resulting force-deformation data is shown in Figure 6.7:

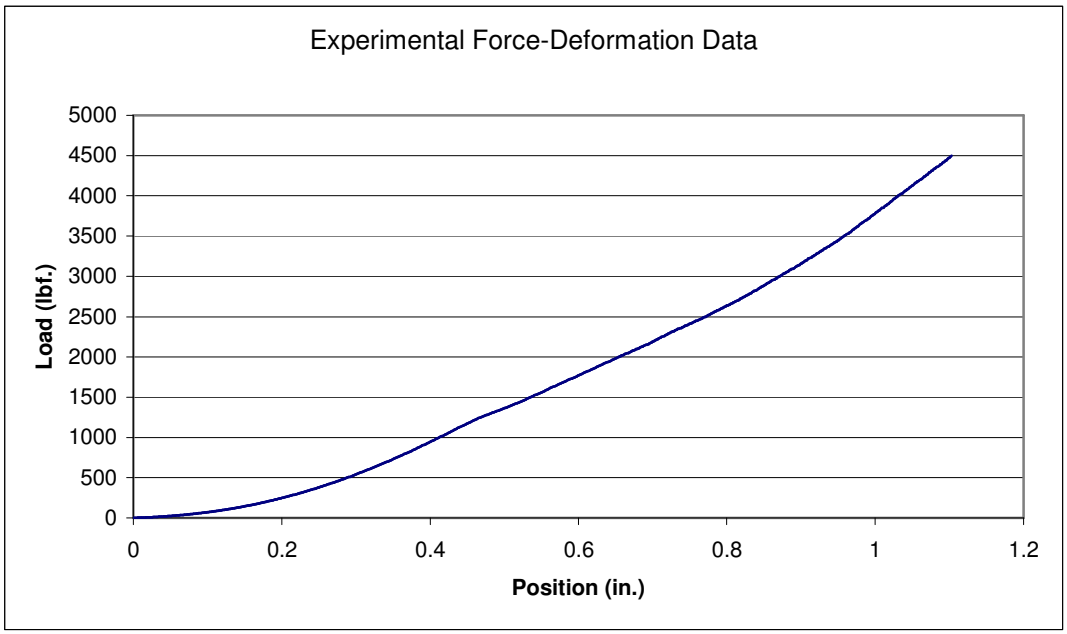

Figure 6.7: Experimental Force-Deformation Data

Buckling of the plate along the outside was observed after about 0.4 inches of deformation. It can be noticed in the data as a change in the slope occurring at this location. Since buckling is not an axisymmetric behavior, the load and position before bucking should provide the best point for validation since the simulation is axisymmetric. At 1000 pounds of applied load there is 0.412 inches of observed deformation. In order to simulate the test in DYNA, a code was written in which the load is ramped up to 4500 pounds (included as Appendix D). Due to computational limitations, the load is applied at a much quicker rate than the experiment, and reaches the final load in 0.1 seconds. Other simulations were run with various loading rates which showed that this has little effect on the deformation as long as the load is not instantaneously applied.

In order to input the load into LS-DYNA, it was necessary to assume the force was evenly applied over the contact area as a uniform pressure. In the axisymmetric

representation each nodal force represents a circumferential line load, so it is necessary to determine the force per unit circumferential length to be applied to each node in order to obtain the desired total force applied to the plate. A simple calculation can be performed accounting for the number of nodes in the contact area as well as the distance of each node from the center. For example, if 100 pounds per inch is applied to a node 0.5 inches from the center, the total force contribution of that node would simply be:

$$100\frac{lb}{in} * 2\pi(0.5in) = (100\pi)lb$$

By summing these circumferential line forces the total force can be obtained. The process of converting an area pressure into multiple circumferential line loads can be seen in the pictorial shown as Figure 6.8:

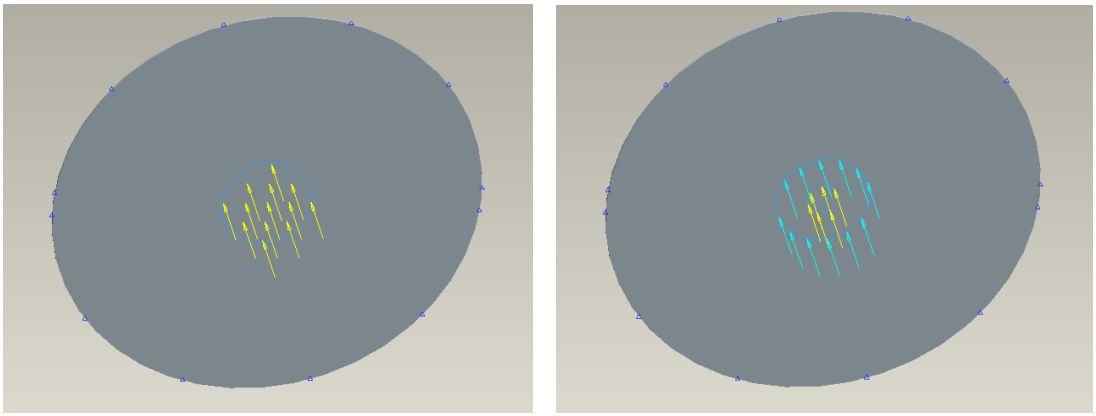

Figure 6.8: Illustration of Converting a Uniform Pressure Into Line Loads

After the required line loads have been determined they can be applied to each node in LS-DYNA, and the code can be run. At 0.02 seconds into the simulation the load has reached the desired 1000 pounds for validation. The deformation is shown in Figure 6.9:

Figure 6.9: Deformation of Plate at 1000 Pound Applied Load

The deformation of the center of the plate at this time in the simulation is 0.334 inches, as compared to the 0.412 inches of deformation measured by the UTM, a difference of about 20%. It is not unreasonable for the UTM test to have slightly more deformation since this measurement includes the compliance of the supporting fixture as well as any possible plate slippage around the bolts (since it is impossible to completely fix the edges of the plate due to physical constraints). In Figure 6.10 it can be seen that the plate is rippling near the edges and the frame is in fact bending, contributing to an inflated displacement measurement:

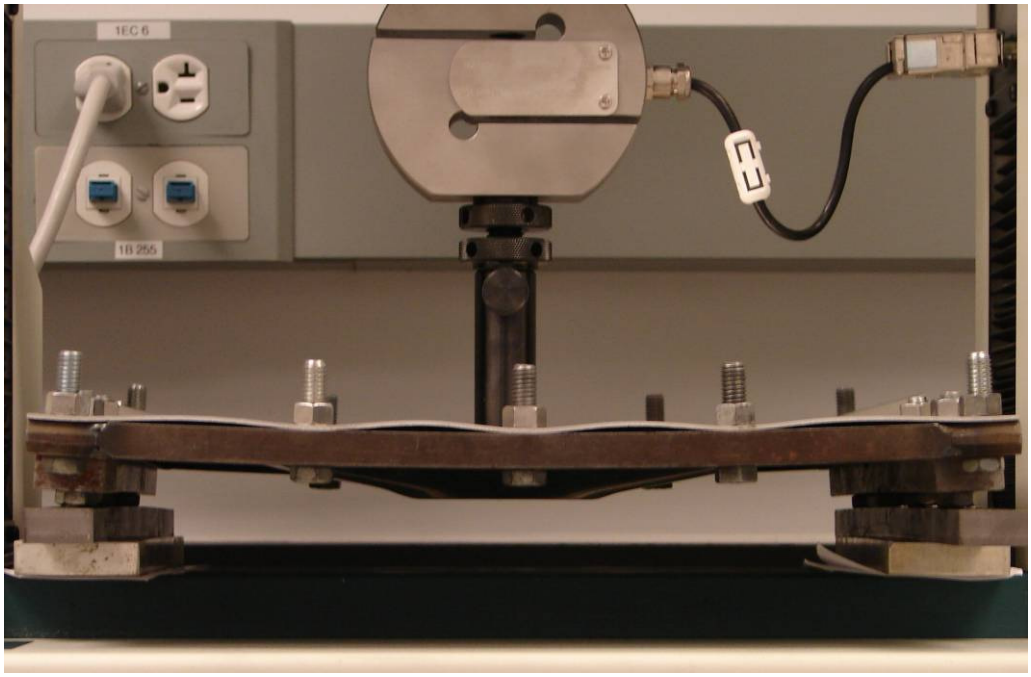

Figure 6.10: Testing Rig

In order to more closely replicate this a second UTM test was conducted with an additional frame on top of the plate to better hold it in place, discourage buckling, and increase frame stiffness. The contact area was also reduced from the 3” diameter previously used to a 1” area cylinder so less applied load would be required to produce deformations, and less stress would be applied to the frame. The second test setup is shown in Figure 6.11:

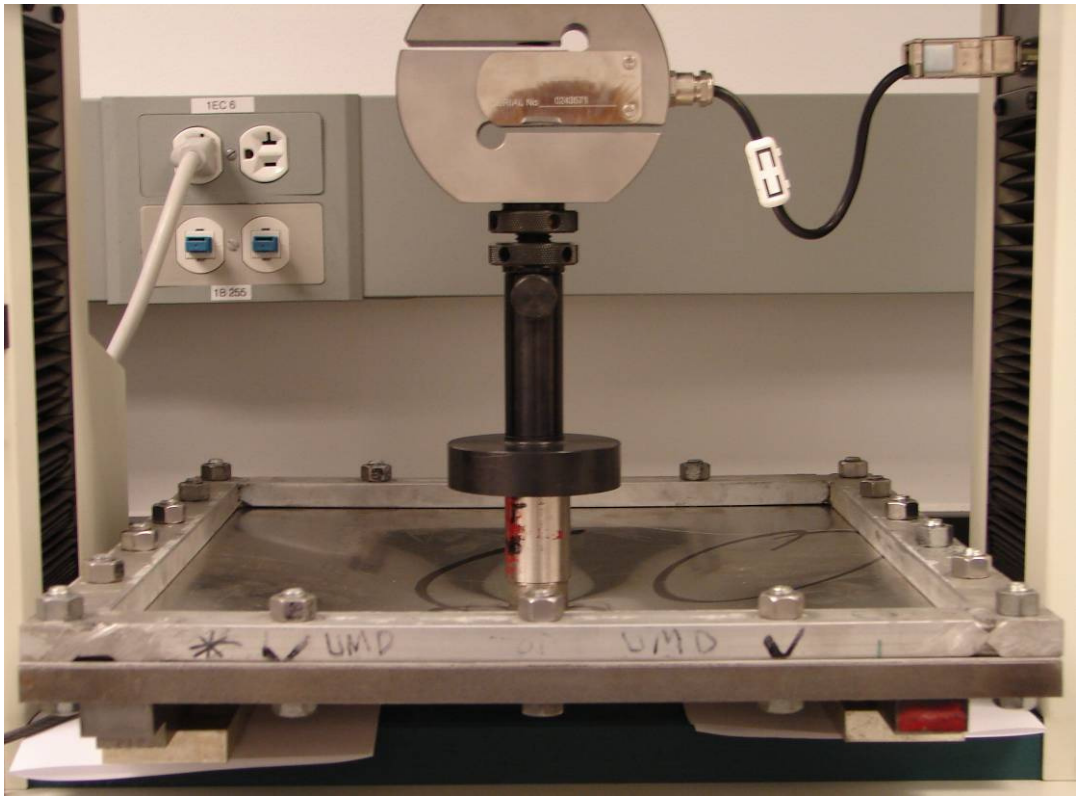

Figure 6.11: Second Test with Clamped Edges

For this second test there is much less bending of the frame, and the plate does not appear to be rippling near the boundaries. A new simulation was run simulating the smaller contact area, and the results are shown in Figure 6.12:

Figure 6.12: Clamped Plate Experimental vs. Simulation Force-Deformation

Two key values are compared from the test and the simulation. The first is the maximum deformation, which was reached at 2500 pounds and obviously includes both plastic and elastic deformation. The second was the final deformation, which was measured after the load was removed from the plate. These values are given in Table 6.1:

	Measured (in)	Simulated (in)	Difference
Final Deformation	0.376	0.464	13%
Maximum Deformation	0.75	0.72	3%

Table 6.1: Measured vs. Computed Deformations

The differences between measured and simulated are much lower than in the first validation test when the plate was not properly clamped and the frame was bending significantly. In the physical tests the rapidly increasing explosive pressures cause significant deformation at the center before the deformation has reached the edges, which is not achievable with the UTM testing rig. The deformation rate was several

orders of magnitude slower than with explosives, and it is impossible to apply the DYNA FEM model to slower deformation rates and a rectangular plate. The difference between the FEM and UTM results could be attributed to the fact that the simulation was modeled as a circle with perfectly fixed boundary conditions. The simulation should model the explosive deformation more accurately then it models the quasi-static UTM test because of the time it takes the deformation to reach the edge of the plate. The rectangular boundary should not contribute the same error in the dynamic case because the plate is mostly done deforming before the edge effects can influence it.

Another potential source of error with this validation test could be that the simulation evenly applies the average force across the entire area of the circular press since the force distribution is not precisely known along the contact area. The simulation does not control the displacement of the contact area like the UTM does, but rather the load, which leads to a slightly different deformed geometry at the contact area. For the physical setup the contact area of the plate remains perfectly horizontal at all times due to the indenter, whereas the simulation allows curvature in this area. All things considered, the validation shows that the code is able to closely replicate a quasi-static test, and is probably even more accurate for explosive tests.

6.5 Generating Pressure Curves for Input

An important aspect of the inverse hybrid method is deriving the initial pressure curves to input into the simulation. This multistep process starts with pressure data obtained from Kolsky bar tests and finishes with time-varying pressure

curve for each node in the simulation. The steps are each described in this section, and are as follows:

1. Obtain pressure plots from Kolsky bar gage tests
2. Fit equations to measured pressures to obtain parameterized curves at known distances from center of plate
3. Fit equation through each parameter to obtain predicted pressure equation at any distance
4. Generate pressure curve for each node in simulation using intermediate parameter values
5. Format curves for input into LS-DYNA keyword file

6.5.1. Obtaining Pressure Data from Kolsky Bar Gage Tests

Data from previously conducted Kolsky bar tests was used as a starting point for determining pressure curves, and two Kolsky bar tests were performed especially for this research effort using 1" DOB and 1.22" SOD (Gage Test 260 and Gage Test 271). The sandbox is prepared as usual and a charge is buried at the DOB of interest. A rigid plate is then mounted at the desired SOD, with a 4 foot long ¼" diameter Kolsky bar centered directly above the charge, and 7 more bars in a line spaced ½" apart. Each bar has a pair of resistance strain gages attached about a foot from the bottom. When the blast "strikes the bottom of the plate, the portion of pressure loading applied to the end of the bars travels up the rod as a compressive loading and goes past the strain gages (where the magnitude of loading is measured) reaches the end of the bar and reflects back down the bar and once again passes the strain gage location" [24]. From this setup pressure-time curves can be extracted at each of these

discrete locations. The entire Kolsky bar setup can be seen in Figure 6.13, and a close-up of the plate can be seen in Figure 6.14:

Figure 6.13: Kolsky Bar Strain Gage Test

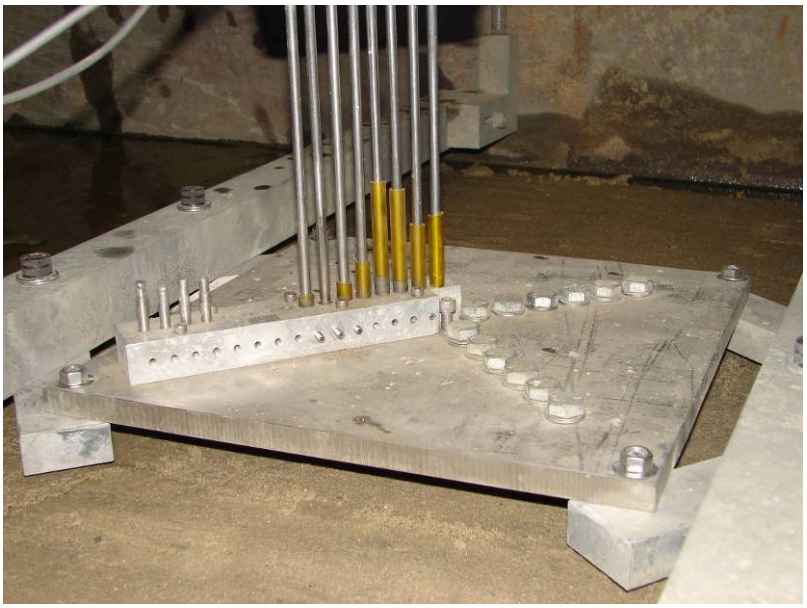

Figure 6.14: Kolsky Bar Strain Gage (Close-up)

The pressure-time curves for the first four bars are shown in Figure 6.15. The pressure was not high enough to obtain data for the bars farther out. This data is the result of the strain gage measurements of the compression wave in the bar caused by the explosive pressure.

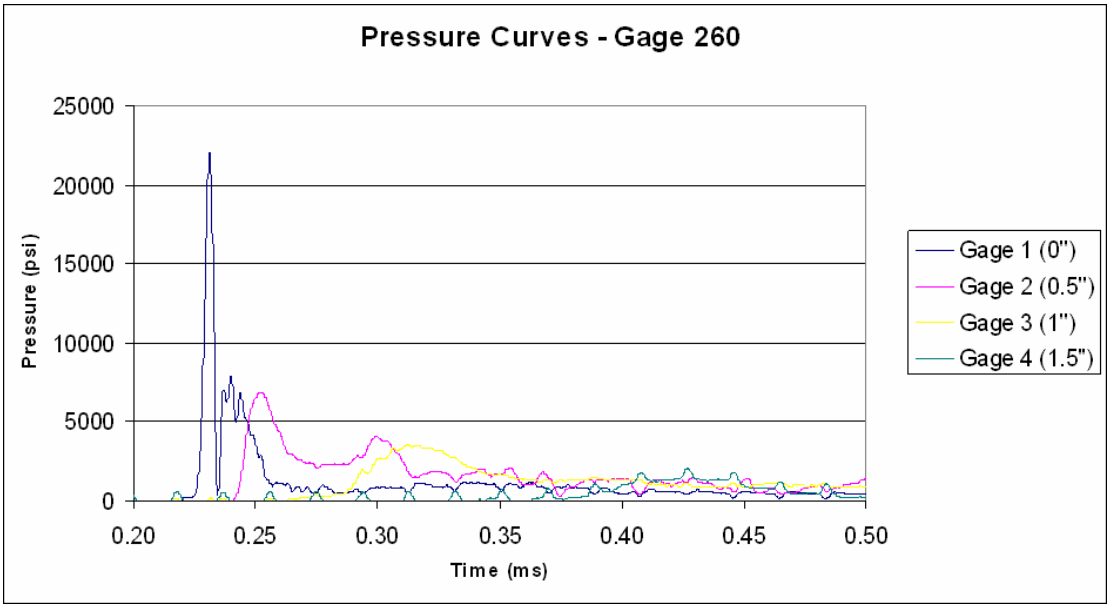

Figure 6.15: Pressure Curves from Kolsky Bar Gage Test 260

A second test was later conducted in order to obtain pressures as far out as 3.5” from the center of the plate, but only the first 3 or 4 gages provided useful data, as shown in Figure 6.16. Interestingly, the gage 0.5” from the center provided a higher pressure reading than the one directly above the charge. After the first few gages the pressure readings do not seem to be accurate because they begin to rise at the exact same time. It is also typical to observe a negative pressure at later times for accurate data. This negative pulse is present for the first three gages, but absent for Gages 4 through 8. Although neither of the Kolsky bar gage tests provided flawless data, they still serve as a good starting point for curve fitting.

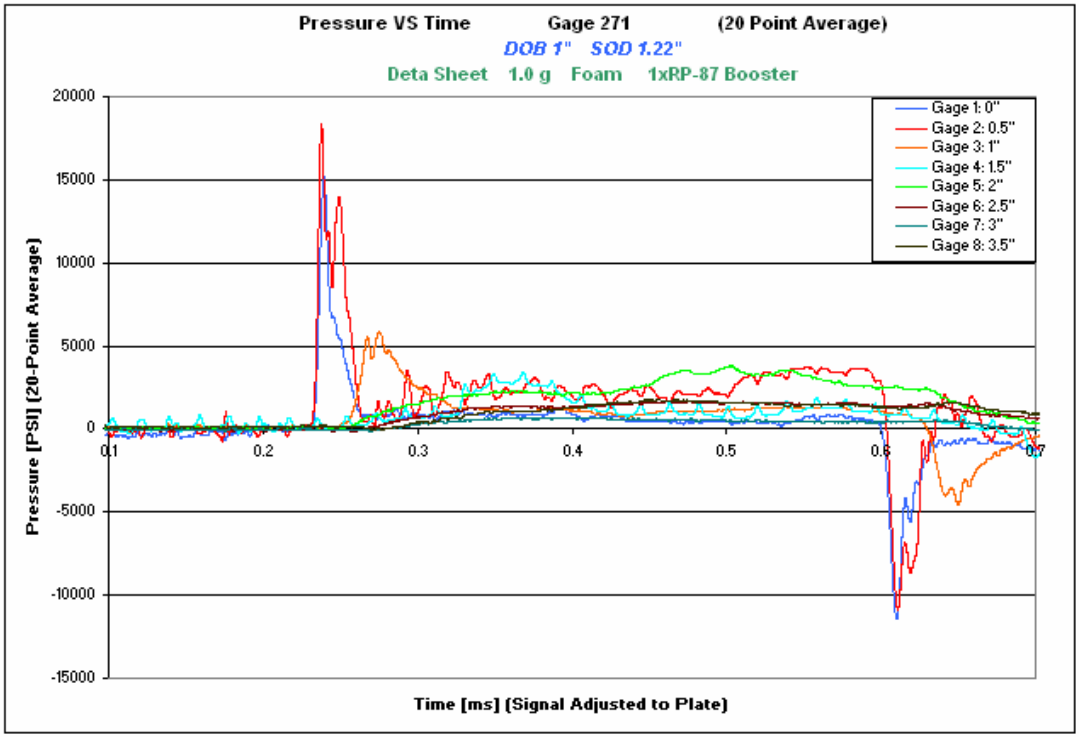

Figure 6.16: Pressure Curves from Kolsky Bar Gage Test 271

To input pressure data into the simulation, a pressure-time curve is necessary for each node. Parameterized curves need to be determined in order to generate curves at intermediate distances from the center and to smooth out any noise.

6.5.2. Fitting Equations to Measured Pressures

In order to fit an equation to the measured pressure data it was first necessary to determine the general form. After examining several different equations, it was determined that $t * e^{-t}$ resembles the quick pressure rise and slower decay characteristic of the pressure-time curves, as seen in Figure 6.17:

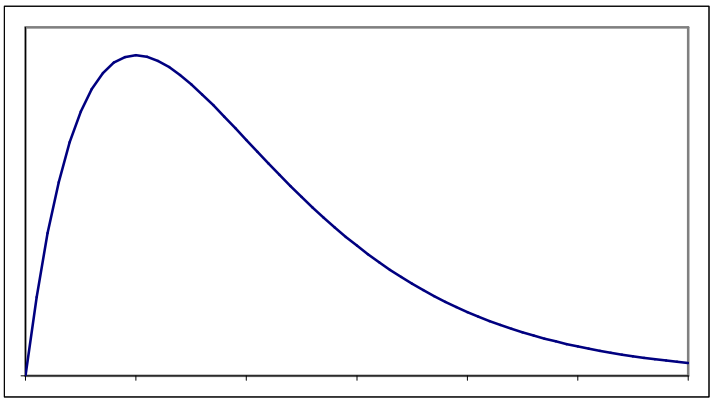

Figure 6.17: Shape of $P(t) = t * e^{-t}$

Using this equation as a starting point, it was necessary to add enough parameters to allow modification of several aspects: the peak pressure value, the rate of pressure decay, the time at which the pressure begins to rise, and the overall shape of the curve. An equation was developed that is of similar form to the Weibull distribution typically used in reliability or statistics:

$$P = c\left(\frac{t-t_0}{a}\right)^b \exp\left(-\left(\frac{t-t_0}{a}\right)^b\right)$$

Where:

a – scales along the t-axis (rate of pressure decay)

b – determines the shape of the curve

c – scales along the y-axis (including peak pressure value)

t_0 – shifts the pressure curve along t-axis (when the pressure begins)

The effect of modifying parameters a, b, and c is shown in Figure 6.18, Figure 6.19, and Figure 6.20:

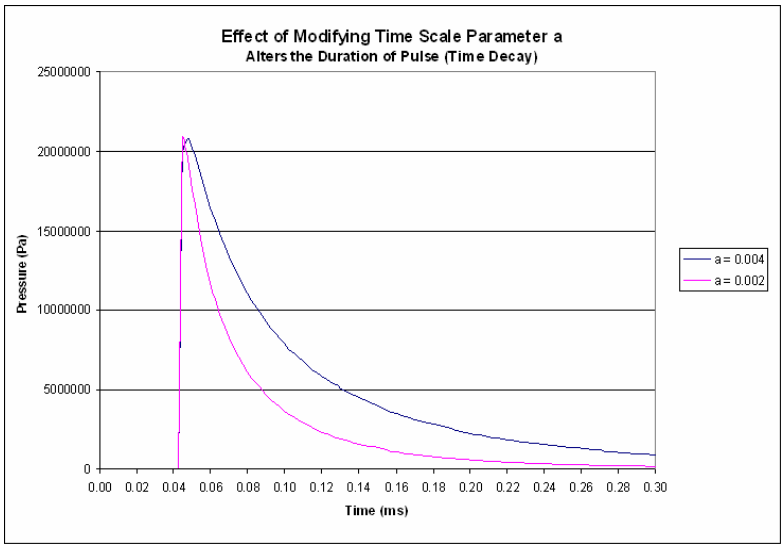

Figure 6.18: Effect of Modifying Parameter a

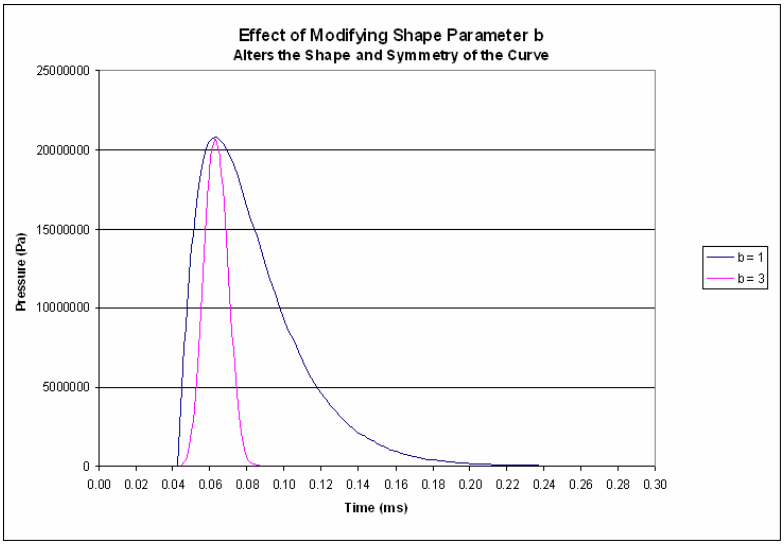

Figure 6.19: Effect of Modifying Parameter b

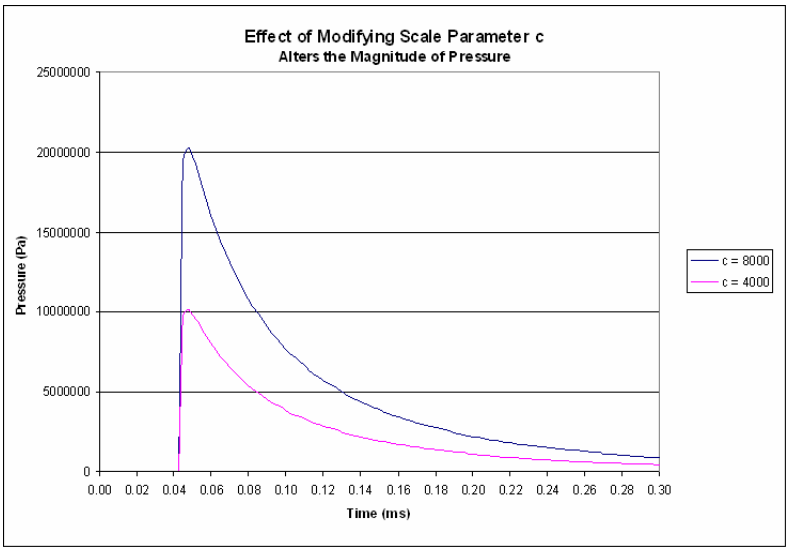

Figure 6.20: Effect of Modifying Parameter c

In order to fit curves these curves to the pressure data, a spreadsheet was created where the parameters could be manually modified. A curve was fit to each of the bar locations one at a time, starting with the Parameter c and t_0. Determining these values is trivial since they shift the entire curve and can easily be set to match the pressure peak and starting point. Determining the values of the time scale parameter a and the shape parameter b is not as straightforward since they closely affect each other. It is also not always intuitive how changing the value of b will change the shape of the curve. A least square fit technique could be applied to obtain the statistically best curve for each pressure reading, but this could result in nonsensical intermediate curves being generated due to the complex interaction of parameters a and b. In general it is ideal to have parameter a and b both continually increasing as the distance from the center increases. Currently it is necessary to manually obtain equations that represent the Kolsky bar data, as shown in Figure 6.21:

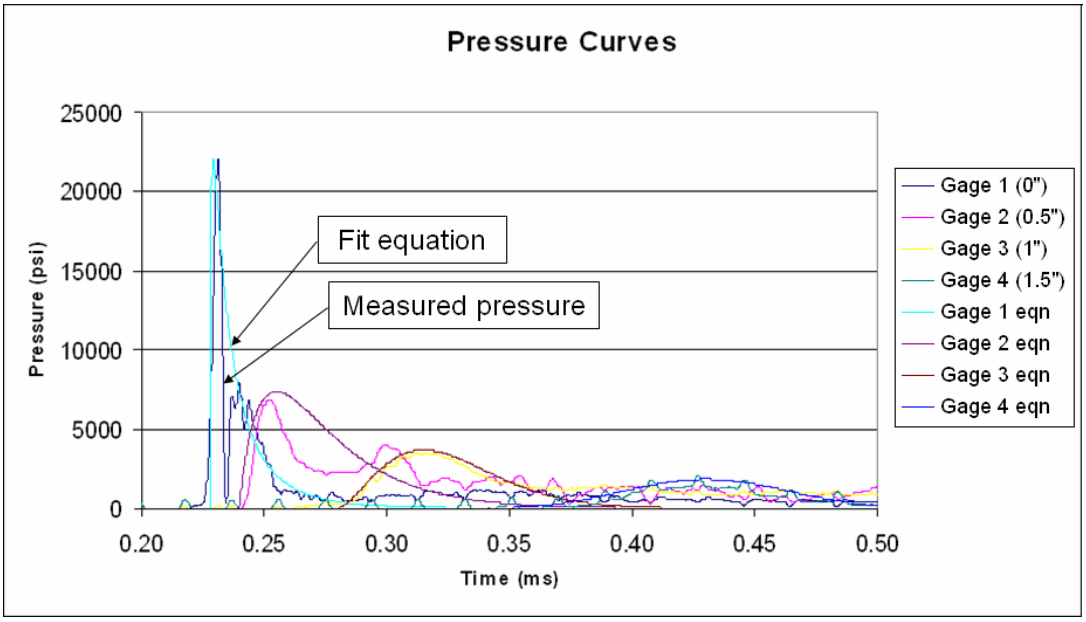

Figure 6.21: Fitting Equations to Gage 260 Experimental Results

From here it is still necessary to determine the intermediate values of the parameters. This is done through a parameter curve-fitting process as described in the next section.

6.5.3. Fitting Equations for Parameters

Interpolation was used to determine the values of the parameters for distances in between where data was originally obtained by the Kolsky bar test. In order to do this the parameter values are plotted as a function of distance from the center of the plate, and an equation is fit through the points. This is typically a second order polynomial, or an exponential equation for the spatial decay (parameter c), as shown in Figure 6.22:

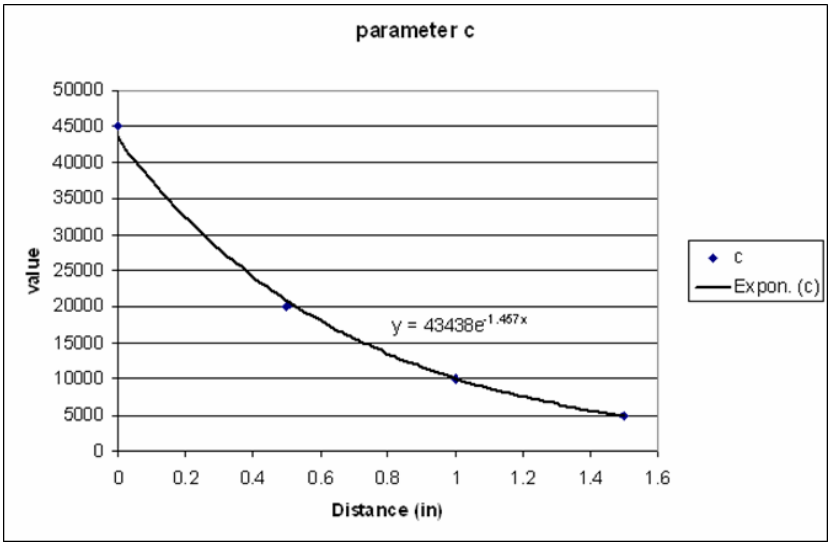

Figure 6.22: Interpolation for Each Parameter

Some judgment is necessary in equation fitting to ensure that the resulting equation makes sense. For example, it is not uncommon to obtain an automatically fit equation for c that significantly underestimates the 0" distance value, which would greatly affect the simulated deformation. However, it is possible to use different equations or fitting techniques in order to obtain a logical interpolation.

6.5.4. Generating Pressure Curves for Each Node

Once an equation has been obtained for each parameter, it is possible to generate a pressure curve for any necessary location. An example of a full set of pressure curves is shown in Figure 6.23:

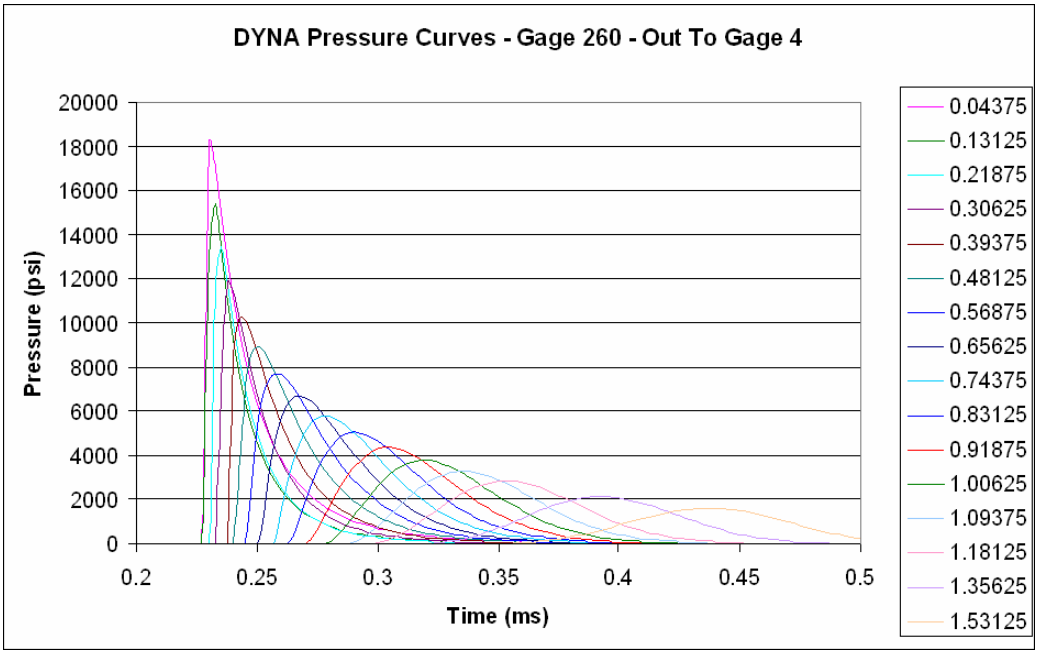

Figure 6.23: Example of Pressure Curves Calculated for Each Simulation Node

Inputting these curves into the LS-PrePost software can be very tedious, especially if the selected grid has a fine resolution. In this case up to 40 curves must be input. In order to make the process easier a macro code was created directly in the Excel spreadsheet in order to properly format the curves for the DYNA keyword file.

6.5.5. Formatting Curves for Keyword File

A spreadsheet and macro were created in order to allow for simple conversion of the Excel generated pressure curves to the keyword file input required by LS-DYNA. The file is titled "Excel to DYNA macro.xls," and the embedded Visual Basic macro code is included as Appendix E. The first step is to create a copy of this file and to enter in the new pressure curves. This is done by either modifying the parameter equations that generate the curves or by directly pasting in the new values from previously generated pressure curves. The macro is started by entering the Visual Basic editor (alt-F11), double-clicking on the user form, and clicking the Run

Sub/UserForm button or pressing F5. The output directory and file name can be specified, as shown in Figure 6.24:

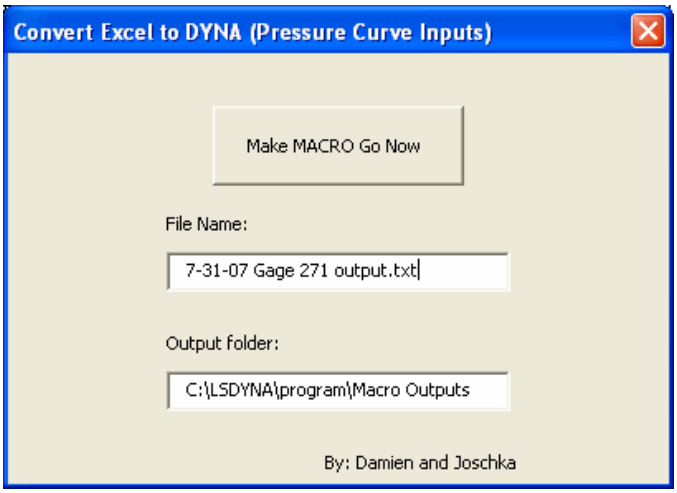

Figure 6.24: Pressure Curve Macro – User Interface

After clicking the Go button, the output file is generated. It can then be copied directly into the desired DYNA keyword file, which is easily edited in Word.

6.6 Initial Simulations

Before the pressure curves were examined, a few basic simulations were run. The first was to determine grid independence. Figure 6.25 shows the model (including a close-up) in LS-PrePost with the typical grid resolution of 4 elements vertically and 40 elements horizontally:

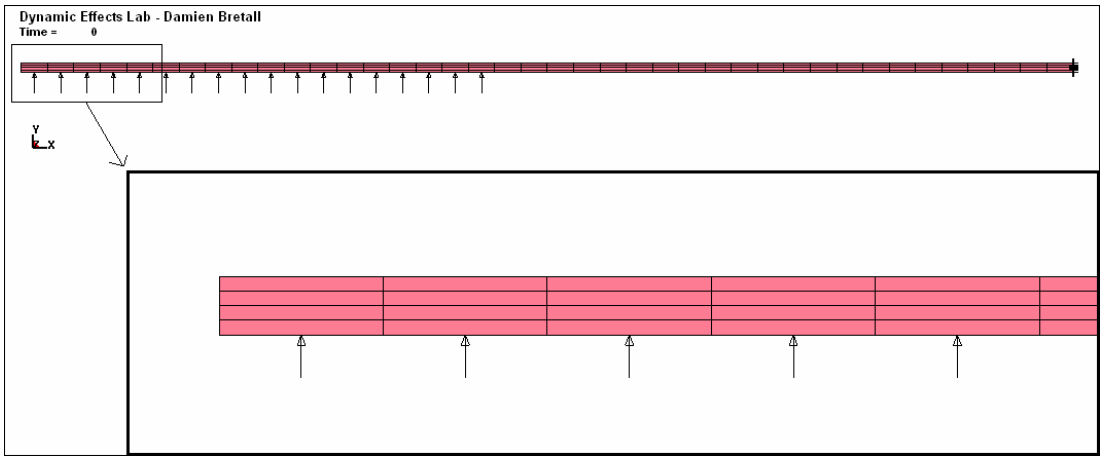

Figure 6.25: LS-PrePost Axisymmetric Model

The right side of the rectangle is the constrained boundary and the left side is the axis of rotation. A finer mesh was then created in order to verify that the solution was not dependent upon the chosen grid. It consists of 8 elements vertically and 80 elements horizontally, at the cost of quadruple run times. The same pressure profiles were input into each simulation, and the final deformations are compared in Figure 6.26:

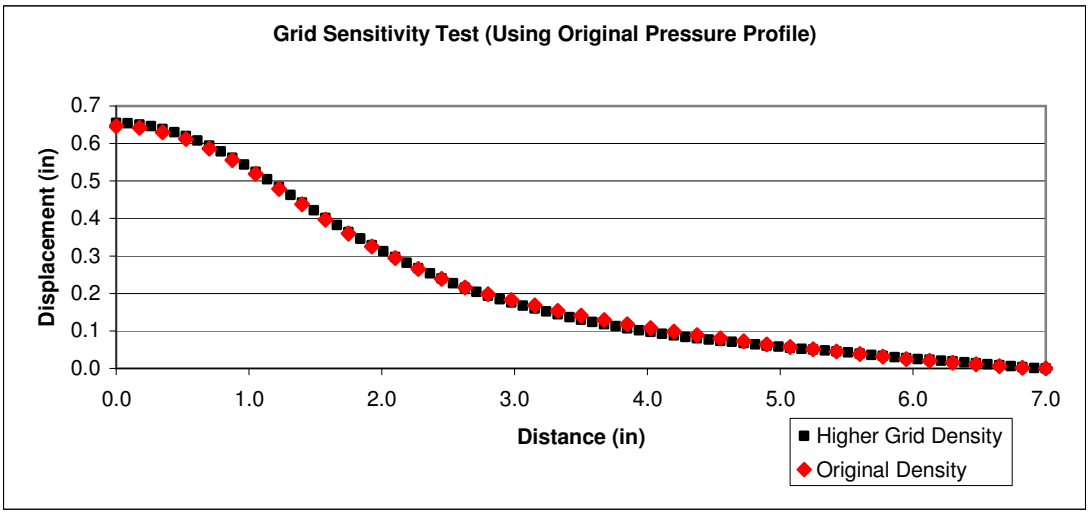

Figure 6.26: Grid Independent Final Deformations

The results are quite similar using either grid, so the rougher grid was selected for all the simulations due to the quicker run times. Due to the axisymmetric simulation only

half of the plate's profile is shown, although the left half of the profile would be a mirror image of the above-shown right half.

Another issue that had to be resolved was how far out on the plate to apply pressure. According to the Kolsky bar tests there is measurable pressure exerted on the plate at least 4" from the center. Initially, pressure curves were only generated and applied up to 3" from the center due to the small values of pressure past this point. A set of curves was then generated all the way out to 4", but this simulation produced nearly identical deformation. To confirm these findings another simulation was run with just this additional pressure (3" to 4" from the center), which produced no visible deformation. When these same pressure values are applied to only the center no permanent deformation occurs either, although it induces significant oscillations of the plate.

In order to fully appreciate what is driving the deformation, a simulation was run where the pressure curve is only applied out to 1.5" (as opposed to 3" out for the original pressure inputs). To clarify, this means that both simulations have the exact same pressures applied for the first 1.5" from the center. The results are shown in Figure 6.27:

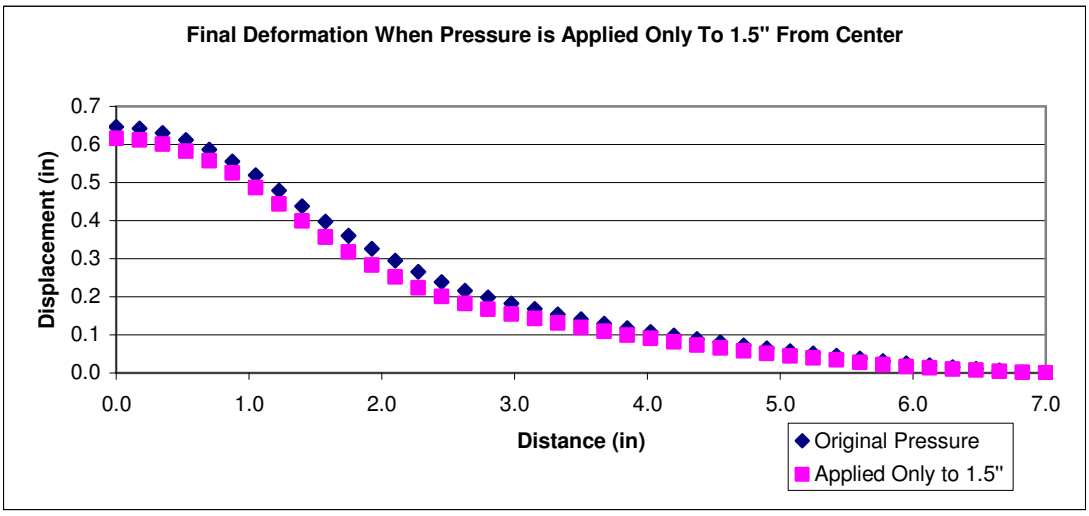

Figure 6.27: Examination of Results with Pressure Applied Only to Center

Although there is less deformation when the pressure is only applied to the center region, it is surprisingly similar. This simulation demonstrates that the majority of deformation is caused by the pressure applied to the center of the plate. This is because of to the higher magnitudes of pressure at the center, but also partially due to the fact that the center of the plate is farthest from the fixed boundary condition.

6.7 Effects of Pressure Curve Modifications

A series of simulations was run in order to better understand how different aspects of the pressure curves affect the resulting final deformation. A baseline pressure profile was first established based on results from the Kolsky bar strain gage tests. This profile will be modified in order to provide higher and lower amounts of deformation, so it was initially scaled to provide a final deformation similar to the 1" DOB test (about 0.65" center deformation). The baseline simulated deformation falls approximately in the middle of the range of experimental final deformations (0.484"

to 1.02”). This baseline pressure profile, also referred to as the original pressure curves, is shown in Figure 6.28:

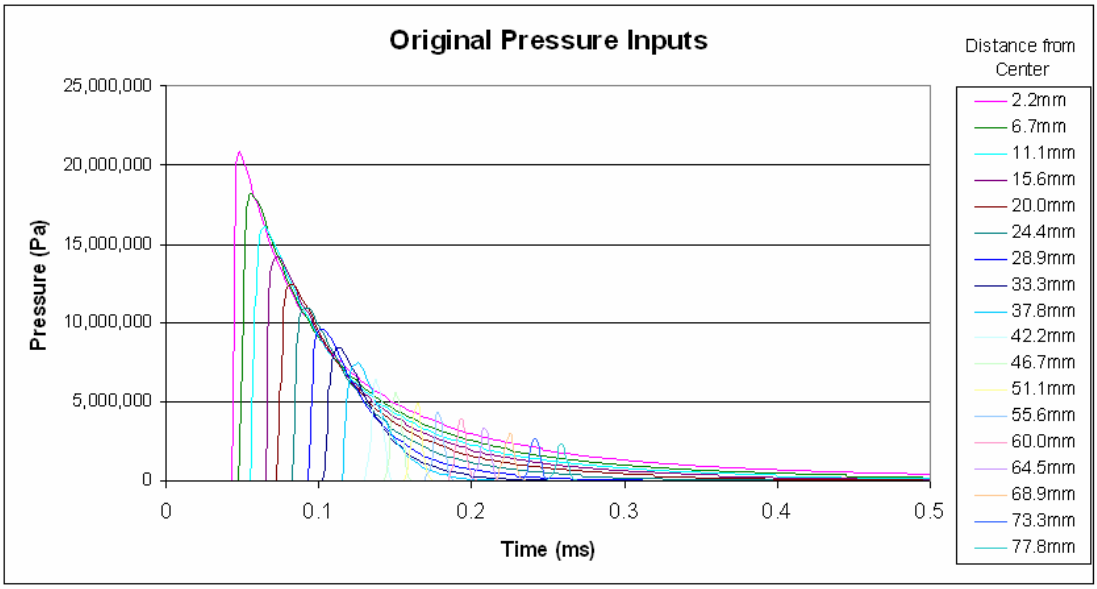

Figure 6.28: Original Pressure Inputs - 3.44 N·s (0.77 lb·s)

The pressure curves have been generated in SI units to simplify DYNA code implementation. In order to obtain a quantitative metric the total impulse applied to the plate was calculated for each set of pressure curves, and is reported in the figure caption. This was done by first calculating the area that each of the pressure curves is applied to. As described in the beginning of this chapter, each of the individual pressure curves is applied uniformly across an area that can be visualized as an annulus on the bottom plate surface. After calculating these areas the pressure curves can be converted into force curves by multiplying them each by their respective areas. The impulse of each curve can then be calculated by integrating with respect to time (using the Riemann sum approximation method). These individual impulses are then added together to obtain the total impulse the pressure profile applies to the plate.

Using this original pressure profile as the baseline, each of the parameters was modified in order determine how different aspects of the pressure profile affect the final deformation. The affect of each parameter on the pressure curve was discussed in Section 6.5.2. The first profile modification investigated is the overall pressure scale, the next is the spatial decay of the pressure curves, and the last is the rate of decay of each curve. A summary of this series of simulations, including which parameter was modified (or which constant in the parameter equation was modified), is shown in Table 6.2:

<-- decreased impulse				increased impulse -->		
Pressure Scale						
c * 0.5	c * 0.666	c * 0.75	c * 1	c * 1.25	c * 1.5	c * 2
PS-3	PS-2	PS-1	original	PS+1	PS+2	PS+3
1.72	2.29	2.58	3.44 N·s	4.30	5.16	6.88
0.39	0.51	0.58	0.77 lb·s	0.97	1.16	1.55
Spatial Decay						
	e^ -1x	e^ -0.85x	e^ -0.7317x	e^ -0.6x	e^ -0.4x	
	SD-2	SD-1	original	SD+1	SD+2	
	2.65	3.06	3.44 N·s	3.95	4.95	
	0.60	0.69	0.77 lb·s	0.89	1.11	
Time Decay						
	a * 0.5	a * 0.75	a * 1	a * 1.5	a * 2	
	TD-2	TD-1	original	TD+1	TD+2	
	1.97	2.71	3.44 N·s	5.79	8.35	
	0.44	0.61	0.77 lb·s	1.30	1.88	

Table 6.2: Pressure Curve Modifications

The total impulse for each of these pressure profiles is also listed in the above table, in both N·s and lb·s. These values are not directly controllable while creating a pressure profile, and are calculated after the fact.

For the pressure scale and time decay simulations, parameters c and a could easily be changed to accomplish the desired pressure profile modification. However,

it was more difficult to modify the spatial decay rate. In order to accomplish this it was necessary to modify the equation used to calculate the value of c based on the distance from the center of the plate, as discussed in Section 6.5.3. For the original pressure curves the equation is c = 8740.8*exp(-0.7317x), where x is the distance along the bottom of the plate, from the center. The negative value in the exponent was modified in order to alter the spatial decay rate. Different names were given to each simulation based on which feature was being modified, and if that results in an increase or decrease of total impulse. For example, the test name "PS+2" indicates that the pressure scale has been increased by two arbitrary levels.

6.7.1. Effects of Pressure Curve Modifications: Pressure Scale

In this investigation the original pressure curve was altered by simply multiplying the y-axis scaling parameter c by different constants. The figures are shown in order of increasing impulse as Figure 6.29 and Figure 6.30:

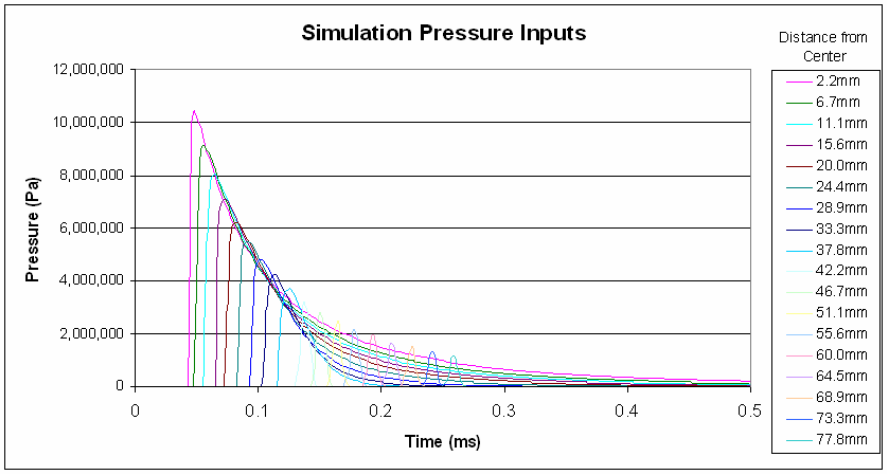

PS-3

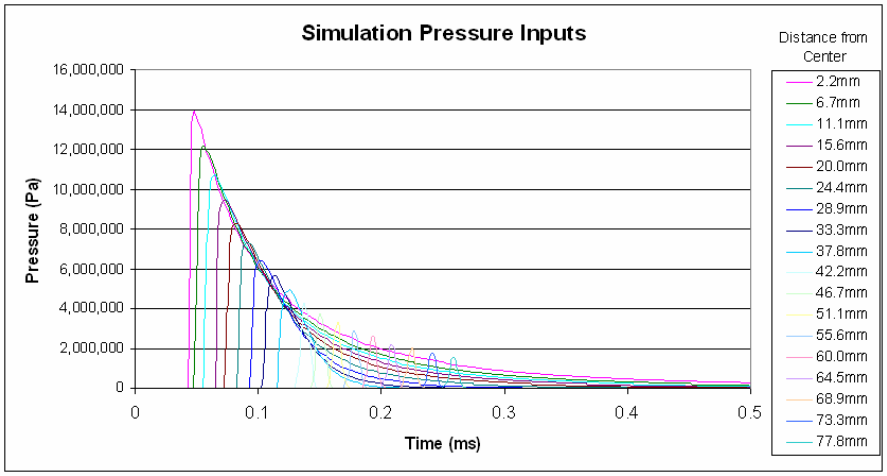

PS-2

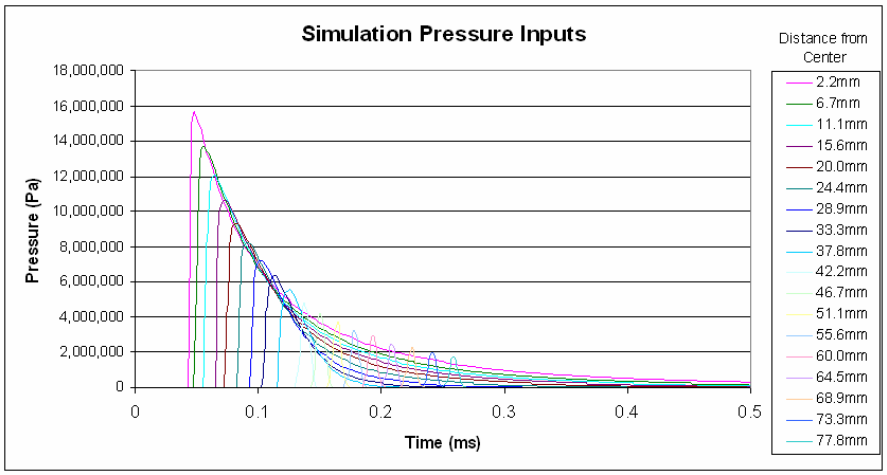

PS-1

Figure 6.29: Decreased Pressure Scale (PS-3, PS-2, PS-1)

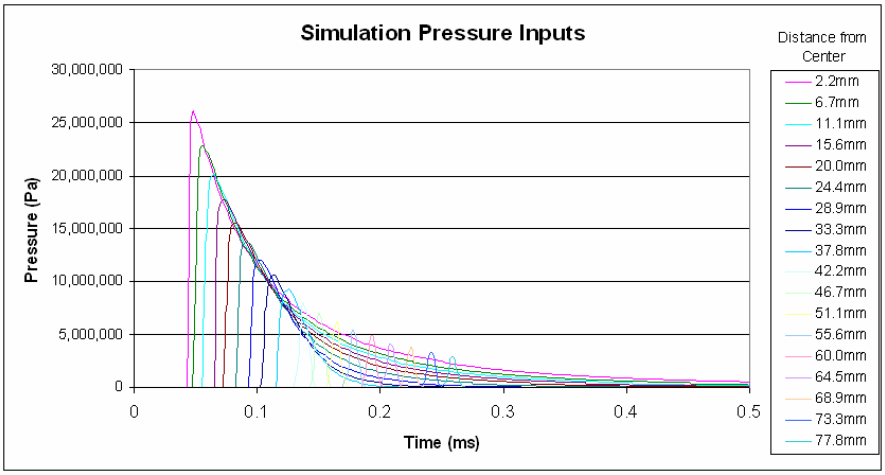

PS+1

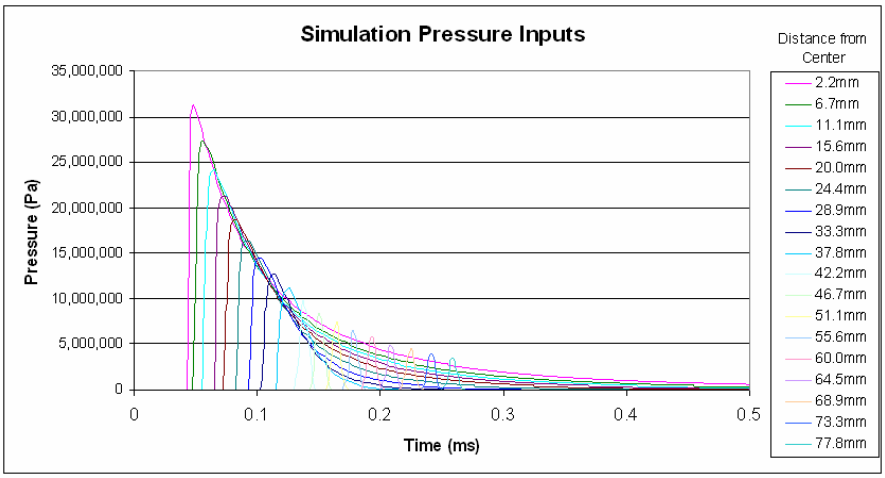

PS+2

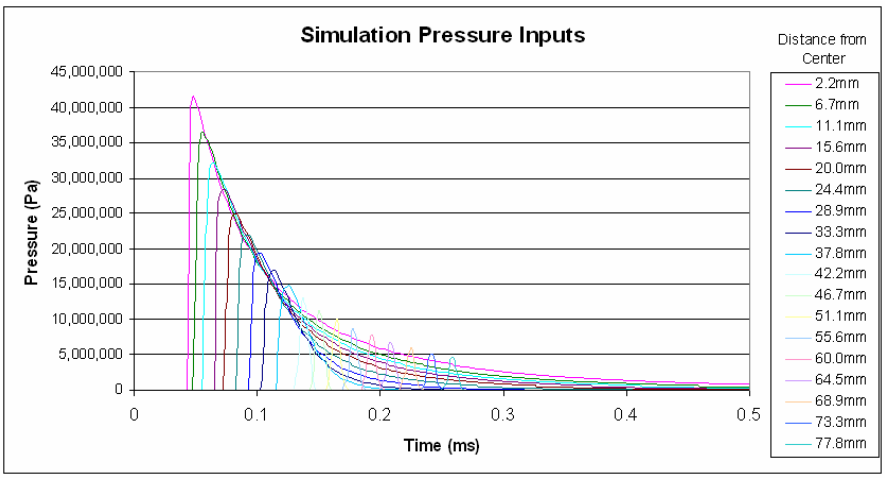

PS+3

Figure 6.30: Increased Pressure Scale (PS+1, PS+2, PS+3)

The resulting final deformation profiles are shown in Figure 6.31:

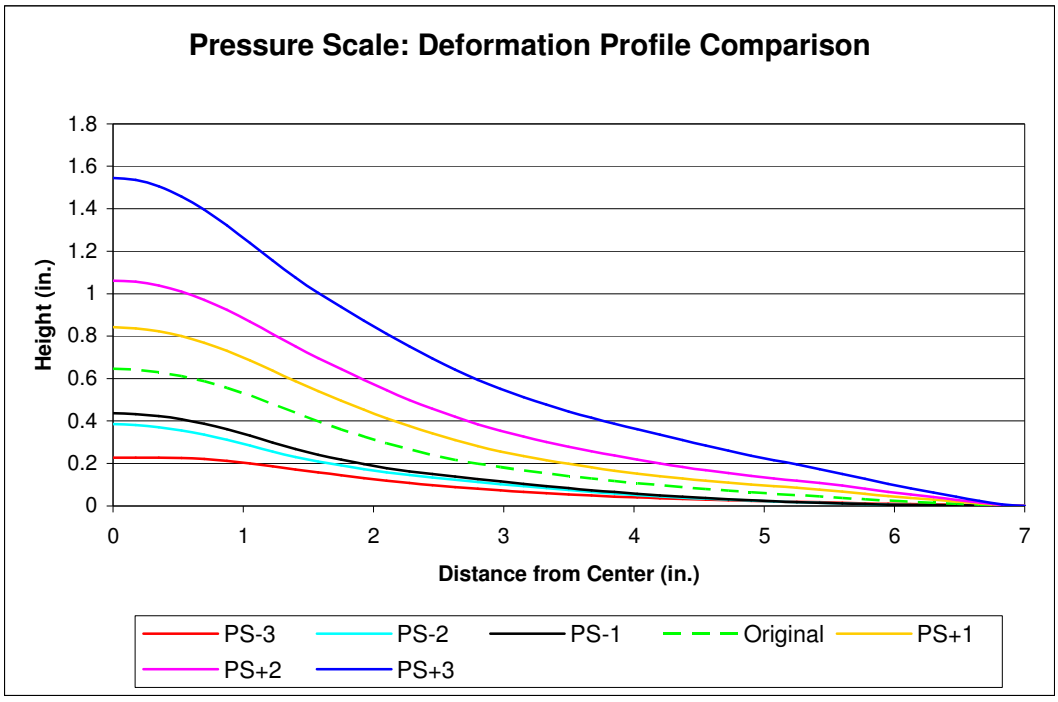

Figure 6.31: Pressure Scale - Effect on Final Deformation

In Figure 6.33 the peak value of the pressure profile is plotted against the resulting center point deformation. This shows the relationship to be approximately linear.

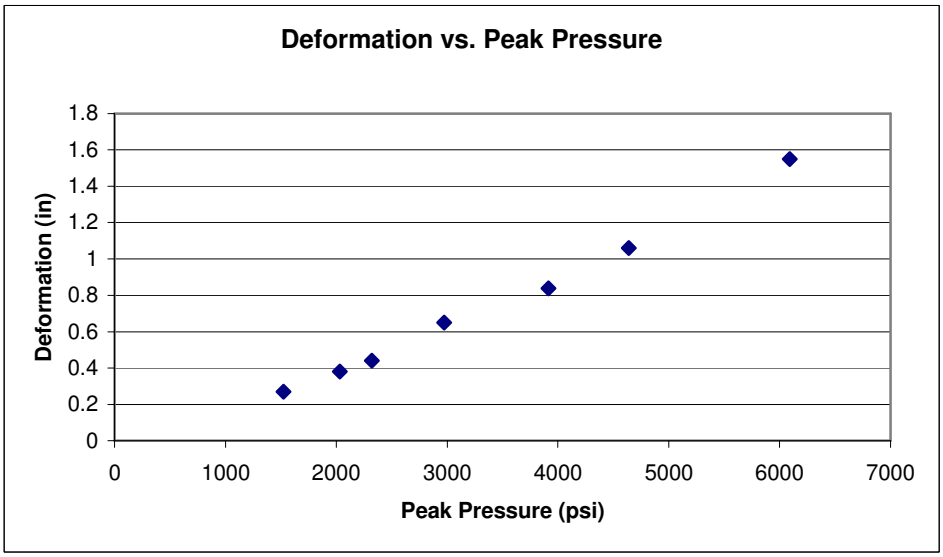

Figure 6.32: Pressure Scale - Effect on Final Deformation

6.7.2. Effects of Pressure Curve Modifications: Spatial Decay

The next pressure profile aspect studied was the spatial decay. This is the rate that the pressure curve peaks decrease with respect to distance from the center of the plate. In order to change this aspect it was necessary to modify the equation for c, rather than simply multiplying c by a constant as was done for the pressure scaling investigation. For the original pressure curve this equation is an exponential function, so the rate of decay can be amplified by decreasing the constant value within the exponent. For example, the original set of pressure curves uses the equation c = 8740.8*exp(-0.7317x) based on a curve fit through the manually determined c values. By changing the equation to c = 8740.8*exp(-0.85x) the peak pressure values decay quicker with respect to distance from the center of the plate. The figures are shown in order of increasing impulse as Figure 6.33, Figure 6.34, and Figure 6.35, including the original pressure curve. An increased spatial decay rate produces a lower total impulse, and these simulations are therefore titled with negative numbers (SD-2 and SD-1).

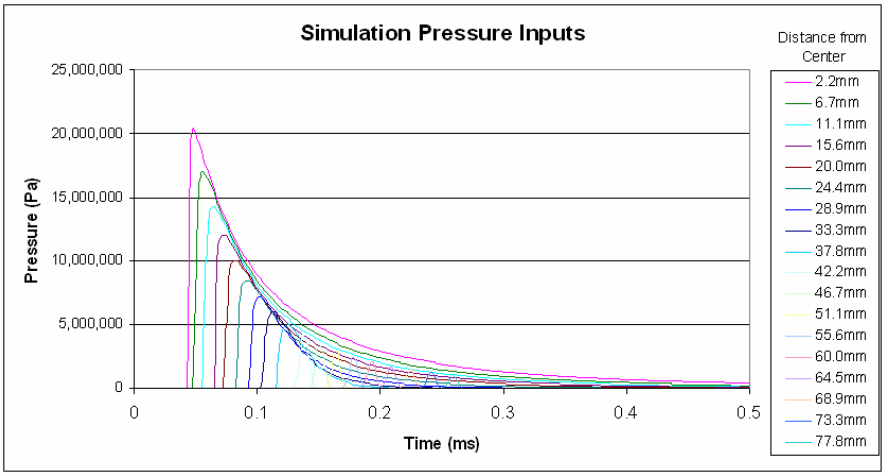

SD-2

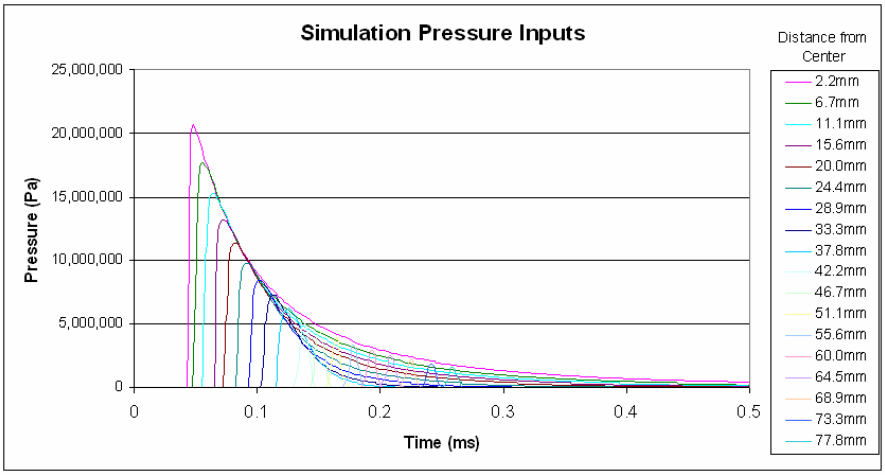

SD-1

Figure 6.33: Increased Spatial Decay (SD-2, SD-1)

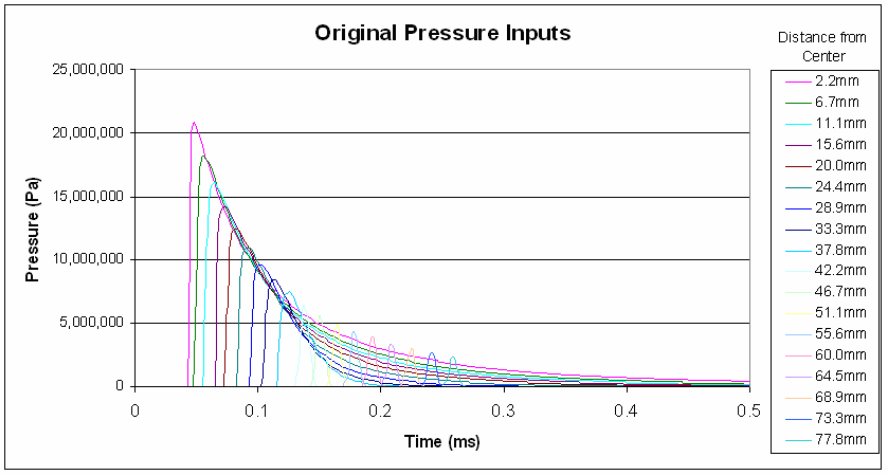

orig.

Figure 6.34: Original Pressure Profile

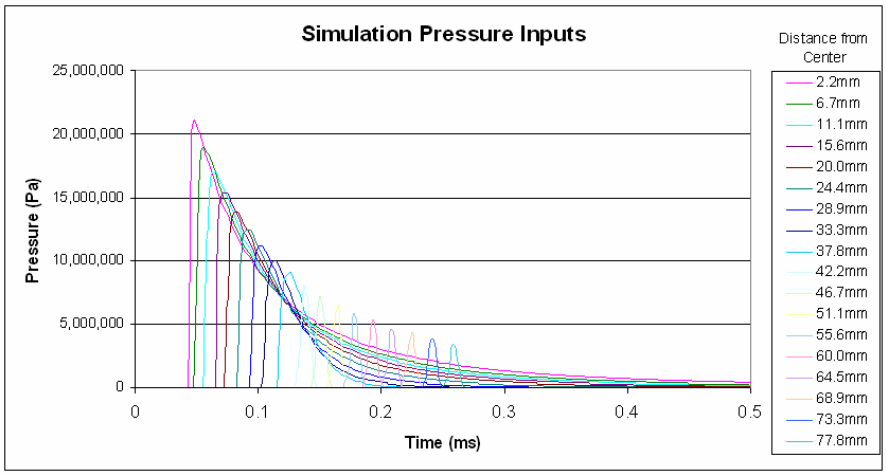

SD+1

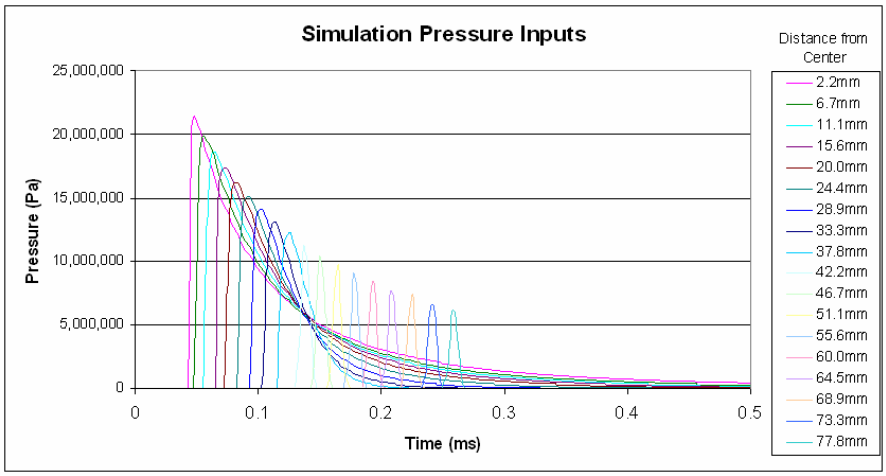

SD+2

Figure 6.35: Decreased Spatial Decay (SD+2, SD+1)

The resulting final deformation profiles are shown in Figure 6.36:

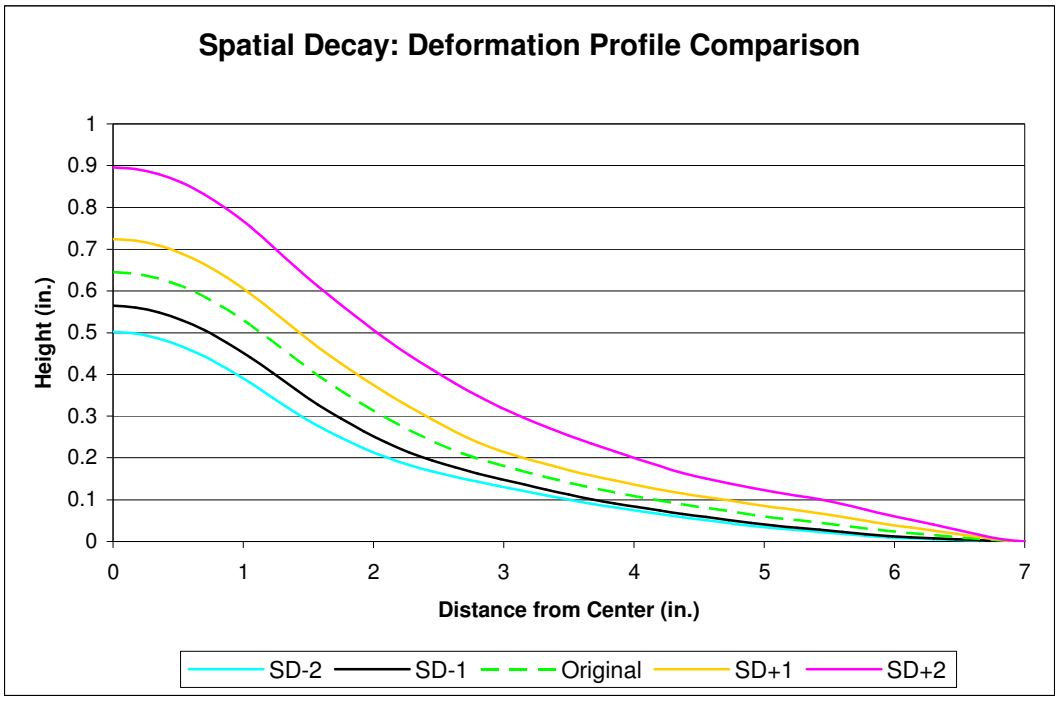

Figure 6.36: Spatial Decay - Effect on Final Deformation

6.7.3. Effects of Pressure Curve Modifications: Time Decay

The final investigated aspect of the pressure profile is the affect of altering the time decay rate. This determines how quickly each pressure curve decays with respect to time, which can be easily altered by simply multiplying the x-axis time scaling parameter a by different constants. The figures are shown in order of increasing impulse as Figure 6.36, Figure 6.37 and Figure 6.38, including the original pressure curve. A increased (faster) time decay rate produces a lower total impulse, and these simulations are therefore titled with negative numbers (TD-2 and TD-1).

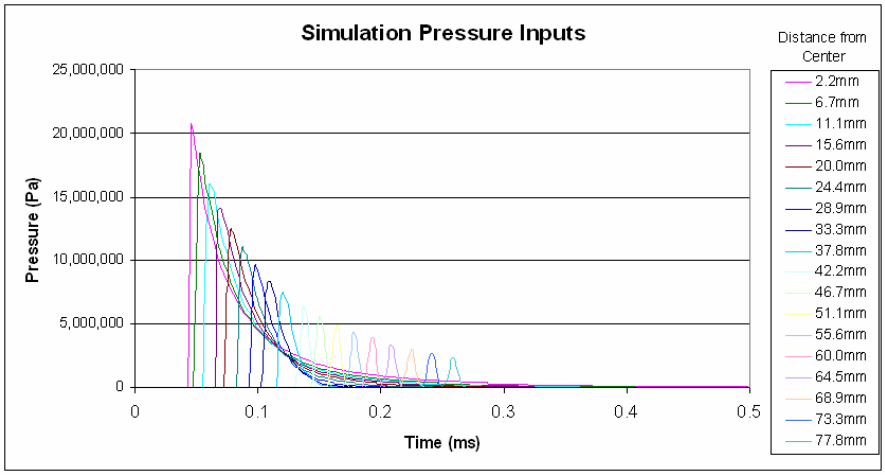

TD-2

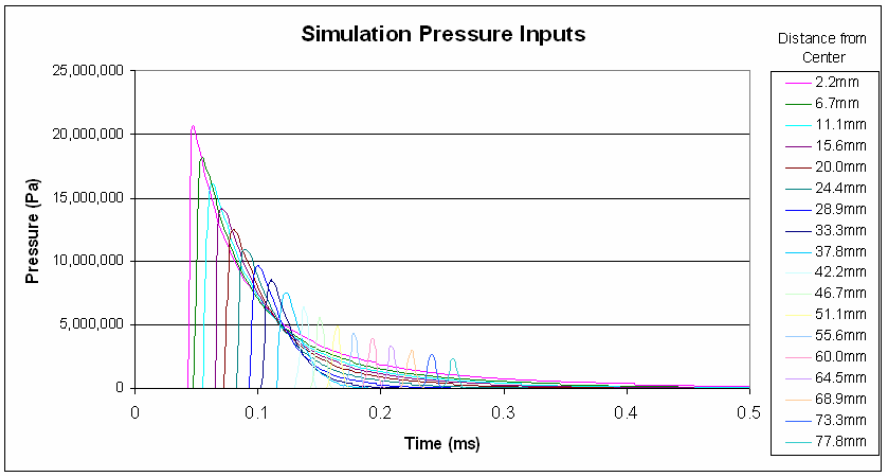

TD-1

Figure 6.37: Increased Time Decay (TD-2, TD-1)

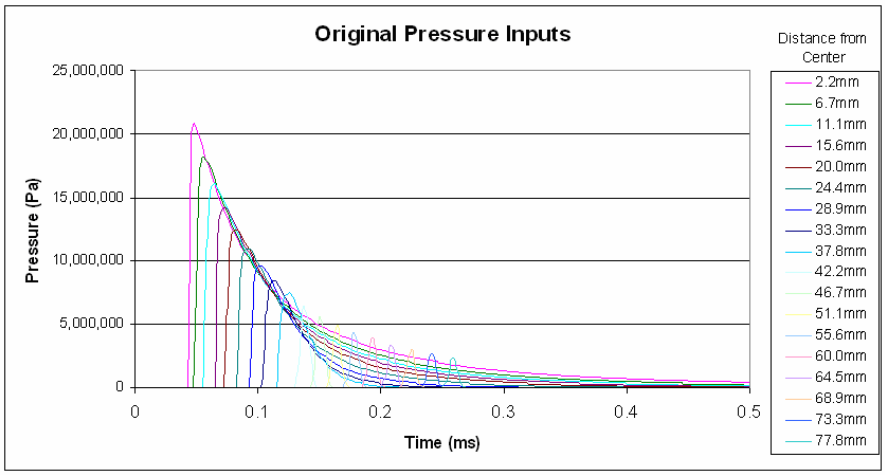

orig.

Figure 6.38: Original Pressure Profile

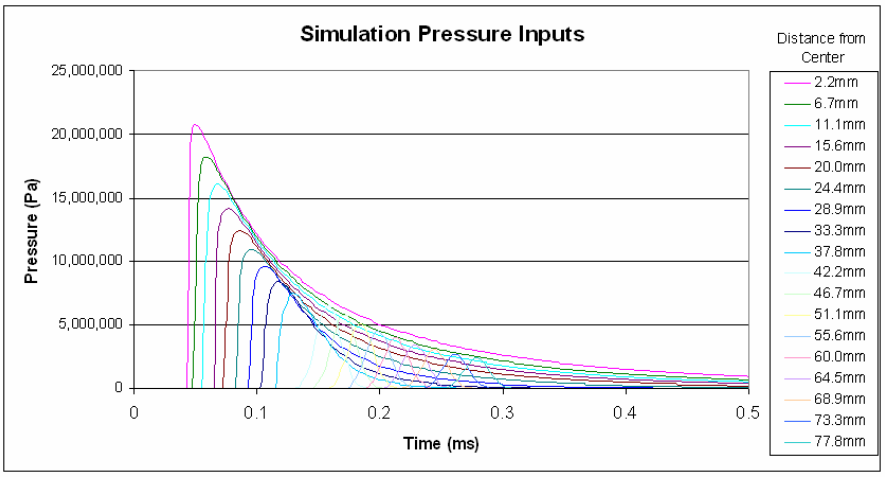

TD+1

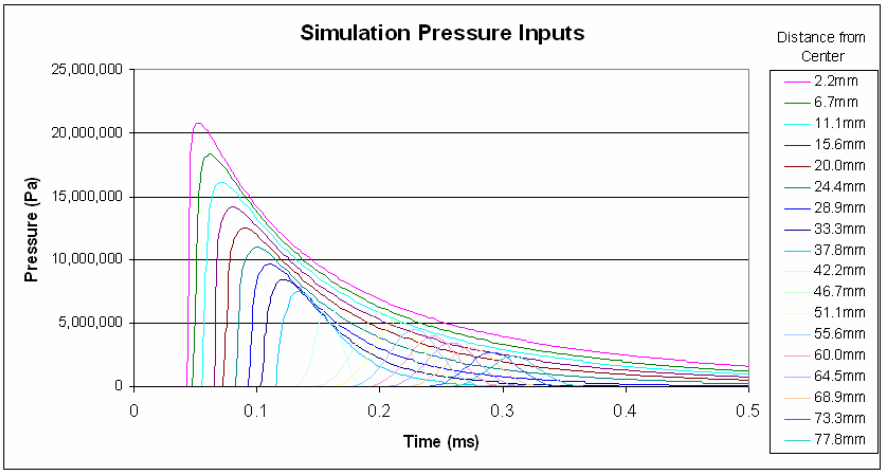

TD+2

Figure 6.39: Decreased Time Decay (TD+2, TD+1)

The resulting final deformation profiles are shown in Figure 6.40:

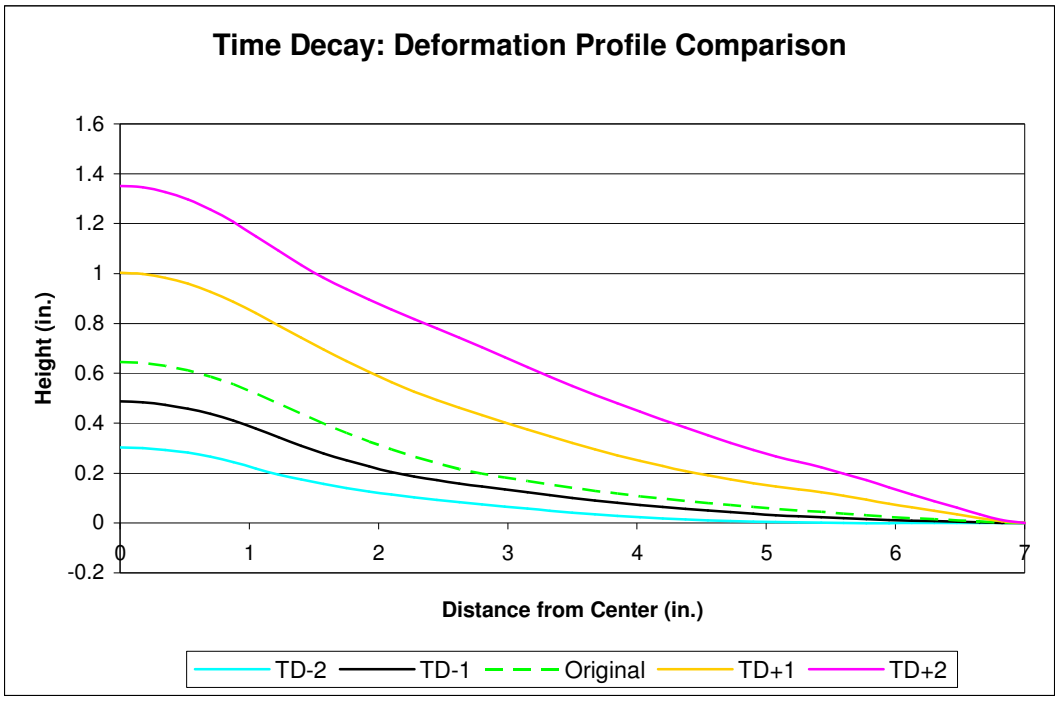

Figure 6.40: Time Decay - Effect on Final Deformation

6.7.4. Effects of Pressure Curve Modifications: Comparisons

In order to quantify the differing pressure curves, the impulse was calculated. This is compared to the simulated final deformation of the center point in Table 6.3 and graphically in Figure 6.41:

	Impulse (lb·s)	Deformation (in.)
Pressure Scale	0.39	0.226
	0.51	0.385
	0.58	0.436
original	0.77	0.646
	0.97	0.842
	1.16	1.062
	1.55	1.545
Spatial Decay	0.60	0.502
	0.69	0.565
original	0.77	0.646
	0.89	0.725
	1.11	0.896
Time Decay	0.44	0.302
	0.61	0.487
original	0.77	0.646
	1.30	1.004
	1.88	1.351

Table 6.3: Impulse vs. Deformation Data

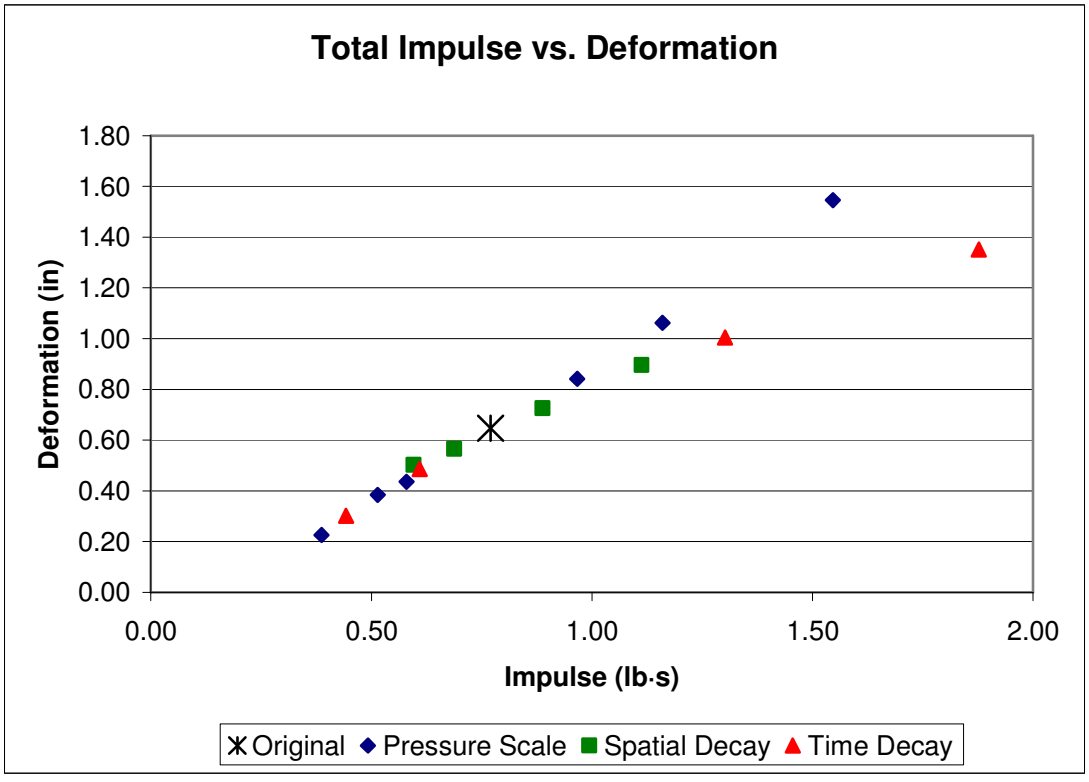

Figure 6.41: Pressure Curve Total Impulse vs. Center Point Final Deformation

By plotting all of the final deformation and impulse data on the same axis, it appears as if there is region for which they have a nearly linear relationship. However, all of these pressure profiles produce similarly shaped deformation profiles. In fact, the one data point that does not seem to fit well with the other data is TD+2, which can be seen in the previously shown Figure 6.40 to have a very linear shape. The discrepancy can be partially attributed to the fact that the value of the maximum final deformation does not adequately represent the entire deformation profile. In some cases profiles that share the same maximum deformation differ as they move away from the center.

Although it would be convenient if the final deformation could be predicted by a single scalar such as impulse, this must not be true for every possibly conceived pressure profile. A smaller load could be applied for a long time, which would represent a high level of impulse yet cause little visible deformation. The pressure curves have thus far all had some commonality. For example, in each of the profiles that demonstrated a linear relationship, the pressure travels along the plate at the same speed and reaches the nodes at the same time.

A completely new pressure curve was generated to see how the impulse and final deformation compare. Another Kolsky bar test was run with the same test parameters as the 1" DOB charge and 1.22" SOD. By fitting curves to this data a pressure profile was generated, as shown in Figure 6.42:

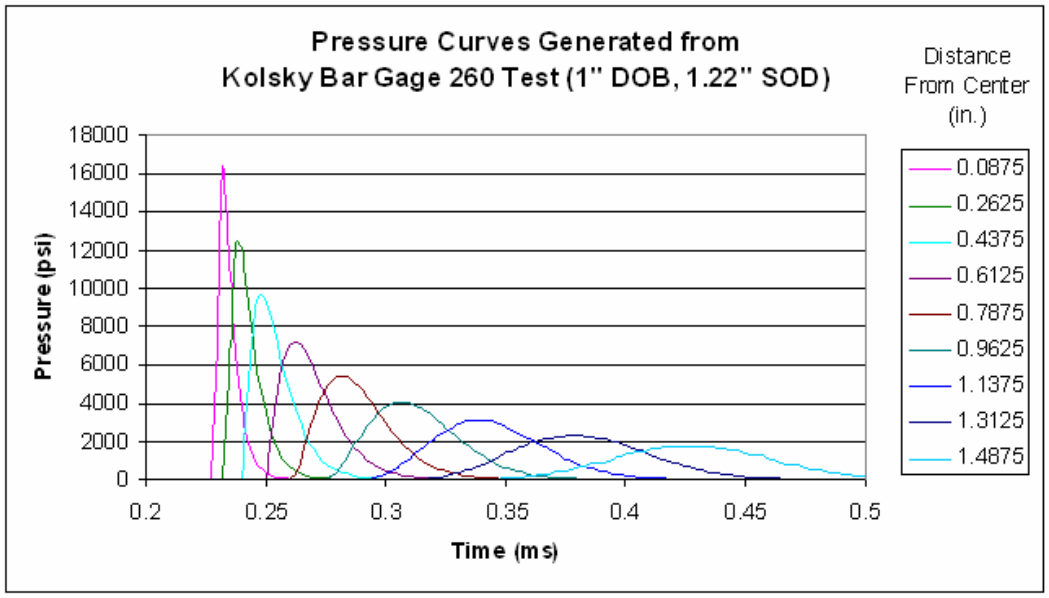

Figure 6.42: Pressure Curves Generated from Gage 260 (1.30 lb·s)

The values are in English units in order to correspond with the Kolsky bar data. The curves had to be scaled down by a factor of 2 in order to obtain a reasonable level of deformation; otherwise the plate became overstretched and the simulation would crash. This is discussed in more detail in Section 6.9. For this pressure profile the curves take longer to travel along the plate than for the previously input profiles. The calculated total impulse for this pressure profile is 1.30 lb·s, and it produces a final deformation of 0.574". Figure 6.43 shows that this pressure profile produces a final deformation that does not agree with the other computations:

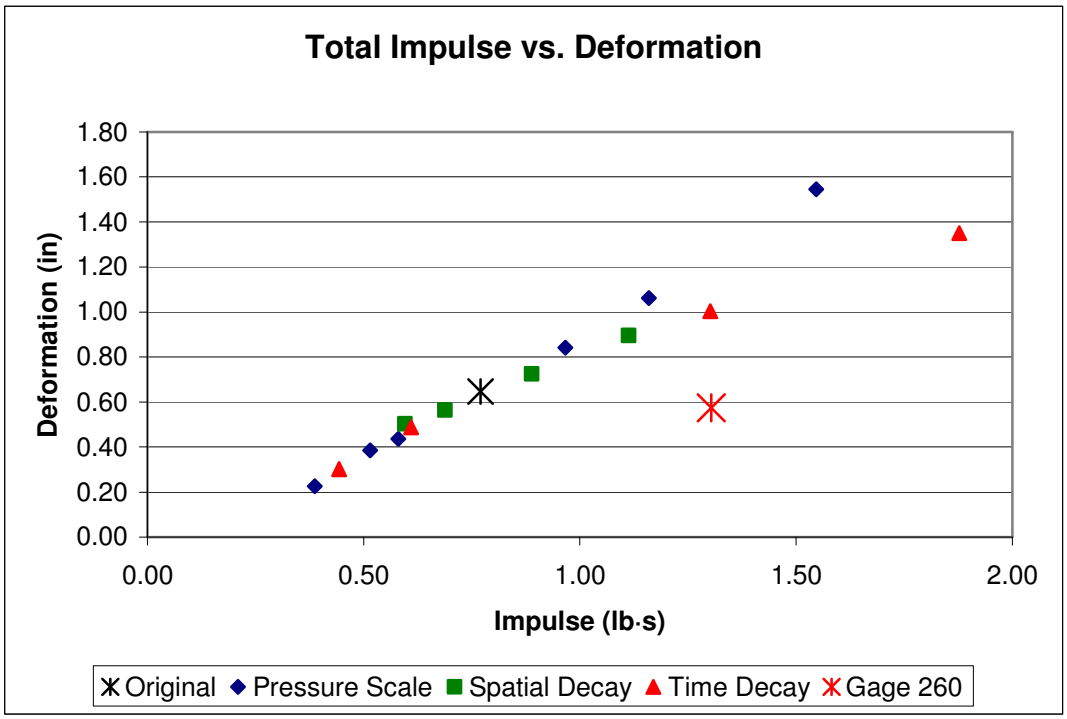

Figure 6.43: Pressure Curve Total Impulse vs. Final Deformation with Gage 260

For this pressure profile the final deformation takes on a different shape than for the previous pressure profiles, which could account for the discrepancy. Figure 6.44 shows the final deformation, which appears more flat along the center of the plate:

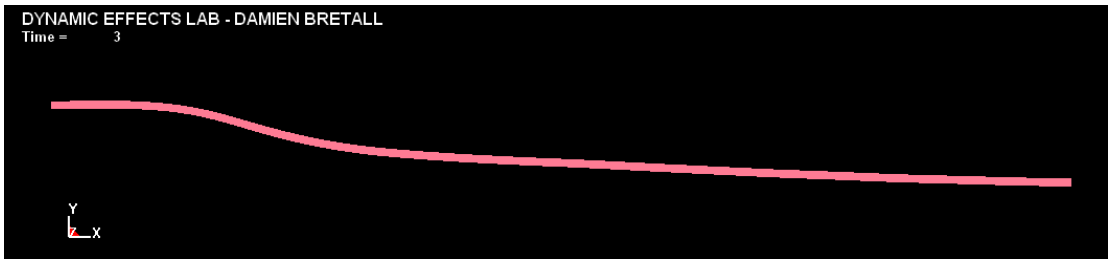

Figure 6.44: Final Deformation from Gage 260 Pressure Inputs (0.5 scale)

Clearly there is a link between the total impulse of the applied pressure curves and the final deformation. It is a very complicated relationship, but happens to be linear when only a single aspect of the pressure profile is modified. In the next section this will be

further explored by modifying several aspects of the pressure curve at the same time, and attempting to obtain drastically different pressure curves having the same total impulse.

6.7.5. Effects of Simultaneous Pressure Curve Modifications

New pressure curves were generated based on the original pressure profile previously shown as Figure 6.28. For the first new profile the amplitude parameter (c) and the time decay parameter (a) were each multiplied by 2. This causes the curves to take on a peak value that is twice as high yet sustain half as long, as shown in Figure 6.45:

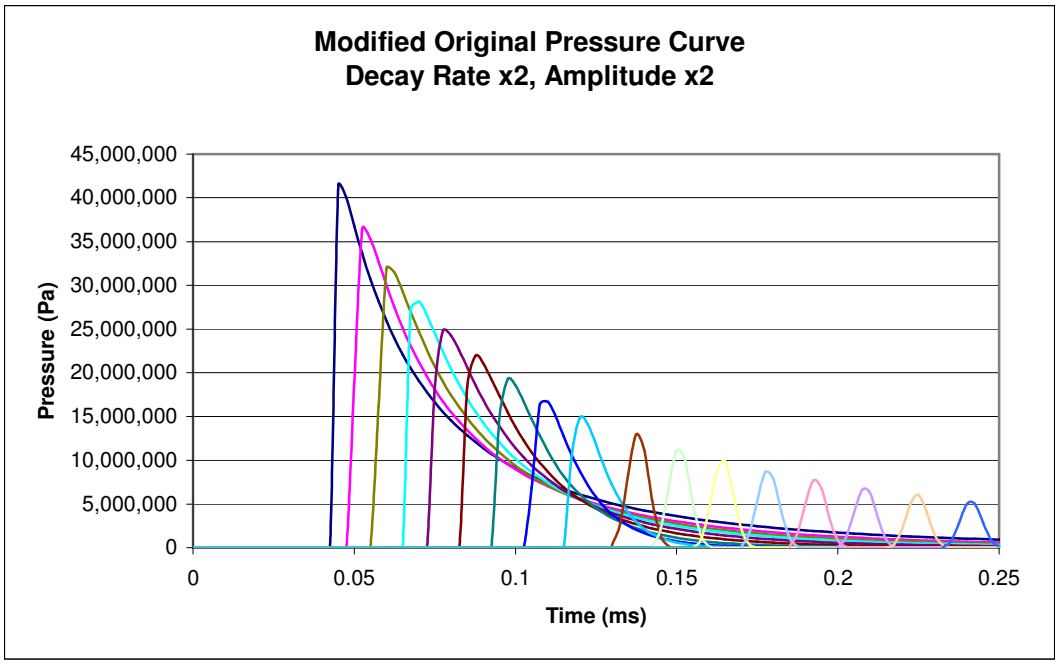

Figure 6.45: Modified Original Pressure Inputs (x2) – 3.94 N·s (0.89 lb·s)

The second profile was created by multiplying each of these parameters by 4, and is shown as Figure 6.46:

a

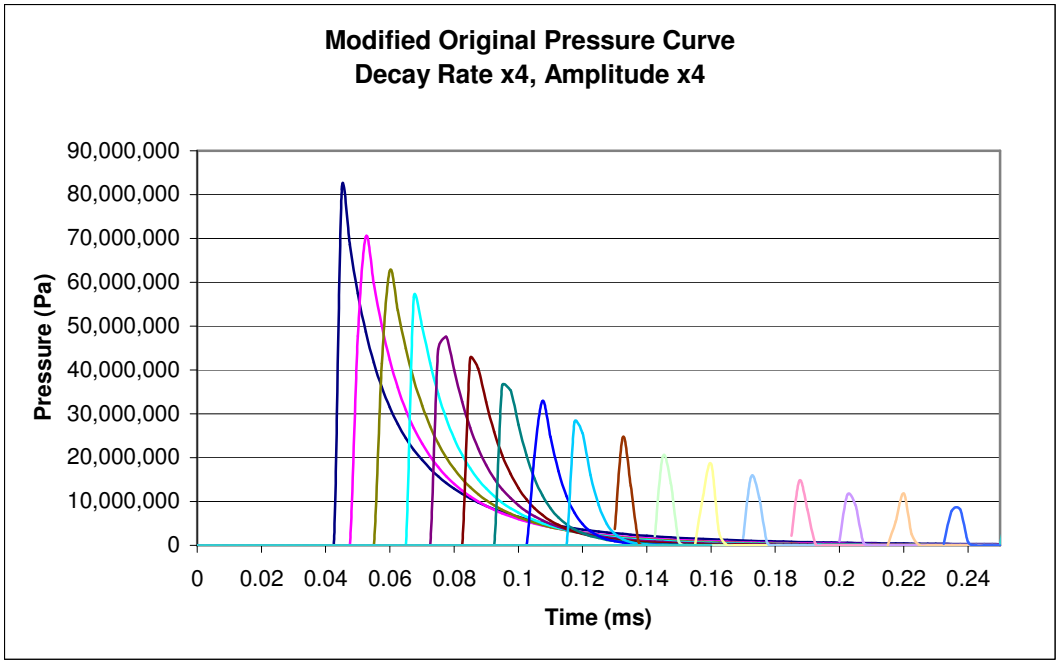

Figure 6.46: Modified Original Pressure Inputs (x4) - 3.97 N·s (0.89 lb·s)

The impulse for each set of pressure curves was calculated, and they ended up both having about 4.0 N•s of impulse, compared to 3.4 N•s for the original pressure curve. The resulting final deformations for the 2x and 4x conditions are shown in Figure 6.47, along with the deformation caused by the original pressure profile:

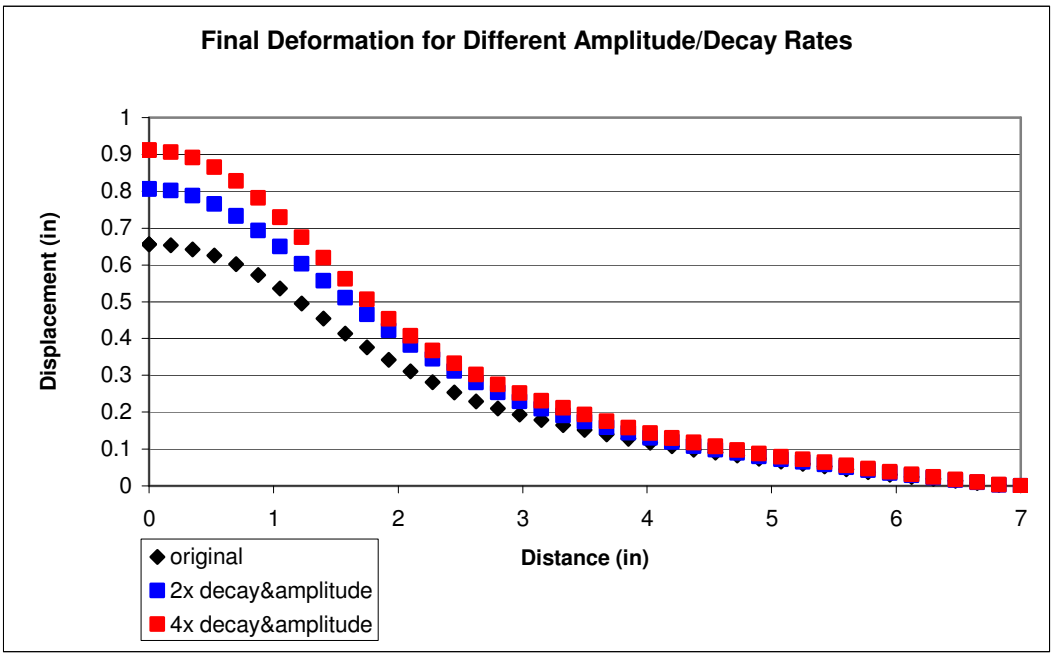

Figure 6.47: Final Deformation from Modified Curves

Even though the two pressure profiles share several similar traits, have the same impulse and cause the same shape deformation, they do not cause the same amount of deformation. The x2 curves produce a final center deformation of 0.806", whereas the x4 curves cause 0.911". However, when plotted on the impulse-deformation curves with the other data (Figure 6.48), the results from these simulations seem to confirm the notion that there is, in fact, a region in which the total impulse linearly affects the final deformation at the center of the plate:

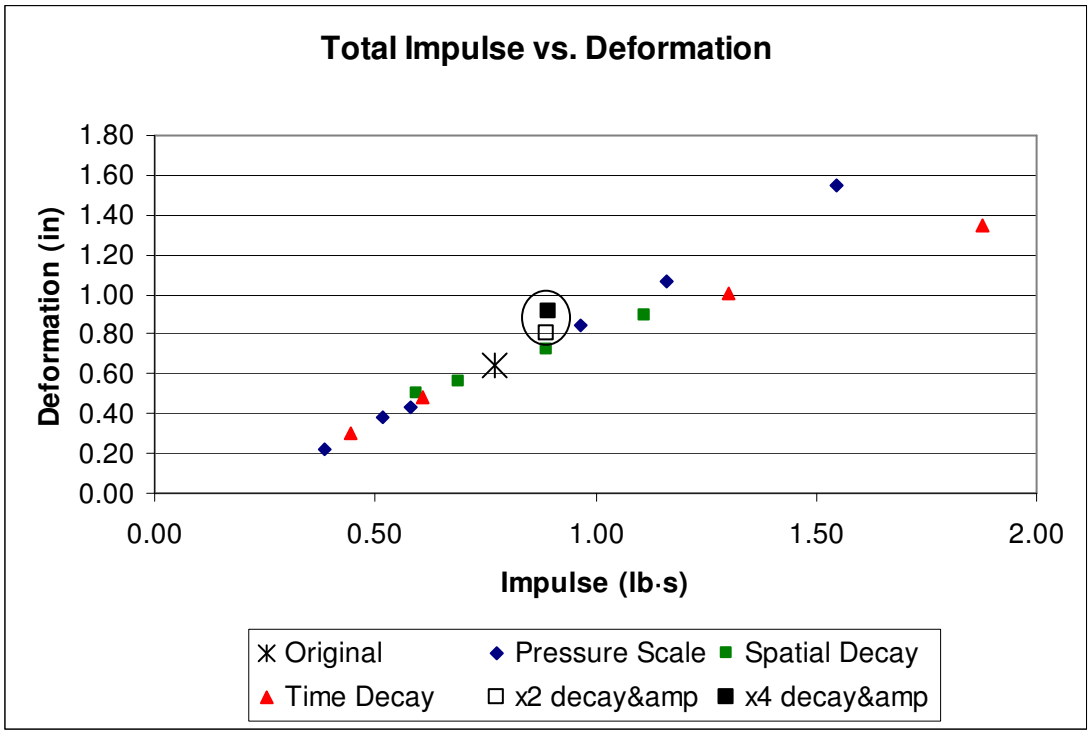

Figure 6.48: Total Impulse vs. Final Deformations with x2 and x4 Tests Circled

This supports the notion that although there is no question the deformation undergone by a flat plate is in fact a complex problem relating to the peak pressures, durations, spatial amplitude decay rate and arrival times, there is a regime where the total impulse of a pressure profile linearly affects the final deformation.

It is important to note that the impulse of the simulation pressure curves are most likely significantly lower than the impulse that would be measured experimentally. This is because in the physical setup the impulse causes both deformation and rigid body motion, whereas for the simulation it only initiates deformation. For instance, the original pressure profile has an impulse of 3.44 N·s, and causes the same deformation as a 1" DOB charge. Referring back to the test results discussed in Table 4.6, the frame of the deforming plate for 1" DOB has an

initial velocity of 4.75 m/s (15.6 ft/s). By multiplying this by the total mass (4.6 kg), the impulse turns out to be about 22 N·s.

6.8 Comparison of Experimental and Computational

Another goal of running the simulations is to determine possible pressure profiles that cause the same deformations as those experimentally measured. The peak pressures, time duration, and spatial decay of the profiles were modified as necessary to determine which combinations produce the final deformation profiles measured by the FARO Arm. In some cases the simulations from the parameter study of Section 6.7 closely matched one such measured deformation, in which case it is reported here. In other cases further tweaking was necessary using the inverse hybrid method in order to obtain the desired deformation. The test conditions are listed in order of increasing deformation, and the simulation results have been mirrored across the y-axis for easier visualization. A summary of the results is shown in Table 6.4:

Description	DOB (in)	Simulation Name	Experimental Deformation (in)	Simulation Deformation (in)	Test
Deepest	1.22	TD-1	0.484	0.487	DT 11
Zero Standoff	*1.22*	SD-1	0.545	0.565	DT 12
Deep	1	original	0.653	0.646	USC 2
Surface/Mid-Depth	0/0.65	PS+1	0.816	0.842	DT 10
Shallow	0.3	x4, scaled 1.1	1.021	1.021	USC 4

Table 6.4: Experimental vs. Simulated Center Point Final Deformation

It is not difficult to generate a pressure curve that produces the desired amount of deformation at the center point. This can be achieved with several iterations of the inverse hybrid method by simply tweaking the scale of any pressure curve until the results agree. However, due to the complexity of the deformation problem it is much more difficult to obtain a pressure profile that produces a similar deformation all

along the plate. Over time an intuition is developed as to which parameters should be modified in order to match a desired deformation, but there is no simple and direct method of determining this other than conducting several iterations. In the following sections the simulated deformation profiles are plotted along with the measured final deformations from several test conditions. The pressure profile used to obtain the desired deformation is also shown.

6.8.1. Matching Pressure Profile to Deformation: Deepest 1.22" DOB

The final deformation from test DT 11 is plotted in Figure 6.49 along with the deformation results from simulation TD-1. The pressure profile input for this test was discussed in the section where the time decay effect was investigated (6.7.3), and is shown once again in Figure 6.50.

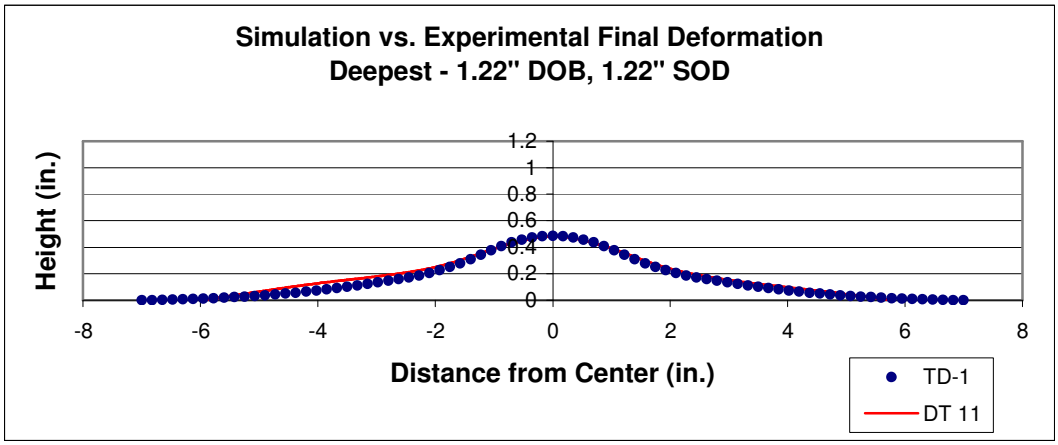

Figure 6.49: Simulation vs. Experimental – 1.22" DOB, 1.22"SOD

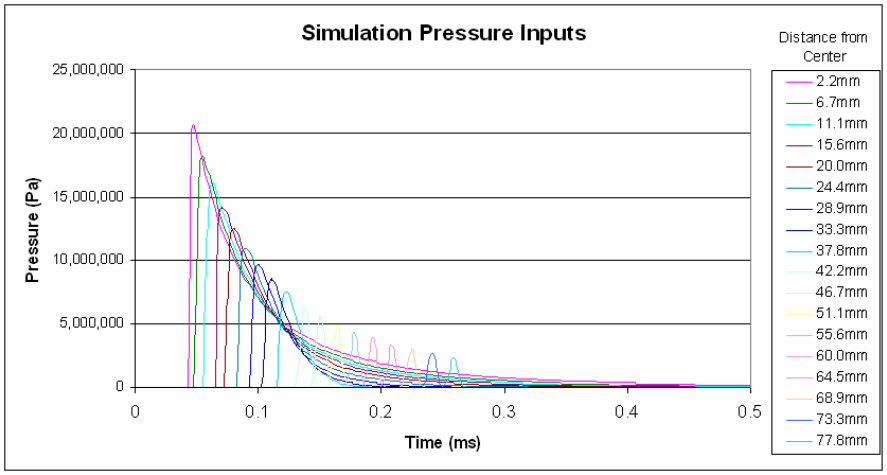

Figure 6.50: Pressure Profile: TD-1

6.8.2. Matching Pressure Profile to Deformation: Zero Standoff 1.22" DOB

The final deformation from test DT 12 is plotted in Figure 6.51 along with the deformation results from simulation SD-1. For this test the pressure profile did not have a great enough spatial decay rate to match the actual deformation further from the center, but the agreement could be improved with minor tweaking. By increasing the spatial decay rate and also increasing the peak pressure values the deformation would become more localized to the center of the plate and better model this test condition. The pressure profile input for this test was discussed in the section where the spatial decay effect was investigated (6.7.2), and is shown once again in Figure 6.52.

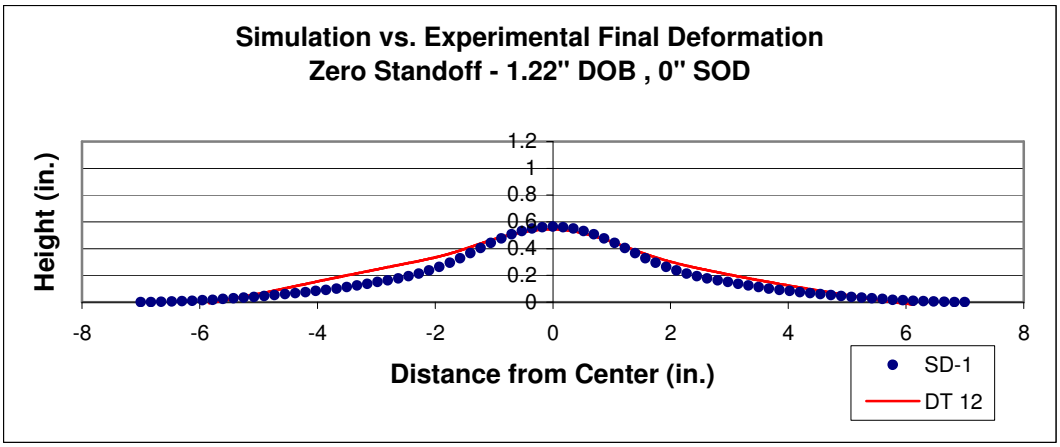

Figure 6.51: Simulation vs. Experimental – 1.22" DOB, 0"SOD

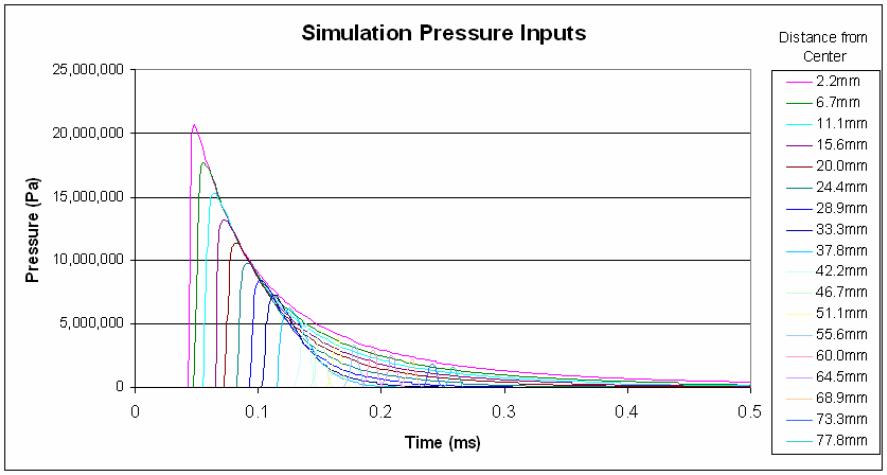

Figure 6.52: Pressure Profile: SD-1

6.8.3. Matching Pressure Profile to Deformation: Deep 1" DOB

The final deformation from test USC 2 is plotted in Figure 6.53 along with the deformation results from the original set of pressure curves. The pressure profile input for this test has been used extensively and discussed in previous sections, but is once again shown in Figure 6.54 for convenience.

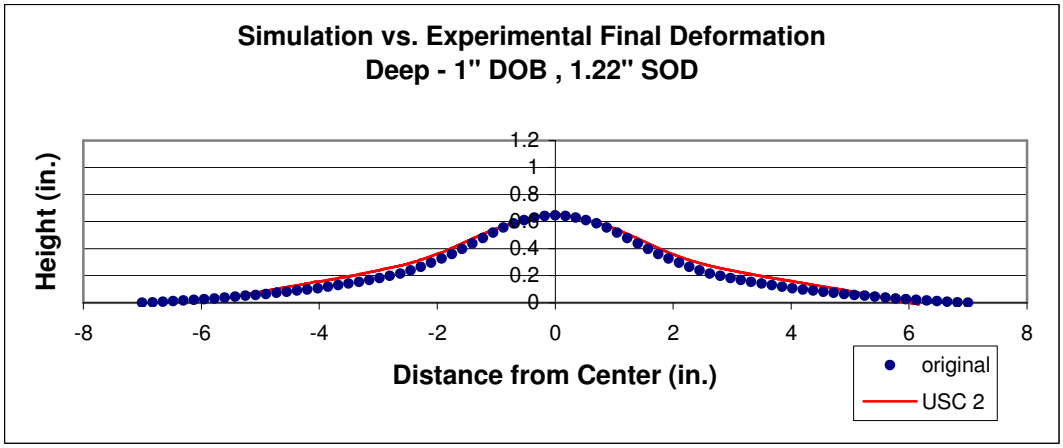

Figure 6.53: Simulation vs. Experimental – 1" DOB, 1.22"SOD

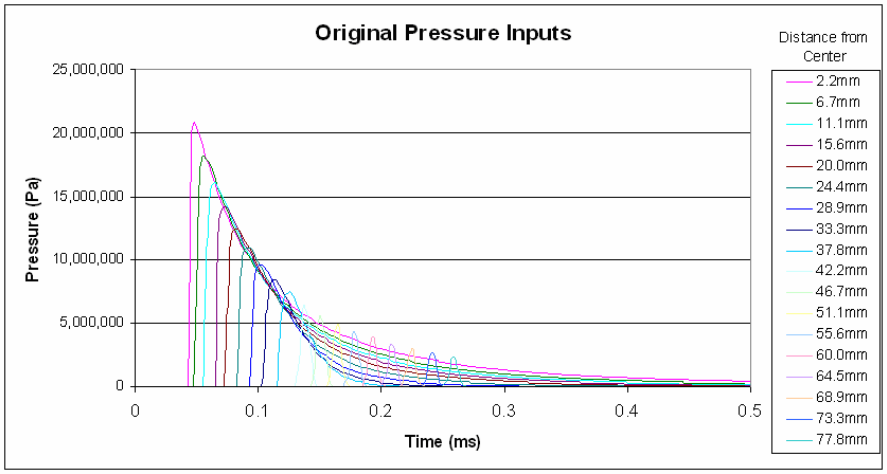

Figure 6.54: Original Pressure Profile

6.8.4. Matching Pressure Profile to Deformation: Surface0”/Mid0.65” DOB

The surface blast and mid-depth charge burial tests had very similar final deformations, so one simulation was used to model both of them. The final deformation from test DT 10 is plotted in Figure 6.55 along with the deformation results from simulation PS+1. The pressure profile input for this test was discussed in the section where the pressure scale effect was investigated, and is shown once again in Figure 6.56.

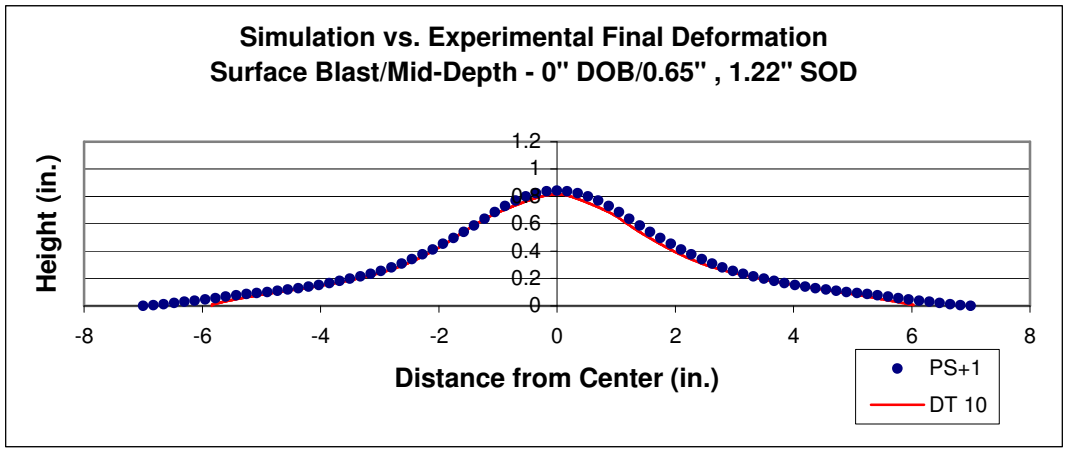

Figure 6.55: Simulation vs. Experimental – 0” DOB / 0.65” DOB, 1.22”SOD

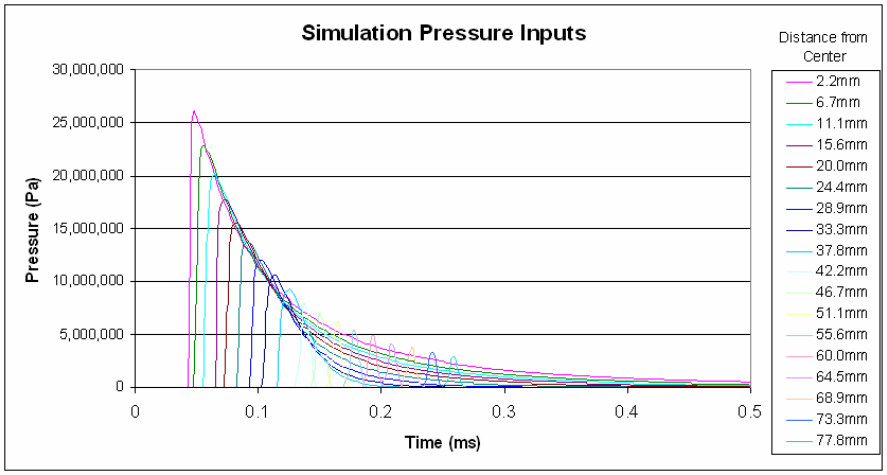

Figure 6.56: Pressure Profile: PS+1

6.8.5. Matching Pressure Profile to Deformation: Shallow 0.3" DOB

The final deformation from test USC 4 is plotted in Figure 6.57 along with the deformation results from a pressure profile tweaked specifically to match this test. The pressure profile input for this test was taken from Section 6.7.5 where original pressure curve was modified to have 4x the decay rate and 4x the amplitude, and is shown once again in Figure 6.58. The pressure profile was also scaled up 1.1 times.

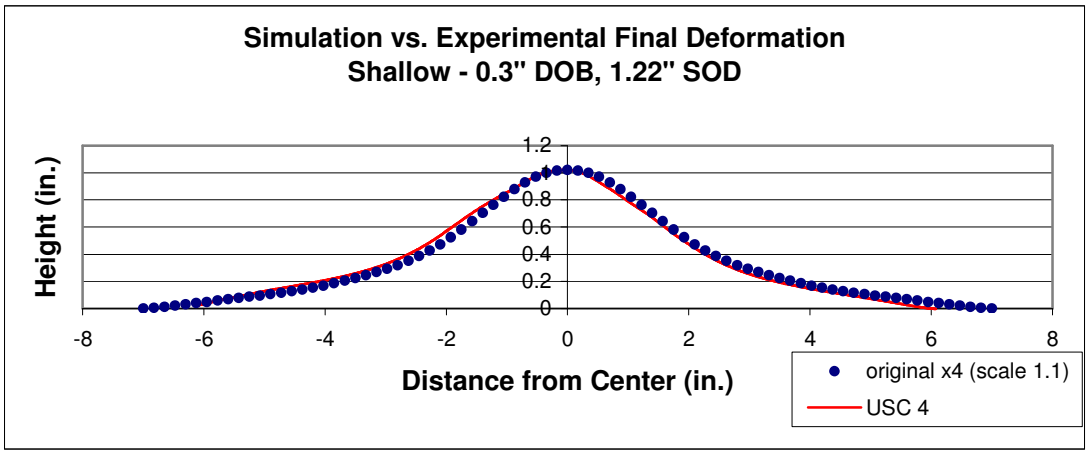

Figure 6.57: Simulation vs. Experimental – 0.3" DOB, 1.22"SOD

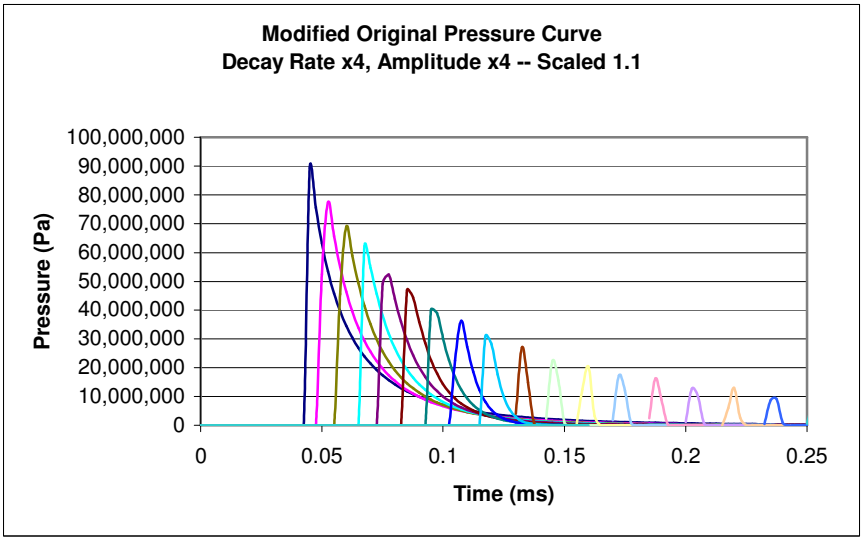

Figure 6.58: Pressure Profile: Modified Original Pressure (x4) with 1.1 Scale

6.9 Comparison of Simulation Pressures to Kolsky Bar Pressure Data

By conducting multiple simulations, it is observed that there are many different pressure profiles that cause the same final deformations. By using the inverse hybrid technique it is impossible to know if any of the pressures obtained actually correspond to what the plate is experiencing. This section will demonstrate that it is possible to obtain drastically different pressure profiles that cause the same deformations.

As mentioned in Section 6.7.4, curves were originally fit to data obtained from Kolsky bar tests, but the magnitude had to be scaled down in order to obtain a reasonable level of deformation. If this was not done, the elements of the simulated plate became deformed too severely and the simulation would crash. The simulation predicted that applying the Kolsky bar pressures would cause more deformation than measured in the physical plate when the same charge size, DOB and SOD were used. One reason for this discrepancy in pressure values could be that the Kolsky bars are held in place by a nondeforming plate, whereas the deformable plate travels away from the explosion. This increases the space between the bottom surface and the explosion, which may cause lower pressures. It is different in the simulation; the code applies these pressures directly to the nodes and they continue to be applied perpendicular to the plate even as it yields. Therefore it is not unreasonable that higher pressures are observed in the Kolsky bar setup than predicted for a deforming plate.

Several simulations were conducted with the goal of finding a pressure profile with the same peak pressure as measured by the Kolsky bars. For Gage Test 271 the

same DOB and SOD was used as for the deep-charge deformable plate test. The maximum recorded pressure from this test was 18,000 psi, so the simulation goal was to use the inverse hybrid method to obtain a pressure profile with this same peak value that produces the same amount of final deformation as the deep-charge test (0.653”). This was done by starting with the original pressure profile that was initially shown as Figure 6.28, which is replotted in units of psi in Figure 6.59 to allow for easy comparison to the Kolsky bar experimental data:

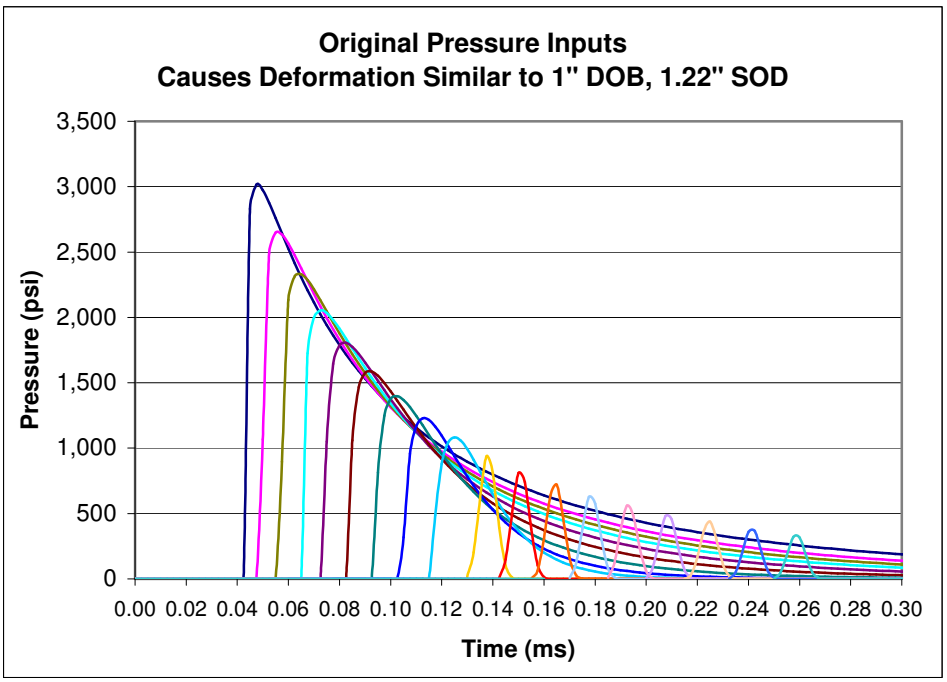

Figure 6.59: Original Pressure Profile – 0.77 lb·s (3.44 N·s)

Several iterations were performed by using this pressure profile and gradually increasing the scale, rate of time decay, and spatial decay until the desired plate shape and amount of deformation was obtained. The modified pressure curve is shown in Figure 6.60 using English units to maintain consistency with the Kolsky bar tests, and the resulting deformation is compared to test USC 2 in Figure 6.61:

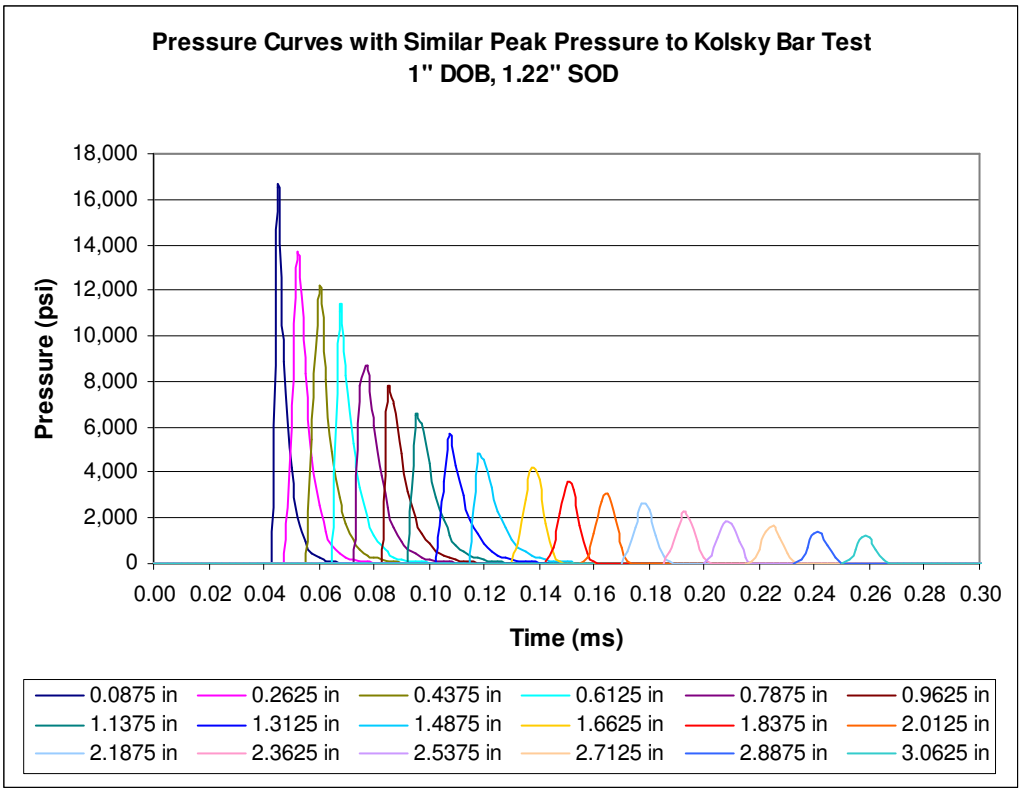

Figure 6.60: Modified Pressure Profile – 0.96 lb·s (4.28 N·s)

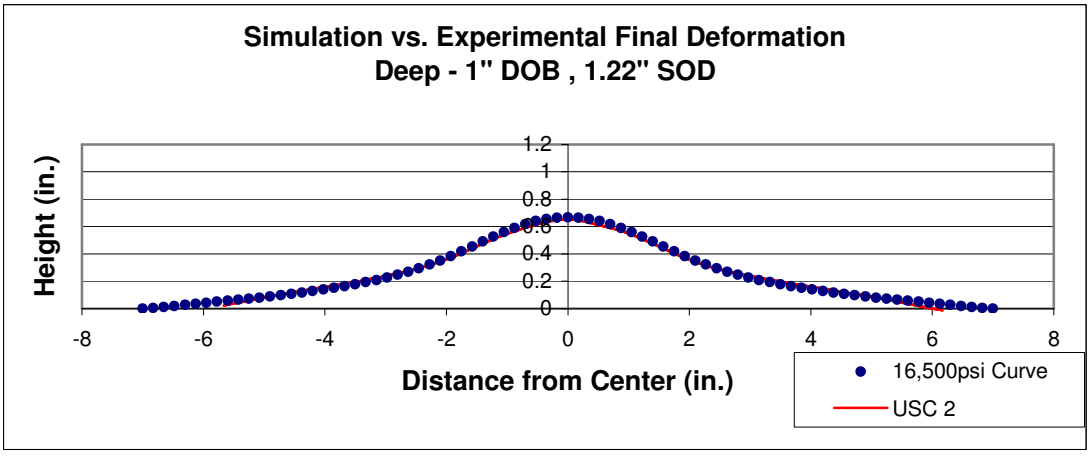

Figure 6.61: Simulation vs. Experimental – 0.3" DOB, 1.22"SOD

This new pressure profile reaches a peak value of 16,500 psi (114 MPa), yet due to the shortened time durations and increased spatial decay it produces a deformation similar to that caused by the original pressure curve with only a 3,000 psi (21 MPa)

peak. The modified pressure profile not only produces a final deformation that agrees more closely to the experimental than the original pressure curve, but has a peak value that is about as high as the Kolsky bar measured peak of about 15,000 psi. The calculated impulse values for the pressure profiles are much more alike than the peak pressure values; the impulse for the original curve is 0.77 lb·s, as compared to 0.96 lb·s for the modified curve.

Although there are currently no means for telling definitively, it is more likely that a pressure profile similar to the modified one was experienced by the plate than the profile with the lower peak value. The simulation and experimentation are not exactly equivalent for several reasons, one of which is that the Kolsky bar pressure reading is not for just the center point of the plate, but rather a ¼" diameter area at the center (due to the size of the bar). However, the Kolsky bar data still provides valuable insight about the accuracy of the simulation pressure curves. The first curves from each pressure profile (which are applied to the center node of the plate) are shown in Figure 6.62 along with the Kolsky bar pressure curve from directly above the charge:

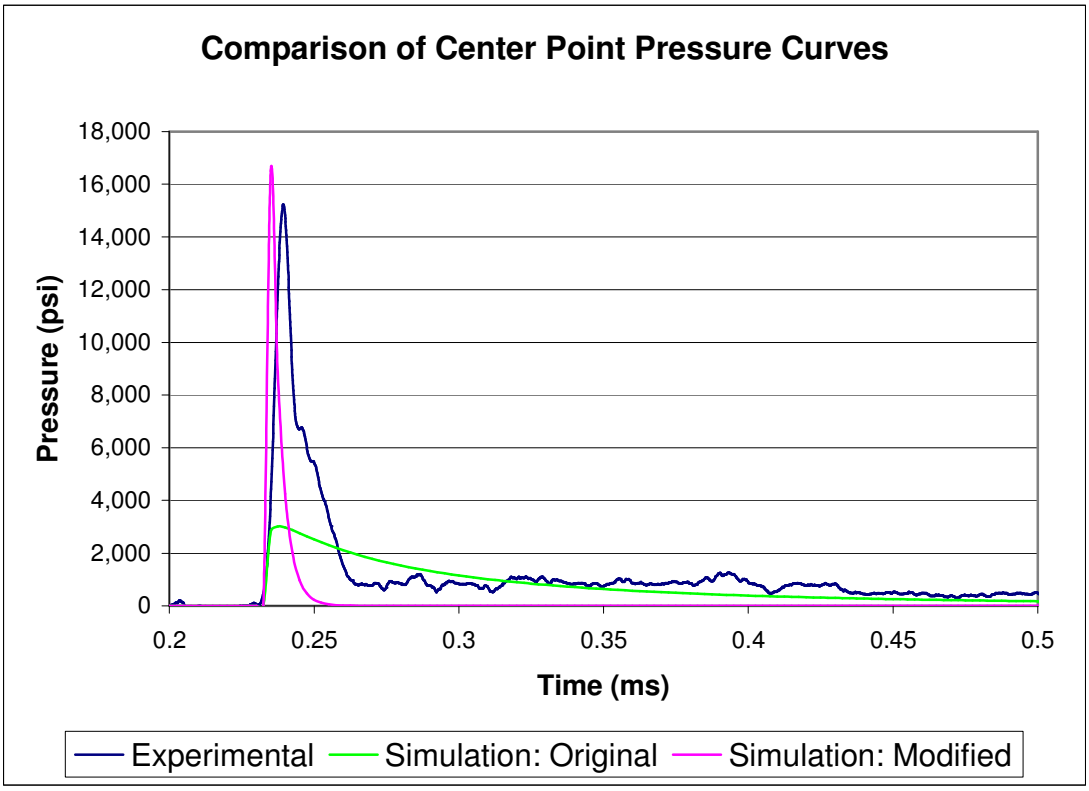

Figure 6.62: Simulated and Experimental Pressure Curves at Center of Plate

Even though both of these simulations output essentially the same final deformation, the pressure profiles are vastly different. From this comparison it appears much more likely that the modified pressure profile is a more accurate interpretation of the explosive loading experienced by the plate. In the next section an attempt is made to analyze the acceleration results from a simulation.

6.10 Center Point Displacement Comparison

The primary goal of running DYNA simulations was to obtain pressure profiles that cause plastic deformation matching the experimental final deformations. However, another aspect of interest is a comparison of the transient center point displacements. Simulation displacement data was compared to the corresponding

experimental data obtained through use of 3D DIC for 1” DOB and 1.22” SOD, as seen in Figure 6.63:

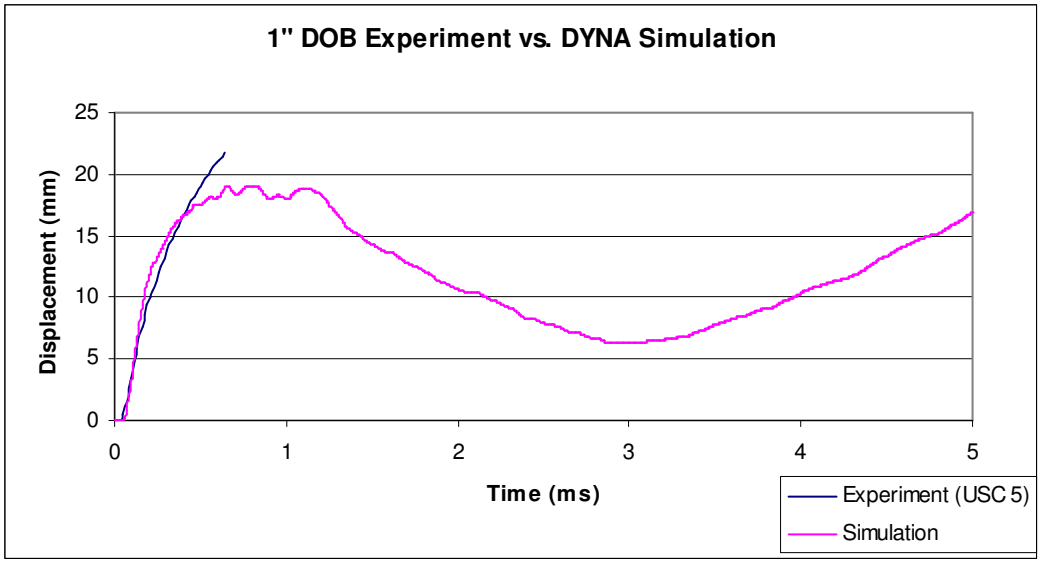

Figure 6.63: Transient Experimental Displacement vs. Simulated

The simulation and experimental results agree quite well in the early stages of deformation. However, the simulation does not include any rigid body motion so the displacements digress as the physical plate begins to translate vertically. Still, this gives credibility to the initial velocity and acceleration values of the simulations. In order to obtain more accurate acceleration values, a very short time frame was necessary. For this reason the beginning portion of the simulation was rerun with an output every 0.1 μs. The reported acceleration values of the center node are shown in Figure 6.64:

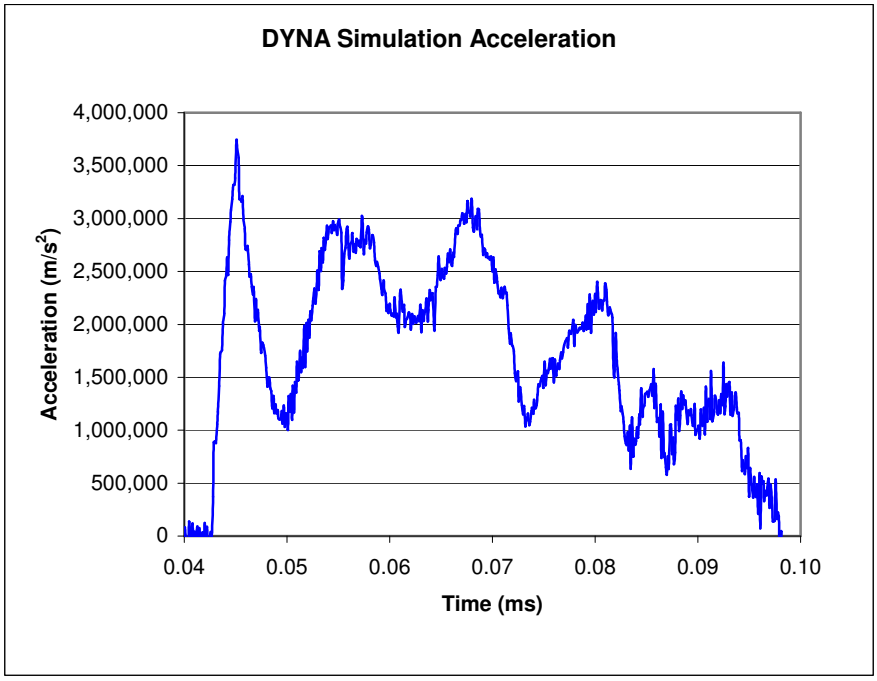

Figure 6.64: Simulated Center Point Acceleration Values

This plot shows that for 1" DOB the plate experiences a maximum acceleration of 3,700,000 m/s^2, or 377,000 *g*. In order to obtain the equivalent full-scale acceleration, this value is divided by the scaling-factor (as discussed in Section 1.3). This equates to a full-scale acceleration 29,000 *g*.

Chapter 7: Conclusion

7.1 Overview of Data Presented

In completing this thesis, small-scale experimentation was conducted with several different test parameters using a variety of data collection techniques and measurements. The typical test used a deformable plate and 1.22" SOD, while varying the depth that the charge is buried. Testing was also conducted with the SOD modified so the plate sat directly on the sand, as well as using a nondeforming plate that was essentially rigid. Manual point tracking was done for this rigid plate (as well as the deep test condition), but for the most part 3D DIC data was obtained for each test condition. The resulting crater was measured for most setups, and the final deformation of the plate was determined using high-accuracy 3D measurement techniques. The type of data presented for each test condition is indicated with an X in Table 7.1:

Description	DOB (in)	SOD (in)	DIC Data	Crater	Final Deformation
Surface Blast	0	1.22	X	X	X
Shallow	0.3	1.22	X		X
Mid-Depth	0.65	1.22	X	X	X
Deep	1	1.22	X	X	X
Rigid plate	*1*	*1.22*		X	
Deepest	1.22	1.22	X	X	X
0" SOD	1.22	0	X	X	X

Table 7.1: Description of Data Available for Each Test Condition

Trends were observed for the obtained data, such as the dependence of crater depth and final deformation on DOB, as well as the relationships between crater volume and volume under the deformed plate. A comparison of the initial velocity was done between that of a rigid plate and the deformable plate/frame rig. 3D DIC

data was also analyzed to provide the initial velocity, center point strains and strain rates, and a rough approximation of maximum acceleration. Although 3D DIC is a well established field, due to digital cinematography limitations it is relatively new to high-speed applications such as an explosively deforming metal.

7.2 Inverse Hybrid Methodology Discussion

Most of the experimental data was obtained in order to support the development of a method for determining the explosive loading on flat plates due to a buried charge. Beginning with data obtained from Kolsky bar experiments, it is possible to fit equations to these pressures and obtain parameterized curves at known distances from the center of the plate. By fitting equations through these parameters, it is then possible to generate a pressure curve for any necessary distance from the center. This allows for nodal loads to be applied in a finite element method model. After running a preliminary simulation, values such as acceleration or final deformation can be compared to the results obtained from 3D DIC experimentation. The pressure profile is then modified and the simulation is rerun until the results agree with the small-scale experimentation. At this point a pressure profile (also known as a set of pressure curves) has been obtained that could possibly have been experienced by the plate during the explosive deformation. Appendix F is a code that can be used to visualize the curves as the pressure distribution across the plate at one instance in time. The inverse hybrid method is depicted as a flowchart in Figure 7.1:

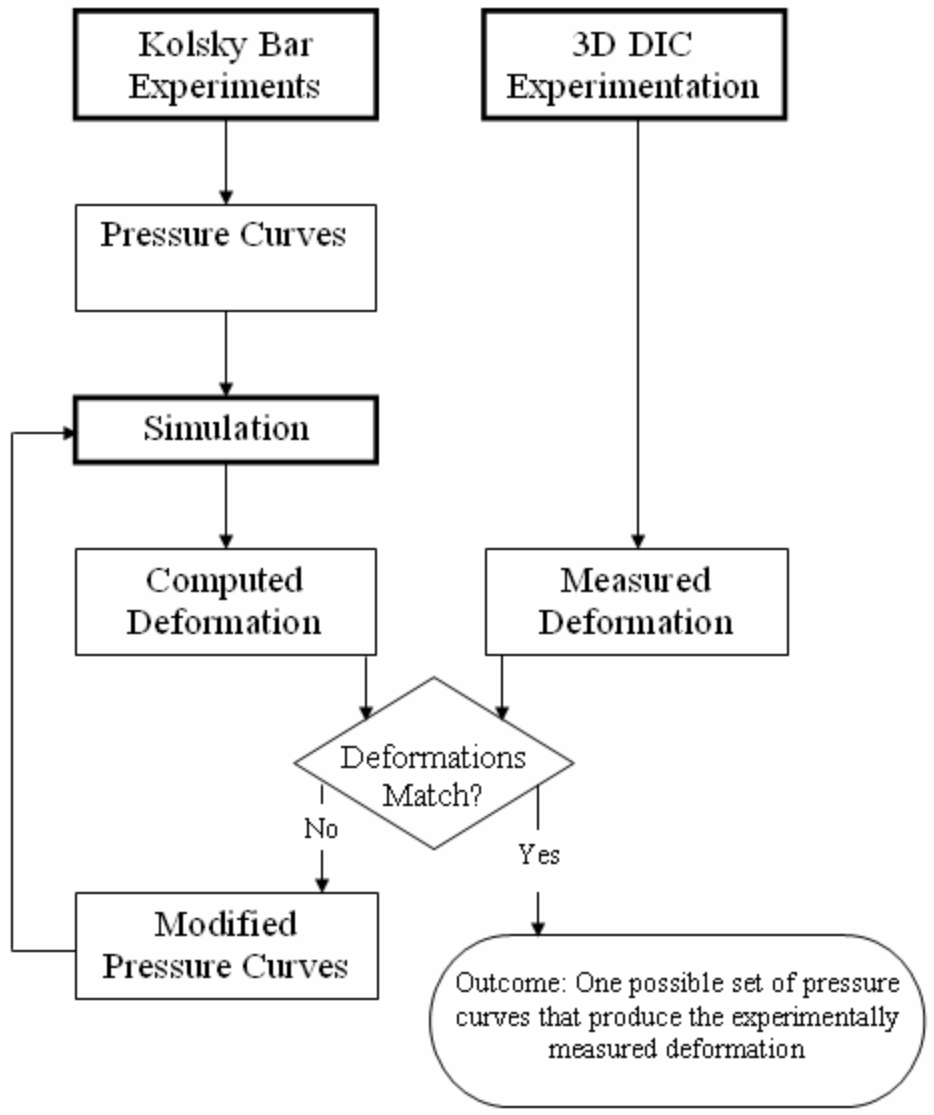

Figure 7.1: Inverse Hybrid Method for Determining Explosive Loading on Plates

By using this method, several important aspects were discovered about the pressures. One realization was that the final deformation is very sensitive to not only the peak pressure value, but also the time and spatial decay, as well as the arrival time of these pressures at different distances along the plate. It was also demonstrated that it is not adequate to classify the explosive force simply by the peak pressure or the total impulse. The simulations demonstrate that there are some situations in which the total impulse of a pressure profile linearly affects the final deformation. For instance,

by only modifying a single curve parameter within a certain regime the final deformation can be predicted based on the known total impulse if a similar pressure curve has already been simulated. However, without this knowledge, the impulse cannot be used to quantitatively predict the amount of deformation. It has also been demonstrated that pressure profiles with the same impulse can generate differing final deformations. This supports the notion that the deformation undergone by a flat plate is in fact a complex problem related to the peak pressures, durations, spatial amplitude decay rate and arrival times, to which the inverse hybrid method can be successfully applied.

In conclusion, this research includes several different types of valuable data, such as the relationship between final deformation profiles to charge depth of burial, and a comparison of crater volume to the volume under the deformed plate. A new inverse hybrid method was developed to allow for better characterization of the pressure profiles experienced by a plate as the blast develops. Based on the research, the following conclusions were made:

- Even though some of the blast's energy is spent deforming the plate, the initial velocity of the rigid body motion is greater than a nondeforming plate of equal mass.
- Simulations showed that the final deformation cannot be determined from only total impulse or peak pressures.
- The final deformation is very sensitive to not only the peak pressure value, but also the time and spatial decay, as well as the arrival time of these pressures at different distances along the plate.

- The inverse hybrid method can be used to determine some of the many possible pressure profiles experienced during an explosion, but experimentation is also necessary to determine which profile is the most accurate.

Appendix A: Matlab CSV Combine Code

```
%CSV/Spreadsheet combining program
%by: Damien Bretall
clear all;
format long;

%values to be edited for each data set
directory = 'G:\Damien - merging computers\Damien\Defomation Tests -
Damien\Deformation Test 9\Complete Recal\Deformation Profiles\'
startfile_num = 01;
endfile_num = 20;
maxpointindex = 200; %if 201 points, max is 200
%also be sure to change the file name below

totalpointindicies = maxpointindex+1;
numfiles = 1 + endfile_num - startfile_num;
data = [0:maxpointindex]';
for i = 1:numfiles  %number of files to read in
    %adjusts for single digit numbers
    if i < 10
        filename = ['DT9_0' num2str(startfile_num + (i-1)) '.csv'];
    else
        filename = ['DT9_' num2str(startfile_num + (i-1)) '.csv'];
    end
    disp(filename)

  %Prescreen files and add in missing Point Indexes

    %need to read in complete file since length could vary
    read_in_temp = csvread([directory filename],2,9);
    read_in = read_in_temp(:,1);
    read_in_index_temp = csvread([directory filename],2,0);
    read_in_index = read_in_index_temp(:,1);

    data_segment = zeros(totalpointindicies, 1);
    index = 1;
    for j = 1:totalpointindicies
        if read_in_index(index,1) == (j - 1)
            data_segment(j,1) = read_in(index,1);
            index = index + 1;
        else
            data_segment(j,1) = 0.0000001;
            %need to use Excel to eliminate these false 0.0000001
values
        end

    end

    data = [data data_segment];

end
csvwrite([directory 'matlab_combined_W.csv'],data)
```

Appendix B : Johnson-Cook 6061-T6 Parameters

Retrieved from the EPIC code's material library (not all were necessary for the code):

Mass properties:

density	=	0.270378E+04	
specific heat	=	0.896167E+03	
conductivity	=	0.167021E+03	
volume expansion coef	=	0.630000E-04	
initial temperature	=	0.294261E+03	
room temperature	=	0.294261E+03	
melting temperature	=	0.925372E+03	
absolute zero temp	=	0.000000E+00	

Johnson-Cook parameters assuming the equation in the form of:

s=(c1+c2*e^n)*(1+C*ln(rate/1/s))(1-T*^m)
where T*=(T-Tr)/(Tm-Tr), s=stress, e=strain, rate=strain rate
(Note the strain-rate in the ln() term is normalized by a reference strain-rate of 1/s)

shear modulus	=	0.275790E+11	
yield stress, c1	=	0.324054E+09	[A]
hardening coef, c2	=	0.113763E+09	[B]
hardening exponent, n	=	0.420000E+00	[n]
strain rate coef, c3	=	0.200000E-02	[C]
softening exponent, m	=	0.134000E+01	[m]
pressure coef, c4	=	0.000000E+00	
max strength (optional)	=	0.000000E+00	

Note that the EPIC code uses different variable names for the parameters than the Johnson-Cook form given in Chapter 6. The letters in brackets have been added to show how they correspond.

Appendix C: DYNA Keywords Used

*CONTROL_TERMINATION – controls how long the simulation will run for

*CONTROL_TIMESTEP – determines the initial timestep (if left blank the solver will calculate an appropriate timesetp. tssfac is set at 0.9 for the validation tests, but 0.67 is used for explosive simulations to provide a smaller timescale.

*DATABASE_BNDOUT, *DATABASE_NODFOR, *DATABASE_SPCFORC – outputs boundary forces, applied nodal forces, and reaction forces. Useful to ensure the simulation is applying forces as expected.

*DATABASE_BINARY_D3PLOT – determines how often the nodal displacements and other data will be output. By entering a value for lcdt the data output frequency can be varied over time (such as to obtain more outputs during the initial high velocity stages). By setting ioopt to 1 the output will occur at the time intervals specified by the load curve at that instance in time on the curve.

*DATABASE_NODAL_FORCE_GROUP – defines nodes for which the forces will be output (works in conjunction with *DATABASE_NODFOR and *SET_NODE_LIST)

*BOUNDARY_SPC_NODE – sets boundary conditions for fixed nodes (most simulations performed hold the X Y Z movement of the boundary nodes fixed, significant nodal rotation is not possible in this geometry so fixing these degrees does not produce different results)

*LOAD_NODE_POINT – applied loads directly to nodes. In axisymmetric simulations this is input as a force per circumferential length (Ex: N/m). dof determines the direction of the load, and lcid refers to the load curve.

*LOAD_SEGMENT – a different method of applying the loads. For the axisymmetric simulation, pressures are input as load curves (Ex: N/m^2) and distributed to the two nodes listed. The solver distributes the pressure as two point loads based on the distance between both nodes. Values for n3 and n4 should either be left blank, or should be repeats of the n2 value.

*PART – assigns the section, material, equation of state to a complete part.

*SECTION_SHELL – defines the section properties as axisymmetric shell elements (elform 14 is an area weighted definition, which is recommended for explosive simulations)

*MAT_JOHNSON_COOK – defines a Johnson-Cook material with the parameters for 6061 aluminum.

*EOS_LINEAR_POLYNOMIAL – required for a Johnson-Cook material. It is simply used to define the bulk modulus for aluminum (which is the same as Young’s modulus since Poisson’s ration is 0.33 for aluminum)

*DEFINE_CURVE – defines the curve for the forces or pressures to be applied

*SET_NODE_LIST – defines a node set, used in this case for nodal force output (see *DATABASE_NODFOR and *SET_NODE_LIST).

*ELEMENT_SHELL – defines each element in terms of 4 nodes. This is generated automatically by the 2Dmesh option in LS-PREPOST.

*NODE – defines the coordinate of each node. Also automatically generated using the 2D mesher.

*END – defines the end of the code

Appendix D: DYNA Validation Code

```
*KEYWORD
*TITLE
$# title
Dynamic Effects Lab - Damien Bretall
*CONTROL_TERMINATION
$#  endtim    endcyc     dtmin    endeng    endmas
  0.200000
*CONTROL_TIMESTEP
$#  dtinit    tssfac      isdo    tslimt     dt2ms      lctm
erode     ms1st
 2.0000E-6  0.900000
$#  dt2msf   dt2mslc     imscl
     0.000         0         0
*DATABASE_BNDOUT
$#      dt    binary
  0.001000         1
*DATABASE_NODFOR
$#      dt    binary
  0.001000         1
*DATABASE_SPCFORC
$#      dt    binary
  0.001000         1
*DATABASE_BINARY_D3PLOT
$#      dt      lcdt      beam     npltc
  0.001000
$#   ioopt
         1
*DATABASE_NODAL_FORCE_GROUP
$#    nsid       cid
         1
*BOUNDARY_SPC_NODE
$#     nid       cid      dofx      dofy      dofz     dofrx
dofry     dofrz
       405         0         1         1         1
       324         0         1         1         1
       243         0         1         1         1
       162         0         1         1         1
        81         0         1         1         1
*LOAD_NODE_POINT
$#     nid       dof      lcid        sf       cid        m1
m2        m3
         2         2         1  1.000000
         3         2         1  1.000000
         4         2         1  1.000000
         5         2         1  1.000000
         6         2         1  1.000000
         7         2         1  1.000000
         8         2         1  1.000000
         9         2         1  1.000000
        10         2         1  1.000000
        11         2         1  1.000000
        12         2         1  1.000000
        13         2         1  1.000000
```

```
        14         2         1  1.000000
        15         2         1  1.000000
        16         2         1  1.000000
        17         2         1  1.000000
        18         2         1  1.000000
        19         2         1  1.000000
*PART
$# title

$#     pid     secid       mid     eosid      hgid      grav
adpopt      tmid
         1         1         1         1
*SECTION_SHELL_TITLE
Axisymmetric_shell
$#   secid    elform      shrf       nip     propt   qr/irid
icomp     setyp
         1        14  1.000000         2         1         0
0         1
$#      t1        t2        t3        t4      nloc     marea
     0.000     0.000     0.000     0.000         0     0.000
*MAT_JOHNSON_COOK_TITLE
Johnson-Cook_6061
$#     mid        ro         g         e        pr       dtf
vp
         1 2703.78002.7579E+106.8900E+10  0.330000
$#       a         b         n         c         m        tm
tr      epso
 3.2405E+8 1.1376E+8  0.420000  0.002000  1.340000 925.37201
294.26099  1.000000
$#      cp        pc     spall        it        d1        d2
d3        d4
 896.16699     0.000  2.000000
$#      d5
     0.000
*EOS_LINEAR_POLYNOMIAL_TITLE
Linear_EOS
$C1 = K = Bulk modulus (same as Elastic modulus since Poisson = .33)
$#   eosid        c0        c1        c2        c3        c4
c5        c6
         1     0.0006.8900E+10
$#      e0        v0
 7.1100E+8  1.000000
*DEFINE_CURVE_TITLE
node_force
$#    lcid      sidr       sfa       sfo      offa      offo
dattyp
         1         0  1.000000  1.000000
$#                a1                  o1
              0.000               0.000
          0.10000000        8500.0000000
          0.20000000        8500.0000000
*SET_NODE_LIST
$#     sid       da1       da2       da3       da4
         1
$#    nid1      nid2      nid3      nid4      nid5      nid6
nid7      nid8
```

```
         1         2         3         4         5         6
7        19
*ELEMENT_SHELL
$#   eid     pid      n1      n2      n3      n4      n5      n6
n7      n8
       1       1       1       2      83      82
       2       1       2       3      84      83
    [...]
     319       1     322     323     404     403
     320       1     323     324     405     404
*NODE
$#   nid               x               y               z      tc
rc
       1           0.000      0.00100000
       2      0.00222250      0.00100000
    [...]
     404      0.17557739      0.00258800
     405      0.17779988      0.00258800
*END
```

Appendix E: Pressure Curves Formatting Macro

Visual Basic code embedded in “Excel to DYNA macro.xls”

```
Option Explicit
Dim X, Y As Integer
Dim lcid As Integer
Dim spacelcid As String
Dim data(300, 60) As String

Private Sub CmdOpen_Click()
lcid = 1

For X = 1 To 300
    For Y = 1 To 60
        data(X, Y) = ""
    Next Y
Next X

For Y = 1 To 60
    For X = 1 To 300
        If Worksheets("Calculated Pressure Curves").Cells(X + 8, Y).Text <> "" Then
            data(X, Y) = Worksheets("Calculated Pressure Curves").Cells(X + 8, Y).Text
        End If
    Next X
    If Worksheets("Calculated Pressure Curves").Cells(9, Y).Text = "" Then GoTo exit1
Next Y

exit1:
Open txtpath.Text & "/" & txtFile.Text For Output As #1

For Y = 2 To 60
    'exit if its reached a blank column
    If data(1, Y) = "" Then GoTo exit2

    'header
    If lcid < 10 Then
        spacelcid = "         "
    Else
        spacelcid = "        "
    End If

    Print #1, "*DEFINE_CURVE_TITLE"
    Print #1, "" & lcid
    Print #1, "$#    lcid      sidr       sfa       sfo      offa      offo    dattyp"
    Print #1, "" & spacelcid & lcid & "         0  0.001000  1.000000"
    Print #1, "$#                a1                o1"

    lcid = lcid + 1

    For X = 1 To 300
        If data(X, Y) <> "" And data(X, Y) <> "#NUM!" Then
            If data(X, Y) <> "0" Then
                Print #1, "          " & Format(data(X, 1), "0.00000000") & "      " &
Format(data(X, Y), "0.0000000E+000")
            Else
                Print #1, "          " & Format(data(X, 1), "0.00000000")
            End If

        End If
    Next X
Next Y

exit2:
Close #1
'opens folder
Shell "explorer.exe " & txtpath.Text, vbNormalFocus
End Sub
```

Appendix F : Matlab Distance-Pressure Profile Generator

Although it was not discussed in the body of the thesis, this Matlab code is a helpful tool for visualizing the pressure-time curves and Kolsky bar data in a different fashion.

```
%Pressure Movie Generator
%by: Damien Bretall
%Description: Converts a set of time-pressure curves into distance-
%pressure profiles at each instance in time, which can be played as
%a movie

clear all
hold off

%variables
columns = 19
rows = 202
units = 'Pa'
data = csvread('C:\LSDYNA\program\8-03-07\Matlab Inputs.csv')

distance = [-fliplr(data(1,2:columns)) data(1,2:columns)]

for timerow = 2:rows
    plot(distance, [fliplr(data(timerow,2:columns))
data(timerow,2:columns)]);
    axis([-4 4 0 25000000]);
    title(['Time: ' num2str(data(timerow,1)) 'ms']);
    xlabel('Distance (in.)')
    ylabel(['Pressure (' units ')'])
    if timerow < 10
        saveas(gcf,['Original 00' num2str( timerow ) '.bmp'])
    elseif timerow >=10 & timerow < 100
        saveas(gcf,['Original 0' num2str( timerow ) '.bmp'])
    else
        saveas(gcf,['Original ' num2str( timerow ) '.bmp'])
    end

    M(timerow-1) = getframe;
end
```

Here is a small sample of a csv file of pressure-time curves used for the Matlab input:

	0.0875	0.2625	0.4375	0.6125	0.7875	0.9625	
0	7724894	7761361	7978224	8592076	8058245	0	
0.0025	7390377	7384015	7532638	8093760	8473320	0	
0.005	7073066	7026502	7108055	7587602	8384920	0	
0.0075	6772032	6688073	6705420	7089786	8037501	3352080	
0.01	6486370	6367876	6324859	6609647	7559396	6058531	…

The columns in this spreadsheet each represent a pressure-time curve applied at a specific distance from the center of the plate (the top row shown in blue), with the times appearing in the leftmost column (shown in red). This code allows for visualization of the data as rows rather than columns, which can then reveal interesting aspects of the pressure profiles.

Beginning with a set of pressure-time curves as shown in the following figure, the code converts them into a series of pressure-distance plots that can be played as a movie to show how the pressure develops on the plate's surface over time, three of which are shown at the bottom of the figure:

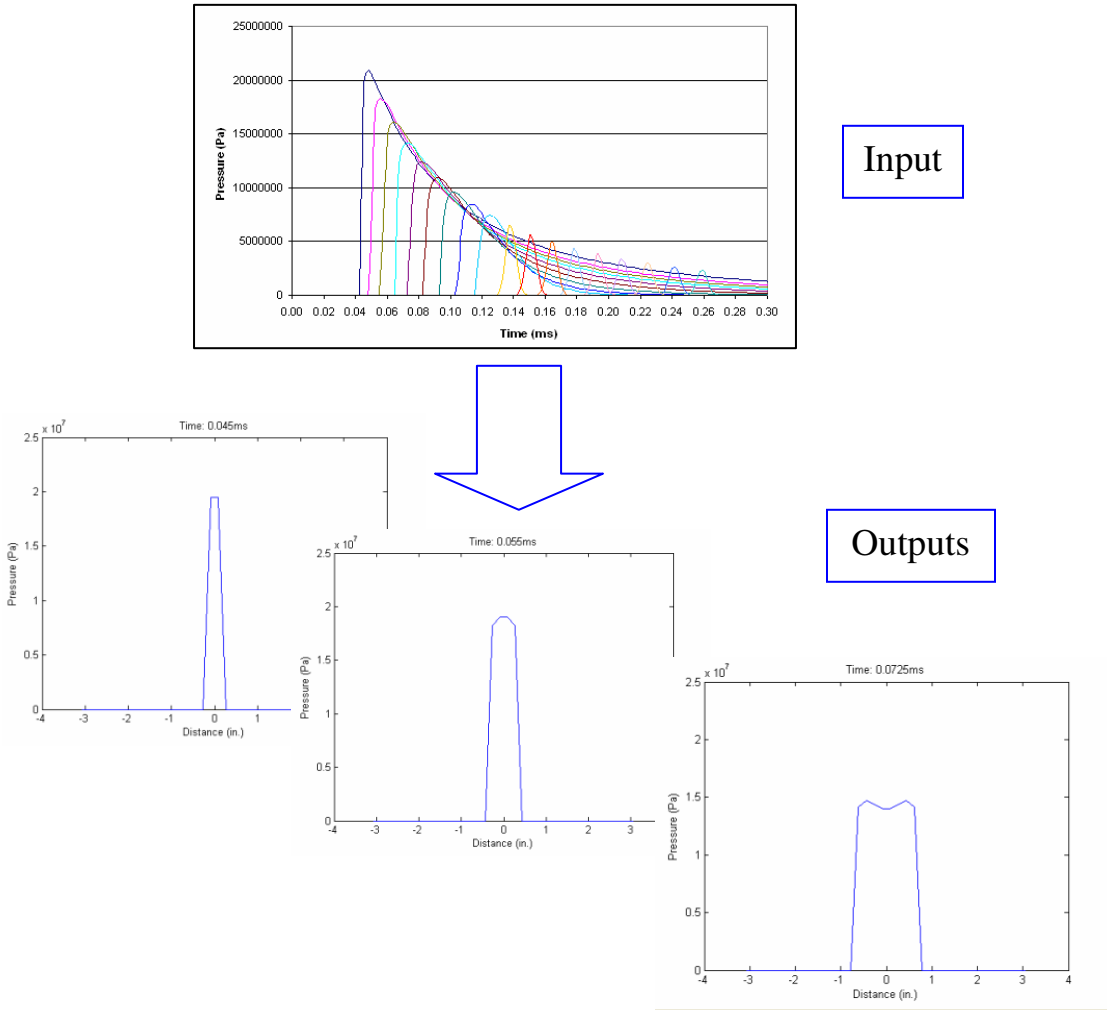

Glossary

axisymmetric: rotational symmetry about an axis; material geometry and properties are identical along every circumferential path

depth of burial (DOB): distance from the top of the explosive to the surface of the sand

Deta sheet: similar to plastic explosives, it is a moldable sheet explosive consisting of 63% PETN by weight

Digital Image Correlation (DIC): a technique to measure deformation of an object's surface; **3D DIC** requires two cameras and can measure out-of-plane deformation

Exploding Bridge Wire (EBW): the type of detonator used to initiate the explosive

FARO: company producing high-accuracy three dimensional measurement devices; the term is also used to refer to the FARO Arm tool used for taking measurements

finite element analysis (FEA): computer simulation technique for finding solutions of complex problems through application of the finite element method

finite element method (FEM): numerical technique for approximating solutions of complex problems

FS-17: firing system used to trigger the EBW

improvised explosive device (IED): unconventional homemade bombs and mines fabricated in many different ways and detonated by various means

inverse hybrid method: technique developed in this thesis for determining possible pressure profiles that could have been experienced by a plate with a measured deformation or rate of acceleration

Johnson-Cook material: commonly used constitutive equation to determine the von Mises flow stress as a function of strain, strain rate, and temperature

Kolsky bar: a long metal rod held in place and subjected to a sudden pressure; several strain gages are mounted along the length to measure the pressure wave

LS-DYNA (aka DYNA): FEA software used to simulate and analyze dynamic events

LS-PrePost: pre- and post-processing software included with LS-DYNA for setting up the FEA model and analyzing the results

PETN: pentaerythritol tetranitrate, a very powerful high explosive

pressure curve: one pressure-time curve that is applied to a single node in the FEA simulations

pressure profile: the full set of pressure-time curves applied to the simulated plate

RDX: cyclotrimethylenetrinitramine, a common military high explosive also known as cyclonite

RP-87: the name of the exploding bridge wire detonator used

standoff distance (SOD): distance from the surface of the sand to the bottom surface of the plate

universal testing machine (UTM): used for performing various material tests by applying deformation at a prescribed rate and measuring the resulting load

References

[1] Genson, Kevin. “Vehicle Shaping for Blast Damage Reduction.” M.S. thesis, University of Maryland, 2006.

[2] Wenzel, Alex. Hennessey, John. “Analysis and Measurements of the Response of Armor Plates to Land Mine Attacks.” Paper II-9.

[3] Anderson, John. Fainaru, Steve. Finer, Jonathan. “Bigger, Stronger Homemade Bombs Now to Blame for Half of U.S. Deaths.” Washington Post, October 26, 2005. <http://www.washingtonpost.com/wp-dyn/content/article/2005/10/25/AR2005102501987.html>, accessed Sept 27, 2007.

[4] “Mine / IED protected Vehicles Design Principles.” Defense Update, Oct 25, 2005. <http://www.defense-update.com/features/du-3-04/vehicle-protection-design.htm>, accessed Sept 27, 2007.

[5] Capaccio, Tony. “Mine More U.S. Troops Die in Iraq Bombings Even as Armoring Improves.” Bloomberg, Oct 13, 2005. <http://www.bloomberg.com/apps/news?pid=10000103&sid=aftH7bcepI8I&refer=us>, accessed Sept 27, 2007.

[6] “U.S. Fatalities by Month.” Iraq Coalition Casualty Count, Sept 23, 2007. <http://icasualties.org/oif/IED.aspx>, accessed Sept 23, 2007.

[7] “Improvised Explosive Devices (IEDs) / Booby Traps.” Jan 11, 2005. <http://www.globalsecurity.org/military/intro/ied.htm>, accessed Sept 27, 2007.

[8] Chabai, Albert. “On Scaling Dimensions of Craters Produced by Buried Explosives.” Journal of Geophysical Research v70.n20 (Oct 15, 1965): p5075-5098.

[9] “RP-87 EBW Detonator.” Teledyne Technologies, Inc. <http://www.teledynerisi.com/products/0products_1ebw_page27.asp>, accessed Oct 1, 2007.

[10] Omni Explosives. <http://www.omniexplosives.com>, accessed Oct 1, 2007.

[11] “FS-17 Firing System.” Teledyne Technologies, Inc. <http://www.teledynerisi.com/products/0products_2fs_page49.asp>, accessed Oct 2, 2007.

[12] "v7.2 Specifications" Vision Research, Inc. <http://www.visionresearch.com/uploads/docs/Discontinued/V7/v7.2spec.pdf>, accessed Oct 4, 2007.

[13] "Platinum FaroArm Product Information" FARO Technologies, Inc. <http://www.faro.com/content.aspx?ct=us&content=pro&item=2&subitem=2>, accessed Jun 22, 2007.

[14] "Principle of Digital Image Correlation" Correlated Solutions, Inc. <http://www.correlatedsolutions.com/index.php?option=com_content&task=view&id=23&Itemid=36>, accessed Nov 1, 2007.

[15] "Experimental Procedures for 3D Image Correlation" Correlated Solutions, Inc. Presentation, delivered 2005.

[16] Clough, Ray. Rashid, Yusef. "Finite Element Analysis of Axi-Symmetric Solids." Journal of the Engineering Mechanics Division, American Society of Civil Engineers v91 (Feb 1965): p71-85.

[17] Daryl, Logan. *A First Course in the Finite Element Method.* Thomson, Toronto. 2007.

[18] Meyers, Marc. *Dynamic Behavior of Materials.* Wiley, New York. 1994.

[19] Haslach Jr., Henry. Armstrong, Ronald. *Deformable Bodies and Their Material Behavior.* Wiley, Hoboken. 2004.

[20] Johnson, Gordon. Cook, William. "A Constitutive Model and Data for Metals Subjected to Large Strains, High Strain Rates and High Temperatures." Proceedings, 7th International Symposium on Ballistics, the Netherlands (1983): p541-547.

[21] EPIC code Material Library, Johnson-Cook Material, 6061-T6. Retrieved by Daniel Casem, Mar 2007.

[22] "LS-PrePost Online Documentation." Livermore Software Technology Corp. <http://www.lstc.com/lspp/content/overview.shtml>, accessed Nov 15, 2007.

[23] "LS-DYNA Keyword User's Manual September 2006 Version 971." Livermore Software Technology Corp. <http://www.dynasupport.com/news/ls-dyna-971-manual-pdf>, accessed Nov 14, 2007.

[24] Fourney, William. Leiste, Uli. Bonenberger, Robert. Goodings, Deborah. "Measurements of Pressure Loading on Plates Due to Explosive Detonation."